REPORT DOCUMENTATION PAGE

AFRL-SR-BL-TR-98-

0512

1. AGENCY USE ONLY (Leave blank)	2. REPORT DATE	3. REPORT TYPE AND DATES COVERED
		FINAL 15 Jun 97 To 14 Jun 98

4. TITLE AND SUBTITLE

ORGANIZATION OF THE 1997 ORGANIC THIN-FILMS FOR PHOTONICS APPLICATIONS TOPICAL MEETING

5. FUNDING NUMBERS

F49620-97-1-0499

62173C   1651/01

61101E   C611/02

6. AUTHOR(S)

Dr David W. Hennage

7. PERFORMING ORGANIZATION NAME(S) AND ADDRESS(ES)

Optical Society of America
2010 Massachusetts ave NW
Washington DC 20036

8. PERFORMING ORGANIZATION REPORT NUMBER

9. SPONSORING/MONITORING AGENCY NAME(S) AND ADDRESS(ES)

AFOSR/NL
110 Duncan Avenue Room B115
Bolling AFB DC 20332-8050

Dr Charles Y-C. Lee

10. SPONSORING/MONITORING AGENCY REPORT NUMBER

11. SUPPLEMENTARY NOTES

12a. DISTRIBUTION AVAILABILITY STATEMENT

Approved for public release;
distribution unlimited.

12b. DISTRIBUTION CODE

13. ABSTRACT (Maximum 200 words)

The meeting was held in Long Beach, CA on Oct 15-17, 1997. A Total of twelve technical sessions plus a poster session was held. The number of presentation and posters totaled over fifty. The sessions covered topics including Interconnects, Poling and Relaxation, Third Order Effects, Emissive Effects, Optical Limiting, Polymer Optical Fibers, Electro-Optic Materials, Second Order Effects, EO Devices and Photorefraction.

19980630 048

14. SUBJECT TERMS			15. NUMBER OF PAGES
			16. PRICE CODE

17. SECURITY CLASSIFICATION OF REPORT	18. SECURITY CLASSIFICATION OF THIS PAGE	19. SECURITY CLASSIFICATION OF ABSTRACT	20. LIMITATION OF ABSTRACT
(U)	(U)	(U)	(UL)

1997

Technical

Digest Series

Volume 14

Organic Thin Films for Photonics Applications

Technical Digest

October 15–17, 1997

Hyatt Regency Long Beach
Long Beach, California

Conference Edition

OSA®
Optical Society of America

Organic Thin Films for Photonics Applications

Technical Digest

October 15–17, 1997

Hyatt Regency Long Beach
Long Beach, California

Volume 14
1997 OSA Technical Digest Series

Conference Edition

Contents

Technical Program Committee Members

George I. Stegeman, *General Chair, CREOL, University of Central Florida, USA*

Hilary S. Lackritz, *General Chair, Purdue University, USA*

William H. Steier, *Program Chair, University of Southern California, USA*

Carl Dirk, *Program Chair, University of Texas at El Paso, USA*

Paul Ashley, *U.S. Army Missile Command, USA*

Donald Burland, *IBM Almaden Research Center, USA*

Steve Forrest, *ATC/POEM, Princeton University, USA*

Dexter Girton, *Lockheed Martin Missiles & Space, Advanced Technology Center, USA*

Zakya Kafafi, *Naval Research Laboratory, USA*

Yasuhiro Koike, *Keio University, Japan*

Mark G. Kuzyk, *Department of Physics, Washington State University, USA*

Robert Norwood, *AlliedSignal Inc., USA*

Peter Palffy-Muhoray, *Liquid Crystal Institute, Kent State University, USA*

Joseph W. Perry, *Jet Propulsion Laboratory, USA*

Nasser Peyghambarian, *Optical Sciences Center, University of Arizona, USA*

Yongqiang Shi, *TACAN Corp., USA*

Charles Spangler, *Optical Technology Center, Montana State University, USA*

Anthony J. Ticknor, *Akzo Nobel Electronic Products, USA*

Joseph Zyss, *Centre National d'Etudes des Telecommunications, France*

International Advisory Committee

Donal D. C. Bradley, *University of Sheffield, U.K.*

Peter Gunter, *ETH Honggerberg, Swiss Federal Institute of Technology, Swizterland*

Winfried H. Horsthuis, *JDS-Fitel, The Netherlands*

Toshikuni Kaino, *Institute of Chemical Reaction, Tohoku University, Japan*

Francois Kajzar, *CEA DTA LETI, France*

Wolfgang Knoll, *Max Planck Institute, Federal Republic of Germany*

Seizo Miyata, *Tokyo University of Agriculture and Technology, Japan*

Almeria Natansohn, *Chemistry Department, Queens University, U.K.*

Andre Pierre Perssons, *Chemistry Department, University of Leuven, Belgium*

Hiroyuki Sasabe, *Frontier Research Program, Insitute of Physical and Chemical Research, Japan*

Yang-Gil Shin, *Electrical Engineering Department, Korea Institute of Science and Technology, Korea*

Giuseppe Zerbi, *Politecnico di Milano, Italy*

Agenda

■ Tuesday
■ October 14, 1997

Seaview Foyer
6:00pm–8:00pm
Registration

■ Wednesday
■ October 15, 1997

Seaview Foyer
7:30am–5:30pm
Registration/Speaker Check-in

Seaview A&B

8:30am–8:45am
Opening Remarks
George I. Stegeman, *General Chair*

8:45am–10:00am
WA ■ Interconnects
Toshikuni Kaino, *Tohoku University, Japan, Presider*

8:45am
WA1 ■ Application of highly scattering optical-transmission polymer to high-quality LCDs, Akihiro Horibe, Eisuke Nihei, Yasuhiro Koike, *Keio Univ., Japan;* Yasuhiro Koike, *Keio Univ. and Kanagawa Academy of Science and Technology, Japan.* We report the highly scattering optical-transmission (HSOT) polymer as a new optical material, and its application to the high-quality backlight system for LCDs. **(p. 2)**

9:00am (Invited)
WA2 ■ Single-mode optical interconnects in ultra-low-loss environmentally stable polymers, Louay Eldada, Lawrence W. Shacklette, Robert A. Norwood, James T. Yardley, *AlliedSignal Inc.* We report a technology for single-mode polymeric interconnects that addresses the telecom industry's need for low-cost components with low insertion loss and temperature/humidity resistance. **(p. 5)**

9:30am
WA3 ■ Vertical tapered mode size transformer in polymer waveguides for efficient fiber coupling, Antao Chen, Vadim Chuyanov, Felix Ignacio Marti-Carrera, Sean Garner, William H. Steier, Jinghong Chen, Shajing Sun, Shane S.H. Mao, Younsoo Ra, Larry R. Dalton, *Univ. Southern California.* We demonstrate a vertical taper section integrated at the ends of polymer devices to improve the coupling between channel waveguides and single-mode optical fiber. **(p. 8)**

9:45am
WA4 ■ Three-dimensional integrated optics using polymers, Sean Garner, Vadim Chuyanov, Antao Chen, Srinath Kalluri, Felix Ignacio Marti-Carrera, William H. Steier, Larry R. Dalton, *Univ. Southern California.* We present simulation, fabrication, and experimental results for vertical waveguide bends and Y-branched vertical splitters. These embody key elements enabling practical three-dimensional integrated optics. **(p. 11)**

Seaview Foyer
10:00am–10:30am
Coffee Break

Seaview A&B

10:30am–12:15pm
WB ■ Poling and Relaxation
Hilary Lackritz, *Purdue University, Presider*

10:30am (Invited)
WB1 ■ Modeling relaxation mechanisms in nonlinear optical polymer films, K.D. Singer, R.D. Dureiko, *Case Western Reserve Univ.* Frequency and time domain harmonic generation and dielectric measurements were carried out on a series of methacrylate polymers. Analysis in relation to the Adam-Gibbs model leads to a predictive model. **(p. 16)**

11:00am
WB2 ■ A stochastic model for chromophore disorientation in guest-host nonlinear optical polymer systems, S.-J. Lee, G.A. Medvedev, J.M. Caruthers, H.S. Lackritz, *Purdue Univ.* A model is developed to describe chromophore disorientation in the guest-host second-order nonlinear optical polymer system, where the structural relaxation is stochastic. **(p. 19)**

11:15am (Invited)
WB3 ■ Mechanisms of chromophore reorientation probed with *in-situ*, pressure second-harmonic generation, L. Michael Hayden, Shane J. Strutz, *Univ. Maryland–Baltimore County.* Second-harmonic generation at hydrostatic pressures up to 3100 atm was used to probe the reorientation of chromophores in 21 different guest-host systems. The data suggests that the dominant mechanism for chromophore reorientation is different above and below T_g. **(p. 22)**

11:45am
WB4 ■ Study of photoinduced orientation of azobenzene amorphous polymer by visible, FTIR and Raman spectroscopy, F. Lagugné Labarthet, T. Buffeteau, C. Sourisseau, *Univ. Bordeaux, France.* The reorientational motions during trans↔cis photoisomerization cycles of azobenzene amorphous polymers have been investigated. Time-dependent linear dichroism measurements have been performed by visible and FTIR spectroscopy. **(p. 25)**

12:00m
WB5 ■ Kinetics of photoinduced orientation of azo-dyes in alignment layers, T. Kosa, P. Palffy-Muhoray, *Kent State Univ.* Dye-doped polymer films can be used to optically align liquid crystals. Orientational relaxation of chromophores in azo-dye-doped thin polyimide films show nonexponential relaxation, which may be explained in terms of dispersive transport. **(p. 28)**

12:15pm–1:30pm
Lunch on your own

Seaview A&B

1:30pm–3:00pm
WC ■ Third-Order Effects
Donal D.C. Bradley, *University of Sheffield, U.K., Presider*

1:30pm
WC1 ■ Laser emission from a monolithic organic single crystal, Denis Fichou, *C.N.R.S., France;* Stéphane Delysse, Jean-Michel Nunzi, *LETI (CEA–Technologies Avancées), France.* We demonstrate optically pumped laser action in single crystals of conjugated octithiophene. Gain narrowing and dual energy dependence of two emissionlines clearly evidence stimulated emission. **(p. 32)**

1:45pm
WC2 ■ Preparation and characterization of single crystal PTS waveguide film, M. Liu, C.K. Hwangbo, L. Friedrich, G.I. Stegeman, *CREOL, Univ. Central Florida.* Crystalline PTS film was prepared by solution method. Wave-guiding and optical characterizations were performed on 1–3-mm-long PTS films at 1.6 micron. **(p. 35)**

2:00pm
WC3 ■ Basic mechanisms involved in the off-resonant nonlinear refractive index of PTS-polydiacetylene, R. Quintero-Torres, M. Thakur, *Auburn Univ.* The sign of n_2 of PTS in the off-resonant domain (650–1064 nm) was found to be negative, which is consistent with saturation of exciton transition being substantially larger than two-photon absorption for off-resonant pumping. **(p. 37)**

2:15pm
WC4 ■ Characterization of push-pull polyenes of increasing size: linear and quadratic polarizabilities in solution, Alain Fort, Jacques Muller, Joel Azoulay, Marguerite Barzoukas, *Institut de Physique et de Chimie des Matériaux de Strasbourg, France;* Valérie Alain, Mireille Blanchard-Desce, *Ecole Normale Supérieure, France.* We have synthesized several series of push-pull polyenes bearing electron donating and withdrawing groups. We have investigated their linear and quadratic polarizabilities in solution. **(p. 40)**

2:30pm
WC5 ■ One- and two-photon-induced photodegradation of DANS films, Qiang Zhang, Michael Canva, George Stegeman, *CREOL, Univ. Central Florida.* The photodegradation quantum efficiency of DANS has been measured from the absorption band to the near-infrared. Its impact on waveguide device performance is being investigated. **(p. 43)**

2:45pm
WC6 ■ Observation of switching phenomena in non-ether PPQ planar waveguide with two-wavelength nonlinear prism coupling, Jun Zhou, *Shandong Institute of Mining and Technology, China;* Zhuangqi Cao, Yingli Chen, Yixin Chen, *Shanghai Jiao Tong Univ., China;* Meng Sun, Diechi Sun, Fuming Li, *Fudan Univ., China.* The research is concerned with the non-ether polyphenylquinoxalines (PPQ) film waveguide, and the switching phenomenon in the waveguide is observed by two-wavelength nonlinear prism coupling. **(p. 46)**

Seaview Foyer
3:00pm–3:30pm
Coffee Break

Seaview A&B

3:30pm–5:30pm
WD ■ Emissive Devices
Zakya H. Kafafi, *U.S. Naval Research Laboratory, Presider*

3:30pm (Invited)
WD1 ■ Conjugated polymers as materials for thin-film solid-state lasers, F. Hide, M.A. Diaz-Garcia, M. McGehee, B.J. Schwartz, A.J. Heeger, *UC–Santa Barbara.* Lasing and gain narrowing are compared for a soluble poly(phenylene vinylene) derivative using two different resonant structures: planar waveguides and microcavities. In both cases, the gain narrowing threshold is at 0.05–0.1 µJ per 10-ns pulse focused to approximately 1.5 mm. Single-mode microcavity lasers are obtained when a cavity resonance occurs at the wavelength where the gain of the polymer is a maximum. Low threshold lasing (threshold more than an order of magnitude below that observed in planar waveguides and microcavities) has also been demonstrated using distributed feedback in a planar thin-film configuration. **(p. 50)**

4:00pm
WD2 ■ Light amplification in polymer optical fibers, Takeyuki Kobayashi, Eisuke Nihei, Keisuke Sasaki, *Keio Univ., Japan;* Yasuhiro Koike, *Keio Univ. and Kanagawa Academy of Science and Technology, Japan.* Graded-index polymer optical fibers doped with fluorescent materials such as organic dyes and rare-earth chelates have been proposed and fabricated for light amplification in the visible and infrared. **(p. 51)**

4:15pm (Invited)
WD3 ■ Liquid crystalline polymers for electroluminescence, D.D.C. Bradley, M. Grell, K.L. Brandon, M.L. Turner, P. Bentley, D.A. Dunmur, *Univ. Sheffield, U.K.;* E.P. Woo, M. Inbasekaran, *The Dow Chemical Co.* Liquid crystalline polymers with the dual attributes of charge transport and light emission capability for application in polarized electroluminescence devices will be reviewed. **(p. 54)**

4:45pm
WD4 ■ Origin of optical gain and stimulated emission in conjugated polymers, Ch. Spiegelberg, A. Schülzgen, M.M. Morrell, B. Kippelen, N. Peyghambarian, *Univ. Arizona;* P.M. Allemand, *Donnelly Corp.* In BEH-PPV polymer films excitonic transitions with a linewidth of 8 nm lead to stimulated emission and optical gain of up to 10.000 per cm. **(p. 55)**

5:00pm (Invited)
WD5 ■ Molecular-level engineering of polymer-based light-emitting devices, Michael Rubner, *Massachusetts Institute of Technology.* Molecular-level processing schemes have been utilized to fabricate light emitting thin film devices from a variety of materials including conjugated polymers and polymers containing tris-chelated Ru(II) complexes. **(p. 58)**

Seaview Foyer
7:30am–5:00pm
Registration/Speaker Check-In

Seaview A&B

8:45am–10:00am
ThA ■ Optical Limiting
A.F. Garito, *University of Pennsylvania, Presider*

8:45am (Invited)
ThA1 ■ Optical limiting and the potential role of organic materials, Eric Van Stryland, Arthur Dogariu, Jin Hong Lim, David J. Hagan, Olga Przhonska, *CREOL, Univ. Central Florida.* We briefly review optical limiting research and present results for several materials exhibiting very different nonlinear mechanisms. We then discuss the most promising organic materials and their characterization. **(p. 60)**

9:15am
ThA2 ■ Optical limiting mechanisms in a neat liquid phthalocyanine thin film, Steven R. Flom, Richard G.S. Pong, James S. Shirk, F.J. Bartoli, Arthur W. Snow, *U.S. Naval Research Laboratory.* In a pure liquid phthalocyanine, optical limiting measurements yield a low threshold and substantial dynamic range. The high fluence limiting is enhanced through optical breakdown. **(p. 61)**

9:30am (Invited)
ThA3 ■ Nonlinear spectroscopy and applications of two-photon absorbing molecules, J. Ehrlich, *Jet Propulsion Laboratory;* A. Heikal, Z.-Y. Hu, I.-Y.S. Lee, H. Röckel, X.L. Wu, *Beckman Institute;* S.R. Marder, J.W. Perry, *Jet Propulsion Laboratory and Beckman Institute.* Large two-photon absorptivities have been observed in bis-donor diphenylpolyenes. Applications of these molecules to two-photon photopolymerization and optical limiting are discussed. **(p. 64)**

Seaview Foyer
10:00am–10:30am
Coffee Break

Seaview A&B

10:30am–12:00pm
ThB ■ Polymer Optical Fibers
Robert A. Norwood, *AlliedSignal Inc., Presider*

10:30am
ThB1 ■ Mode-coupling effects in plastic optical fibers, G. Jiang, R.F. Shi, A.F. Garito, *Univ. Pennsylvania.* Mode coupling in plastic optical fibers is observed through optical pulse broadening measurements that show characteristic change over from linear to square root length dependence. **(p. 66)**

10:45am (Invited)
ThB2 ■ High-speed polymer optical fiber and related photonics polymer, Yasuhiro Koike, *Keio Univ. and Kanagawa Academy of Science and Technology, Japan.* Recent progress of the polymer optical fiber (POF) and related photonics polymer for high-speed telecommunication is reviewed. The high-bandwidth perfluorinated GI POF, which has no serious absorption loss from visible to 1.3-μm wavelength, is proposed as a promising candidate for "the last one mile." **(p. 69)**

11:15am
ThB3 ■ Polymer thin-film overlays for passive side-polished fiber devices, S.G. Lee, J.P. Sokoloff, H. Sasabe, *Institute of Chemical and Physical Research (RIKEN), Japan.* Several polymers often used as "hosts" in "guest-host" organic thin-film systems were investigated for their suitability as overlays for side-polished fiber devices. **(p. 70)**

11:30am (Invited)
ThB4 ■ Plastic optical fibers: yesterday, today, and tomorrow, Toshikuni Kaino, *Tohoku Univ., Japan.* In the past, when lowering the optical loss of plastic optical fibers (POF) was the main issue, deuteration/fluorination technologies were effectively applied. Today, POF transmission bandwidth is of special interest, and graded-index POF attract many people. In the near-future, the important point will be the use of short-wavelength optical sources to open new horizons for POF applications. **(p. 73)**

12:00m–1:30pm
Lunch on your own

Seaview A&B

1:30pm–3:00pm
ThC ▪ Electro-Optic Materials
Carl Dirk, *University of Texas at El Paso, Presider*

1:30pm
ThC1 ▪ Noncentrosymmetric ionically self-assembled thin films for second-order nonlinear optics, J.R. Heflin, Y. Liu, C. Figura, D. Marciu, R.O. Claus, *Virginia Tech.* We have demonstrated that a fast and inexpensive self-assembled monolayer technique can produce noncentrosymmetric thin films with $\chi^{(2)}$ values comparable to that of quartz. **(p. 78)**

1:45pm
ThC2 ▪ Multifunctional photoresponses in carbazole main-chain polymers, Tatsuo Wada, Yadong Zhang, Hiromi Kimura-Suda, Hiroyuki Sasabe, *CREST, JST, and RIKEN, Japan;* Tetsuya Aoyama, Su-An Choi, *Institute of Physical and Chemical Research (RIKEN), Japan.* We have developed photoconductive and electro-optic carbazole main-chain polymers with shoulder-to-shoulder, head-to-tail, and hyperbranched arrangements for multifunctional materials. **(p. 81)**

2:00pm
ThC3 ▪ Quadrupoling for second-order nonlinear optics, K.D. Singer, S.F. Hubbard, R.G. Petschek, N. D'Sidocky, C. Hudson, L.C. Chien, *Kent State Univ.;* C.C. Henderson, P.A. Cahill, *Case Western Reserve Univ.* Hyper-Rayleigh scattering measurements revealed a sizable chiral quadrupolar nonlinearity in camphorquinone molecules. These may be exploited to form electro-optic materials in axially aligned polymers. **(p. 84)**

2:15pm
ThC4 ▪ Thiophene-based nonlinear optical chromophore functionalized epoxy polymers for electro-optic applications, K.G. Chittibabu, L. Li, *Molecular Technologies, Inc.;* X. Wang, J. Kumar, S.K. Tripathy, *Univ. Massachusetts Lowell.* Thiophene-based nonlinear optical chromophore functionalized epoxy polymers containing strong electron-withdrawing groups such as tricyanovinyl and nitro, with high optical nonlinearities were synthesized by post-functionalization. **(p. 87)**

2:30pm
ThC5 ▪ Electro-optic effect and propagation loss in polymer films containing nano-sized droplets of liquid crystal, Shiro Matsumoto, Yasuyuki Sugiyama, Seizou Sakata, Takayoshi Hayashi, *NTT Integrated Information & Energy Systems Laboratories, Japan.* Polymer materials containing nano-sized liquid crystal showed a large electro-optic effect ($\Delta n = 0.001$ at 8 V/μm), low propagation loss (2.5 dB/cm), and fast response time (<10 μs). **(p. 90)**

2:45pm
ThC6 ▪ High glass transition temperature syndioregic second-order nonlinear optical polymers in Langmuir-Blodgett-Kuhn films, M.J. Roberts, G.A. Lindsay, J.D. Stenger-Smith, R.A. Hollins, A.P. Chafin, *U.S. Navy;* R.G. Gratz, *Mary Washington College.* Langmuir-Blodgett-Kuhn processing of the polymers yields uniformly deposited films with stable noncentrosymmetric order to temperatures of 95°C. **(p. 93)**

Seaview Foyer
3:00pm–3:30pm
Coffee Break

Seaview A&B

3:30pm–4:30pm
ThD ▪ Second-Order Effects
Joseph Zyss, *France Telecom/CNET, France, Presider*

3:30pm (Invited)
ThD1 ▪ Nonlinear optics of chiral media, Thierry Verbiest, Sven Van Elshocht, Gunter Beelen, Carlo Boutton, Martti Kauranen, André Persoons, *Univ. Leuven, Belgium.* We give an overview of our recent work on second-harmonic generation from chiral surfaces and the electro-optic effect in chiral isotropic media. **(p. 98)**

4:00pm
ThD2 ▪ Thiophene-based hydrazones: a new class of nonlinear optical molecular crystals, Christian Bosshard, Pan Feng, Man Shing Wong, Martin Bösch, Urs Meier, Peter Günter, *Institute of Quantum Electronics, Switzerland.* We have developed new nonlinear optical molecular crystals that can easily be grown in large sizes and describe their high second-order nonlinearities and their potential for applications. **(p. 101)**

4:15pm
ThD3 ▪ Difference in relaxation time between coherent and incoherent second-harmonic generation, Koen Clays, Geert Olbrechts, David Van Steenwinckel, André Persoons, *Center for Molecular Electronics and Photonics, Belgium.* The difference in relaxation time between coherent and incoherent second-harmonic generation is explained by diffusion over the coherence length and over the wavelength, respectively. **(p. 104)**

Seaview C

4:30pm–7:00pm
ThE ∎ Poster Session

5:30pm–7:00pm
Conference Reception

ThE1 ∎ Third-order nonlinear optical property of platinum group metal complexes with square planar configurations, Takehito Kodzasa, Toshihide Kamata, Hirobumi Ushijima, Hiro Matsuda, Fujio Mizukami, *National Institute of Materials and Chemical Research, Japan.* Abstract not available. **(p. 108)**

ThE2 ∎ Nonlinear absorption in CuPc-SiO$_2$ composite, E. Blanco, R. Litrán, M. Ramírez-del-Solar, *Univ. Cádiz, Spain;* F.J. Aranda, D.V.G.L.N. Rao, S. Tripathy, *Univ. Massachusetts;* D. Narayana Rao, J.A. Akkara, M. Nakashima, *U.S. Army Natick Research Development and Engineering Center.* We present results for the effective excited-state absorption cross section for copper pthalocyanine in solution in sulfuric acid as well as in a pthalocyanine-silica composite. **(p. 111)**

ThE3 ∎ Electro-optic measurements of dye-doped linear polymers, Fassil Ghebremichael, Randall J. Knize, *USAF Acad.* A modified Mach-Zehnder interferometer was used *in situ,* for temperature-dependent linear electro-optic studies. Electronic feedback system achieved optimum and stable interferometer phase. Film thickness variation was compensated for more accurate and sensitive nonlinear coefficient measurements, resulting in the detection of both the α- and β-relaxations of poly(methyl methacrylate) +2%wt. (4-dimethylamino-4'nitrostilbene) films. **(p. 114)**

ThE4 ∎ Linear and second-order nonlinear optical properties of urethane-urea copolymers, Masaaki Tsuchimori, Osamu Watanbe, Akane Okada, *Toyota Central Research and Development Laboratories Inc., Japan.* Urethane-urea copolymers showing large and stable nonlinear optical properties were synthesized. Linear optical properties including propagation loss were studied for slab and channel waveguides. **(p. 117)**

ThE5 ∎ Orientational relaxation of nonlinear optical dipole moments transversely aligned to the main backbone in the linear polyurethane, Naoto Tsutsumi, Osamu Matsumoto, Wataru Sakai, *Kyoto Institute of Technology, Japan.* Relaxation of oriented NLO dipole was studied for linear polyurethane corona-poled at two temperatures. Remarkable orientational stability for sample poled at 94°C was ascribed to higher effective T_g resulting from smaller free volume. **(p. 120)**

ThE6 ∎ Hyper-Rayleigh scattering and two-photon absorption-induced fluorescence of chromophores with enhanced thermal stability, Chia-Chen Hsu, *National Chung Cheng Univ., Taiwan;* Ching-Fong Shu, Tzer-Hsiang Huang, Jiunn-Lih Lin, Yuh-Kai Wang, Yi-Liang Zang, *National Chiao Tung Univ., Taiwan;* C.H. Wang, *Univ. Nebraska-Lincoln.* The first hyperpolarizabilities (β) and thermal stabilities of thiophene-incorporated polyene chromophores with and without a configuration-locked trans-triene bridge were compared by the hyper-Rayleigh scattering (HRS) and thermal stability experiments, respectively. From HRS and thermal stability experiments, it is found that the configuration-locked trans-triene bridge can enhance both β value and thermal stability in thiophene-incorporated polyene chromophores. **(p. 123)**

ThE7 ∎ Nonlinear optical films from pairwise-deposited semi-ionomeric syndioregic polymers, M.J. Roberts, G.A. Lindsay, J.D. Stenger-Smith, P. Zarras, R.A. Hollins, A.P. Chafin, M.P. Nadler, *U.S. Navy;* K.J. Wynne, *Office of Naval Research.* A polymeric salt formed on a Langmuir trough, after transfer, gives a polar film that uses primarily ionic and hydrogen bonding to maintain noncentrosymmetric order. **(p. 126)**

ThE8 ∎ Nonlinear optical properties of *bacteriorhodopsin* in multilayer Langmuir-Blodgett films, A.V. Kir'yanov, I.A. Maslyanitsin, V.V. Savranskii, N.A. Tkachenko, *General Physics Institute, Russia;* H. Lemmetyinen, *Technical Univ. Tampere, Finland.* Nonlinear optical properties of multilayer Langmuir-Blodgett films (LBF) of *bacteriorhodopsin* (bR) were studied experimentally. The samples were deposited in Y- and Z-configurations (Z-type bR films up to 50 layers were manufactured at first). The method of second-harmonic generation and the Z-scan technique were used in order to evaluate the elements of susceptibility second-order tensor and to determine the sign and approximate magnitude of the refractive-index nonlinear part for the samples studied. **(p. 129)**

ThE9 ∎ Molecular orientation in protein films deposited on substrates coated with Langmuir-Blodgett and self-assembled monolayers, Paul L. Edmiston, Laurie L. Wood, John E. Lee, S. Scott Saavedra, *Univ. Arizona.* We have been investigating techniques for creating macroscopically ordered protein films formed by covalent bonding between a unique site on the protein and an appropriately derivatized substrate surface. Assemblies consisting of heme proteins immobilized on substrates coated with self-assembled monolayers and Langmuir-Blodgett are being examined. Macroscopic film order is probed using a combination of total internal reflectance fluorescence and planar integrated optical waveguide-attenuated total reflection spectroscopies, from which the orientation distribution of heme tilt angles in the protein film is determined. **(p. 130)**

ThE10 ■ Fabrication of the one-dimensional superlattice in the epitaxially grown film of platinum dioxime complexes, Kaoru Yamamoto, Toshiaki Ohta, *Univ. Tokyo, Japan;* Toshihide Kamata, Kiyoshi Yase, Yuji Yoshida, Fujio Mizukami, *National Institute of Materials and Chemical Research, Japan.* The one-dimensional superlattice was prepared by depositing two types of platinum dioxime complexes alternately. The structure was investigated by XRD, TED, UV-Vis, and AFM measurements. **(p. 134)**

ThE11 ■ *Bacteriorhodopsin* optoelectronic synapses, D.P. Shelton, *Univ. Nevada Las Vegas.* A *bacteriorhodopsin* thin film can provide a combination of vector multiplication, associative learning, and memory storage functions in a neural network. **(p. 137)**

ThE12 ■ Beam splitting in nonlinear polymeric waveguide induced by photobleaching, Aaron Wilkosz, *Nichols Research Corp.;* Sergey Sarkisov, *Alabama A&M Univ.* Theoretical and experimental results are reported on optical beam splitting in dye-doped polymeric slab waveguide as a result of photobleaching with low power light. **(p. 140)**

ThE13 ■ Field-induced spatial deformations in chiral smectic A liquid crystals, F.J. Bartoli, J.R. Lindle, S.R. Flom, B.R. Ratna, R. Shashidhar, *U.S. Naval Research Laboratory.* Field-induced layer deformations in chiral smectic A liquid crystals are investigated. The relationship of the deformation angle and the electroclinic tilt angle is discussed. **(p. 143)**

ThE14 ■ Electro-optic modulation in waveguides based on single crystal films of organic materials, Jianjun Xu, M. Thakur, *Auburn Univ.* Electro-optic modulation has been demonstrated in two different waveguide structures based on organic single crystal films. **(p. 146)**

ThE15 ■ Enhanced degenerate four-wave mixing in an endohedral metallofullerene through metal-to-cage charge transfer, D. Marciu, C. Figura, S. Wang, J.R. Heflin, P. Burbank, S. Stevenson, H.C. Dorn, *Virginia Tech.* The $\chi^{(3)}$ of the endohedral metallofullerene $Er_2@C_{82}$ has been found to be orders-of-magnitude larger than that of the corresponding empty-cage fullerenes. **(p. 149)**

ThE16 ■ Fabrication of vertical tapers in polymer thin films by oxygen reactive ion etching with a shadow mask for photonic device applications, Antao Chen, Felix Ignacio Marti-Carrera, Sean Garner, Vadim Chuyanov, William H. Steier, *Univ. Southern California.* A simple technique for making vertical tapers in polymer thin films by reactive ion etching with a shadow mask is demonstrated. **(p. 152)**

ThE17 ■ Spontaneously self-assembled polar multilayers with high second-order nonlinearity, M.S. Johal, J.M. Robinson, D.W. McBranch, D.Q. Li, *Los Alamos National Laboratory;* L. Smilowitz, *Boston Univ.;* W.S. Yang, Y.W. Cao, X.D. Chai, Y.S. Jiang, T.J. Li, *Jilin Univ., China.* Second-harmonic generation is used to determine the magnitude of the second-order nonlinear optical coefficient and average molecular orientation of a polar multilayer on silica. **(p. 155)**

ThE18 ■ Modified attenuated total reflection for the fast and routine electro-optic measurements of nonlinear optical polymer thin films, Antao Chen, Vadim Chuyanov, Sean Garner, William H. Steier, Larry R. Dalton, *Univ. Southern California.* Attenuated total reflection with a simple algorithm and a scratch-resistant metal electrode for fast evaluation of corona poled electro-optic polymer thin films is presented. **(p. 158)**

ThE19 ■ Return loss measurements for the determination of critical materials parameters for polymer optical waveguides, Robert A. Norwood, *AlliedSignal, Inc.* For optical network applications it is necessary to know how a material's optical properties change with wavelength, temperature, and humidity. We demonstrate a simple technique for obtaining this information by measuring return loss. **(p. 161)**

ThE20 ■ Optical measurement of the glass transition temperature of polymeric waveguides for integrated optics, Harald Bock, Stefan Christian, *Max-Planck-Institut für Polymerforschung, Germany;* Wolfgang Knoll, *Max-Planck-Institut für Polymerforschung, Germany and The Institute of Physical and Chemical Research (RIKEN), Japan;* Jan Vydra, *Institut für Angewandte Physik, Technische Hochschule Darmstadt, Germany.* Influence of processing steps on the glass transition temperatures of polymeric waveguides for integrated optics has been investigated using a novel nondestructive optical technique. **(p. 164)**

ThE21 ■ Passive alignment of optic fiber array using silicon V-grooves monolithically integrated with polymer waveguide devices, Antao Chen, Mehrdad Ziari, William H. Steier, *Univ. Southern California.* Experimental results of a passive array alignment technique between optic fiber and polymer waveguides using silicon V-grooves made on the waveguide substrate are presented. **(p. 167)**

ThE22 ■ Ionization-assisted deposition of polyurea thin films for nonlinear optical applications, H. Usui, H. Kikuchi, K. Tanaka, S. Miyata, T. Watanabe, *Tokyo Univ. Agriculture and Technology, Japan;* W. Knoll, H. Bock, *Max-Planck-Institut für Polymerforschung, Germany.* Polyurea thin films were polymerized with an ionization-assisted deposition method, which enabled us to control the dipole orientation during the film formation process. **(p. 170)**

Seaview Foyer
7:30am–5:30pm

Seaview A&B

8:30am–10:00am
FA ■ EO Devices I
William H. Steier, *University of Southern California, Presider*

8:30am (Invited)
FA1 ■ Electro-optic polymer devices for fiber-optic gyros and other applications, Paul R. Ashley, *U.S. Army Missile Command;* Jeffrey S. Cites, *Aegis Research Corp.*
Integrated photonic components based on polymeric materials have been developed, which enhance the integration of fiber-optic gyroscopes. New active and passive polymeric materials, device designs, and component integration on optoelectronic substrates are reviewed.
(p. 196)

9:00am
FA2 ■ Push-pull polymer integrated Mach-Zehnder modulators, Wenshen Wang, Yongqiang Shi, David J.
Olson, Weiping Lin, James H. Bechtel, *TACAN Corp.* An optical push-pull structure has been realized on an integrated Mach-Zehnder intensity modulator based on the laser diode 3 electro-optic polymer. The devices have exhibited a 50% reduction in the halfwave voltage compared to the non-push-pull devices. **(p. 198)**

9:15am
FA3 ■ Nonlinear optical chromophores containing fused terthiophene as a new type of electron relay,
O.-K. Kim, *U.S. Naval Research Laboratory and Collège de France, France;* A. Fort, M. Barzoukas, *IPCMS, France;* J.-M. Lehn, *Collège de France, France.* Nonlinear optical chromophores containing fused terthiophene (DTT) were synthesized. They exhibited a large molecular nonlinearity, indicating DTT as a highly efficient relay with anomalous solvatochromism and remarkable thermal stability.
(p. 201)

9:30am
FA4 ■ Thermo-optic switches using fluorinated polyimide waveguides, Junya Kobayashi, Tohru Maruno,
Yasuhiro Hida, *NTT Opto-Electronics Laboratories, Japan;* Tohru Matsuura, Shigekuni Sasaki, *NTT Science and Core Technology Laboratory Group, Japan.* We fabricated Y-branching-type TO switches using fluorinated polyimide waveguides. Extinction ratio was above 20 dB for driving powers above 160 mW. PDL was below 0.4 dB. **(p. 204)**

Seaview Foyer
10:00am–10:30am
Coffee Break

Seaview A&B

10:30am–12:00m
FB ■ Polymer Integrated Optics
Yasuhiro Koike, *Keio University, Japan, Presider*

10:30am (Invited)
FB1 ■ Control of the photoinduced micro-patterning of nonlinear organic thin films: from molecular to photonic engineering, Sophie Brasselet, Joseph Zyss,
France Telecom-Centre National d'Etudes des Télécommunications, France. Experiments and theory jointly evidence the possibility of photoinducing any desired spatial micro-pattern for the $\chi^{(2)}$ tensor of functionalized organic films via adequately polarized "write" beams.
(p. 208)

11:00am
FB2 ■ In-situ trimming of polymer optical waveguides by rapid photobleaching for tuning device specifications, Antao Chen, Felix Ignacio Marti-Carrera, Vadim
Chuyanov, Sean Garner, William H. Steier, Shane S.H. Mao, Younsoo Ra, Larry R. Dalton, *Univ. Southern California;* Yongqiang Shi, *TACAN Corp.* We present a novel post-fabrication trimming technique that can adjust the power splitting ratio, the extinction ratio, and coupling constant of polymer waveguide devices. **(p. 211)**

11:15am
FB3 ■ Application of surface relief gratings created on azobenzene functionalized polymer films as phase masks, Lian Li, *Molecular Technologies Inc.;* Xin Li Jiang,
Dong-Yu Kim, Jayant Kumar, Sukant Tripathy, *Univ. Massachusetts Lowell.* Photofabricated surface relief gratings on azobenzene functionalized polymer films were used as phase masks to transfer the pattern to different azopolymer films. **(p. 214)**

11:30am
FB4 ■ Self-imaging holographic optical waveguides,
H. Grebel, J.L. Graziani, S. Vijayalakshmi, *New Jersey Institute of Technology;* L.W. Shacklette, K.M.T. Stengle, L. Eldada, R. Norwood, J.T. Yardley, *AlliedSignal.* We have studied holographic pattern, along the wave propagation direction and extended throughout the entire guide. Various self-imaging guides have been analyzed and realized.
(p. 217)

11:45am
FB5 ■ Application of UV-cured epoxy resin to polymeric optical waveguide components, Satoru
Tomaru, Koji Enbutsu, Makoto Hikita, Ryoko Yoshimura, Saburo Imamura, Tohru Maruno, Junya Kobayashi, *NTT Opto-Electronics Laboratories, Japan.* We have realized both a low loss (0.06 dB/cm) multimode optical waveguide at 0.83 µm and a passive fiber alignment using UV-cured epoxy resin. **(p. 220)**

12:00m–1:30pm
Lunch on your own

Seaview A&B

1:30pm–3:00pm
FC ■ EO Devices II
Paul R. Ashley, *U.S. Army Missile Command, Presider*

1:30pm (Invited)
FC1 ■ Next generation ultrahigh frequency integrated EO modulators, Datong Chen, Harold R. Fetterman, Boris Tsap, *UC–Los Angeles;* Antao Chen, William H. Steier, Larry R. Dalton, *Univ. Southern California;* Wenshen Wang, Yongqiang Shi, *TACAN Corp.* Our new generation of polymer electrooptic modulators, with integrated micro-wave transitions, has been demonstrated up to 113 GHz. Low cost arrays involving Mach–Zehnders in parallel and series configurations are now feasible for meaningful signal processing roles. **(p. 224)**

2:00pm
FC2 ■ Characterization of electro-optic polymer films using decal deposited reflection Fabry-Perot modulators, L.-M. Wu, Ph. Prêtre, R.A. Hill, A. Knoesen, *UC–Davis.* Reflection-mode Fabry-Perot modulators have been used for the complete determination of dispersive linear optical and electro-optic properties of poled nonlinear optical polymers. **(p. 226)**

2:15pm (Invited)
FC3 ■ Integrated electro-optic polymer devices for optical communications, Yongqiang Shi, Wenshen Wang, James H. Bechtel, *TACAN Corp.;* William H. Steier, Larry Dalton, *Univ. Southern California;* Harold R. Fetterman, *UC–Los Angeles.* The design, fabrication, and test of high-speed electro-optic (EO) polymer modulators are presented. Preliminary applications in analog and digital optical communication systems are demonstrated. Recent developments in optimizing EO polymer device performances will be discussed. **(p. 229)**

2:45pm
FC4 ■ Recent advances in the translation of large microscopic nonlinearities to large macroscopic nonlinearities in electro-optic polymer films, Aaron W. Harper, Mingqian He, Fang Wang, Jinghong Chen, Jingsong Zhu, Sam S. Sun, Larry R. Dalton, Antao Chen, Sean M. Garner, Araz Yacoubian, William H. Steier, *Univ. Southern California;* Datong Chen, H.R. Fetterman, *UC–Los Angeles.* Theoretical and experimental results relative to the generation of high electro-optic activity in poled polymer films are presented. **(p. 232)**

Seaview Foyer
3:00pm–3:30pm
Coffee Break

Seaview A&B

3:30pm–5:15pm
FD ■ Photorefraction
Kenneth D. Singer, *Case Western Reserve University, Presider*

3:30pm (Invited)
FD1 ■ High-performance photorefractive polymers and their applications, B. Kippelen, B.L. Volodin, E. Hendrickx, D.D. Steele, Sandalphon, Y. Enami, J.F. Wang, H. Röckel, F. Meyers, N. Peyghambarian, *Univ. Arizona;* S.R. Marder, *California Institute of Technology.* Recent advances in photorefractive polymer development will be discussed. Materials with unprecedented refractive-index modulation amplitudes, long shelf lifetimes, good photostability, and spectral sensitivity in the near-infrared will be presented. **(p. 236)**

4:00pm
FD2 ■ Organic photorefractive composite dynamics, J.D. Shakos, A.M. Cox, D.P. West, K.S. West, T.A. King, *Univ. Manchester, U.K.;* R.D. Blackburn, *Liverpool John Moores Univ., U.K.* Charge mobility restricts the response rate of reorientationally enhanced photorefractive polymer composite materials, according to degenerate four-wave mixing and Mach-Zehnder interferometric measurements. **(p. 239)**

4:15pm (Invited)
FD3 ■ Recent advances in high-gain photorefractive polymers, A. Grunnet-Jepsen, W.E. Moerner, *UC–San Diego.* High-gain photorefractive polymers with improved stability are described, and the achievement of beam fanning, self-pumped phase conjugation, and large two-beam coupling gains are discussed. **(p. 242)**

4:45pm
FD4 ■ Phase stability of guest-host photorefractive polymers studied by light-scattering experiments, E. Hendrickx, B.L. Volodin, D.D. Steele, J.L. Maldonado Rivera, J.F. Wang, B. Kippelen, N. Peyghambarian, *Univ. Arizona.* We report on new photorefractive polymers with high efficiency and long shelf lifetimes. Phase stability is studied by light-scattering experiments. **(p. 245)**

5:00pm
FD5 ■ Reduced hole mobility in photorefractive polymers due to the chromophore dipole moment, Arosha Goonesekera, Stephen Ducharme, *Univ. Nebraska-Lincoln.* Photorefractive polymers contain electro-optic chromophores whose large dielectric dipole moments significantly reduce the photocarrier mobility, thus reducing photorefractive speed and sensitivity. **(p. 248)**

5:15pm–5:30pm
Closing Remarks

Interconnects

Wednesday, October 15, 1997

Toshikuni Kaino, Tohoku University
Presider

WA
8:30am–10:00am
Seaview A&B

Application of Highly Scattering Optical-Transmission Polymer to high quality LCDs

Akihiro Horibe, Eisuke Nihei, Yasuhiro Koike
Faculty of Science and Technology, Keio University,
3-14-1, Hiyoshi, Kohoku-ku, Yokohama 223, JAPAN
Telephone : International +81 45 563 1141 ext.3454

Yasuhiro Koike
Kanagawa Academy of Science and Technology
1-1-1, Fukuura, Kanazawa-ku, Yokohama 236, JAPAN
Telephone : International +81 45 785-3730

More efficient LCD backlights have been strongly required to achieve lower electric power consumption and higher brightness on the LCD panel.

For the conventional LCD backlight system which has one lamp at an edge of light pipe (transparent PMMA), complicated dot printed or sand blasted patterns are necessary at the bottom of the PMMA light pipe to obtain uniform luminance. Here, a diffuser film is indispensable to hide these patterns. In case of our backlight system consisting of the highly scattering optical transmission (HSOT) polymer plate, although the concentration of the scatterer in the HSOT polymer plate is uniform, the luminance is almost uniform all over the surface of the plate. It is suggested that the high-order scattering inside the polymer would make the luminance from the surface uniform.

All conventional edge-light type backlight systems have consisted of a transparent PMMA plate as a light pipe and surrounding light-controlling devices (such as diffuser film, dot patterns, etc.). Our proposal is to use the only HSOT polymer plate for the backlight system without other complicated light-controlling devices used in conventional systems.

The HSOT polymer materials were prepared by polymerization of MMA solution including a small amount of other material with a different refractive index as scatterer. As shown in our previous papers[1,2], the scattering property of the HSOT polymer can be changed by controlling a correlation length defined in Debye scattering theory[3]. The correlation length which means the size of heterogeneous structure can be controlled by selecting a suitable scatterer.

The scattering phenomenon inside the HSOT polymer was exactly confirmed by Monte Carlo simulation[3]. In this simulation, scattering angle "θ" and photon path length "L" are calculated by the following equations.

$$\theta = F^{-1}(random1) \tag{1}$$

$$F(\theta) = \sum_{a=0}^{\theta} I(a) / I_{all} \tag{2}$$

$$L = -\ln(random2) / \pi r^2 CK \tag{3}$$

Here, random1 and 2 are random number, r is particle radius, C is particle concentration, K and I are scattering efficiency and scattering intensity profile of single scattering respectively, which are calculated by Mie theory[4]. One million photons are traced to draw illumination profile from the HSOT

polymer light pipe. Since the simulation result is in good agreement with the experiment (shown in Figure 1), the designing of optimum performance for the HSOT polymer can be easily made. Figure 2 is the simulation result with 100 photons which shows the illumination from all over the surface of the HSOT polymer light pipe. The circles in this figure denote the output point of the photons and are randomly located in the HSOT plate, which shows the uniformity of illumination.

Figure 3 shows a comparison of luminance distribution of our HSOT backlight system with the conventional one. The angular dependence of luminance of the HSOT system (see curve (a)) has not only brighter luminance but also no hollows of luminance near ±45degree observed in conventional backlight (see curve (b)). It is confirmed that the hollows of luminance have a bad influence on the viewing angle for the LCD panels. In case of the backlight for the latest LCD panels which have the wide viewing angle, not only higher luminance but also high quality illumination without the hollows are required. New HSOT backlight system satisfies the high performance of the latest LCDs.

Table 1 summarizes the comparison of the luminance between the conventional and the HSOT polymer backlight system. The HSOT polymer backlight system was adopted to a new model of 2.5 inches LCD TV on the market from November, 1996. In spite of being a quite simple system, the luminance from the HSOT backlight system is two times brighter than that of the conventional system. The luminance profile of the HSOT system has no hollows which is observed in the conventional system. Therefore, the illumination intensity and quality of the wide viewing angle of the LCDs can be dramatically improved by the new HSOT system.

Recently, the requirement of both higher efficiency and visual quality for LCD is increasing more and more.
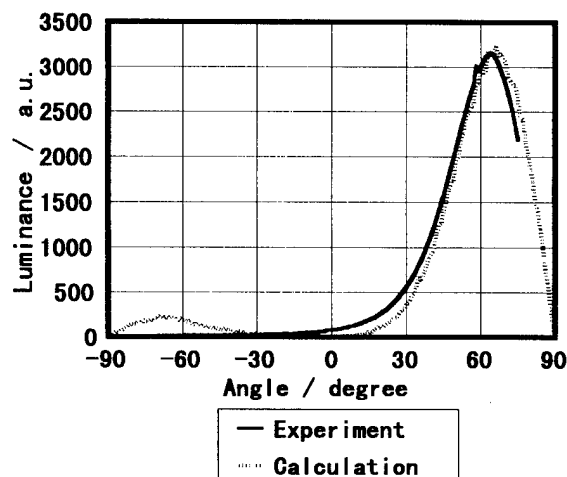
Figure 1   Angular dependence of luminance of HSOT polymer.
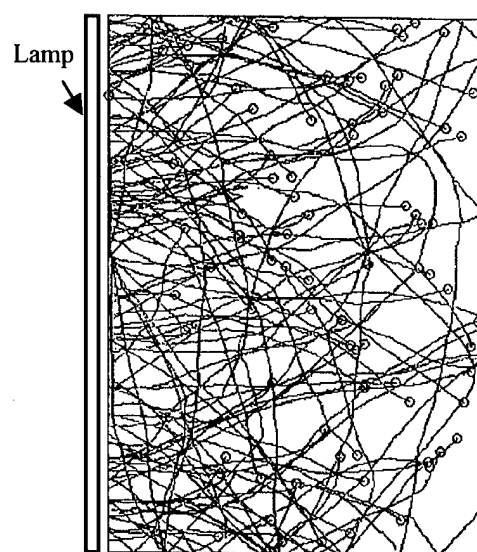
Figure 2.   Ray tracing simulation.
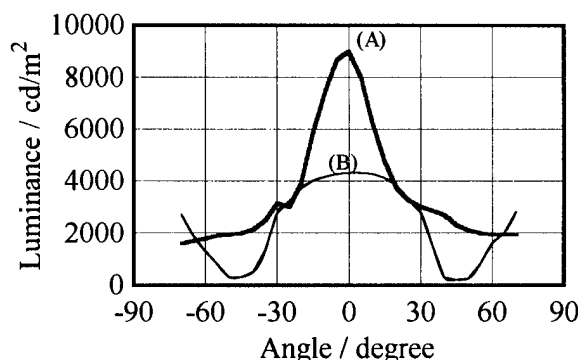
Figure 3   Comparison of angular dependence of luminance
(A) HSOT backlight system
(B) Present conventional backlight system

The illumination properties of the HSOT backlight system do fit to the latest LCDs. This new material, the HSOT polymer, is suitable for the backlight of the LCDs which require to achieve lower electric power consumption and higher quality of the visual property.

Table 1   Comparison of luminance for 2.5 inches backlights

	Conventional	HSOT
Luminance (cd/m^2)	**4300**	**9000**
Components	Prism film Diffuser film Transparent light pipe Dot printing pattern White reflector	Prism film HSOT light pipe Silver reflector

Reference

1. A. Horibe, M. Izuhara, E. Nihei, Y. Koike, "Brighter Backlights Using Highly Scattered Optical-Transmission Polymer", J of SID, 3/4, 169 (1995).

2. A. Horibe, E. Nihei, Y. Koike, "Bright LCD Backlight Using High-Scattering Optical-Transmission Polymer", SID'96 Digest, 577 (1996).

3. I. Lux, L. Koblinger, "Monte Carlo particle transport methods: Neutron and photon calculations", CRC Press (1991)

4. G. Mie, Ann. der phys., 25 377 (1908)

Single-Mode Optical Interconnects in Ultra-Low-Loss Environmentally-Stable Polymers

Louay Eldada, Lawrence W. Shacklette, Robert A. Norwood, and James T. Yardley

AlliedSignal Inc., Electronic & Optical Materials Division, 101 Columbia Road, Morristown, NJ 07962

Telephone: (201) 455-3069, Facsimile: (201) 455-3008, e-mail: eldada@research.allied.com

I. INTRODUCTION

SINGLE-MODE passive optical components need to be produced in high volume and at low cost in order to meet the ever-increasing demands of the telecom industry. Although glass optical fibers provide a very convenient means for carrying optical information over long distances, they are very inconvenient for complex high-density circuitry. Devices produced in glass fibers are difficult to fabricate — especially when they have a high port count — and as a result are quite expensive. Polymeric materials, on the other hand, offer the potential to create low-cost highly-complex optical interconnection circuitry on a planar substrate. In addition, they provide the possibility for a much higher degree of ruggedness and hermeticity. We have developed in detail one technology for single-mode polymeric optical interconnection which addresses the needs of the telecom industry. Our polymeric waveguiding structures are very low loss (0.06 dB/cm at 1550 nm), temperature resistant (they can endure more than 65 years at 100°C before a loss of 0.1 dB/cm is thermally induced), humidity resistant (no humidity effects were observed on a bare device after 600 hours at 85°C 85% RH), and exhibit low dispersion and low birefringence.

II. MATERIALS

We have developed a wide variety of photochemically-set optically transparent polymers which are based on combinations of multifunctional acrylate monomers/oligomers and various additives. Upon photochemical exposure, these monomer systems form highly crosslinked networks which exhibit low intrinsic absorption in the wavelength range extending from 400 to 1600 nm. Fig. 1 shows a subset of our monomers which, when fully cross-linked, span a refractive index range of 1.3 to 1.6. Any two monomers are miscible, permitting continuous tailoring of the refractive index in this range, which can be achieved with 10^{-4} accuracy. This control of refractive index allows us to fabricate step-index optical waveguide structures with well-defined numerical apertures (NA's). At the same time, other physical properties of the materials such as flexibility and toughness as well as such important properties as surface energy and adhesion can be tailored to meet the needs of specific applications. Thin films of optical quality from 1 to 500 μm have been prepared by spin casting or slot coating then photo-exposing at room temperature. Waveguide structures have been fabricated by either mask photolithography or direct laser writing.

Fig. 2. Absorption losses for three AlliedSignal polymer systems. Acrylic with full CH content is solid line. Dashed line is for material with 30% CH content; dotted line is for material with 20% CH content.

The results of a waveguide spectrometry study[1] performed in our standard acrylates are shown in Fig. 2. Notable features are the region of transparency around the datacom/computing wavelength of 840 nm, the C-H vibrational overtones which are most pronounced beyond 1 μm, and the windows of transparency near 1.3 and 1.55 μm, the wavelengths of interest for telecom. Modifying a molecule by substituting fluorine for hydrogen in C-H bonds has the effect of greatly increasing the reduced mass, thereby lowering the energy of the fundamental bond vibration and its overtones and virtually eliminating absorption from 1 to 2 μm (see Fig. 3). The solid line in Fig. 2 represents the loss of our standard acrylates; these materials exhibit loss values of 0.02, 0.15, and 0.45 dB/cm at 840, 1300, and 1550 nm, respectively. The dashed and dotted lines show the results of partial fluorination (70% and 80%, respectively). This partial fluorination makes the losses as low as 0.001, 0.03, and 0.06 dB/cm at 840, 1300, and 1550 nm, respectively.

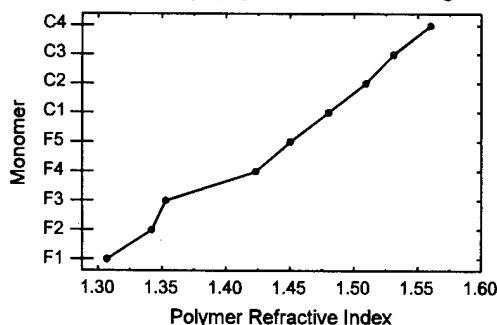Fig. 1. Refractive index of polymers corresponding to a set of AlliedSignal monomers. Continuous adjustment of the refractive index is achievable between 1.3 and 1.6.

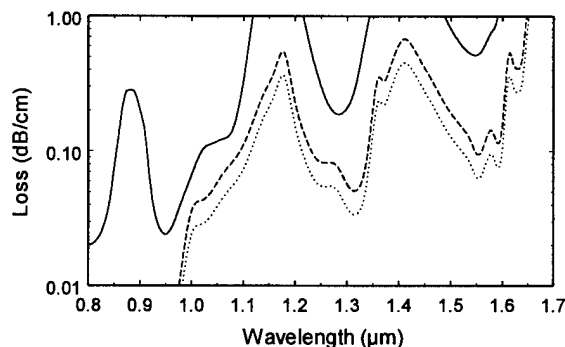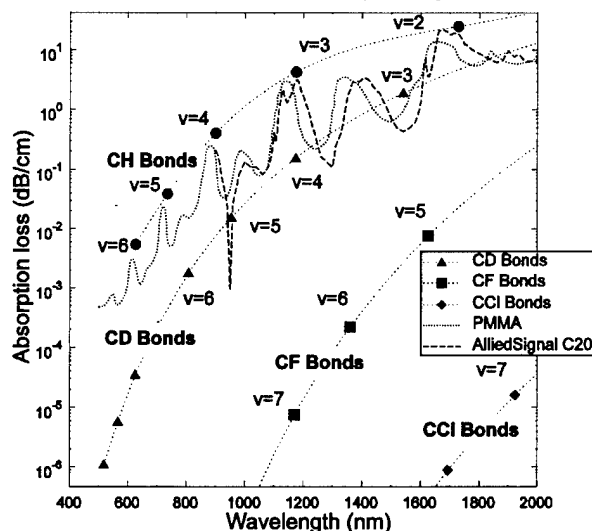Fig. 3. Calculated absorption losses for various vibrational motions normalized to the observed absorption loss for PMMA. Also shown are experimental losses for PMMA and for a non-modified AlliedSignal polymer, an acrylate with a comparable concentration of CH bonds.

Our polymers were subjected to humidity cycling tests. The test guides were pigtailed but not packaged or protected in any way. A thin cladding was printed around the core layer to give a short path for the diffusion of water. The sample was cycled between rigorously dry and humid (85°C 85% RH) conditions for 600 hours. Transmission measurements were performed at 1550 nm. The results are shown in Fig. 4 and they reveal that no increase in loss was observable. The fact that humidity has very little effect on our polymers was expected. When fully cured, these materials have a very high level of crosslinking, resulting in a tightly bound network with a low level of voids, leaving little space for water to be absorbed. The present observations also give no evidence of mechanical failure of devices due to water incursion, such as delamination or loss of integrity at the interface with the glass fibers.
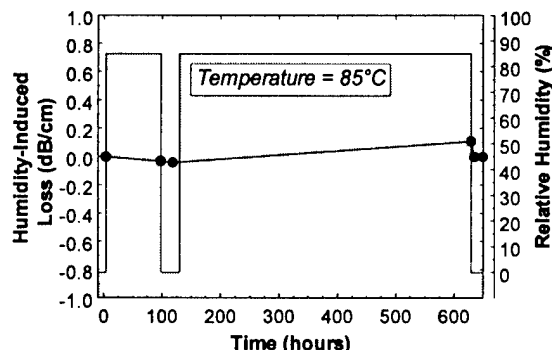

Fig. 4. Results of humidity cycling experiment showing no humidity-induced loss after 600 hours.

A key characteristic for practical applications is thermal stability of optical properties since organic materials may be subject to yellowing upon thermal aging. Because of their highly crosslinked nature, these polymers are quite stable thermally. Thermal stability of the waveguide materials was studied by a variety of techniques including TGA (Thermal Gravimetric Analysis), spectrophotometry, and in-situ optical loss measurement. The thermal decomposition temperature, defined as the 5% weight loss temperature at a heating rate of 10°C/min., is 415°C, making our polymers the only acrylates reported to have a decomposition temperature above 400°C. However, much more important is the retention of high optical transmission upon thermal aging. In order to investigate this phenomenon, we carried out loss measurements on 5-cm-long fiber-pigtailed straight waveguides. These data are presented in Fig. 5 and they show conclusively that the thermal stability of these polymer waveguides is excellent, with practical stabilities (time for thermally inducing 0.1 dB/cm loss) at 840 nm of about 65 years at 100°C, 10 years at 120°C, one year at 150°C, two weeks at 200°C, and one day at 250°C.
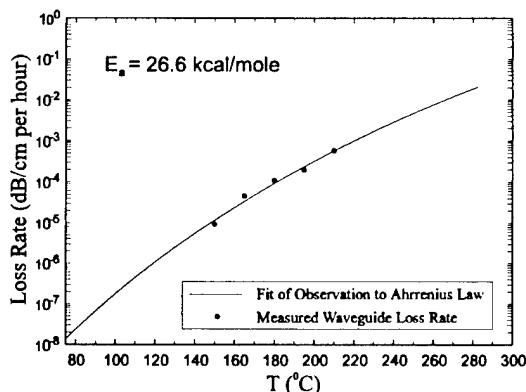
Fig. 5. Thermal stability data with Ahrrenius fit.

Thermal stability at longer wavelengths is even greater, as demonstrated in Fig. 6. It has also been observed that these polymeric devices are mechanically robust; no mechanical failure such as cracking or delamination occurs after extended treatment at 250°C.
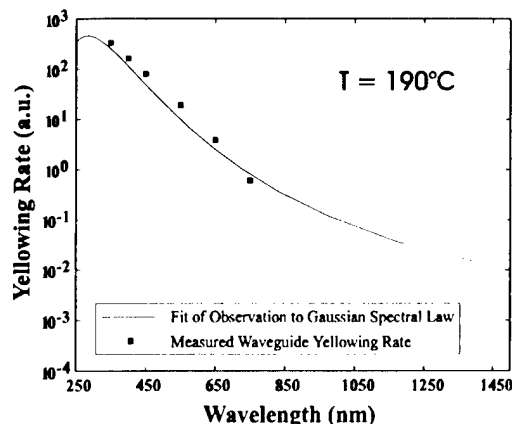
Fig. 6. Loss induced in AlliedSignal polymers by thermal exposure at 190°C as a function of wavelength. Higher stability is achieved at longer wavelengths.

In WDM systems where components rely on controllable optical phase delays or gratings, the refractive indices of the waveguide materials and their sensitivity to temperature and wavelength changes are of considerable importance. Below their glass transition temperature, glassy polymers generally have a dn/dT of $10^{-4}/°C$, which may be unacceptably large for some applications. For our highly cross-linked acrylate systems, dn/dT is as low as $5\times10^{-5}/°C$. As for $d\Delta n/dT$ for a core/cladding polymer pair, it is essentially zero. The lower dn/dT and $d\Delta n/dT$ can be made, the fewer measures are necessary to control temperature, thus reducing the overall cost of a system.

Many WDM schemes rely on having no wavelength-dependent optical effects other than those geometrically designed into the system. Therefore, material dispersion is generally to be avoided. We have measured $dn/d\lambda$ in our polymers at several wavelength ranges of interest. The values obtained at 1300 and 1550 nm are -4×10^{-6} and -2×10^{-6} nm^{-1}, respectively. These values are comparable to those for SiO_2 and are much lower than those for semiconductors and doped glasses.

A key material property impacting polarization transparency is the birefringence and its dispersion. We have measured the TE and TM indices for our standard polymers. The birefringence was measured to be $\Delta n \equiv n_{TE} - n_{TM} = -0.0008$ at 543.5 nm. This value decreases for longer wavelengths and varies with processing conditions.

III. SINGLE-MODE DEVICE FABRICATION

Polymeric optical waveguide devices may be fabricated in many ways. For the materials described above, a photolithographic fabrication scheme is most appropriate. Within our approach, photosensitive polymerization initiators are added to the monomer mixtures to provide a means for photochemically initiating the polymerization. Device fabrication is achieved by either conventional mask photolithography (Fig. 7a) or by laser direct-writing (Fig. 7b). These lithographic processes offer very high contrast responses allowing us to define polymeric features with dimensions ranging from a few microns to a few millimeters with a high degree of accuracy and process latitude. The ridges seen in the sidewalls of the mask-produced guide in Fig. 7a are due to the staircasing in the photomask, and the fact that they are sharply reproduced across the entire depth of the structure demonstrates the high contrast in the materials.
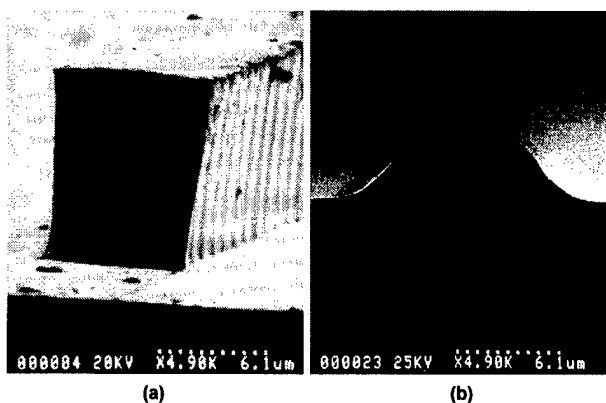
Fig. 7. Scanning electron micrographs of (a) mask-fabricated and (b) laser-defined single-mode waveguides.

Another useful aspect of these materials is that, owing to the nature of the lithographic process, selective undercutting can be performed to make structures that can grip optical fibers, resulting in a simple and inexpensive fiber pigtailing process.[2] Fibers can be "snapped" into these grippers after development, when the crosslinked polymer is highly elastomeric.

By selecting an appropriate pair of acrylate mixtures as core and cladding materials, the NA of a waveguide as well as its mode profile can be very accurately controlled. For example, single-mode waveguides that match single-mode glass fibers have been produced,[3] as shown in Fig. 8.
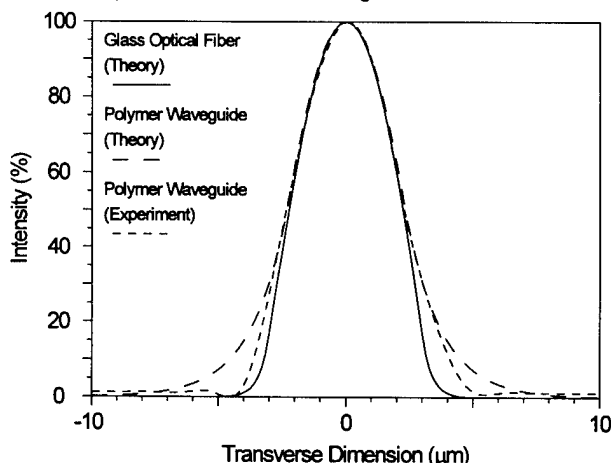
Fig. 8. Overlap of the modal profiles for a single-mode glass optical fiber and one of our single-mode waveguides (as expected from theory and as measured experimentally).
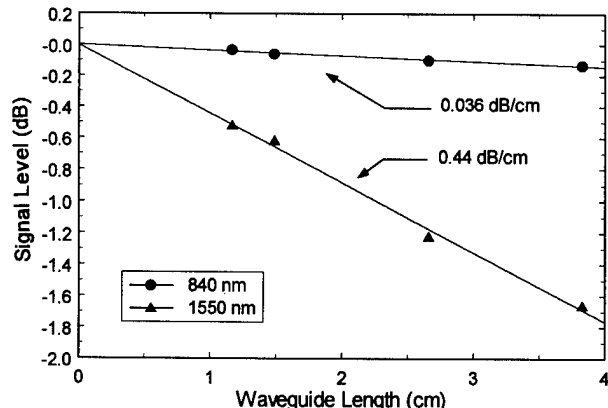
Fig. 9. Results of a cleave-back loss measurement on a single-mode waveguide fabricated in standard AlliedSignal polymers on silicon.

In the waveguide spectrometry studies described above, absorption was measured on slab waveguides where fabrication imperfections are easily avoidable. However, we also performed loss measurements on channel waveguides. Fig. 9 shows the results of a cleave-back experiment that was performed on a single-mode waveguide fabricated in our standard acrylates on silicon, and it reveals that the two-dimensionally confining guides exhibited propagation losses of 0.036 and 0.44 dB/cm at 840 and 1550 nm, respectively, indicating that, remarkably, the loss in our guides is practically absorption-limited.

We have also fabricated low-loss single-mode bends, Y-branches (Fig. 10) and directional couplers that behave in accordance with theoretical predictions.[3] For example, directional couplers made by laser writing exhibited the predicted sinusoidal transfer functions that agree well with beam propagation method calculations. Fig. 11 shows the output from a set of evanescent couplers as a function of interaction distance. This power transfer function follows a $\sin^2$ law as expected from theory, giving a coupling length of 1.65 mm. Beam propagation calculations for these devices predicted a coupling length of 1.6 mm, in good agreement with experiment.
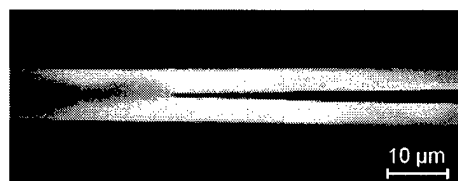
Fig. 10. SEM micrograph of the splitting region in a Y-branch.
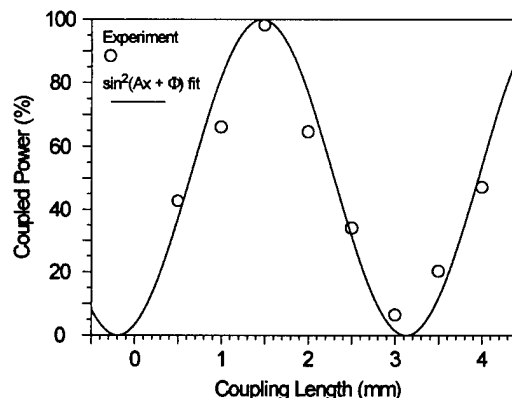
Fig. 11. Output of a single-mode directional coupler as a function of interaction length.

Beside having the intrinsic material properties required in a WDM device, AlliedSignal optical polymers lend themselves easily to the fabrication of WDM components. WDM devices typically utilize either gratings or phased arrays to separate wavelength channels. Our materials have the contrast needed to produce both types of elements, as demonstrated recently.[4]

IV. CONCLUSION

We have extensively verified the technical and commercial viability of an advanced polymer technology and have demonstrated the practical efficacy of our polymers for single-mode passive waveguiding components. As the telecom industry needs become more demanding, we are confident that our low-cost high-performance polymeric materials will play a key role in this market.

V. REFERENCES

1. K.W. Beeson et al., *Nonlin. Opt.* **3**, 205 (1992).
2. L. Eldada et al., *Proc. SPIE* **3006**, 344 (1997).
3. L. Eldada et al., *J. Lightwave Technol.* **14**, 1704 (1996).
4. L. Eldada et al., *Proc. LEOS Summer Topical Meet.* (1997).

Vertical tapered mode size transformer in polymer waveguides for efficient fiber coupling

Antao Chen, Vadim Chuyanov, Felix Ignacio Marti-Carrera, Sean Garner, and William H. Steier
Department of Electrical Engineering - Electrophysics
University of Southern California, Los Angeles, CA 90089-0483, (213) 740 8659

Jinghong Chen, Shajing Sun, Shane S. H. Mao, Younsoo Ra, and Larry R. Dalton
Department of Chemistry
University of Southern California, Los Angeles, CA 90089-1062, (213) 740 8659

Recent years have seen significant progress in photonic devices based on electrooptic (EO) and passive polymers. Recently an EO polymer modulator that works at a record high speed of 113 GHz has been reported(1), and a system demonstration incorporating EO polymer modulators has also been made(2). As polymer waveguide devices are entering fiber optic telecommunication and data communication systems, practical issues concerned by system designers have become increasingly important. One of such issues is the insertion loss of the polymer device.

The insertion loss of an optical waveguide device packaged with optical fibers comes from two major sources: fiber coupling loss and the propagation loss in the waveguide. At the telecommunication wavelength of 1.3 µm, the fiber coupling loss is the most part of the device insertion loss(3). It basically comes from the mode mismatch between the optical fiber and waveguide. Due to the single mode and the low operation voltage requirements, polymer waveguides are usually 1-2 µm thick, and the polymer waveguide mode is typically a 5 µm (lateral) by 1-2 µm (vertical) ellipse. The mode of a standard 1.3 µm single mode fiber is a circle typically 10 µm in diameter. The difference in size and shape between the two modes makes the coupling between fiber and waveguide inefficient.

In this paper, we describe a unique taper mode size transformer to improve coupling between single mode channel waveguides and standard single mode fibers. The taper transformer(4) also provides an additional benefit of increasing fiber misalignment tolerance. Our approach can keep the waveguide structure optimized for device function, and use independent transformer sections integrated at the ends of device chip to expand mode size(3). This technique keeps the total thickness of the device small for low voltage operation, and the mode expansion is achieved without suffering from metal loss due to electrodes.

Fig. 1 illustrates our proposed vertically tapered mode size transformer. The transformer is fabricated on a device chip with waveguide and electrodes already made. No change of previous device fabrication steps is needed. The upper cladding near the end of the chip tapers off until the core layer is exposed. Then a new cladding with a refractive index higher than the index of the original upper cladding is put in the taper area. Since the index difference between this new cladding and the core layer is smaller, the mode is less confined from the top. As light propagates along the taper, the mode size gradually grows in that direction. The confinement by the lower cladding is not affected. Therefore no additional propagation loss is introduced because the mode does not expand toward metal and lossy substrate. The lateral confinement is also hardly affected because the change of the effective index difference in the lateral direction is negligible. The transformed mode is bigger and more circular, which matches better with fiber mode. These adiabatic tapers are typically 1000 µm long and 5 µm deep, slow enough to avoid the radiation and reflection losses. Coupling losses of 1.6 dB with standard 10 µm fiber and 1 dB with 6.3 µm bending insensitive fiber are predicted by mode overlapping at the wavelength of 1.3 µm.

Only two steps are needed to fabricate the mode size transformer: taper etching and coating of the new cladding. Two special but simple reactive ion etching techniques, shadow masked

etching(5, 6) and tapered photoresist etching mask(7), are used for making the vertical taper.

The test samples are made with inverted ridge waveguides with a mode size transformer fabricated at one end. The cross section of the waveguide prior to taper etching is given in Fig. 2. The polymers used for upper cladding and core are Epoxylite 9653-2 resin and PU-DR19(8), respectively. A vertical taper is etched in the upper cladding and slightly into the core layer. The final thickness of the core layer is 1.2±0.2 μm. The refractive index of the new cladding is 1.6265 at the wavelength of 1.3 μm. In order to observe the waveguide mode at various positions in the taper, some samples had tapers aligned at an angle with the end of the sample. In this way, the outputs from different channel waveguides show the mode at different points in the taper. The observed mode expansion, as shown in Fig. 3, are very close to the calculation results shown in Fig. 1. An increase of fiber vertical misalignment tolerance is also observed.
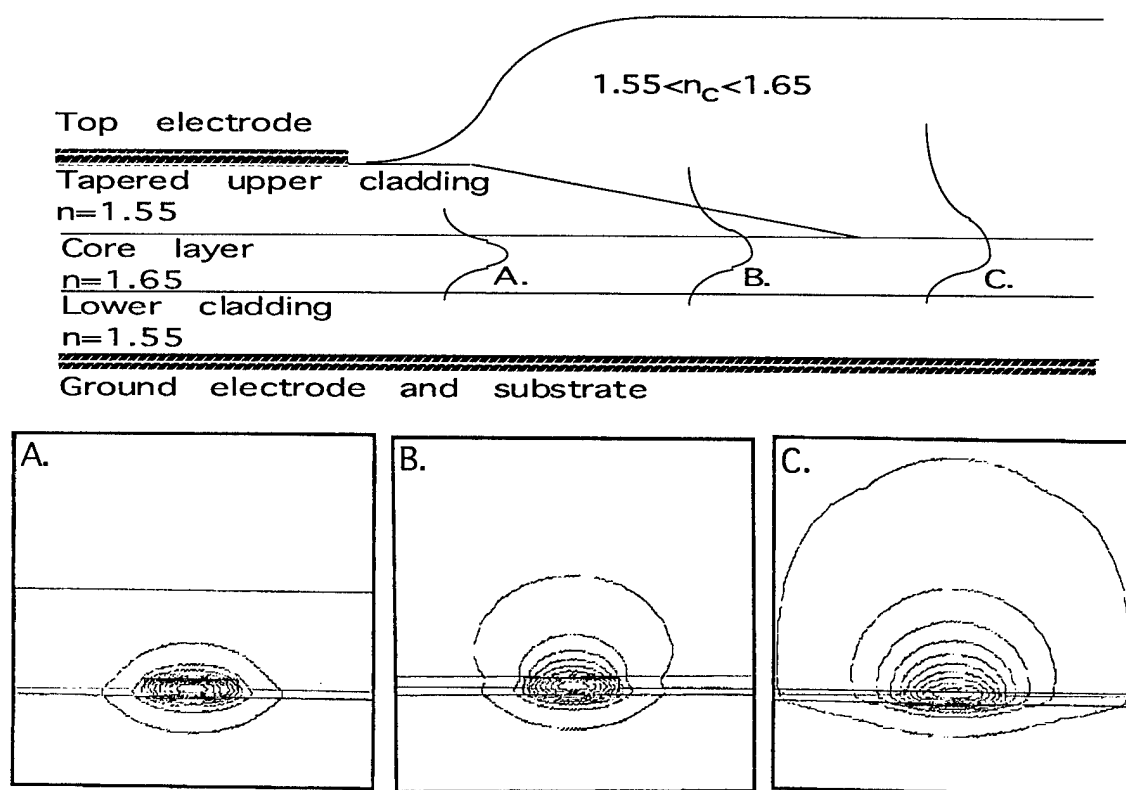
Fig. 1. Mode size transformation by the vertical taper.
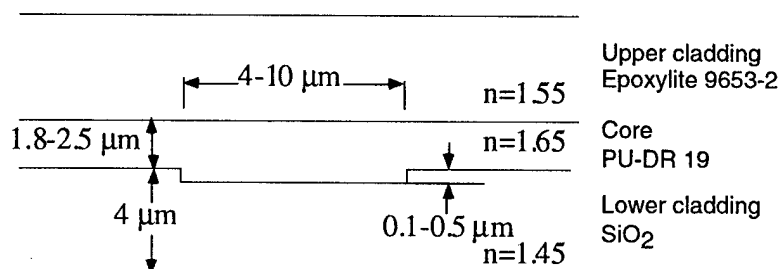
Fig. 2 The cross section view of the waveguide in the test samples.

The improvement of coupling efficiency is obtained by comparing the insertion loss of the

sample when a single mode fiber with 10 µm mode size is coupled to the tapered end with the insertion loss when the fiber is coupled to the non-tapered end. The reduction of coupling loss for different waveguide widths and two polarizations is summarized in Table 1. These values are repeatable from several samples, but they are still about 1 dB higher than theoretical predictions. A complete 3D beam propagation analysis of the taper is in progress to find the source of the extra loss. Therefore the coupling can be further improved by optimizing taper parameters and processing. The fact that the improvement of coupling is independent of waveguide width indicates that the lateral confinement of waveguides are not affected by the vertical expansion of mode. The experimental results also demonstrated that the performance of this taper mode size transformer is polarization insensitive, a very desirable property for many integrated optics devices.
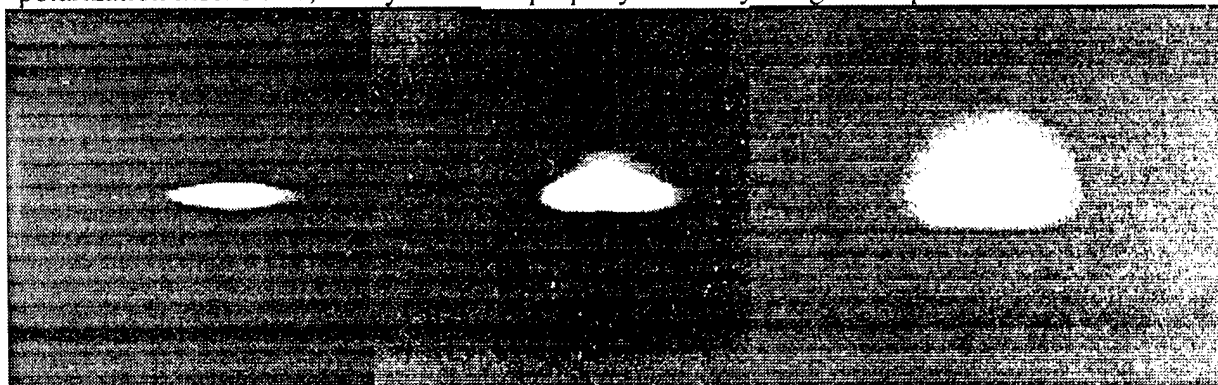
Waveguide   In the Taper   Output

Fig. 3. Photographs of waveguide mode under various stages of expansion.

Table I. The improvement of fiber coupling in dB from 8-9 waveguides of each width.

Polarization	Waveguide width (µm)			
	4	5	6	9
TE	1.8±0.3	1.7±0.3	1.4±0.4	1.8±0.4
TM	2.2±0.1	1.9±0.3	2.1±0.3	1.8±0.5

In summary, a novel mode size transformer with a vertical taper in the polymer waveguide is demonstrated. These tapers are easy to fabricate. The taper section is made as the final processing steps of the device, and there is no need to change previous device processing steps. Mode expansion and a 1.8 dB polarization insensitive reduction of fiber coupling loss is observed in our preliminary experiment. Further improvement is expected. This taper mode size transformer is a simple approach to get substantial improvement of fiber coupling.

References

1.   D. Chen, H. R. Fetterman, A. Chen, W. H. Steier, L. R. Dalton, *Proceedings of SPIE* **3006**, 314-317 (1997).
2.   Y. Shi, et al., *IEEE Journal of Selected Topics in Quantum Electronics* **2**, 289-299 (1996).
3.   A. Chen, et al., *Proceedings of SPIE* **3005**, paper 11, in press (1997).
4.   I. Moerman, et al., *Microelectronics Journal* **25**, 675-690 (1994).
5.   A. Chen, F. I. Marti-Carrera, S. Garner, V. Chuyanov, W. H. Steier, *to be presented in the Organic Thin Films for Photonics Applications, Long Beach, CA, October, 1997* (1997).
6.   B. Jacobs, R. Zengerle, K. Faltin, W. Weiershausen, *Electronics Letters* **31**, 794-796 (1995).
7.   T. J. Suleski, D. C. O'Shea, *Applied Optics* **34**, 7507-7517 (1995).
8.   M. Chen, L. R. Dalton, L. P. Yu, Y. Q. Shi, W. H. Steier, *Macromolecules* **25**, 4032-4035 (1992).

Three Dimensional Integrated Optics Using Polymers

Sean Garner, Vadim Chuyanov, Antao Chen, Srinath Kalluri, Felix Ignacio Marti-Carrera, and
William H. Steier
Department of Electrical Engineering - Electrophysics
University of Southern California, Los Angeles, CA 90089-0483   (213) 740-8781

Larry R. Dalton
Department of Chemistry
University of Southern California, Los Angeles, CA 90089-1062   (213) 740-8659

Two dimensional integrated optical circuits have been demonstrated with considerable complexity and size. For example, 19x19 integrated star couplers[1] have shown the large-scale routing capabilities of optical waveguides. As the two dimensional area and complexity of these circuits increases, problems can arise, for example, if the signals require similar optical time delays. The vertical integration of optical devices into a three dimensional structure can offer a significant increase in the integration density without increasing the time delays or the integration area. In 3-D integrated optics, one envisions several layers of 2-D integrated optics with the various layers coupled together vertically at appropriate locations by vertical waveguide bends, vertical waveguide power splitters, or vertical voltage controlled switches.

The realization of 3-D integration requires a material system in which (i) additional guiding and cladding layers can be fabricated above completed layers of integrated optical circuits, (ii) there is a sufficient range and fine adjustment of indices of refraction to minimize the overall structure height, and (iii) can be processed into both vertical and horizontal waveguide structures. Polymers meet all of these material requirements. Spun cast polymers offer adhesion to virtually any substrate and can be patterned by standard photolithography. Also, the lower levels of polymer integrated circuits can be hardened by crosslinking to allow the fabrication of upper layers. Chemically engineered polymers can possess a wide range of refractive indices, and these indices can be "fine tuned" by mixing of compatible polymers. Low loss polymer waveguides fabricated by reactive ion etching (RIE) or by photobleaching have been demonstrated. In addition EO polymers make possible integrated vertical electro-optic devices.[2,3] Furthermore, a photoresist etch mask and RIE enable easy device alignment and fabrication with high precision. We will present data to show that polymers can be vertically patterned by RIE, and that this enables fabrication of vertically sloped waveguides and multiple layers of devices. These general material properties of polymers make them ideal candidates for three dimensional integrated optics.

Similar to traditional 2-D integrated optics, practical 3-D integration requires basic building blocks. Among these basic structures are vertical waveguide bends to passively route optical signals among the various layers and vertical Y-branches to controllably divide optical power among the stacked waveguides. Here, we present fabrication, insertion loss, and waveguide simulation results showing the practicality of vertical waveguide bends and Y-branched vertical splitters.

The fabrication of vertically sloped waveguides requires three key steps (Figure 1). First, a spun-cast photoresist layer, above an existing cladding layer, is partially exposed (Figure 1a). The following section discusses two unconventional photolithography methods for accomplishing this. After development, the photoresist film possesses a vertical pattern. Next, this sloped photoresist
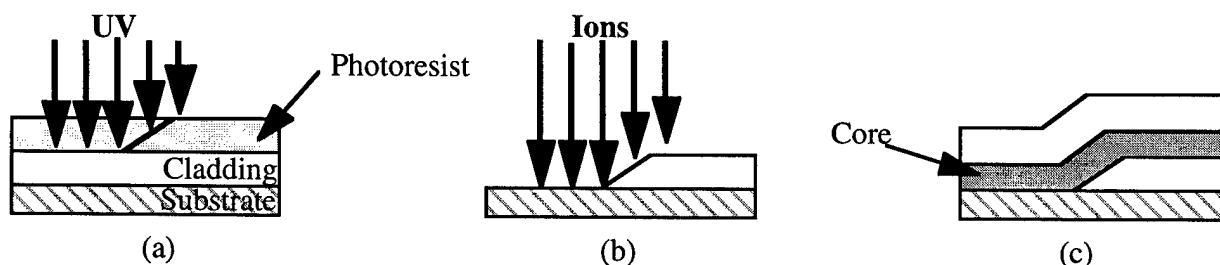

Figure 1: Key fabrication steps for a vertically sloped waveguide

layer serves as an RIE etch mask (Figure 1b). Since oxygen plasma etches both photoresist and the polymer cladding, RIE efficiently transfers the slope downward. The final step involves spin casting a guiding and cladding layer on top of the sloped lower cladding (Figure 1c). For the small separation angles (0.1-5°) and thin films (0.8-5μm) involved, the subsequently spun layers effectively follow the contours of the underlying surface. The above process can also fabricate vertically sloped structures above and alongside of existing waveguide devices. In this way, processing steps specific to polymer films, enable the fabrication of 3-D integrated structures.

As mentioned previously, the partial exposure of photoresist enables the fabrication of vertically sloped waveguides. A standard mask aligner can control the energy and placement of this partial exposure to produce slopes with micron accuracies, and evaluation after development can assure the quality of the photoresist slope before permanently etching into the cladding. An alternative method uses RIE to etch a slope directly into the cladding.[4] To partially expose photoresist, we used two unconventional photolithography techniques: gray-scale masking, and non-contact exposure.

Gray-scale masking[5] involves a photolithography mask with variable transmission to control the photoresist exposure over the entire sample surface (Figure 2a). The mask is made by first obtaining a computer generated gray-scale image on a 35mm slide. A photographic set-up transfers this image onto a holographic film plate which serves as the gray-scale mask. The chosen computer gray level determines the exposure of the photoresist. In this way, computer designed patterns can produce pre-determined contours across the entire sample surface. The resolutions of the 35mm slide and the photographic set-up determine the feature-size limit. In our case, this was about 10μm. After a multi-step process to generate a mask, gray-scale masking enables repeatable control of the entire surface contour.

Non-contact exposure also produces vertical slopes in photoresist (Figure 2b). It utilizes a standard photolithography mask with a straight edge pattern. By vertically separating the mask from the sample, the UV can diffract around the straight edge to expose the underlying photoresist. The separation angle of the resulting slope depends on the exposing energy density, mask separation height, and photoresist thickness. The ability to control the separation angle within 0.2° by varying the exposure time will be shown. Although this method cannot produce the diverse contour shapes possible with the gray-scale mask, it does provide a fast single-mask method for producing a variable range of separation angles.
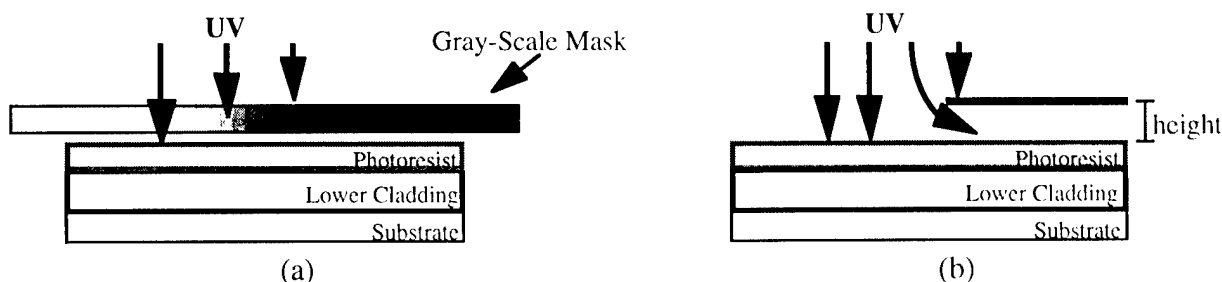
Figure 2: Variable photoresist exposure techniques

The controllable range of separation angles, from 0.1 to 5°, offers incredible opportunities in fabricating vertically integrated structures. The small separation angles of <1° enable vertical mode transformers[4] and adiabatic mode splitters.[6] These devices rely on the slowly tapered slopes to avoid any modal conversion. The large separation angles allow short vertical connections within multi-layer structures. The short length reduces the distance traveled over the etched vertical slope and minimizes any scattering loss that this may entail. The above fabrication techniques can, therefore, produce repeatable vertical slopes for a wide range of device requirements.

To evaluate the quality of the above fabrication procedures, we made single-mode ridge waveguides with vertical waveguide bends. The waveguides traversed a 2mm long slope with a separation angle of 0.3°. The total sample length was approximately 1cm. The insertion losses measured in the sloped waveguides were only 1.5dB higher than planar waveguides of comparable

length. Since the core and cladding refractive indices were 1.65 and 1.55, respectively, at $\lambda=1.3\mu m$, strong vertical confinement existed. We believe radiation loss, therefore, produced <0.1dB of this total,[7] and scattering from the etched slope accounted for the rest. By optimizing the etch parameters and incorporating different cladding materials we hope to reduce this insertion loss.

The realization of vertical waveguide bends shows great potential for practical 3-D integrated optical circuits. Not only can vertical bends route single waveguides, but they also enable Y-branched vertical splitters. One approach involves fabricating a vertical ridge waveguide bend above an existing straight channel waveguide pattern. The waveguides of the two layers are vertically aligned to produce a branching structure. Figure 3 shows a 1x4 splitter composed of a vertical Y-branched splitter followed by two vertically stacked planar Y-branches. One fabrication issue of this structure involves spin casting equal thicknesses of the two core layers. Accurate control of the power splitting ratio requires similar effective indices of the two branch arms and, therefore, core thicknesses within $0.1\mu m$. Currently, we are looking into ways to compensate for thickness errors due to spin casting by varying the index of the upper cladding. An alternative approach to vertical power splitting includes fabrication of a standard 2-D integrated Y-branch. By incorporating a vertical waveguide bend at one output and keeping the other output on the same plane, the structure splits the optical power to two vertical waveguide layers. This method incorporates current Y-branch technology and waveguide bend fabrication. Further beam propagation analysis and fabrication procedures of Y-branched vertical splitters will be presented.
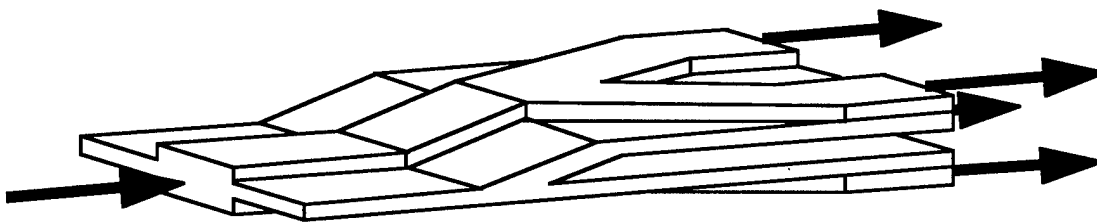
Figure 3: Vertically integrated 1x4 splitter (Only the core layer is shown for clarity.)

To our knowledge, this represents the first analysis and fabrication of vertical waveguide bends and Y-branched vertical splitters. We have shown that photolithography techniques can accurately produce vertical bends with controllable separation angles. These slopes enable vertical structures ranging from vertical adiabatic mode splitters to short vertical waveguide routers. Combining the vertical waveguide bends with standard straight waveguides or Y-branches produces Y-branched vertical splitters. These vertical splitters enable the division of optical power among vertically integrated optical layers. The vertical waveguide bend and the Y-branched vertical splitter represent key elements needed for practical three dimensional integrated optics. By unlocking the third dimension, they enable existing technologies of 2-D integration and multi-layer device fabrication[2] to dramatically increase the density and complexity of integrated optical circuits.

References:
[1] C. Dragone, C.H. Henry, I.P. Kaminow, and R.C. Kistler, *IEEE Photon. Technol. Lett.*, vol. 1, pp. 241-243, 1989.
[2] T.A. Tumolillo,Jr. and P.R. Ashley, *Appl. Phys. Lett.*, vol. 62, pp. 3068-3070, 1993.
[3] M. Hikita, Y. Shuto, M. Amano, R. Yoshimura, S. Tomaru, and H. Kozawaguchi, *Appl. Phys. Lett.*, vol. 63, pp. 1161-1163, 1993.
[4] A. Chen, V. Chuyanov, F.I. Marti-Carrera, S. Garner, W.H. Steier, J. Chen, S. Sun, and L.R. Dalton, *Proceedings of SPIE* **3005**, in press, 1997.
[5]. T.J. Suleski and D.C. O'Shea, *Appl. Opt.*, v. 34, pp. 7507-7517, 1995.
[6] W.K. Burns and A.F. Milton, *IEEE J. Quantum Electron.*, v. QE-11, pp. 32-39, 1975.
[7] D.L. Lee, *Electromagnetic Principles of Integrated Optics*, New York: Wiley, 1986.

Poling and Relaxation

Wednesday, October 15, 1997

Hilary Lackritz, Purdue University
Presider

WB
10:30am–12:15pm
Seaview A&B

Modeling Relaxation Mechanisms in Nonlinear Optical Polymer Films

K.D. Singer and R.D. Dureiko

Department of Physics, Case Western Reserve University, Cleveland, Ohio 44106-7079

The thermal and temporal relaxation of polar order in polymeric electro-optic materials remains an important problem in the realization of these materials in applications. Fortunately, much progress has occurred in the development of more stable high-temperature materials. These developments, however, require that a regime for accelerated testing be established. Thus, measurement techniques and associated models which can connect the time and temperature behavior of new materials need to be refined. To this end, we report here on progress in the development of a new frequency domain technique for measurement, as well as progress on the development of a widely applicable model for chromophore orientational relaxation.

In the present study we have adapted a relatively new technique introduced by J.A. Cline and W.N. Herman to observe chromophore relaxation in the frequency domain.[1] Using a mode-locked Ti:Sapphire laser, a more quantitative analysis of frequency domain chromophore relaxation has been made. Broadening the frequency range to include frequencies from 10 mHz to 40 kHz, has allowed measurements to be made at temperatures from slightly below T_g to temperatures far above T_g.

Assuming the chromophores have only one predominant hyperpolarizability tensor component, β_{333}, then the macroscopic susceptibility can be written as,[2]

$$\chi_{zzz}^{(2)} = N\left(f_z^\omega\right)^2 f_z^{2\omega}\left[\beta_{333}\left\langle\cos^3\theta\right\rangle + \gamma_{3333}f_z^0 E_z^0\left\langle\cos^4\theta\right\rangle\right]$$

where θ is the angle between the applied field and the dipole moment, μ, N is the number density of chromophores, f_i is the local field factor in the direction i, and z is direction of the applied field. The statistical averages may be performed by inferring the angular dipole orientation distribution to be described by a Boltzmann distribution. In the case of a dc applied field, these averages reduce to $\langle\cos^3\theta\rangle = \mu f^0 E/5kT$ and $\langle\cos^4\theta\rangle = 1/5$ provided $\mu f^0 E/kT \ll 1$. So, with the assumption that the second order nonlinear optical susceptibility varies linearly with respect to the applied electric field, $\chi^{(2)}$ can be rewritten as,[2]

$$\chi^{(2)} = A\sin(\omega t + \phi)$$

where ω is the frequency of the applied field and ϕ is the phase lag of the chromophore orientation with respect to the applied field. Since the SH intensity varies as the square of $\chi^{(2)}$,

$$I^{2\omega} \propto \left(A\sin(\omega t + \phi)\right)^2 = \frac{A^2}{2}\left(1 - 2\cos(2(\omega t + \phi))\right).$$

Thus, by setting a lock-in amplifier to lock in at twice the applied voltage frequency, both the in phase component and the out of phase component of $\chi^{(2)}$ can be measured directly.

Figure 1 shows the measured $\chi^{(2)}$ components for one of the NLO polymer systems in this study.
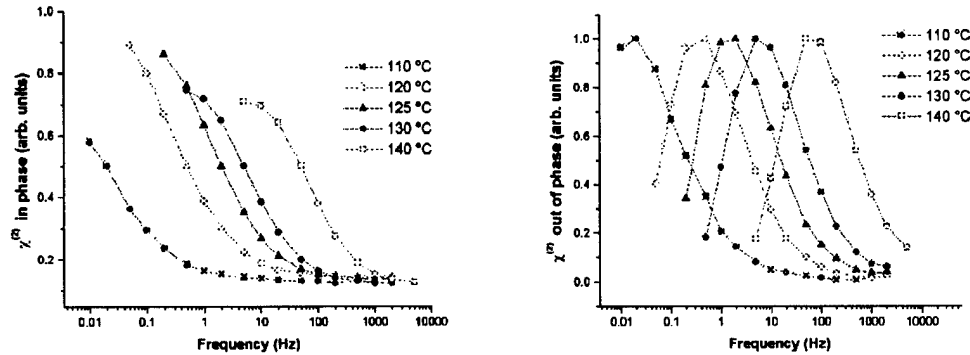
Figure 1. In phase and out of phase components of $\chi^{(2)}$ for DR1-MMA.

The chielectric relaxation spectra for the out of phase components were fit to the Dissado-Hill line shape function,

$$\chi(\omega) = \chi(0)\left(1 + i\omega/\omega_p\right)^{n-1} {}_2F_1\left(1-n \;\; ; \;\; 2-m \;\; ; \;\; 2-n; \left(1+i\omega/\omega_p\right)^{-1}\right)$$

$$\chi''(\omega) \propto \omega^{n-1} \quad \omega >> \omega_p$$

$$\chi''(\omega) \propto \mathrm{Im}\left(1+i\omega/\omega_p\right)^{-1} \quad \omega \cong \omega_p$$

$$\chi''(\omega) \propto \omega^m \quad \omega << \omega_p$$

where ${}_2F_1$ is the Gaussian hypergeometric function,[3] n and m are shape parameters ranging from 0 to 1, and ω_p is a characteristic relaxation time.

Chielectric measurements were made by first converting the SH light into an electrical voltage using an avalanche photodiode, and then using this voltage as the input to an SRS850 dual lock-in amplifier. The experimental frequency range was 10mHz to 40 kHz. Figure 2 shows a reduced temperature plot of τ for the two guest-host systems, PMMA\DCM, PMMA\DR1, and one side-chained system,DR1-MMA[4], in this study.

By scaling the temperature with respect to T_g of each system, the measured τ values appear to lie on a single master curve as suggested by other studies.[5] The model line in Figure 2 correspond to an Adam-Gibbs model for DR1-MMA where the fictive temperature was determined by calorimetry measurements. The Adam-Gibbs model fits well at all temperatures, and also well approximates the behavior of the related guest-host polymer systems, and thus represents a "universal" curve for these methacrylate materials. This leads to predictive capabilities for the useful lifetime of the electro-optic properties of polymer-chromophore systems. We are currently investigating a wider variety of NLO polymeric media, including higher T_g guest/host systems, polyimides, and also cross-linked

polymers, to determine if the results found in this limited study can be applied in general. If they can, the techniques discussed here may prove to be a useful tool in predicting which NLO media will be viable in device applications.
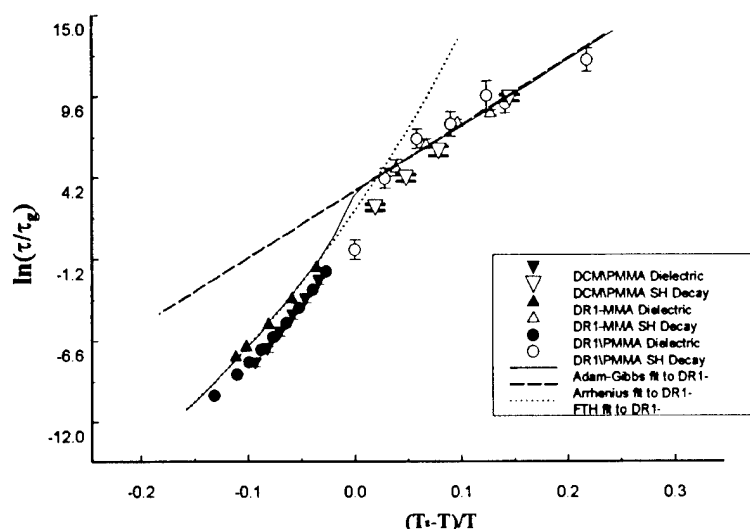
Figure 2. Reduced temperature dependence of chromophore relaxation time, τ, in guest-host and side-chained polymer systems .

References
[1] J.A. Cline; W.N. Herman., Tech. Digest, "Organic Thin Films for Photonic Applications", *Opt. Soc. Am.* p. MD39 (1995).
[2] A. Dhinojwala, G.K. Wong, and J.M. Torkelson, *Macromolecules* **26**, 5943 (1993).
[3] L. J. Slater, "Generalised Hypergeometric Functions", Cambridge University Press, Cambridge (1966).
[4] Purchased from IBM Almaden Research Center- San Jose, CA.
[5] P. Kaatz, P. Pretre, U. Meier, U. Stalder, C.Bosshard, P. Gunter, B. Zysset, M Stahelin, M. Ahlheim, F. Lehr, *Macromolecules* **29**, 1666 (1996).

A stochastic model for chromophore disorientation in guest-host nonlinear optical polymer system

S.-J. Lee, G.A. Medvedev, J.M. Caruthers, H.S. Lackritz
School of Chemical Engineering, Purdue University, West Lafayette, IN 47907
(Phone)765-494-4058 (FAX)765-494-0805

The temporal and thermal stability of nonlinear optical (NLO) properties of polymers doped with optically active chromophores has been studied by many researchers [1] because of its importance to predict the long term performance of these systems for practical applications. Until recently most of these efforts were focused on attempting to fit experimental data to empirical functions, such as stretched exponential [2] or lognormal [3], with no direct mechanistic interpretation of the parameters. It has been established that the decay of the second harmonic generation (SHG) signal after poling is clearly nonexponential, and its characteristics depend, in a complex manner, on processing and thermal history. Whereas there is general agreement that the complex character of the decay in NLO properties is caused by the coupling of the chromophores disorientation to the structural relaxation of the polymer matrix, the mechanism of this coupling is poorly understood. This research involves the application of a stochastic model, recently developed by our group, for structural relaxation in glasses [4] in order to describe orientational relaxation of chromophore particles, which is responsible for SHG decay in chromophore doped polymer glasses.

The Debye model for rotary diffusion in a viscous fluid is a reasonable point-of-departure for describing chromophore disorientation. Unfortunately, this model only predicts an exponential decay of the orientational correlation [5] and, therefore, is not capable of describing NLO behavior in chromophore doped polymers. In order to obtain nonexponential behavior, some researchers [6] have attempted to introduce temperature dependence into the diffusion model. Although these models, in some cases, are able to fit experimental data for certain thermal histories, all the models fail to reproduce nonexponential behavior in the isothermal case. For a fully equilibrated material all these models predict exponential decay of the SHG signal, and the Debye model is recovered.

We believe that a model for chromophore mobility must acknowledge the spatial and temporal heterogeneity of glass forming materials near and below the glass transition temperature (T_g) is taken into account. The heterogeneity, which results from the "freezing" of the density fluctuations while system approaches the glass transition, has been confirmed experimentally by techniques such as NMR [7] and photobleacing experiments[8]. The stochastic model, details of which can be found elsewhere [4], is able to successfully describe the structural relaxation in the glassy polymer systems. This model is based on the single relaxation time Kovacs volume relaxation equation with the random noise term being introduced to represent instantaneous fluctuations of the specific volume,

$$\frac{d}{dt}[V - V_e(T)] = -\frac{1}{a(T,V)\tau_0}[V - V_e(T)] + R(T,V;\xi(t)) \qquad (1)$$

where $V_e(T)$ is the equilibrium specific volume which is a function of temperature, and R is the stochastic term which depends on $\xi(t)$, the standard Wiener process. The stochastic term is uniquely determined by the fluctuation dissipation theorem, which requires that in the limit of large time the volume distribution should approach stationary distribution that is consistent with the equilibrium thermodynamics. The intensity of fluctuations is controlled by the width of the equilibrium distribution of specific volume which in turn depends on the size of the domain.

The underlying stochastic model for the specific volume relaxation is then utilized to describe the chromophores orientational relaxation. The minimum set of implicit postulates used is as follows: (i) the rate of chromophore reorientation is controlled by the local thermodynamic state; (ii) the local domain surrounding the chromophore is of sufficient size that the continuum postulate is still valid, but so small that thermal fluctuations are important; and (iii)the local fluctuations in density that occur in the pure polymer are unaffected by the presence and motion of the chromophores. This implies that any chromophore belonging to a given local environment experiences rotary diffusion of Debye type with a single relaxation time. The nonexponential SHG decay is obtained when summation over these contributions from all chromophores throughout the sample is fulfilled.

To obtain the rotational diffusion coefficient of chromophore which includes dependence on the instantaneous state of the polymer matrix, it is assumed in the first approximation that $D=D_0/a(V,T)$, where D_0 is the diffusion coefficient at some reference state and $a(V,T)$ is the same shift factor employed in Eqn (1). Thus, for the weak poling field condition

$$\chi^{(2)}_{normalized}(t) = \exp[-\int_0^t D(t')dt'] = \exp[-D_0 t^*] \quad ; t^* = \int_0^t \frac{dt'}{a(T(t'), V(t'))} \tag{2}$$

Eqn (2) indicates that the chromophore disorientation process is controlled by the "material time" t^*, which measures the net amount of relaxation occurring in polymer matrix on the polymer time scale.

The simulation of the SHG decay using the stochastic model yields nonexponential behavior as shown in Fig. 1 and fits the experimental data with only one parameter, D_0. To study the influence of thermal and pressure histories on the characteristic of the SHG decay several simulations using material parameters for PMMA+ 2wt.% DANS have been performed. It should be emphasized that the traditional models for both volume [9] and SHG relaxation generally require an increasing number of phenomenological parameters when dealing with more complex thermal histories. However, the stochastic model uses the same set of physically significant parameters determined at equilibrium conditions. The stochastic model has been successfully used to describe the specific volume behavior for various thermal histories, thus we anticipate that SHG relaxation can also be described for these thermal histories. In the numerical simulation of the temperature down jump experiments, the dependence of the SHG decay on the annealing temperature, cooling rate, and equilibration time has been studied; and we obtain trends that are in qualitative agreement with experimental data [10]. The important result determined from the simulations is that the extent of deviations

from equilibrium experienced by the system during processing control the long term stability of SHG signals.
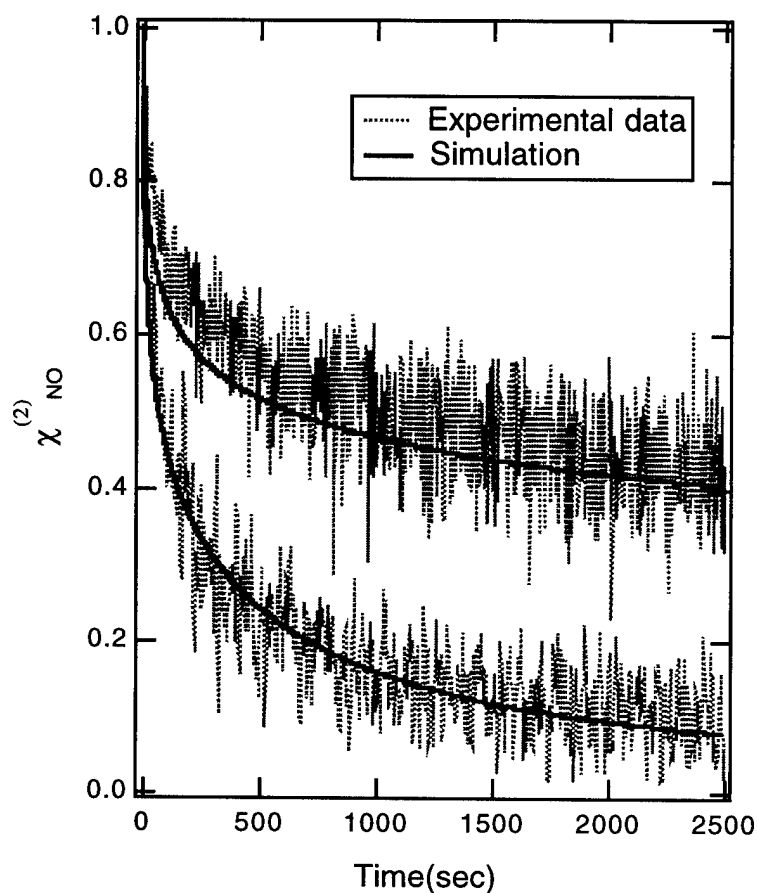
Fig. 1 Comparison of simulation results for the normalized second order susceptibility, $\chi^{(2)}$ to experimental data for PMMA+2wt.%DANS, (DC poling field 0.2 MV/cm, T_g=88^{0}C); down temperature jump with cooling rate 35K/min (i) from T_g+5^0 to T_g-10^0 ($D_0\tau_0$=1.5), (ii) from T_g+5^0 to T_g-5^0 ($D_0\tau_0$=2),

References

1. For example; H.L.Hampsch, J.Yang, G.K.Wong, J.M.Torkelson, Macromolecules 21 (1988) 526

2. J.C.Hooker, J.M.Torkelson, Macromolecules, 28 (1995) 7683

3. S.Schussler, U.Albrecht, R.Richert, H.Bassler, Macromolecules, 29 (1996) 1266

4. G.A.Medvedev, S.-J.Lee, J.M.Caruthers, H.S.Lackritz, Macromolecules, (1997) submitted

5. (a) J.W.Wu, J.Opt.Soc.B, 8 (1991) 142
   (b) M.A.Firestone, M.A.Ratner, T.J.Marks, Macromolecules 28 (1995) 6296

6. (a) L.Y.Liu, D.Ramkrishna, H.S.Lackritz, Macromolecules 27 (1994) 5987
   (b) S.C.Brower, L.M.Hayden, Appl.Phys.Lett., 63 (1993) 2059

7. K.Schmidt-Rohr, H.Spiess, Phys.Rev.Lett., 66 (1991) 3020

8. M.T.Cicerone, M.D.Ediger, J.Chem.Phys., 103 (1995) 5684

9. For example; G.B.McKenna in Glass Formation and Glassy Behavior; Comprehensive Polymer Science, 2, 311-362: Pergamon Press; Oxford (1989)

10. D.Randell, H.S.Lackritz, paper in preparation

Mechanisms of chromophore reorientation probed with in-situ, pressure second harmonic generation

L. Michael Hayden and Shane J. Strutz

Department of Physics, 1000 Hilltop Circle, University of Maryland Baltimore County
Baltimore, MD 21250
(410) 455-3199, hayden@umbc.edu

Introduction

Research to determine the mechanisms which tie chromophore reorientation to polymer relaxation is crucial to the development of thermally stable NLO polymers.[1] Most of the work to date has been performed above or near the glass transition temperature where the decay of the NLO properties of the material is tied to the glass transition and the α-motion of the polymer backbone. Devices which rely upon permanently poled polymer films for their NLO characteristics are not designed to operate near or above the glass transition because their nonlinear properties would quickly dissipate. A study of the coupling between polymer motion and chromophore reorientation below the glass transition temperature is necessary to gain insight into the reorientional dynamics of the chromophores at common device temperatures. Using the results of elevated temperature studies to predict the behavior of the NLO properties below T_g may not be accurate if the mechanisms responsible for chromophore reorientation are not the same in both regimes.

Low temperature studies of the reorientation of NLO chromophores have been avoided because of the time required for such experiments. By applying pressure to a polymer system the T_g can be raised.[2,3,4,5] This change in T_g allows for the investigation of chromophore reorientation far below the atmospheric pressure glass transition while maintaining experimental temperatures near the atmospheric glass transition temperature.

Here we present an experimental study using high pressures to determine the temperature dependence of the activation volume associated with chromophore reorientation in a guest host polymer consisting of 4-diethyl amino-4'nitrotolane (DEANT) in polymethylmethacrylate (PMMA). By measuring the activation volume as a function of temperature using SHG, we are able to identify two separate relaxation processes related to chromophore reorientation in doped PMMA.

Previously, we determined the activation volumes for chromophore reorientation in a side chain system and several guest host systems near T_g.[6,7] To measure the activation volume associated with the motion of dopants in a polymer system, we use hydrostatic pressure in a second harmonic generation configuration.[8] The technique for measuring the activation volume involves recording the SH radiation emitted from a film under pressure and fitting with a Kohlrausch-Williams-Watts (KWW) stretched exponential. In this study, as in earlier

studies, we find that the pressure dependence of the shift factor a_p is given by

$$\ln a_p = \ln \frac{\langle \tau(P) \rangle}{\langle \tau(P_0) \rangle} = \frac{\Delta V^*(P - P_0)}{RT} \qquad [1]$$

where R is the gas constant, T is the absolute temperature, and ΔV^* is the activation volume.

The host polymer was PMMA. The dopant, 4-diethyl amino-4'-nitrotolane (DEANT) was obtained from Dr. Robert Twieg. The dye was combined with the polymer to 3% by weight and dissolved in chloroform to 8% by weight before spreading onto microscope slides using a knife edge technique. After baking to remove the solvent, the T_g (105°C) was measured with a Dupont 2100 Differential Scanning Calorimeter (DSC).

After thermal erasure at T_g+10°C for 30 minutes, the films were corona poled at T_g+10°C. The films were then cooled at 3°C/min for 5 minutes, removed from the poling device, grounded, and left to cool until they reached room temperature. The films were then stored at room temperature for 2 days to allow the bulk of the remaining charge deposited through corona poling to dissipate.

The apparatus used to measure the SHG signal as a function of pressure consisted of an enclosed optical cell filled with a light silicone oil (Dow Corning 200 Fluid) placed in a standard SHG configuration.

Free standing films were placed in the optical cell and maintained at 2400 atm while heating the cell to the desired temperature. This procedure significantly minimized the motion of the polymer and the subsequent reorientation of the chromophores during the heating process. Once the experimental temperature was reached, the system was brought to the experimental pressure and the decay of the SHG signal was recorded. Activation volumes at a given temperature were extracted from decay data taken at several pressures at the given temperature.

Results and Discussion

Figure 1 shows representative decays of the SHG signal vs time for various pressures. As the experimental pressure was increased, the rate of chromophore reorientation decreased dramatically due to a decrease in polymer mobility. The SHG data was fit to a KWW stretched exponential to obtain values for the parameters τ and β_{KWW}. The value of β_{KWW} decreased from high values (0.7-1) at low pressures and high temperatures to (0.3-0.5) at low temperatures or high pressures. The decrease in β_{KWW} corresponds to an increase of the distribution of decay times. This same broadening of relaxation times was also observed in the dielectric relaxation spectra of polycarbonate[9] and the poly(alkyl

methacrylates)[10] where it was shown that the width of both the α and β relaxation broadened as temperature was lowered. As the temperature is decreased (similar to increasing the pressure) the segmental motion of the polymer is restricted, decreasing the number of configurations available for polymer relaxation. Therefore, in order for chromophore reorientation to occur many more individual motions of polymer segments are required.
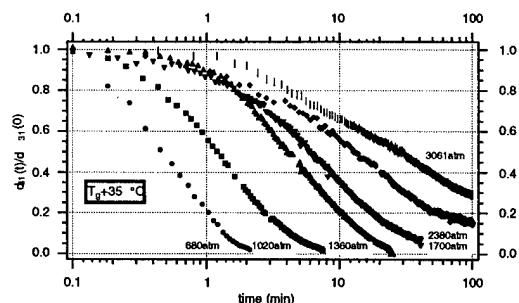

Figure 1. Decay of SHG signal in corona poled films of 3% DEANT/PMMA at T_g+35°C.

Plots of ln a_p vs pressure are shown in Figure 2 for T_g-15°C, T_g+10°C, and T_g+15°C. Since the data appears to show a different dependence at low and high pressures for all temperatures, we fit Equation (1) to each region separately and found one slope for decays performed at lower pressures and another slope for decays at higher pressures.
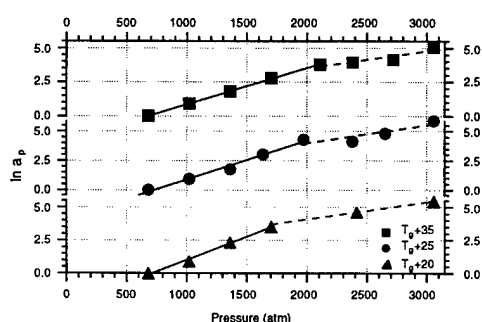

Figure 2. Natural log of the shift factor vs. pressure for 3% DEANT/PMMA for a selection of experimental temperatures. The regions of high slope (solid lines) and low slope (dotted lines) correspond to regions of long range and local relaxation respectively.

The activation volumes from the low pressure region are larger than those in the high pressure region at any given temperature. This trend is in agreement with activation volumes determined from dielectric relaxation measurements upon neat PMMA by Sasabe and Saito[7] who found a large activation volume (88 Å^3) for the merged $\alpha\beta$ relaxation process and a smaller activation volume (35 Å^3) for the β process. The activation volume can be thought of as the volume of the polymer that cooperatively participates in the reorientation of the chromophore. Using this model, in the low pressure region, the large activation volumes would be indicative

of chromophores coupling with the long range α-type polymer relaxation. The β process of PMMA, which is local, also contributes to the reorientation in this range of temperatures and pressure, but has a smaller effect compared with the α or backbone motion of the polymer. Because both processes are active in this regime, we refer to this activation volume as $\Delta V_{\alpha\beta}^*$.

To understand the high pressure region, we recall that increasing the pressure of the system causes the T_g to increase. At high pressures, the region of lesser slope in Figure 2, the polymer is depressed far enough into the glassy region to impede the large scale motion of the polymer. Chromophore reorientation then becomes coupled to the local relaxations, resulting in a smaller activation volume. We designate this smaller activation volume as ΔV_{β}^*.

The activation volume, $\Delta V_{\alpha\beta}^*$, remained approximately constant within the temperature range T_g-25°C to T_g+10 °C (Figure 3). At higher temperatures, the activation volume decreased with increasing temperature. This is consistent with dielectric relaxation studies of poly(methyl acrylate)[11] and polypropylene oxide[12] and photon correlation studies of poly(methyl acrylate)[13] and poly(ethyl acrylate)[14] where it was found that above T_g, the activation volume decreased with increasing temperature. This decrease in activation volume implies that the number of cooperative segments of the polymer chain which allow for chromophore reorientation, decreased with increasing temperature. This is reasonable since the density of the polymer decreases with increasing temperature. The decreased density allows greater freedom of motion for the imbedded chromophores; thus, fewer polymer segment motions are required for chromophore reorientation.
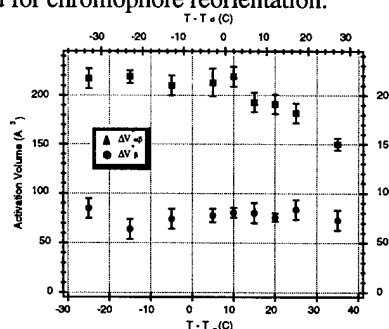
Figure 3. The activation volumes $\Delta V_{\alpha\beta}^*$ and ΔV_{β}^* versus temperature for 3% DEANT/PMMA. The activation volumes were calculated from the slope of ln a_p vs pressure.

The activation volume ΔV_{β}^* was much smaller than $\Delta V_{\alpha\beta}^*$ and remained approximately constant from T_g-25°C to T_g+35°C with an approximate value of 77±10 Å^3. This is in agreement with previous work in dielectric relaxation which showed that the temperature and pressure dependence of the β relaxation process in neat

PMMA is much weaker than the corresponding α relaxation process and that ΔV_β^* is much smaller than $\Delta V_{\alpha\beta}^*$.[15]

As mentioned above, $\Delta V_{\alpha\beta}^*$ decreased linearly with temperature above T_g +10°C. In order to better understand why the break occurs at T_g +10°C and not at the glass transition temperature, one must look at the meaning of $\Delta V_{\alpha\beta}^*$. This activation volume is associated with the reorientation of the chromophore. The T_g determined by differential scanning calorimetry (DSC) is not related to chromophore reorientation but merely chromophore concentration. Realizing this, a more appropriate method for relating the activation volume to a transition temperature may be to compare $\Delta V_{\alpha\beta}^*$ to the depoling temperature, T_d. To determine T_d, we heated a poled sample at 10°C/min while recording the SHG intensity at atmospheric pressure. During this test, the SH intensity decayed slightly below the T_g ; whereas, near and above the T_g the signal rapidly decreased. We define the depoling temperature as the midpoint of the transition. The T_d of 3% DEANT/PMMA at atmospheric pressure is 113 ±2°C, which is 8°C higher than the DSC determined T_g in identically prepared samples. The fact that $\Delta V_{\alpha\beta}^*$ breaks at approximately the depoling temperature is further indication that the activation volumes we measure are a gauge for understanding chromophore mobility.

Aside from the direct measurements of activation volumes, we also found that the position of the critical pressure, the location of the bend in the graph of ln a_p vs. pressure, decreased with temperature. This critical pressure designates the separation point between the low pressure region, where chromophore reorientation is predominantly coupled to the motion of the polymer backbone, and the high pressure region were the α motion is restricted. Since the critical pressure decreased linearly with temperature, there may be a temperature where the steep portion of the graph of ln a_p vs pressure would not occur. This point would occur at approximately T_g-35°C if a strict linear relationship were followed. This implies that below T_g-35°C, the long range motion of the polymer would be entirely restricted leaving only secondary relaxations to influence chromophore reorientation and SHG decay.

Conclusions

The above results are in agreement with the recent work of Kaatz et. al.,[16] where they observed that, deep in the glass, chromophore reorientation is much more coupled to α-type relaxation processes in side-chain NLO polymers than in guest-host systems. To more fully confirm their prediction, we are repeating our work on several side-chain systems.

The experiment used high pressures to increase the T_g of the doped polymer allowing the investigation of chromophore reorientation far below the atmospheric glass transition. This procedure decreases the amount of time needed to probe such sub-T_g relaxations since the available phase space has been reduced but the actual temperature which governs the rate of searching the space has not. Our data suggests that there would be a temperature below which the long range, backbone motion of the polymer would be frozen out (approximately T_g-35°C). Below this temperature, secondary relaxation processes would be the key factor determining the stability of chromophore order and the subsequent stability of NLO devices. Further studies are still needed to connect the activation volumes measured here to molecular mechanisms. Possibly, through molecular modeling of the chromophore activation volumes, the polymer-chromophore coupling responsible for the secondary relaxations may be identified, leading to the design of new, more stable polymers.

Though the material studied in this experiment has limited technological application, the results from this study may still be valid due to the continued interest in guest-host systems based on high T_g polyimides and polyquinolines. This experiment is a step toward understanding the temporal instability of NLO devices which are operated far below the glass transition temperature. Experiments such as this need to be performed on technologically promising materials in an effort to understand whether the trends exhibited in the DEANT/PMMA system are common to the other main classes of NLO systems.

References

1 Polymers for Second Order Nonlinear Optics, Lindsay G. A. and Singer K. D. , (ACS Symp. Series 1995, 601, Washington, DC).
2 Olabisi, O.; Simha, R. Macromolecules 1975, 8, 206.
3 Quach A.; Simha R. J. Appl. Phys. 1971, 42, 4592.
4 Tribone, J. J.; O'Reilly, J. M.; Greener, J. J. Polym. Sci.:Part B: Polym. Phys. 1989, 27, 837.
5 O'Reilly, J. M. J. Polym. Sci. 1962, 57, 429.
6 Brower, S. C.; Hayden, L. M. J. Polym, Sci: Part B Polym. Phys. 1995, 33, 2391.
7 Brower, S. C.; Hayden, L. M. submitted to Macromolecules.
8 S. C. Brower, Ph.D. dissertation, University of Maryland Baltimore County, 1996.
9 Mc Crum, N.G.; Read, B. E.; Williams, G. Anelastic and Dielectric Effects in Polymeric Solids, (John Wiley and Sons, London, 1967).
10 Ishida, Y.; Yamafuji, K. Kolloid-Z. 1961, 177, 97.
11 Williams, G. Trans. Faraday Soc. 1964, 60, 1556.
12 Fontanella, J. J.; Wintersgill, M. C.; Smith, M. K.; Semancik, J; Andeen, C. G. J. Appl. Phys. 1986, 60, 2665.
13 Fytas, G.; Patkowski, A.; Meier, G.; Dorfmuller, T. J. Chem Phys. 1984, 80, 2214.
14 Fytas, G.; Patkowski, A.; Meier, G.; Dorfmuller, T. Macromolecules 1982, 15, 870.
15 Sasabe, H; Saito, S. J. Polym. Sci. A-2 1968, 6, 1401.
16 Kaatz, P.; Prêtre, P.; Meier, U.; Stadler, U.; Bosshard, C.; Gunther, P.; Zysset, B.; Stähelin, M.; Ahlheim, M.; Lehr, F. Macromolecules 1996, 29, 1666.

Study of photoinduced orientation of azobenzene amorphous polymer by Visible, FTIR and Raman spectroscopy.

F.Lagugné Labarthet, **T.Buffeteau** and **C.Sourisseau**
Université de Bordeaux 1, U.R.A.124-C.N.R.S.
351, Cours de la Libération, 33405 Talence, FRANCE.

Azo-dye containing polymeric systems have been a subject of intensive research in the last few years in the areas of photofunctional applications such as photon mode optical memories, transducing optical information, photoswitching of electron conductivity. The main interest of such doped or functionalized systems is due to their dichroic and birefringent properties when they are illuminated by a polarized light. Such an effect is a consequence of the reversible "trans↔cis" photoisomerisation with respect to the N=N double bond which causes a redistribution in the orientation of photochromic entities. In this respect, Dumont et al.[1] have already reported the basis of a simple three-level theoretical model in order to explain the reorientation mechanisms of the azo molecules within a photoisomerisation cycle. Hereafter we thus report the results of a dynamical study of the photoisomerisation-induced reorientation of DR1-azo-dye in a polymer matrix (PMMA) by *in-situ* time dependent Visible and polarisation modulation FTIR spectroscopy measurements. The last part concerns the generation of high-efficiency diffraction patterns obtained by holographic way.

1 Linear dichroism measurements in the visible region.

The absorption spectrum of a 5% DR1-doped PMMA film displays an intense maximum at 492 nm. In any isotropic starting film (pump off), it is checked that the absorbances in both the $A_\perp$ and $A_{//}$ directions are identical. In contrast, after a writing process with a linearly polarized radiation and after a photoisomerization cycle including thermal back-relaxation, one notes significant absorbance variations in the parallel ($A_{//}$ decreases) and perpendicular ($A_\perp$ increases) directions. Dynamical experiments under various pump conditions (0.8 to 400mW/cm2) have been performed[2] *in situ* on samples which are simultaneously pumped (λ pump=514.5 nm) and probed (λ probe=492 nm). In fact, if we assume a cylindrical symmetry for such rod-like dye molecules, one can define the macroscopic order parameter $<P_2>=(A_{//}-A_\perp)/(A_{//}+2A_\perp)$, which can be compared in such uniaxial systems with the second order Legendre's polynomial $<P_2(\cos\theta)>$. It appears that at least two regimes are involved in the writing process (figure 1):
-a fast one, due to the pump efficiency, is expected proportional to $I_0.\cos^2\theta$ (where θ is the angle between the long molecular axis and the direction of the incident pump light); such an angular dependent optical pumping from trans to cis ("Angular hole burning") causes a redistribution in the orientation of the photochromic entities. One notes significant differences in the kinetics since stronger is the pump intensity, more efficient is the hole-burning mechanism at short time. Nevertheless, for the stronger pump irradiances (80-400mW/cm²) maximum values of orientation are reached which implies that there is an saturation threshold in the orientation-selective orientation. Angular redistribution is evidenced during the relaxation process in which molecules diffuse by thermal back
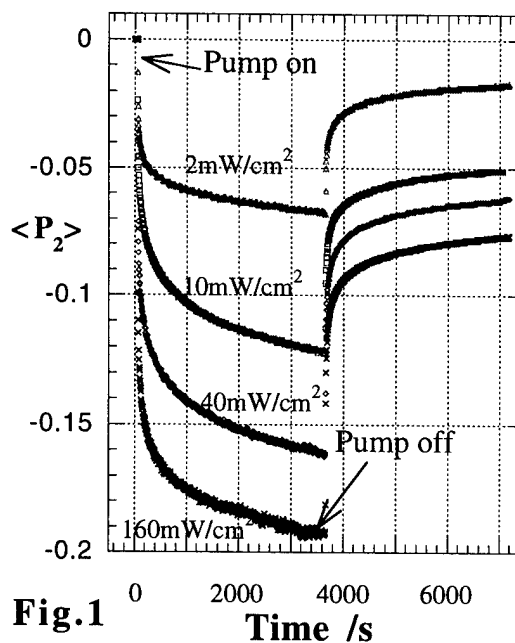

Fig.1

relaxation: the final redistribution of molecules is thus expected to be strongly dependent on the size of the various free volumes, with different constrained geometries, available in the host medium.

2 Linear dichroism measurements by polarisation modulation FTIR spectroscopy (PM-IRLD).

Infrared linear dichroism is a well-suited technique to characterize the molecular orientation in samples showing optical anisotropy such as oriented azo-doped polymers[3], since it can provide direct information on the orientation of different chemical groups of the dye. This information is obtained by measuring the dichroic difference $\Delta A = A_{//} - A_\perp$ where $A_{//}$ and $A_\perp$ are the absorbances measured with the infrared radiation polarized parallel and perpendicular to the reference direction (laser polarisation), respectively. The sensitivity of the this method comes from the fact that the dichroic difference spectrum is measured directly by modulating the polarisation of the infrared beam at high frequency (62kHz) with a photoelastic modulator. Therefore, for an uniaxial orientation and cylindrical symmetry, the signal obtained by polarization modulation is related to the normalized orientational parameter $F_\theta = (A_{//} - A_\perp)/3A_0$ where A_0 is the absorbance of a given vibrational mode in the isotropic sample.

As seen on fig. 2, the signal to-noise ratio on the difference spectrum is remarkable, even for ΔA as low as 0.01. All the bands observed on the PM-IRLD spectrum are assigned to the azobenzene derivative and exhibit negative ΔA values. Since the vibrations associated with these bands have their transition dipole moment essentially parallel to the long axis of the azobenzene groups, the difference spectrum clearly demonstrates that the irradiation of the polymer film produces a preferred orientation of these groups perpendicular to the writing polarisation direction.

Fig.2   **Wavenumber /cm^{-1}**
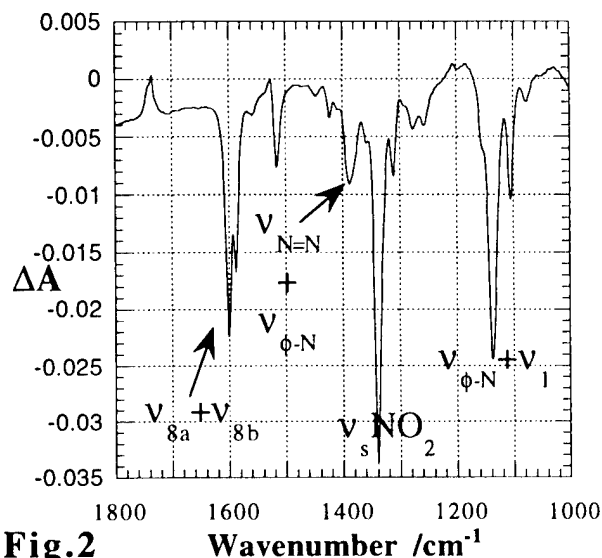
In figure 3, variations of F_θ values for two representative vibrations ($v_s NO_2$ and $vN=N+v\phi-N$) in a DR1-doped PMMA matrix are represented as a function of time for the irradiation period (pump on) and after the writing laser was turned off.

From the normalized results upon pumping it is possible to compare the degree of orientation of several chemical groups.

In addition, by comparing PM-IRLD and Visible data and using the Legendre's polynomials additive property, it is then possible to estimate the orientation of each vibrational mode with respect to the main molecular axis; for instance it is found that the 1339cm^{-1} mode ($v_s NO_2$) makes a 15° angle. Various results will be presented and discussed for either functionalized or doped polymer systems.

Fig.3   **Time /s**
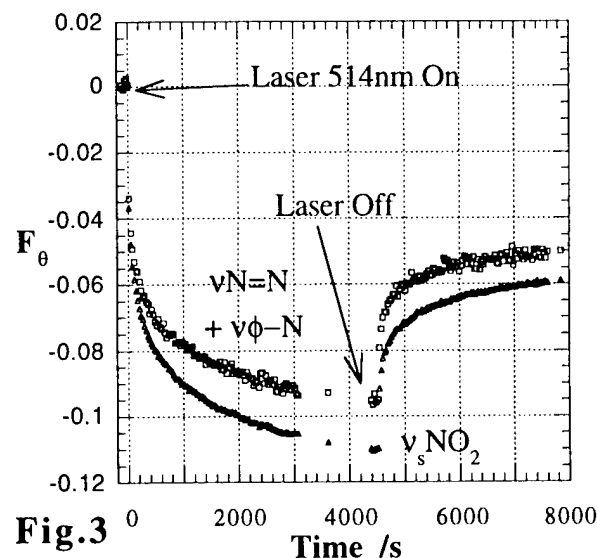
3 Optically induced high-efficiency diffraction gratings.

The ability of these azo-polymer systems to change their refractive indexes has lead several groups[4,5] to investigate the possibility of using these films as erasable holographic storage media and to investigate their properties when used as holographic volume gratings.

We have obtained similar results (Fig.4) concerning the dynamic of grating induced by the interference of two laser beams with different polarisation recording conditions. Two processes are observed: the faster regime (10 seconds - 0.3% diffraction efficiency) corresponds to a weak refractive index modulation ($\Delta n = 10^{-3}$). A second and slower process takes place over several decades of minutes and leads to high diffraction efficiencies up to 20%. Atomic Force Microscope measurements have revealed a perfectly spaced and sinusoidal surface modulation[4].
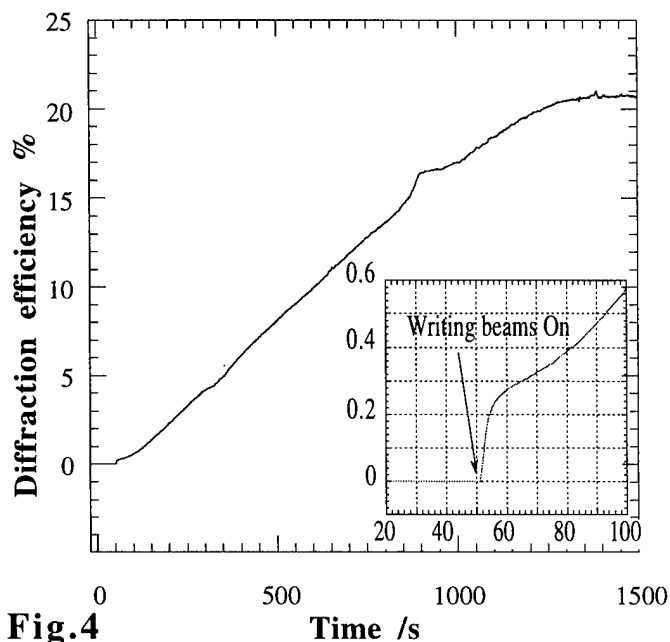
In order to get a better insight into the molecular orientations in the different areas of the pattern, we have developed the phenomenological equations taking account of the various polarisation conditions for the pump and the probe beams. In addition, polarized Resonance Raman measurements[6] in confocal microspectrometry have been performed. Fig.5 displays the intensity of Raman image for the vibrational mode at 1339cm^{-1} in a pDR1A-blend-pMMA grating (grating period=2.5μm) on a 20*20μm^2 area. From this powerful technique one can get orientational molecular information in the various regions of the grating with a 1μm spatial resolution.

Fig.4

Fig.5   Micrometers
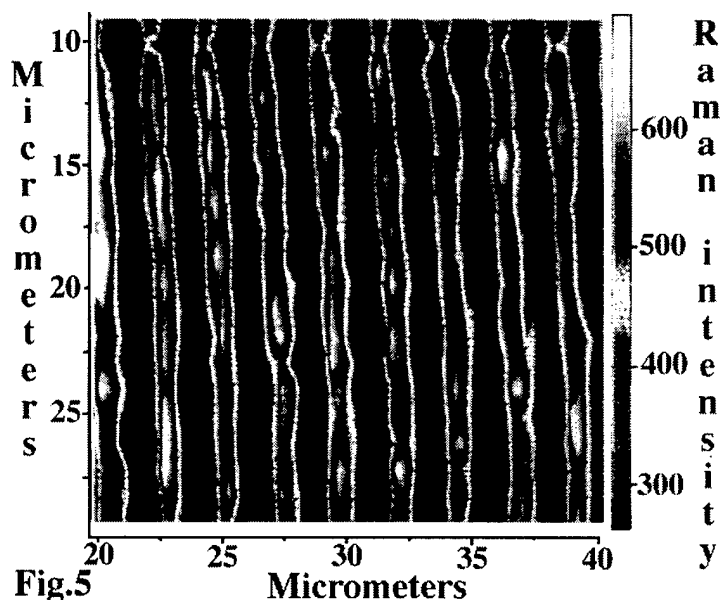
References

[1] M.Dumont and Z.Sekkat, Synthetic Metals 54, 373, 1993.
[2] F.Lagugné Labarhet and C.Sourisseau, New Journal of Chemistry, in press.
[3] T.Buffeteau and M.Pézolet, Applied Spectroscopy 50, 948, 1996.
[4] C.Barret, A.Natansohn, P.Rochon, J.Phys Chem. 100, 8836, 1996.
[5] X.L.Jiang, L.Li, J.Kumar, D.Y.Kim, V.Shivshankar and S.Tripathy, Applied Phys.Letter 68, 2618, 1996.
[6] F.Lagugné Labarhet and C.Sourisseau, J.Raman Spectrosc.27,491, 1996.

Kinetics of Photoinduced Orientation of Azo-dyes in Alignment Layers

T. Kosa* and P. Palffy-Muhoray
Liquid Crystal Institute, Kent State University, Kent OH, 44242
*On leave from Research Institute for Solid State Physics, P.O. Box 49, Budapest, H-1525, Hungary

Address: Liquid Crystal Institute,
          Kent State University, Kent OH, 44242
          tel: (330) 672-4056
          e-mail: tik@scorpio.kent.edu

Optical buffing of alignment layers [1] for liquid crystal device applications has generated considerable interest recently. In order to make efficient use of optical alignment, detailed understanding of photoinduced orientation of azo-dye molecules in the alignment layer and the coupling between the dye and the bulk liquid crystal is necessary. A simple model for the latter has already been proposed [2]. In this paper we study the time evolution of photoinduced anisotropy in azo-dye doped polyimide films. The orientational kinetics of chromophores in polymers is also of interest to the $\chi^{(2)}$ materials community.

Light induced orientation of azo-dyes occurs via selective excitation and depopulation of certain orientational states. We have measured phase retardation due to photoinduced birefringence in polymide films doped with the dye Disperse Orange. Reorientation cycles of the dye were induced by periodically alternating the polarization of the pump beam between two orthogonal states. The induced birefringence, shown in Fig. 1., is well approximated by the Williams-Watts-Kohlrausch[3] stretched exponential form over its entire range. The feature that the orientational relaxation does not follow a single exponential form suggests that the underlying mechanism is dispersive transport characteristic of random amorphous materials. Our pump-probe experiment utilises a photo-elastic modulator and allows the measurement of phase retardation with a precision of $\sim 10^{-5} rad$. Phase retardation in our samples was typically in the neighborhod of $\sim 10^{-2} rad$.
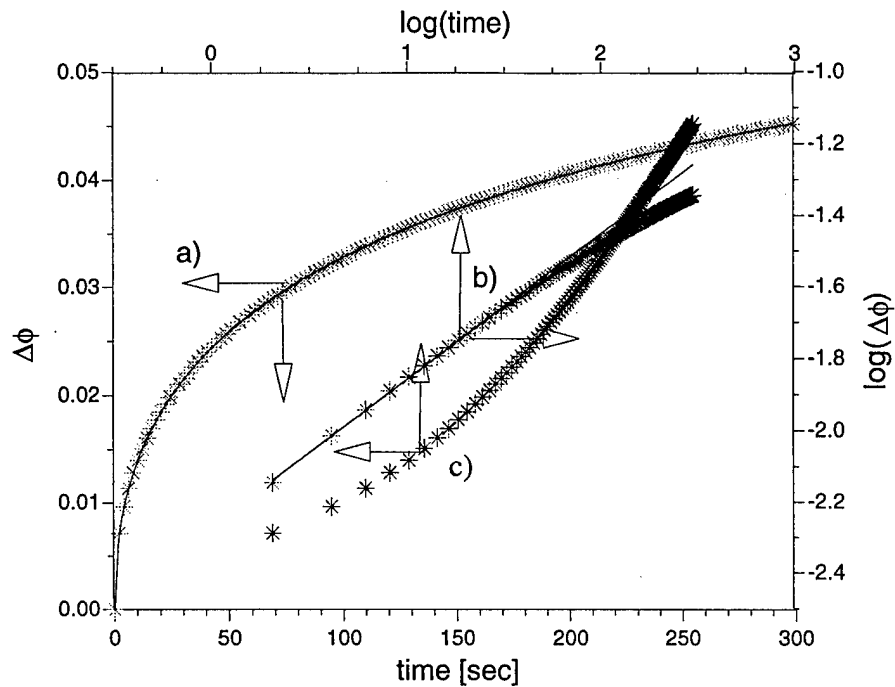
FIG.1: Time dependence of induced phase retardation on **a)** linear scale (solid line is a stretched exponential fit) and **b)** log-log scale (solid line is a power law fit).
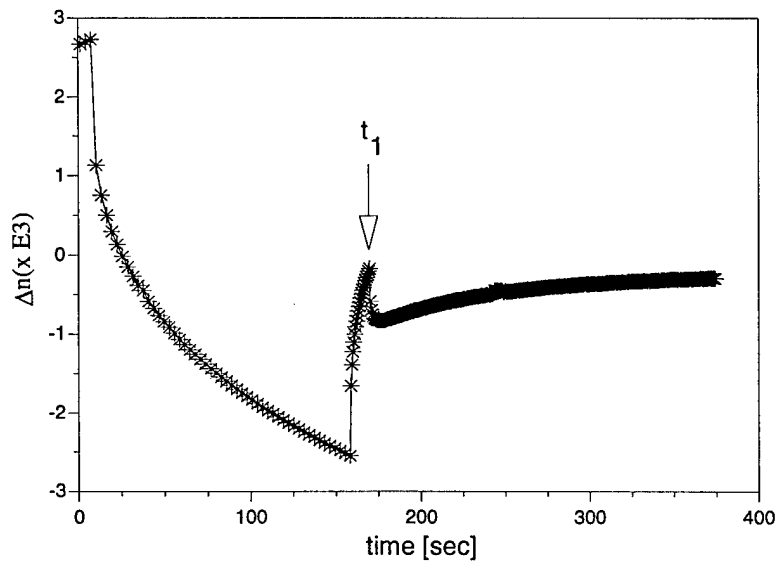
FIG.2: Birefringence induced by circularly polarized light. When the sample birefringence is zero (at t_1), the polarization of pump beam changed from plane to circularly polarized. The birefringence increases ('recoil'), then slowly decays to zero.

Although the stretch exponent β is expected to be a material property, we find in our experiments that β depends on the pump intensity. In addition, on short time scales, a power-law time dependence is observed (Fig.1.). As shown in [4], this suggests that for short relaxation times the distribution of relaxation times also follows a power-law dependence. This translates into an exponential distribution of activation energies.

Following the approach of Dumont [5], we have solved rate equations for the orientational dynamics. Comparing the results with experiment gives information about dispersive orientational diffusion.

An interesting 'recoil' effect, also exhibited by other systems [4], is shown in Fig.2. This effect is predicted by our model of orientational dynamics.

[1] W. Gibbons, T. Kosa, P. Palffy-Muhoray, P.J. Shannon, S.T. Sun, *Nature* **377**, 43, (1995).

[2] T. Kosa, P. Palffy-Muhoray, *Pure Appl. Opt.* **5**, 595, (1996).

[3] G. Williams, D.C. Watts, *Trans. Faraday Soc.*, **66**, 80, (1970).

[4] T. Kosa, I. Janossy, *Phil. Mag. B*, **64**, 355, (1991).

[5] M. Dumont, *European Opt. Soc. Topical Meetings Digest Series*, **7**, (1996).

Third-Order Effects

Wednesday, October 15, 1997

Donal D.C. Bradley, University of Sheffield, U.K.
Presider

WC
1:30pm–3:00pm
Seaview A&B

LASER EMISSION
FROM A MONOLITHIC ORGANIC SINGLE CRYSTAL

Denis FICHOU [(1)], Stéphane DELYSSE [(2)], and Jean-Michel NUNZI [(2)]

(1) Laboratoire des Matériaux Moléculaires, UPR 241, C.N.R.S.,

2, rue Henry Dunant, 94320 Thiais, France

Phone (+33) 1 49 78 12 41

Fax (+33) 1 49 78 13 23

E-mail fichou@glvt.cnrs.fr

(2) LETI (CEA - Technologies Avancées)

DEIN / SPE, Groupe Composants Organiques,

CEA Saclay, 91191 Gif sur Yvette, France

Recently, the possibility to realize a polymer laser diode has been investigated and it has been shown that optically pumped conjugated polymers generate stimulated emission in solution [1,2] and thin films [3-5]. In the latter case, it is necessary to build a microcavity around the polymer film in order to induce lasing. We demonstrate here that ultra thin (a few microns) single crystals of octithiophene (8T) naturally behave as luminescent optical resonators and are adapted to produce optically driven laser emission.

Single crystals of 8T are obtained by slow vacuum sublimation as bright red lamellae [6]. The 8T molecules have a planar *all-trans* -conformation and are all parallel to each other in a herringbone packing. The 8T crystal used throughout this study has an elongate ovoid shape (length=3.5 mm, width=1.5 mm) and thickness=3.5 μm. It is positionned with its (b,c) plane normal to the laser pump beam. The excitation source is a Q-switched mode locked Nd:YAG laser doubled by a type II KDP crystal to deliver 532 nm pulses (33 ps at 10 Hz).

At pump energies below ~0.1 μJ, photoluminescence (PL) consists in two broad bands at 640 nm and 695 nm and a weak shoulder around 760 nm. At pump energies higher than ~0.1 μJ up to ~10.0 μJ, the broad band at 695 nm is progressively gain

narrowed down to a line width of fwhm~8 nm and its maximum red-shifted to 700 nm. When the pump energy is increased above 10.0 µJ, the emission at 640 nm also emerges as a gain narrowed line whose intensity approaches half that of the dominating line at 700 nm for an energy of 50.0 µJ. Similar results are obtained using a laser pump at 355 nm. The two lines peaking at 640 nm and 700 nm coincide with the two maxima of the broad PL spectrum and would then correspond to transitions from the vibrational ground level of the S_1 excited state to the first and second vibrational levels of the fundamental state S_0.

Importantly, both emission lines do not have the same intensity dependence on the pump energy. The intensity of the 640 nm line increases exponentially while that of the 700 nm line follows a saturation behavior in the 0.1-50.0 µJ energy range. Such a dual energy dependence can be easily interpreted according to the basic principles of laser operation [7]. Gain narrowing and dual energy dependence of the two emission lines are clear signatures of stimulated emission (SE) thus ruling out other processes.
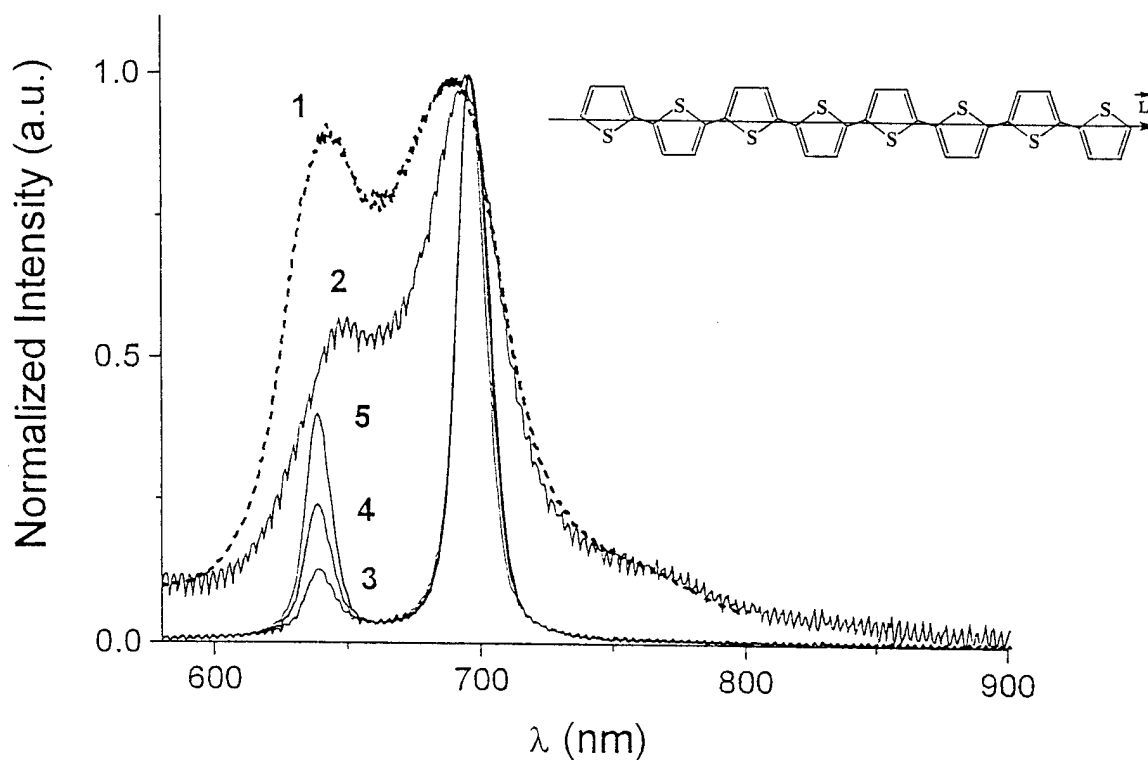
Fig.1 Normalized SE spectra from a 8T single crystal under pulsed laser pumping at various energies 1/ 0.1 µJ, 2/ 1.0 µJ, 3/ 13.0 µJ, 4/ 27.0 µJ, 5/ 50.0 µJ.

Finally, spectral SE selection can be monitored by simply scanning the spatial position of the laser beam on the crystal. From one crystal site to the other the relative intensities of both SE lines can be totally inverted. This originates from two sharply delimited thickness domains and can be interpreted from simple resonator theory for transverse modes.

In conclusion, 8T single crystals are naturally adapted to generate laser emission upon optical pumping. Low-threshold gain narrowing results from a net alignment of molecular dipoles in a crystal having the dimensions and optical quality of a resonator. Since 8T is a semiconducting conjugated model oligomer, it bridges the gap between conventional laser dyes and luminescent conjugated polymers such as PPV. This particular situation in the world of organic laser materials should, in the future, allow to control local laser processes in polymers on the way to the polymer laser diode. Although a few dye-doped lasing organic crystals have been reported [8], oligothiophenes single crystals constitute to our knowledge the first family of monolithic (undoped) organic laser crystals.

References

[1] D. Moses, *Appl. Phys. Lett.* **60**, 3215 (1992).

[2] W. Holzer, A. Penzkofer, S-H. Gong, A. Bleyer and D.D.C. Bradley, *Adv. Mater.* **8**, 974-978 (1996).

[3] N. Tessler, G.J. Denton and R.H. Friend, *Nature* **382**, 695-697 (1996).

[4] F. Hide, M.A. Diaz-Garcia, B. J. Schwartz, M. R. Anderson, Q. Pei and A. J. Heeger, *Science* **273**, 1833-1836 (1996).

[5] D.G. Lidzey, D.D.C. Bradley, S. F. Alvarado and P. F. Seidler, *Nature* **386**, 135 (1997).

[6] D. Fichou, B. Bachet, F. Demanze, I. Billy, G. Horowitz and F. Garnier, *Adv. Mater.* **8**, 500-504 (1996).

[7] W. Koechner, Solid State Laser Engineering, Springer Series in Optical Sciences, Springer Verlag, vol. 1, 1976.

[8] N. Karl, *Phys. Status Solidi (a)* **13**, 651-655 (1972).

Preparation and Characterization of Single Crystal PTS Waveguide Film

M. Liu, C.K. Hwangbo, L. Friedrich, and G. I. Stegeman
Center for Research and Education in Optics and Lasers, University of Central
Florida, Orlando, FL 32816-2700
Tel. (407) 823 6918
Fax: (407) 823 6955

Spatial optical solitons have been receiving an increasing amount of attention due to their potential application for all-optical interconnects. Bright solitons arise as a compensation of natural diffraction of an optical beam by a self-focus nonlinearity. They have been observed in semiconductor, glass and CS_2 waveguides at powers of 500W, 400KW and 500KW [1,2,3]. Recently, conjugated polymer poly[2,4-hexadiyn-1, 6-diol-bis(p-toluenesulfonate)] (PTS) was reported to have large positive nonlinearity (2.2×10^{-12}W/cm^2) and a very small two-photo absorption at around 1.6μm [4]. The large off-resonant positive nonlinearity would allow the one-dimensional (1D) spatial soliton at a practical power level on PTS slab waveguide. We now report the preparation and waveguiding of PTS films.

It has been known that PTS polymer single crystal could be abtained from solid polymerization of monomer crystal by UV exposure or annealing. The PTS polymer crystals were prepared both as a bulk and a thin film in our laboratory. Large ($3 \times 1.5 \times 1$cm^3) bulk polymer PTS crystals were prepared by slow solvent evaporation method and annealing polymerization process, to confirm the reported optical nonlinearity and absorption. The optical characterizations showed a good agreement with published data.

Monomer PTS film was grown by slow solvent evaporation. The principal procedures are as follows: (1) the monomer PTS was dissolved into acetone. The polymer powder in the solution, which came from the partially polymerized monomer and was insoluble in acetone, was filtered out. (2) The concentration of PTS solution was adjusted to 0.4g/ml by carefully controlled acetone evaporation. (3) The PTS solution was brought into the gap between a pair of precleaned glass substrates by capillary effect. The thickness of the gap will eventually determine the film thickness of grown film. (4) Put the substrate-solution-substrate assembly into a controllable nitrogen flowing desiccator to achieve a slow solvent evaporation.

The PTS monomer crystalline films grown by the above procedure was typically 15-20 mm^2 in area with thickness of 4-6 μm depending on the gap between substrates, and extremely smooth surface. The surface orientation of as-

grown film was (100). The polymer chain (b axis), along which the largest nonlinearity can be achieved, was parallel to the substrate surface. Two different morphologies of the monomer crystalline film, hexagonal or needle-like, can be grown depending on the growth condition. In a waveguide application point of view, hexagonal form was more desirable than needle-like morphology in which the polymer chain ran perpendicular to the long side. After monomer growth, the film was polymerized by UV exposure or annealing at 50°C in nitrogen atmosphere for one week. In most cases the cracking in the film was accompanied by the polymer percentage increase during the polymerization process due to a very large shrink (5%) of b dimension [5]. But, the PTS polymer film with 1 mm wide, which is wide enough for optical soliton measurements, could be obtained with hexagonal morphology.

Good end faces of PTS polymer film were achieved by the cleavage of the crystalline film due to its aniostropic nature [5]. 1-3 mm long PTS films for end face coupling could be fabricated reliably by cutting the glass substrates along b axis. Optical waveguiding was demonstrated on our PTS films with length varying from 1 to 3 mm. Figure 1 shows the output image of a 3mm long PTS film at 1.6 μm. The soliton generation and other nonlinear optical measurements are under investigation.
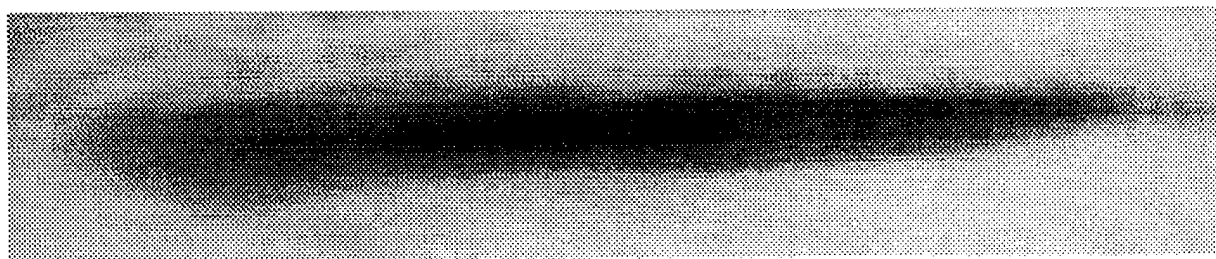
Fig. 1: Output image of a 3 mm long PTS slab waveguide

References:

1. J. S. Aitchison, A.M. Weiner, Y. Silberberg, M. K. Oliver, J. L. Jackel, D. E Leaird, E. M. Vogel, and P. W. E. Smith, Opt. Lett. 15, 471(1990).
2. J.S. Aitchison, K. Al-Hemyari, C. N. Ironside, R. S. Grant, and W. Sibbett, Electron. Lett. 28, 1879(1992).
3. S. Maneuf, R. Desailly, and C. Froehly, Opt. Commun. 65,193(1988).
4. Lawrence, W. E. Torruellas, M. Cha, M. L. Sundheimer, G. I. Stegeman, J. Meth, S. Etemad, and G. Baker, Phys. Rev. Lett. 73, 2773(1994).
5. Krug, E. Miao, M. Derstine, and J. Valera, J. Opt. Soc. Am. B., 6(4), 726(1989).

Basic Mechanisms involved in the Off-resonant Nonlinear Refractive Index of PTS-Polydiacetylene

R. Quintero-Torres and M. Thakur

Auburn University, AL 36849

Phone: (334)844-3326

Polydiacetylene single crystal, PTS, is known to have the largest off-resonant nonlinear refractive index (n_2). Recently we have demonstrated picosecond all-optical switching using PTS-polydiacetylene in a Fabry-Perot cavity[1]. This measurement was performed using a pump-probe technique with 90ps pulses at 1.06μm wavelength. In that measurement, besides demonstrating a large modulation depth, we showed that the sign of n_2 was negative. In another work, however, a positive sign for n_2 was reported from a z-scan measurement[2] and two photon resonances were used to explain the positive sign and the off-resonant nonlinear optical processes in PTS. In this work we have made detailed measurements of the sign using Michelson interferometry and z-scan. These and previous measurements using pump-probe technique at different off-resonant wavelengths show that the sign of n_2 of PTS is negative over the wavelength of 650 - 1064nm.

To measure the nonlinear refractive index of PTS a Michelson interferometer was constructed. Laser pulses of 60ps duration at 10Hz repetition rate and 1.06μm wavelength were used for this measurement. In one arm of the interferometer, a PTS sample was placed while the the beam in the other arm passed through air. The fringes were observed using a CCD camera and the direction of the fringe shift as a function intensity was recorded photographically. For calibration of the sign, the PTS sample was replaced by an 100μm thick glass slip and the fringe shift was recorded as the glass slip was rotated. The rotation of the glass slip introduced positive changes in phase and the corresponding direction of the fringe shift was noted as the calibration of the sign of phase change. For the PTS sample the phase change as the intensity was increased was unequivocally negative. The total phase change we measured was $\pi/2$ for an increase in

intensity of 150MW/cm^2 and a crystal thickness of 200μm. The results clearly showed that the magnitude of n_2 was ~10^{-5} cm^2/MW and the sign was negative.

The z-scan measurement was performed using the same sample (200μm thick crystal) and the same laser (60ps pulses, 10Hz, 1.06μm wavelength) using the established procedure.[3] The typical results of the z-scan are shown in Fig.1. As these results show (a peak followed by a valley), the measured sign of n_2 is negative. To obtain these z-scan results special care was taken to avoid stray scattering which significantly affects z-scan data particularly for n_2 measurements requiring an aperture in the far field. For cases where the stray scattering was not avoided we observed z-scan data that were completely misleading in terms of the sign of n_2. The results in Fig.1 were reproduced for several samples. The magnitude of n_2 determined from the z-scan data was ~10^{-5} cm^2/MW, consistent with the Michelson interferometry results.

Our measurements clearly show that the correct sign of n_2 of PTS at 1.06μm wavelength is negative. The Michelson interferometry in particular provides unambiguous information regarding the sign. Another measurement involving heterodyne detection[4] reported previously also showed a negative sign at 1.06μm. Other detailed measurements have established that the sign of n_2 in the wavelength range between 620 - 751nm is negative.[5] This implies that the sign is negative all the way from 620 to 1064nm. The peak of the excitonic absorption in PTS occurs at 620nm. The excitation becomes off-resonant at a wavelength beyond about 650nm. Thus the sign is negative in the resonant as well off-resonant domains. The negative sign of the off-resonant n_2 is due to saturation of the exciton transition that far outweighs two photon resonances. The measured[5] saturation (α_2) for excitation at or beyond about 729nm, is about -17 cm/MW which is substantially larger than the highest two photon absorption peak (0.7 cm/MW at 2.7eV) reported[2] for PTS. Therefore, saturation dominates over two photon absorption to determine the nonlinear refractive index.
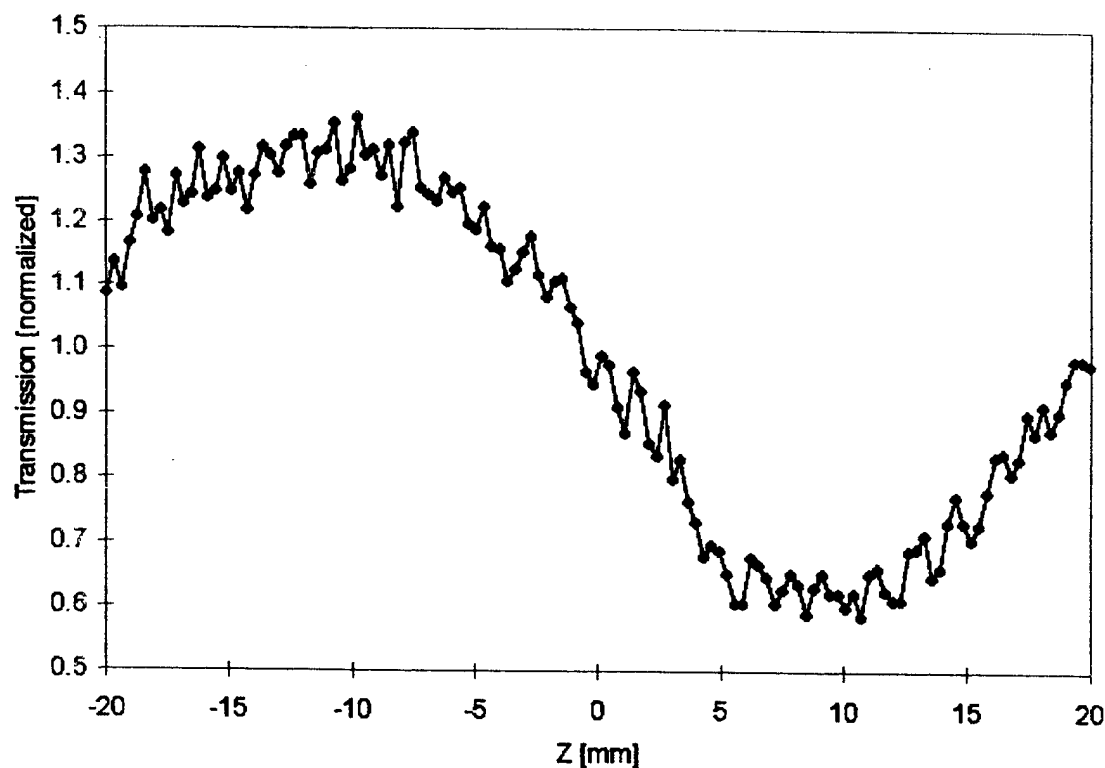
Fig. 1. Z-scan data (n_2 measurement) for an intensity of $150MW/cm^2$.

References:

1. R. Quintero-Torres and M. Thakur, Appl. Phys. Lett., 66 1310 (1995).

2. B. Lawrence, W.E. Torruellas, M. Cha, M. L. Sundheimer, G. I. Stegeman, J. Meth, S. Etemad and G. Baker, Phys. Rev. Lett., 73 597 (1994).

3. M. Sheik-Bahae, A.A. Said, T.-H. Wei, D.J. Hagan and E.W. Van Stryland, IEEE J. Quant. Electron, 26 760 (1990).

4. S.T. Ho, M. Thakur and A. LaPorta, IQEC, paper QTuB5, 8 40 (1990).

5. B. I. Green, J. F. Muller, J. Orestein, D. H. Rapkine, S. Schmitt-Rink, and M Thakur. Phys. Rev. Lett., 61 325 (1988); B. I. Green, J. Orestein, M. Thakur and D. H. Rapkine, MRS Symp. Proc., 109 159 (1987).

Characterization of Push-Pull Polyenes of Increasing Size: Linear and Quadratic Polarizabilities in Solution

Alain Fort, Jacques Muller, Joel Azoulay, Marguerite Barzoukas

Institut de Physique et de Chimie des Matériaux de Strasbourg, Groupe d'Optique Nonlinéaire et d'Optoélectronique (UM 046), 23 rue du Loess, 67037 Strasbourg Cedex, France, Tel: (33) 3 88 10 70 87

Valérie Alain, Mireille Blanchard-Desce

Ecole Normale Supérieure, Département de Chimie (URA 1679), 24 rue Lhomond, 75231 Paris Cedex 05, France, Tel: (33) 1 44 32 33 33

Push-pull molecules have been extensively studied for their properties in the field of quadratic nonlinear optics. Such molecules consist of electron-donor and electron-acceptor substituents connected via a conjugation path. The partial intramolecular charge transfer (ICT) between these end groups can lead to large ground-state dipoles μ. Also, they can display huge static quadratic hyperpolarizabilities $\beta(0)$ related to the occurence of the ICT transition between the ground and first-excited states [1].

Recently, we have developed a two-form two-state model of push-pull molecules wherein the ground and first-excited states are linear combinations of the neutral and zwitterionic or charge-separated forms (see Scheme 2) [2,3]. To characterize the mixing between these limiting-resonance forms, we have defined a parameter MIX equal to the difference between the respective weights of these forms in the ground state.

neutral form   zwitterionic form

Scheme 2

Actually, MIX is proportional for push-pull polyenes to the geometrical Bond Length Alternation (*BLA*) parameter that has been developed by S. Marder and coworkers [4,5]. We have studied analytically the variations of the linear and nonlinear polarizabilities as functions of *MIX*.

In this work, we present a thorough experimental investigation on two series of push-pull polyenes of increasing size bearing aromatic electron-donating end groups and various electron-withdrawing moieties (see Scheme 1). The total number n of double bonds in the conjugation path was equal to 1, 2, 3, 4 and 5.
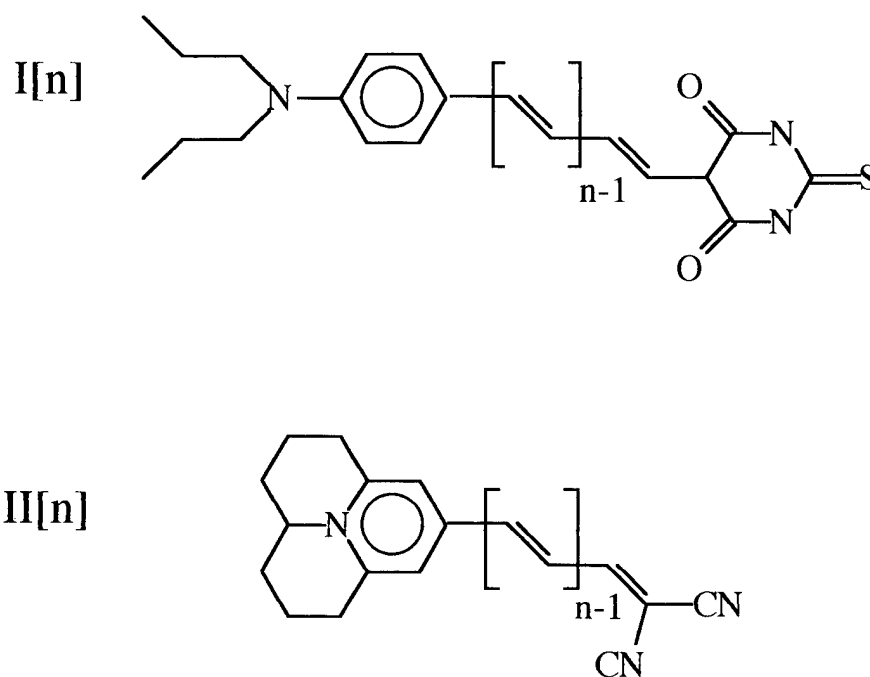
Scheme 1

For each compound in series I[n] and II[n] , we have determined in solution:

- the ground-state dipole μ using capacitive measurements

- the static quadratic hyperpolarizability $\beta(0)$ using the well known electric-field-induced-second-harmonic (EFISH) technique

- the static linear polarizability $\alpha(0)$ using a new experimental set-up, based on transmission ellipsometry, that we have developed [6]

Finally, we have used the two-form two-state model to analyse these experimental results. We have shown that both the maximum linear polarizability $\alpha_{max}(0)$ and quadratic hyperpolarizability $\beta_{max}(0)$ are affected by the nature of the donor/acceptor end groups as well as the size of the polyenic linker. We have also shown that the variation of *MIX* with increasing chain length depends on the donor/acceptor pair.

REFERENCES:

[1] J.-L. Oudar and D.S. Chemla, J. Chem. Phys. 66 (1977) 2664.

[2] M. Barzoukas, C. Runser, A. Fort and M. Blanchard-Desce, Chem. Phys. Lett. 257 (1996) 531.

[3] M. Barzoukas, A. Fort, M. Blanchard-Desce, New J. Chem. 21 (1997) 309.

[4] C.B. Gorman and S.R. Marder, Proc. Natl. Acad. Sci. U.S.A. 90 (1993) 11297.

[5] S.R. Marder, C.B. Gorman, F. Meyers, J.W. Perry, G. Bourhill, J.-L. Brédas and B.M. Pierce, Science 265 (1994) 632.

[6] A. Fort, J. Muller, O. Cregut, L. Mager, J.-P. Vola, M. Barzoukas, to be submitted

One and Two Photon Induced Photodegradation of DANS Films

Qiang ZHANG, Michael CANVA, George STEGEMAN

Center for Research and Education in Optics and Lasers (CREOL)
P.O. Box 162700 - 4000 Central Florida Boulevard
University of Central Florida, Orlando FL 32816-2700 - USA
Phone : (1) 407 - 823 6916 - Fax : (1) 407 - 823 6955
qiang@soliton.creol.ucf.edu, canva@mail.creol.ucf.edu, and george@creol.ucf.edu

Dye doped solids have been investigated for a decade for non-linear optical applications, especially for integrated optics. In some areas, their "single shot" performance has now reached levels which compete with the best ferroelectrics materials and thus encourages their practical usage. However, a key question remains to be answered : how stable is their performance with time when used in given devices and under operational conditions ?

In this presentation, we shall report the theoretical and experimental investigation of the impact of dye degradation on the performance of an infra-red waveguide polymer. We first modeled the degradation processes in terms of one photon (1PA) and two photon absorption (2PA). We then chose the well known DANS polymer on which to conduct experiments. The wavelength dependence of the one photon degradation process was characterized at different wavelengths ranging from the visible absorption band to the near infra-red. In this latter part of the spectrum the absorption of light pulses is mainly due to two photon absorption which also leads to photodegradation and which was quantified. Then, the evolution of the index decrease in the waveguiding regions was correlated to the dye degradation kinetics. Finally, given the one and two photon absorption spectra, and the associated quantum efficiencies of photodegradation, the model predicts the maximum lifetime of any device based on DANS, assuming the limitation is solely due to one and two photon absorption induced photodegradation.

Photodegradation studies have already been reported in many papers. Usually they were performed with 1PA excitation in the dye absorption band. To fit the data and take into account the non-uniformity of the degradation along the propagation axis (i.e. the front area is bleached before the back area of the sample), mostly numerical solutions were proposed, both taking or not taking into account the change in the losses due to the bleaching process. Some papers have reported analytical approximate solutions and we shall use one of them which is valid at wavelengths where the dye absorbs more than the photoproduct, the absorption of the latter being overall small [1]. It allows us to indirectly measure the quantum efficiency of photodegradation, or its inverse which corresponds to the averaged expected number of excitation/de-excitation cycles the dye molecule undergoes before degradation. This number is defined as B. In the case of 2PA, only the excitation mechanism is different, and a similar average cycle lifetime B_2 (as B_1 in the 1PA case) may be correlated to the de-excitation mechanism. The B parameters may be wavelength and excitation mechanism dependent.

To validate our theoretical model and experimental procedures, we chose the well known nonlinear dye DANS. Figure 1 shows its 1PA and 2PA spectra. The linear spectrum of DANS is given in the 200-1600 nm range, on a log scale. Data in the infra-red were acquired through waveguide loss measurements [2]. The nonlinear absorption spectrum had been obtained around 900 nm from z-scan experiments [3]. Our goal is to study the degradation under different experimental conditions and to asses its impact on waveguiding device performances.
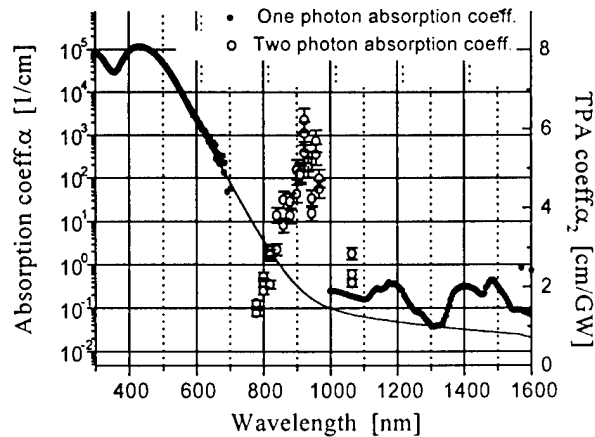
Figure 1 : *One and two photon absorption spectra of DANS.*

To actually measure the photodegradation quantum efficiency accurately and easily, it is best to measure an intensity and cumulative energy change in transmission from a few percent to a few tens of percents. In the case of micrometer thick films of DANS, we chose to measure the degradation effect at the 543.5 nm line of a green He-Ne laser (the absorption being about 1.3×10^4 cm^{-1}, the initial transmission is about 27 %). For all other longer wavelengths of the pump, this green beam was used to probe intermittently (i.e. without inducing any noticeable bleaching) the evolution of the material absorption. This pump and probe technique allows us to conduct experiments at different wavelengths up to 1.06 μm where accurate measurements of absorption evolution would have been difficult.

The trend seems to be that the B_1 parameter associated with the 1PA process increases noticeably with increasing excitation wavelength when getting outside of the absorption band. In the infra-red region, no noticeable 1PA was recorded at low powers and we focused on 2PA excitation regime experiments. The B_2 parameter measured at 1.06 μm was found to be very similar to the value of B_1 in the absorption band.

Detailed experimental procedures and results shall be reported at the conference. Typical results are shown in the case of 1PA at 543 nm c.w., figure 2a, and at 1.06 μm in case of 1PA c.w. and 2PA pulsed, figure 2b. Data are fitted with the model previously described and referenced.
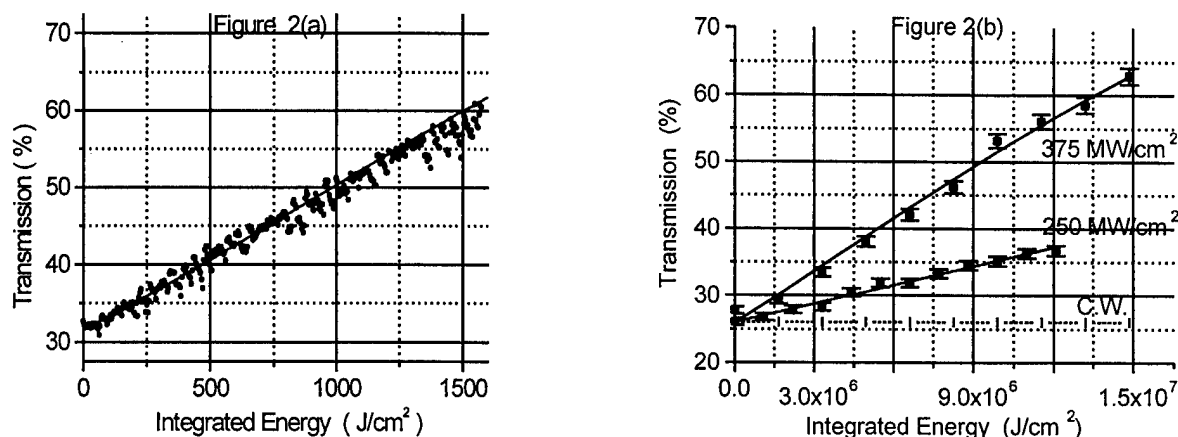
Figure 2 : *Probe (543.5 nm) transmission as a function of accumulated input energy when pumped at : (a) at 543.5 nm c.w. 2 mW/cm², (b) at 1060 nm, c.w. 5.4 kW/cm², pulsed 250 MW/cm² and 375 MW/cm² peak intensities.*

The increase in transparency is due to a decrease in the active dye concentration and is thus linked to a decrease in optical index in the infrared. In the case of a waveguide structure can lead to a strong decrease in the overall transmission if the cut-off is reached for the operational wavelength. This evolution of the material's optical index is illustrated in experiments in which launching pulses in a tapered waveguide and outcoupling them with a grating shows an evolution of the emission angle with time.

In conclusion, we are currently investigating the wavelength dependence of photodegradation quantum efficiency induced by one photon absorption, $B_1(\lambda)$, and two photon absorption processes, $B_2(\lambda)$. The first results from these studies show that the $B_1(\lambda)$ tends to actually increase with increasing wavelength. This, and the fact that the absorption decrease, makes 1PA degradation effects quickly negligible compared to 2PA effects when using pulses. Concerning 2PA, the first results seem to show that $B_2(2\lambda)$ is similar $B_1(\lambda)$. Plugging those results into a simulation actually allows us to predict the evolution of the local dye concentration as a function of the material's illumination history. In the case of waveguide structures, it can forecast when cut off will be reached. We plan to extend this study to at 1.3 and 1.5 μm.

References :
[1]   A. Dubois, M. Canva, A. Brun, F. Chaput and J.P. Boilot, *"Photostability of dye molecules trapped in solid matrices"*, Applied Optics, **35**, 3193-3194, (1996).
[2]   A. Otomo, M. Jäger, G. Stegeman, M. Flipse and M. Diemeer, *"Key trade-offs for second harmonic generation in poled polymers"*, Applied Physics Letters, **69**, 1191-1993, (1996).
[3]   M. Cha, W. Torruellas, G. Stegeman, W. Horsthuis and G. Mollmann, *"Two photon absorption of di-alkyl-amino-nitro-stilbene side chain polymer"*, Applied Physics Letters **65**, 2648-2650, (1994).

Observation of Switching Phenomena in Non-ether PPQ Planar Waveguide with Two-wavelength Nonlinear Prism Coupling

Jun Zhou

(Institute of Engineering Physics, Shandong Institute of Mining and Technology,
Taian, Shandong 271019, China)

Zhuangqi Cao   Yingli Chen   Yixin Chen
(Institute of Optical and Photonics, Department of Applied Physics,
Shanghai Jiao Tong University, Shanghai 200030, China)

Meng Sun   Diechi Sun   Fuming Li
(State Key Laboratory of Materials Modification by Photon, Ion and Electron Beam,
Fudan University, Shanghai 200043, China)

In the past two decades, third-order nonlinear optical properties of organic and polymeric materials have attracted considerable attention to realize all-optical signal processing devices.[1,2] Especially, the large off-resonance third-order optical nonlinearities of conjugated organic polymers with delocalized π--electron systems, such as polydiacetylenes[3,4], are considered to be potential candidates. Although conjugated polymer is reported to have large $\chi^{(3)}$ and fast response time, many of them are highly intractable materials that are difficult to process to form the low-loss waveguide structures required for their application[5]. Recently, many techniques for fabricating low-loss planar waveguides in thin films of solution processible conjugated polymer have been developed[7,8] besides third-order nonlinear optical polymers that exhibit low absorption have been reported[6] Furthermore, numerous different schemes which aim is all-optical switching and all-optical logic operations have been suggested for practical devices. They are included in nonlinear prism and grating couplers and nonlinear directional couplers[9,10], such as two-channel nonlinear directional couplers, nonlinear Mach-Zehnder interferometers, nonlinear distributed-feedback grating reflectors and adiabatic polymer-glass-waveguide all-optical switch[11,12]. However, though the prism coupler has attracted partially significant attention both theoretically[13] and experimentally[14], as so far we know the nonlinear prism coupling to organic polymer waveguide has

only been demonstrated in single beam experiments on intense-dependent nonlinear effects[15].

In this paper we present a nonlinear switching phenomena, which is observed in the planer waveguide fabricated with non-ether polyphenylquinoxalines (PPQ) material by two-wavelength nonlinear prism coupling. The molecular structure of non-ether PPQ is shown in Fig. 1, the quinoxaline rings each linked with a benzene ring is connected to each other by either a single bond or a benzene ring, this forming a delocalized π--electron system and having a large near-resonance third-order nonlinear optical susceptibility[16]. The absorption spectrum of non-ether PPQ/ chloroform solution is shown in Fig.2. From the spectrum, the peak of absorption is at 395 nm, and when the wavelength is longer than 700 nm, the optical loss of neat non-ether PPQ is calculated to be less than $1 cm^{-1}$. Furthermore, the glass-transition temperature T_g of non-ether PPQ is reported to be $337°C$, which suggests the material would have good thermal stability at high temperature[17].

In the process of sample preparation, the solid non-ether PPQ was nominally mixed 5% by weight with chloroform and dissolved into solution by overnight at home temperature. In order to prevent the formation of microbubbles in the solution additional stirring or shaking wave avoided. Before preparing the planar waveguides, the polymer solution was filtered through a 0.2 μm pores filter, then the filtered solution of non-ether PPQ was dropped on the substrate of quartz

glass and spin-coated with a rotation speed in the range between 800 rpm and 1200 rpm leading to uniform thin film between $1.0 \mu m$ and $2.0 \mu m$ thickness, then the film was softly baked to remove residual solvent at $50°C$ for no less than 12 hours. Finally, the sample of polymer planar waveguide was made successfully out. Here, we should point out that the substrates have to be pre-cleaned very accurately.
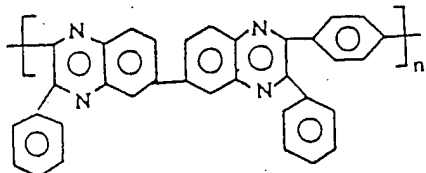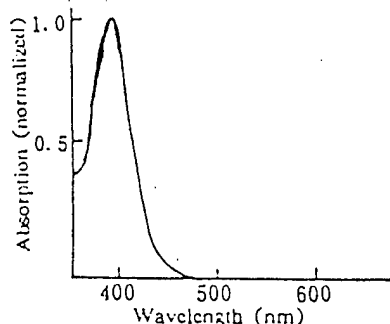

Fig.1 Molecular structure of non-ether PPQ

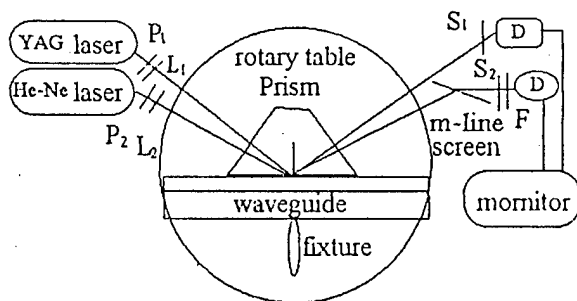Fig.2 Optical absorption spectrum of non-ether PPQ/chloroform

Fig.3 Experimental setup of the two-wavelength nonlinear prism coupling.

(P_1 , P_2 --polarizer; L_1 , L_2 --lens; D--detector; S_1 , S_2 --narrow seam; F--632.8nm pass filter.)

In this experiment the m-lines spectroscopy technique[15] had been used to characterize the guiding modes and the switching phenomenon in waveguide is observed with two-wavelength nonlinear prism coupling. The experimental setup is shown in Fig. 3. The pump light of a mode-

locked Q-switched Nd:YAG laser system ($\lambda = 1.064$ μm, 7 ns pulse width, the maximum repeat frequency 10Hz, the maximum of putout energy 300 mJ) and the probe light of He-Ne laser ($\lambda = 632.8$nm, 10mW) are used to coupled into the waveguide, respectively. Both beams are TE polarized and focused onto the base of the coupling prism. As the waveguide and the coupling prism mounted on the motorized rotary is rotated and translated assembly, due to the pump beam and probe beam are coupled into the waveguide, the dark m-lines are seen at the specific coupling angles in the reflected filed. At this time an m-line of probe light is then imaged onto narrow seam that is mounded on the front of the photomultiplier detector(PTM). As the pump beam is switched on or off, the intense pump pulse beam induces the ultrafast electronic nonlinear Kerr effects originated from intensity-dependent of refractive index so that the changes of refractive index of the polymer film waveguide cause an angular shift of the m-lines. Thus the signal of the PTM detector is switched on or off with the shift of m-line on the narrow seam. The experimental results are shown in Fig. 4. In the mean times, the intensities of switching signal of PTM which changes with the input intensities of pump light are showed in Fig. 5. From the picture, the intensities of switching signals are changed nonlinearilly with the pump power and the saturation will appear when the pump intensities is larger than 30 Mw/cm^2, which means that the half-high widths of the signals pulse will be constant in the range of higher pump intensities. It is also seen the threshold power intensity of switching effect is about 2 MW/cm^2 at an estimating coupling efficiency of 6%.

According to our analyses, it can be conclude that the switching phenomenon is mainly caused by the electronic effect. From Fig. 2, the absorption of PPQ material for the light of $1.064 \mu m$ wavelength can be nearly neglected so that the thermal effect due to the absorption of material is considered to be small. On the other hand, from the contrast of the Fig. 4(a) and Fig. 4(b) we know that the half-high width of the probe light is less than the half-high width of the pump pulse in the same time scaling limit, we estimated the response time of the switching effects is about several nanoseconds, which suggests that the ultrafast electronic nonlinearity

of non-ether PPQ material plays the main role other than slow thermal nonlinearity. Because the third-ordernonlinear effects of non-ether PPQ material mainly comes from the contribution of electron effect of material, the nonlinear response time of the non-ether PPQ should be much fast than 35 picoseconds[18]. Thus, though the
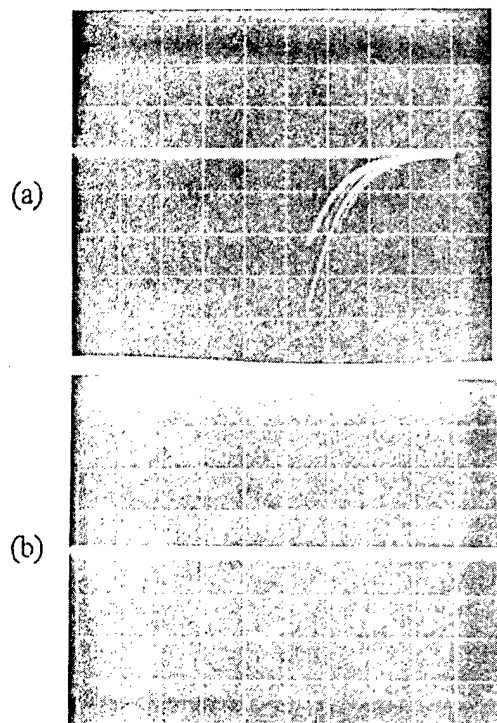

(a)

(b)

Fig.4 Switching Phenomena as ultrafast optical Kerr effect in the waveguide
(a) signal pulse detected pump pulse beam;
(b) signal pulse as the m-lines shift of probe light
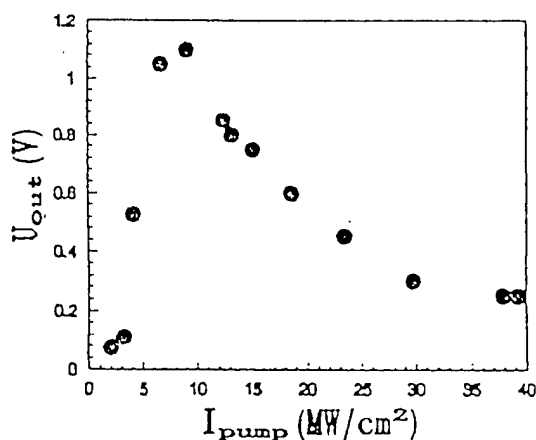
Fig.5 The signal intensities of m-lines of probe light versus various intensities of pump beam

switching response time of the waveguide should be at the picosecond orders of magnitude, the measured switching time is the nanosecond orders

of magnitude in this experimental because of the limitation by the pulse width of pump beams used in the nonlinear prism coupling and the response factor of the PTM detector.

In summary, we have initially realized the switching effects with two-wavelength nonlinear prism coupling into the non-ether PPQ waveguide. Furthermore, the analyses have been taken to identify the dominant effect due to electronic nonlinearity in the case of high intense pump beam. The measured switching time in this experiment is shorter than several nanoseconds, and the power intense of switching effect is about $2\ MW / mm^2$. All these parameters suggest a good application prospect of the switch phenomenon in the waveguide.

. References
1. N. Bloembergen, Int. J. of Nonlin. Opt. Phys., 3, 439(1994)
2. D. S. Chemla and J. Zyss, Eds., Nonlinear Optical Properties of Organic Molecules and Crystals, (Academic Press, Orlando, Florida, 1987). Vol.2
3. S.Okada and H. Nakanishi, Int. J. of Nonlin. Opt. Phys., 3, 501(1994)
4. J.Zhou, Y. Chen, Z. Cao, J. Liu, Y. Zhao, H. Zhu, D. Sun and F. Li, Proc. SPIE, 2897, 165, Beijing(1996)
5. T. Hasegawa, K. Ishikawa, T. Kanetake, T. Koda, K. Takeda, H. Kobayashi and K. Kubodera, Chem. Phys. Lett., 171, 239(1990)
6. H. S. Nalwa, Adv. Mater. 5, 341(1993)
7. W. Krug, E. Miao and M. Derstine, J. Opt. Soc. Am. B, 6, 726(1989)
8. W. A. Pender, A. J. Boyle, P. Lambkin, W. J. Blau, K. Mazaheri, D. J. Westland, V. Skarda and M. Sparpaglion, Appl. Phys. Lett. 66, 786(1995)
9. G. Assanto, J. of Mod. Opt., 37, 855(1990)
10. G. I. Stegeman and E. M. Wright, Opt. Quantum Electron, 22, 99(1990)
11. P. D. Townsend, J. L. Jackel, G. L. Baker, J. A. Shelburne, III, and s. Etemad, Appl. Phys. Lett. 55, 1829(1989)
12. J. Y. Chen and S. I. Najafi, Appl. Opt., 33, 3375(1994)
13. C. Liao, G. I. Stegeman, C. T. Seaton, R. L. Shoemaker and J. D. Valera, J. Opt. Sco. Am. A, 2, 590(1985)
14. W. Lukosz, P. Pirani and V. Briguet, Opt. Lett. 12, 263(1987)
15. H. Rigneault, F. Flory and S. Monneret, Appl. Opt., 34, 4358(1995)
16. S. C. Mehandale and K. C. Rustagi, Optics Comm., 28, 359(1979)
17. P. M. Hergenrother, Polymer Eng. Sci., 16, 303(1976)
18. J. Yan, J. Wu, H. Zhu, X. Zhang, D. Sun, F. Li and M. Sun, Optics Comm., 116, 425(1995)

Emissive Devices

Wednesday, October 15, 1997

Zakya H. Kafafi, U.S. Naval Research Laboratory
Presider

WD
3:30pm–5:30pm
Seaview A&B

Conjugated Polymers as Materials for Thin Film Solid State Lasers

F. Hide, M.A. Diaz-Garcia, M. McGehee, B. J. Schwartz and A. J. Heeger

Institute for Polymers and Organic Solids

University of California at Santa Barbara

Santa Barbara, CA 93106

Optically pumped gain narrowing and lasing have been demonstrated in submicron thick films, neat and undiluted, of photoluminescent conjugated polymers. The dramatic collapse of the emission line width occurs at very low pump energy thresholds (~ 10 $\mu J/cm^2$). Gain narrowing is found in over a dozen different conjugated polymers representing a variety of molecular structures, including poly(p-phenylenevinylene), poly(p-phenylene) and polyfluorene derivatives; the emission wavelengths in these materials span the visible spectrum. The short gain lengths in conjugated polymers are attributed to the high density of chromophores, the large density of states associated with the interband (π-π^*) transition in quasi-one-dimensional systems, and the Stokes shift which minimizes self-absorption and allows optical pumping to the excited state without simultaneously stimulating emission (thereby yielding population inversion). Lasing and gain narrowing are compared for a soluble poly(phenylene vinylene) derivative using two different resonant structures: planar waveguides and microcavities. In both cases, the gain narrowing threshold is at 0.05 - 0.1 μJ per 10 ns pulse focused to approximately 1.5 mm. Single mode microcavity lasers are obtained when a cavity resonance occurs at the wavelength where the gain of the polymer is a maximum. Low threshold lasing (threshold more than an order of magnitude below that observed in planar waveguides and microcavities) has also been demonstrated using distributed feedback in a planar thin film configuration.

Light Amplification in Polymer Optical Fibers

Takeyuki Kobayashi, Eisuke Nihei, Keisuke Sasaki, Yasuhiro Koike
Faculty of Science and Technology, Keio University
3-14-1, Hiyoshi, Kohoku-ku, Yokohama 223, JAPAN
Telephone: International +81-45-563-1141 ext. 3454

Yasuhiro Koike
Kanagawa Academy of Science and Technology
1-1-1, Fukuura, Kanazawa-ku, Yokohama 230, JAPAN
Telephone: International +81-45-785-3730

1. Introduction

Polymer optical fibers (POF) have attracted increasing attention because of their clear technical advantages over glass fibers, such as flexibility and a large core diameter, which enable efficient coupling and connection. Recently, we developed low-loss (100 dB/km) high-bandwidth (5.12 GHz for 100-m transmisson) graded index POF[1]. Polymer optical fibers that regenerate signal light in the visible and infrared are potentially important because of their adaptability for POF-based short span optical local distribution networks such as premise wiring and LAN.

We have chosen organic dyes[2,3] and rare earth chelates as gain media and incorporated them into the core region of POF. The synthetic polymer shows much better compatibility with organic compounds and amenability to high dopant concentration, which results in a high gain in a short length of fiber.

2. Organic dye-doped POF

The most important characteristic of organic dye-doped POFs for practical applications is their ability to provide high-power output tunable over a wide range. In order to demonstrate the tunability of organic dye-doped POFs, we carried out amplification experiments. The fiber was end-pumped at 532 nm with a frequency-doubled Nd: YAG laser. We used a monochromator to separate the amplified output signal from any broad band spontaneous emission or remnant pump before detection with a photomultiplier.

Figure 1 shows theoretical (curves) and experimental (points) gain versus the signal wavelength for a rhodamine B doped-POF for 2.8 kW of pump power at 532 nm. Signal inputs were 0.3 W. Amplification over the range 560-600 nm has been achieved with a best observed gain of 33 dB at 580 nm. The theoretical calculation was carried out based on the measured spectroscopic data.

Table 1 shows measured signal gains obtained so far with POF doped with several different dyes. As shown in Table 1, organic dye-doped polymer fiber amplifiers can operate covering a wide range in the visible.
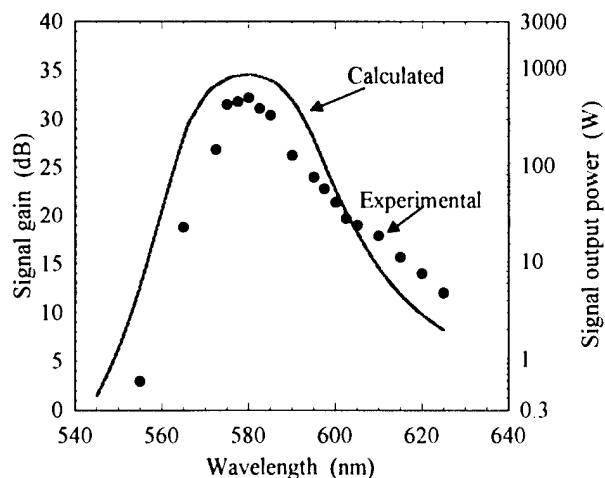
Figure 1   Measured and calculated signal gain as a function of the signal wavelength for a Rhodamine B-doped POF, 1 m in length, 300 μm in core diameter. The dye concentration was 1 ppm-wt.

Table 1   The measured signal gains for organic dye-doped POFs.

Dye	Gain (dB/times)	Signal wavelength (nm)	Fiber Length (m)
Rhodamine B	36/4000	580	0.9
Rhodamine 6G	26/400	572	1.2
Rhodamine 101 P.C.	13/20	598	2.2
Pyrromethene 567	14/25	567	1.5
Perylene orange	18/63	580	1.1
Perylene red	20/100	597	1.6
Oxazine 4	18/63	649	1.0

3. Rare earth chelate-doped POF

Rare earth chelates show sharp line emissions characteristics of rare earth ions. We chose β-diketone of trifluoroacetylacetone (TFAA) as a chelating agent, and synthesized europium chelate in tris form. We fabricated a fiber preform rod containing 1 wt% Eu(TFAA)₃ using the interfacial gel polymerization technique[2]. The preform rod was heat-drown into a fiber.

Figure 2 shows the emission spectrum of an $Eu(TFAA)_3$-doped POF, 0.1 m in length, end-pumped at around 350 nm with an argon ion laser. The chelate concentration was 1 wt%.

The 614 nm emission line is dominant, which corresponds to the $^5D_0$-$^7F_2$ transition, and the fluorescence linewidth was found to be 10 nm.

4. Conclusions

A Rhodamine B-doped POF, 1 m in length, 300 μm in core diameter, exhibited more than 20 dB signal gain for signal wavelength spanning 40 nm range between 560 nm and 600 nm. The optical amplification covering most of the spectral range from 560 nm to 650 nm has been obtained with POFs doped with several selected dyes. The broad spectral coverage demonstrates the versatility of the organic dye-doped POFs. Also, we successfully incorporated Eu chelate into POF. The emission spectrum was presented.
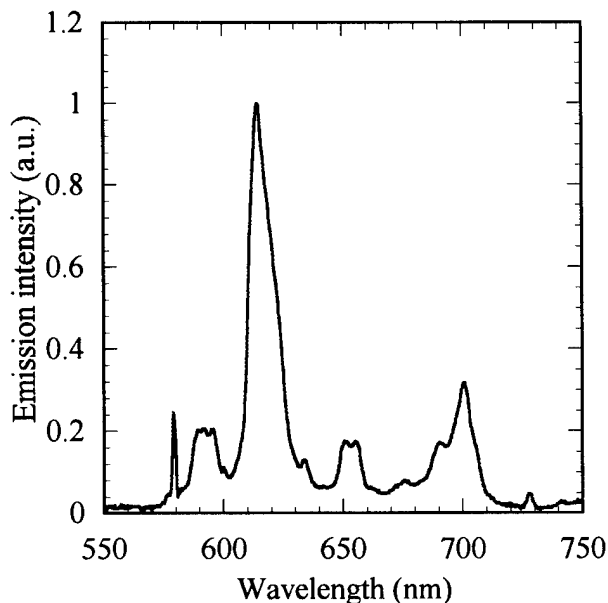
Figure 2 Emission spectrum of $Eu(TFAA)_3$-doped POF, 0.1 m in length, 300 μm in core diameter. The chelate concentration was 1 wt%.

We have a prospect that the wide choice of organic dyes and rare earth chelates offers light amplification covering most of the spectral range from visible to infrared. Polymer optical fiber laser can be easily constructed with a proper choice of wavelength-selective elements.

References

1) Y. Koike, T. Ishigure, and E. Nihei, J. Lightwave Technol., **13** 1475 (1995).

2) A. Tagaya, Y. Koike, T. Kinoshita, E. Nihei, T. Yamamoto, and K. Sasaki, Appl. Phys. Lett., **63**, 883 (1993).

3) T. Kobayashi, A. Tagaya, S. Nakatsuka, S. Teramoto, E. Nihei, K. Sasaki, and Y. Koike: to be published in *Polymers for Advanced Optical Applications* ed. S. A. Jenekhe, and K. J. Wynne (ACS Symposium Series, ACS Books, Washington, DC).

Liquid Crystalline Polymers for Electroluminescence

D.D.C. Bradley, M. Grell, K.L. Brandon
Department of Physics and Centre for Molecular Materials, University of
Sheffield, Hounsfield Rd, Sheffield, UK

M.L. Turner, P. Bentley, D.A. Dunmur
Department of Chemistry, University of Sheffield, Western Bank, Sheffield, UK

E.P. Woo, and M. Inbasekaran
Central & New Businesses R&D, The Dow Chemical Co., Midland, Michigan, MI 48674, USA

Organic electroluminescence is attracting strong interest for applications in lighting and displays. Polymer devices offer some advantages for low cost processing over large areas and with extended molecular architectures there is the possibility of polarised emission. This is attractive for backlighting liquid crystal displays and also for development of sources for optoelectronics. In order to achieve polarised emission there is a need to obtain highly oriented samples. Further, to allow construction of efficient electrolumiescent diodes it is necessary to achieve this orientation in thin films deposited on suitable electrode surfaces. We believe that mesophase formation is an attractive approach to achieve these dual goals and we have thus undertaken a programme of work to produce liquid crystalline polymers with the dual attributes of charge transport and light emission capability that can allow application in electroluminescence devices. This paper reports on recent progress in materials preparation, processing and device fabrication.

Origin of Optical Gain and Stimulated Emission in Conjugated Polymers

Ch. Spiegelberg,[*] A. Schülzgen, M. M. Morrell, P. M. Allemand,[**]
B. Kippelen, and N. Peyghambarian

Optical Sciences Center, University of Arizona, Tucson, AZ 85721, USA
**Donnelly Corporation, Tucson, AZ 85721-1108.*
[*] *tel: (520) 621 2382, fax: (520) 621 4442, e-mail: christis@u.arizona.edu*

Recent reports on a spectrally narrow emission peak have generated a lot of excitement in the scientific community. Hide et al. [1] and Frolov et al. [2] reported dramatic photoluminescence (PL) line narrowing in a variety of PPV derivative films for exciton densities above 10^{17} cm^{-3}, indicating stimulated emission (SE). The SE linewidth (7 to 9 nm) has been attributed to either amplified spontaneous emission [1] or superradiance [2].

We present a detailed analysis of SE, as well as of absorption changes above and below the excitonic absorption edge of BEH-PPV films using femtosecond pump-probe spectroscopy. From spectra taken at very early times after photoexcitation, where spectral diffusion has not yet occurred, we can identify several excited excitonic states and show that the homogeneous linewidth of these states is only about 8 nm. Gain narrowing, ASE, or superradiance arguments are not needed to explain the origin of the narrow SE spectrum. We show that the optical gain is due to inversion of the exciton-phonon transitions [3].

Thin films of the soluble PPV-derivative Poly (2,5-bis(2'-ethyl-hexyloxy)loxy)-1,4-phenylenevinylene [4] were fabricated by spin coating from xylene-solution. The samples were resonantly excited in their absorption edge at 555 nm, using an amplified CPM laser system which provides intense excitation and spectrally broad probe pulses of 100 fs duration.

The low density PL spectrum (Fig.1) is similar to the one observed in electroluminescence. It exhibits

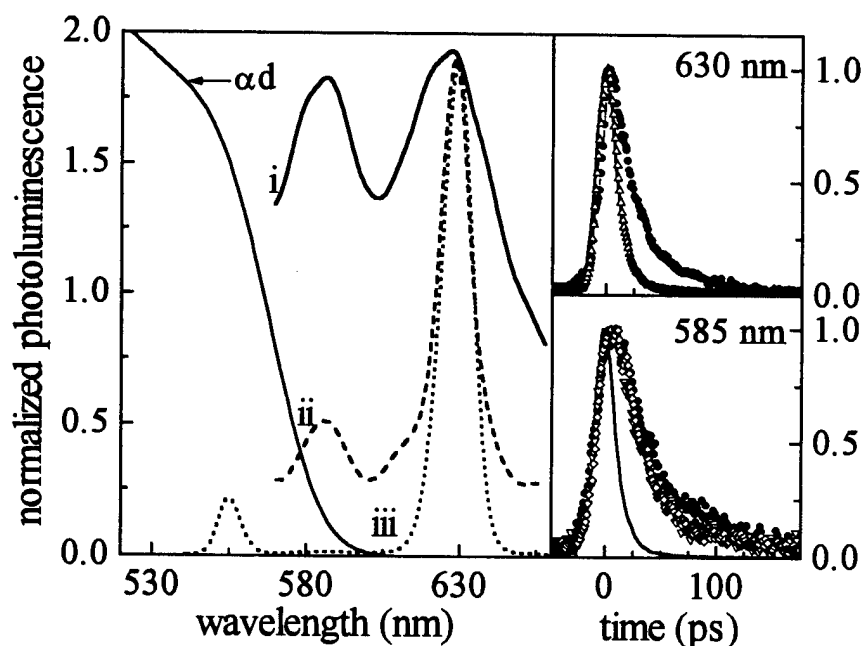Fig.1 Normalized PL for 30, 50 and 120 μJ/cm² excitation (i-iii). Inset: PL decay at 630 nm for 30 (solid dots) and 50 μJ/cm² (open triangles) and at 585 nm for 30, 50 and 800 μJ/cm² (open diamonds). The solid line is the apparatus function of the setup.
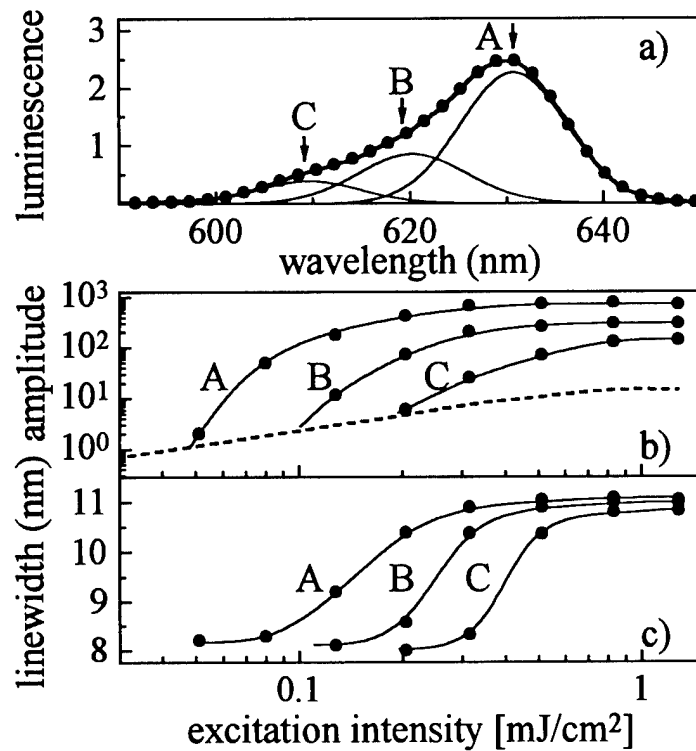
Fig.2 a) PL for 500 µJ/cm² excitation. Dots and thin lines represent a lineshape fit; b): Amplitude of peak A, B, and C. Dashed: PL amplitude at 585 nm; c): FWHM of peak A, B, and C. Solid lines are to guide the eye

the well known vibrational structure with an energy spacing of about 150 meV, corresponding to the frequency of phenylene backbone vibrations. For increasing excitation intensity, the initial 120 nm broad PL spectrum narrows into a 9 nm broad emission line at the photon energy of the 1- phonon line. This transition happens when the excitation is increased to about 50 µJ/cm² analogous to an average exciton density of $n_{eh} = 5 \times 10^{18}$ cm^{-3}. At the excitation intensity where a narrow line is observed, the decay time at 630 nm decreases drastically from about 60 ps to a time shorter than 10 ps, the time resolution of the streak camera. The rapid decay of the PL is typical for SE. At the 0- phonon line no change on the PL decay time is observed, even when the excitation is increased up to 800 µJ/cm².

A further increase of excitation, however, changes the spectrum of the emission at the 1- phonon line: additional structures appear on the high energy side. In Figure 2a) we plotted the PL spectrum for an excitation of 500 µJ/cm². For all the different excitation levels used in our experiment, the narrow emission spectrum can be very accurately fitted by three different levels with a Gaussian shape peaking at $\lambda = 632$, 621, and 609 nm, labeled A, B, and C respectively. The intensity dependence of amplitude and linewidth (FWHM) of these three peaks are shown in Fig. 2 b) and c). While the spontaneous emission at the 0- phonon line (the dotted line in Fig. 2b represents a Gaussian fit to the PL at 585 nm) increases linearly, the amplitude of all 1- phonon transitions exhibits a clear threshold behavior with increasing excitation, followed by saturation. Doubling the excitation intensity at the threshold results in an increase of the emission of peak A by more than two orders of magnitude. Typical for SE, the very fast recombination shortcuts slower nonradiative processes that determine the quantum efficiency and the kinetics at low excitation densities resulting in a dramatic increase of the quantum efficiency above the SE threshold. In the unsaturated regime we find for all three transitions a common linewidth of 8 nm. This linewidth increases to 11 nm at saturation. As revealed by our pump-probe measurements, the excitation regime above 500 µJ/cm² is characterized by less efficient optical pumping due to absorption bleaching at the excitation wavelength.

The right part of Fig.3 shows the net optical gain ($\Delta\alpha d$-αd_{lin}) measured in the transparent region of a BEH-PPV layer by pump-probe experiments at zero time delay between pump and probe pulse and for different excitation intensity. Since the film thickness is only 190 nm, a net gain of 0.185 translates into a gain coefficient of almost 10^4 cm^{-1}, by far the largest value reported for a

semiconducting polymer. The gain spectra exhibit several peaks, separated by approximately 35 meV. These findings are in very good agreement with the results of the PL lineshape analysis. We find that the three major gain peaks at 632, 621 and 609 nm correspond exactly to transitions A, B, and C observed in the emission (see Fig. 2). The left part of Fig. 3. shows the corresponding relative absorption change ($\Delta\alpha/\alpha$) in the spectral region around the excitation wavelength (555 nm) for zero time delay between pump and probe pulse. Absorption bleaching is ob-
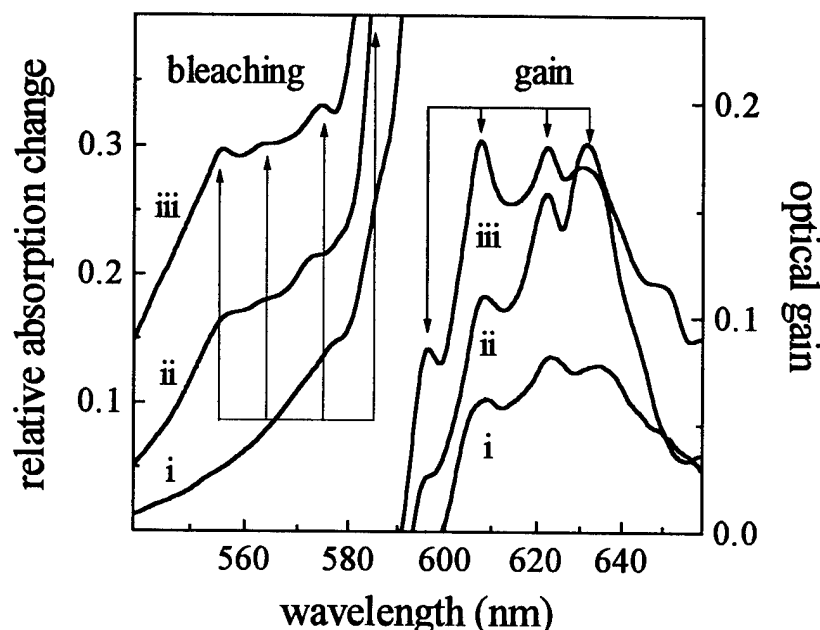
Fig.3 Relative absorption bleaching ($\Delta\alpha/\alpha_{lin}$) and net optical gain ($\Delta\alpha-\alpha_{lin}$) for 0.1, 0.4 and 1 mJ/cm² (i-iii) at zero time delay.

served in a broad spectral region that covers more than 180 meV around the excitation wavelength. Three different transitions can be distinguished in the energetic region below the excitation wavelength. Since their energy separation is identical to that of the levels observed in the optical gain and PL (see right part of Fig. 3., Fig.2), they can be assigned to the same energy levels. The energy shift between the transitions seen in absorption bleaching and those seen in the gain and emission spectra is always about 155 meV, the energy of the prominent phonon mode. We therefore attribute the large optical gain to exciton-phonon scattering processes. The gain at zero delay reveals very fast (< 150 fs) energy relaxation of at least part of the resonantly excited excitons at 555 nm into the energetically lower lying states. The relative bleaching is always largest at the exciton ground state (585 nm) and is larger for higher excitation (as high as 0.8). With increasing excitation the excited states become more and more occupied and the corresponding initial gain increases accordingly.

In conclusion, we have demonstrated spectral hole-burning in the absorption and gain region of the conjugated polymer BEH-PPV. Strong coupling of excitons to high-energy phonons (150 meV) results in high optical gain of up to 10^4 cm⁻¹ in a spectral region where the material is transparent. The lifetime of the gain corresponds to the density-dependent exciton lifetime.

References

[1] F. Hide et al., Science **273**, 1833 (1996).
[2] S. V. Frolov et al. Phys. Rev. Lett, **78, 729** (1997).
[3] Ch. Spiegelberg et al., submitted (1997)
[4] E. Harlev and F. Wudl, private communication

Molecular-Level Engineering of Polymer-Based Light-Emitting Devices

Michael Rubner
Massachusetts Institute of Technology

Molecular-level processing schemes have been utilized to fabricate light emitting thin film devices from a variety of materials including conjugated polymers and polymers containing tris-chelated Ru(II) complexes.

Optical Limiting

Thursday, October 16, 1997

A.F. Garito, University of Pennsylvania
Presider

ThA
8:45am-10:00am
Seaview A&B

"Optical Limiting and the Potential Role of Organic Materials"

Eric Van Stryland, Arthur Dogariu, Jin Hong Lim, David J. Hagan and Olga Przhonska
CREOL
P.O. Box 162700
University of Central Florida
Orlando, Florida 32816-2700

We will present a brief review of past work on passive sensor protection devices including the materials studied (e.g. semiconductors, organics and ink) and some of the requirements of optical limiting devices. The nonlinear mechanisms potentially useful for optical limiting include nonlinear absorption, nonlinear refraction and nonlinear scattering. We present methods for characterizing nonlinear materials using Z-scan and related techniques and describe ways to differentiate the nonlinear mechanisms. We will specifically discuss two-photon absorption and excited-state absorption (referred to as reverse-saturable absorption), as well as bound electronic n_2 and excited-state refraction. We also show how to examine organic thin films using a modified Z-scan with enhanced sensitivity called EZ-scan. The organic materials studied include phthalocyanine and polymethine dyes. The potential of organics for real optical systems remains to be seen. For example, the most promising organic limiting materials are effective over somewhat smaller spectral ranges than desired. Mixing of different materials in solution or solid matrices may extend the spectral range, and potentially extend the dynamic range as well.

Optical Limiting Mechanisms in a Neat Liquid Phthalocyanine Thin Film

Steven R. Flom, Richard G.S. Pong, James S. Shirk, F.J.Bartoli
Code 5613,Optical Sciences Division, (202) 767-3795
Arthur W. Snow
Code 6120, Chemistry Division
Naval Research Laboratory, Washington DC 20375

This paper describes some of the novel physical, photophysical, and optical properties of a new material, lead tetrakis-(β-ethyl-terminated-polyethyleneoxide)phthalocyanine (PbPc(β-PEO)$_4$). These novel properties were achieved by molecular engineering of the long polyethylene oxide (PEO) side chains. In the material described here, the PEO side chains are $O(CH_2CH_2O)_nCH_2CH_3$ and have an average molecular weight of 350 implying that n=7. PbPc(β-PEO)$_4$ is a viscous liquid in the pure form. It readily forms thin films of high optical quality by capillary action. By comparison, the usual unsubstituted phthalocyanine forms polycrystalline thin films that sublime only at temperatures above 400C. The feature of this material most important to our group is that this neat liquid maintains many of the photophysical properties of the phthalocyanine electronic system. Here we emphasize the physical properties that are useful for optical limiting applications.

As will be shown PbPc(β-PEO)$_4$ has the essential photophysical properties that a material must have to function as a low threshold limiting material based on reverse saturable absorption (RSA). First its excited state absorption cross sections exceed those of the ground state over a large portion of the visible spectrum. Second the ground state absorbs a sufficient proportion of the incident light energy to ensure population of the excited state. Third its excited state lifetime is comparable to or longer than the light pulse to be limited. Further, since it can be used for limiting as a pure material, it provides a high number density of active material within the a small focal volume typical of a low f/ number optical system. The nature of the side chains leads to the expectation of large volume thermal expansivities and thus strong variations of the refractive index with temperature which can lead to large thermal refractive contributions in an optical limiter.

The ground and excited stated cross sections are shown in figure 1. The ground state absorption cross sections, determined from the linear absorption spectrum, show no evidence of strong intermolecular interactions. The excited state cross sections were calculated from transient absorption spectra reported previously[1]. The
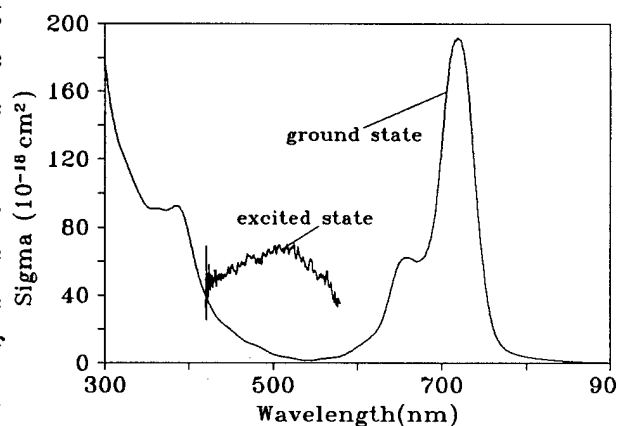

Figure 1 Ground and excited state absorption cross section for pure PbPc(β-PEO)$_4$.

excited state cross sections exceed the small ground state cross sections over a broad region of the visible spectrum satisfying the first two conditions for an RSA limiter. The decay of the transient absorption spectrum[1] indicates that the lifetime of the state responsible for the excited state cross sections is 9 ± 1 ns.

Figure 2 shows a log plot of the copolarized degenerate four-wave mixing data taken at a number of different excitation fluences. The traces have been normalized to one another at their peak for ease of comparison. The fluences used, listed in the inset to the figure, result in ~20% of the ground state molecules being excited at the highest fluence. Two qualitative features are immediately apparent. First, there is little decay of the signal again indicating a long lived excited state. Second, the traces are nearly super-imposable and demonstrate that fluence dependent processes such as exciton-exciton annihilation are unimportant in the excited state dynamics.

Figure 2 Copolarized DFWM signal for PbPc(β-PEO)$_4$ at differing excitation fluence.

Figure 3 shows the limiting performance of a thin cell of PbPc(β-PEO)$_4$. The solid squares are the result of collecting all of the light transmitted through the sample while the asterisks are data taken with an f/5 aperture in the collection optics. The f/0.8 collection optics demonstrate the limiting due only to the absorptive part of the limiting mechanism. With an aperture included in the collection optics the limiting performance is significantly better. This is a result of the both the excited state refractive response as well as the thermal mechanisms. Also shown as pluses in the figure is the "Encircled energy" which is an indication of how well the light can be refocused after passing through the limiter. A four level model of the limiting response using the parameters determined above fits the initial part of the limiting curve very well. However, at higher fluences, the nonlinear absorption from a four level model saturates and is a poor predictor of the limiting. Additional mechanisms are contributing to the limiting at high fluence.

Figure 3 Log-log plot of the relative transmission of PbPc(β-PEO)$_4$ at 532 nm

The mechanism responsible for the high fluence limiting is attributed to the absorption and scattering due to optical breakdown and subsequent plasma formation. Separately we have shown

that thin films of PbPc(β-PEO)$_4$ exhibit a photovoltaic effect and photoconductivity.[2] Further, pure PbPc(β-PEO)$_4$ samples showed clear evidence of optical breakdown at moderate fluence. The observed photovoltage saturated and there was a drop in the electrical resistance of the sample. When the incident energy exceeded 100-200 nJ, corresponding to peak incident fluences of about 1 J/cm^2 on the PbPc(β-PEO)$_4$ film, broad band light emission from a plasma could be seen visually from the sample. The threshold for the optical breakdown, on the order of 0.5 to 1 J/cm^2, is comparable to the observed threshold for optical breakdown in a carbon black suspensions. The threshold for laser induced electric breakdown in any dielectric material is lowered by the presence of charge. The available electrons initiate the electron avalanche ionization.[3] In PbPc(β-PEO)$_4$ the low threshold for breakdown is apparently due photo produced charge in this material.

In conclusion, these experiments show that an f/5 limiter using a pure thin film of PbPc(β-PEO)$_4$ possesses a low limiting threshold and a substantial dynamic range. The observed limiting threshold is almost as low as that observed for the best RSA limiters. This material is a strong nonlinear absorber that also possesses a large thermal contribution to the limiting and the *potential* to be self healing. In previous phthalocyanine limiters, high fluence limiting is aided both by higher excited states and by thermally induced lensing. Here the high fluence limiting is enhanced through optical breakdown. The subsequent plasma formation leads to scattering centers that absorb and scatter the light, in analogy with the dominant limiting mechanism in carbon black suspension limiters.[4] PbPc(β-PEO)$_4$ is the first material to exhibit RSA and photoconductivity that leads to plasma formation at low fluences.

<u>References</u>

1. S.R. Flom, R.G.S. Pong, J.S. Shirk, F.J. Bartoli, R.F. Cozzens, M.E. Boyle and A.W. Snow "Optical Limiting in Phthalocyanine Solutions and In Pure Liquid Phthalocyanines" *Proc.Mat. Res. Soc.* (in press).

2. R.G.S. Pong, J.S. Shirk, S.R. Flom, A.W. Snow, "Limiting Mechanisms in a Photoconducting Liquid Phthalocyanine" *Proc. Mat. Res. Soc.* (in press).

3. C. Sacchi; *J. Opt. Soc. Am. B* **8**, 337 (1990) and references therein.

4. K. Mansour, M.J. Soileau, E.W. Van Stryland; *J. Opt. Soc. Am. B* **9**, 1100 (1992).

Nonlinear Spectroscopy and Applications of Two-Photon Absorbing Molecules

J. Ehrlich†, A. Heikal§, Z.-Y. Hu§, I.-Y. S. Lee§, S. R. Marder†§, J. W. Perry†§, H. Röckel§ and X. L. Wu§

† Jet Propulsion Laboratory, California Institute of Technology, Pasadena, CA 91109

§ Beckman Institute, California Institute of Technology, Pasadena, CA 91125

Molecules exhibiting strong two-photon absorption hold great potential for a wide range of applications including: two-photon fluorescence microscopy , three-dimensional (3D) optical data storage, 3D microfabrication, and optical limiting. (1-4) From a fundamental point of view, knowledge of molecular two-photon spectra and structure/property relationships are also important for a more complete understanding of the third order polarizabilities of conjugated molecules. However, very little is known or understood about two-photon states and spectra of conjugated molecules or how they correlate with structure. We have observed large two-photon absorptivities in bis-donor diphenylpolyene derivatives, that appears to be correlated to simultaneous charge transfer from the end groups to the pi-conjugated bridge in the molecule. These molecules are also excellent photoexcitable electron donors that can initiate charge-transfer reactions. In initial applications of these materials we have demonstrated their use in two-photon initiation of polymerization and optical limiting.

Measurements of the dispersion of the nonlinear absorption for bis-donor diphenylpolyenes of varying polyene length and with dialkylamino or diphenylamino end-groups have been performed using nanosecond and picosecond pulses. On the nanosecond timescale the effective two-photon absorptivity (TPA) for these molecule is exceptionally large, on the order of 1 x 10-46 cm4 s/photon, which is over an order of magnitude larger than for the dye Rhodamine B. (5) On the picosecond time scale the effective TPAs are on the order of 2 - 3 x 10-48 cm4 s/photon, which is still large relative to most commonly used two-photon fluorophores. These results indicate that a dynamic nonlinear absorption process is taking place, consistent with two-photon induced excited-state absorption.

Motivated by the large nonlinear absorptivities observed, we have investigated the optical limiting performance of bis-donor stilbenes and diphenylpolyenes. Significant optical limiting is observed for a bis-donor stilbene for 5-ns, 600-nm pulses. (6) The strong optical limiting by two-photon absorption in this material is particularly interesting because the linear transmission is very high, > 95%, for the samples employed. We have observed that on going from bis(dialkylamino) to bis(diphenylamino) stilbene that the TPA shifts to the red by ~90 nm, while the one photon absorption shifts only by ~15 nm. A mixture of the two compounds exhibits broadband nonlinear absorption and high linear transmission. Thus, these molecules hold potential as broadly transparent two-photon optical limiting materials. Two-photon initiated polymerization holds tremendous promise for ultrahigh density optical memory and 3D microfabrication. (2) One can selectively polymerize very small volumes of polymer near the focus of a laser beam, thus creating a change in refractive index and permitting data storage densities of 1012 bits/cm³. The bis-donor diphenylpolyenes are excellent electron donors and we have shown that upon excitation they are able to initiate polymerization of acrylate monomers and multifunctional acrylates. These materials have allowed us to develop a new class of two-photon photopolymers, that have high writing speed as a result of their large two-photon absorptivity. The two-photon photopolymer blends are composed of a two-photon absorbing initiator, a crosslinkable monomer, and a polymer binder. Using such two-photon photopolymers, we have written micrometer dimension crosslinked polymer spots in two- and three-dimensional patterns. We have also utilized these two-photon photopolymers for the fabrication of photonic bandgap-like periodic three-dimensional polymer microstructures.

References
(1) W. Denk, J. H. Strickler, and W. W. Webb, Science, 248, 73 (1990).
(2) J. Strickler and W. W. Webb, Optics Lett., 16(22), 1780 (1991).
(3) G. S. He, R. Gvishi, P. N. Prasad and B. Rhinehardt, Opt. Commun., 117, 133 (1995).
(4) J. D. Bhawalkar, G. S. He, Chi-Kyun park, C. F. Zhao, G.Ruland, and P. N. Prasad, Opt. Commun., 124, 33-37 (1996).
(5) C. Xu and W. Webb, J. Opt. Soc. Am. B, 13, 481 (1996).
(6) J. E. Ehrlich, X.-L. Wu, I.-Y. S. Lee, Z-.-Y. Hu, S. R. Marder, and J. W. Perry, Optics Lett., submitted.

Polymer Optical Fibers

Thursday, October 16, 1997

Robert A. Norwood, AlliedSignal Inc.
Presider

ThB
10:30am-12:00m
Seaview A&B

Mode Coupling Effects in Plastic Optical Fibers

G. Jiang, R.F. Shi, and A.F. Garito, Department of Physics and Astronomy, University of Pennsylvania, Philadelphia, PA 19104, (215)898-7938

In optical fibers for data transmission applications, a most important characteristic along with total attenuation is the optical bandwidth that defines the limit of information carrying capacity.[1] Besides compensation for modal dispersion through a parabola-like graded index profile, mode coupling is a mechanism important to increased fiber bandwidth performance. Mode coupling changes the length dependence of the bandwidth, or equivalently, the inverse pulse broadening, from linear to square root behavior, usually through extrinsic features which might include micro bends, diameter variations, micro voids, cracks etc. In this paper, we report the observations of mode coupling effects in plastic optical fibers (POFs) using time-domain bandwidth measurements of high quality step index (SI) POF.[2-4] Our results are directly verified by independent measurements of the far-field radiation patterns.

The fiber used in our experiment was ESKA Premier GH 4001P (Mitsubishi Rayon Co., Ltd.). Measurements were first performed to establish the fiber length dependence of the pulse broadening by focusing input light into the fiber by using one of four micro objectives (5X, 0.12 NA; 10X, 0.25 NA; 20X, 0.40 NA; and 40X, 0.65 NA), which provide a source with controllable launch numerical aperture (NA).
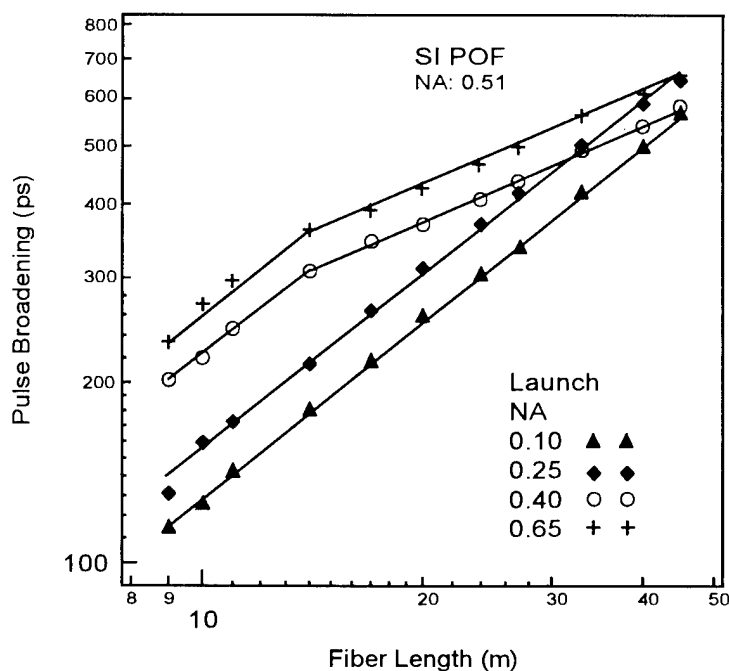
Fig. 1. Log-log plot of output pulse width as a function of fiber length with launch numerical aperture (NA) as parameter.

Fig. 1 shows the log-log plot of the optical pulse broadening (σ) versus the fiber length (L). A fit of the pulse broadening (σ) to the following relation

$$\sigma \propto L^{\alpha} \qquad (1)$$

shows that $\alpha = 0.99 \pm 0.01$ for NA = 0.12 and $\alpha = 0.97 \pm 0.02$ for NA = 0.25. These results indicate that for under-filled launching cases, the pulse broadening is nearly a linear function of the fiber length. More importantly, when the light is coupled into the fiber using a high NA microscope objective, the pulse broadening clearly shows two distinct regions. In the first region, a fit to Eq. (1) yields $\alpha = 0.97 \pm 0.03$ for NA = 0.40 and $\alpha = 0.96 \pm 0.10$ for NA = 0.65. In the second region, the pulse broadening slows down significantly, with the fit producing $\alpha = 0.54 \pm 0.01$ for NA = 0.40 and $\alpha = 0.57 \pm 0.01$ for NA = 0.65.

A diffusion theory of mode coupling in an optical fiber has been established by Gloge[5]. The theory predicts that after light travels a certain fiber distance, or coupling length, mode coupling is complete, and equilibrium mode distribution (EMD) is established. Correspondingly, the optical pulse broadening changes from being linearly proportional to the fiber length ($\alpha = 1$) to varying as the square root of the length ($\alpha = 0.5$). Our results clearly demonstrate good agreement between diffusion theory and experiment. In addition, our measurement indicates that the coupling length is around 15 to 20 m. The much shorter coupling length compared to glass optical fibers (GOFs) which have a typical coupling length of several kilometers[6] shows that mode coupling is much more significant in POFs than in GOFs.

We also carried out far-field radiation pattern measurements[7] to study mode coupling effects under different launching conditions. Fig. 2 shows angular scans of the far-field intensity under a variety of launch conditions.

(a)   (b)

Fig. 2. Far-field radiation patterns from a 30m-long POF under (a) low NA launch conditions: launch NA=0.12, (b) high NA launch conditions: launch NA=0.4.

For each experiment, light was launched into a 30 m-long SI POF at an angle with respect to the fiber axis of from 0 to 25 degrees in 5 degree increments. In Fig. 2 (a), the light was launche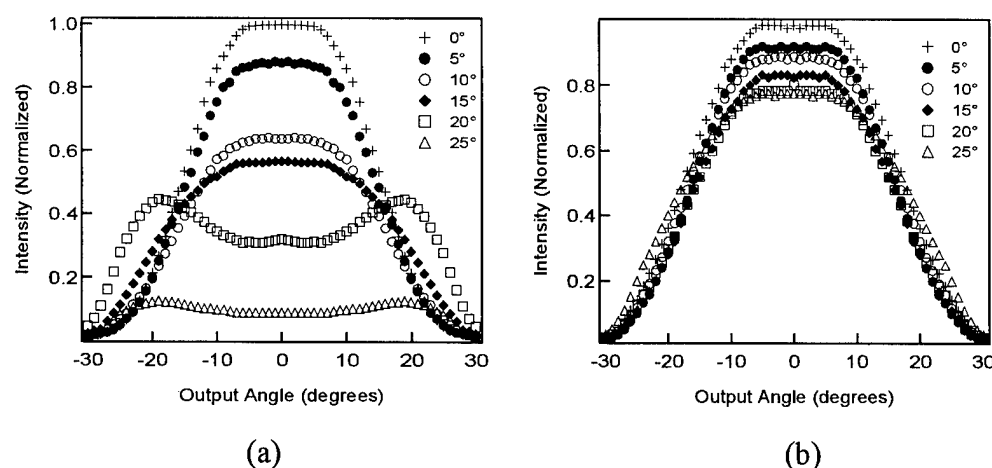d into the fiber using a low NA (0.12) microscope objective. We can clearly see that the far-field pattern changes from being a disk to a ring when the incidence angle exceeds 20°, suggesting that only a group of high order modes is excited. This finding is in agreement with our previous observation in the time domain bandwidth measurements that mode coupling is far from being complete. In contrast, as can be seen in Fig. 2 (b), when the input laser light was launched into the fiber with a high NA (0.40) microscope objective, the output distribution consists of a disk that is essentially independent of the launch angle. This behavior demonstrates that the mode coupling is complete and the EMD condition is achieved.

In summary, we have observed mode coupling effects in high quality SI POFs with its characteristic change over in the dependence of the pulse broadening on fiber length from linear to square root behavior. The EMD condition can readily be achieved in SI POFs at lengths (~15-20m) much shorter than in GOFs. Our results were directly verified by independent measurements of the far field radiation patterns under different launching conditions.

References:

[1]. Paul E. Green, Jr. "Optical networking update," *IEEE J. Select. Areas Commun.* **14**, 764 (1996).

[2]. R.F. Shi, W.D. Chen, and A.F. Garito, "Measurements of graded-index plastic optical fibers," *Proc. Fourth International Conference on Plastic Optical Fibers and Applications*, 1995, pp. 59-62.

[3]. W.D. Chen, "High speed plastic optical fibers for data communications," Ph. D. dissertation, University of Pennsylvania, Philadelphia, PA (1996)

[4]. G. Jiang, R.F. Shi, and A.F. Garito, "Mode coupling and equilibrium mode distribution conditions in plastic optical fibers," *IEEE Photonics Technology Letters*, (In press).

[5]. D. Gloge, "Optical power flow in multimode fibers," *Bell Syst. Tech. J.*, 1972, **51**, pp. 1767-1783.

[6]. E.L. Chinnock, L.G. Cohen, R.D. Standley, and D.B. Keck, "The length dependence of pulse spreading in the CGW-Bell-10 optical fiber," *Proc. IEEE Lett.*, 1973, **61**, pp. 1499-1450.

[7]. W.A. Gambling, D.N. Payne, and H. Matsumura, "Mode conversion coefficients in optical fiber," *App. Opt.*, 1975, **14**, pp. 1538-1542.

High Speed Polymer Optical Fiber and Related Photonics Polymer

Yasuhiro Koike

[1]Faculty of Science and Technology, Keio University

[2]Kanagawa Academy of Science and Technology

[1]3-14-1, Hiyoshi, Kohoku-ku, Yokohama 223 Japan

[2]1-1-1, Fukuura, Kanazawa-ku, Yokohama 236 Japan

With the growing interest focused on the broadband network systems, optical fiber network for high speed telecommunication becomes more important in the premise network area. Silica base single mode fiber is an ideal medium for long distance communication because of its high transparency and high bandwidth, while its much low attenuation is minor advantage in the short distance network. As many data distributions and fiber connections are required in the premises wiring and LANs, low coupling and distribution losses must be maintained. Therefore, we have proposed a large-core, high-bandwidth graded-index polymer optical fiber (GI POF) for high speed data "transmission" medium, and we succeeded in several gigabit transmission in 100 m GI POF link. However, as the GI POF was composed of poly methyl methacrylate (PMMA), its high attenuation of transmission limited the GI POF link length to approximately 100 m. Recently we proposed the low-loss perfluorinated (PF) polymer base GI POF which enables more than 300-m transmission with maintaining high data rate.

Perfluorinated polymer provided great advantage in the infrastructure of the POF network. Low intrinsic absorption loss of the PF polymer enabled the dramatic decrease in the attenuation of GI POF that is as low as 50 dB/km at 1.3-μm wavelength. The theoretical attenuation limit of the PF polymer base POF was estimated by the aspects of intrinsic scattering and absorption losses. The minimum attenuation of 0.3 dB/km of the PF polymer base GI POF indicates that the POF link is possible to cover several kilometers without repeaters. With increasing the link length, the pulse distortion due to the material dispersion comes to limit the bit rate of POF link. It was clarified that the low material dispersion of the PF polymer compared with PMMA and silica allows more than 10 Gb/s transmission even in 1 km link.

Furthermore, no modal noise effect was observed even when 200-μm misalignment was occurred at the fiber-to-fiber coupling because a large number of modes are transmitted in the large core GI POF.

Polymer Thin Film Overlays for Passive Side Polished Fiber Devices

S. G. Lee, J. P. Sokoloff, and H. Sasabe

Frontier Research Program,

The Institute of Chemical and Physical Research (RIKEN)

2-1 Hirosawa, Wako-shi, Saitama 351-01, Japan

Corresponding author: Sang Goo Lee (+81) 48-462-1111 ext 6324

Side polished fibers (SPF) are interesting devices because they represent a method of altering a light wave's amplitude or phase as it travels in an optical fiber. This eliminates many of the practical problems associated with fiber-optic devices made up of components, such as the optical mode-mismatches and losses resulting from "pigtailing" an optical fiber to a non-fiber device component. In SPFs a portion (~1 mm in length) of the fiber clad is polished away permitting the light wave to interact with an overlay material placed on the polished area. A variety of overlays have been used with SPFs to make both passive and active SPF devices. [1]

Polymer thin films can also be used as SPF overlays. This paper investigates several common host polymers to determine their suitability as SPF overlays. Introducing a guest dopant into the overlay, which can have its optical properties modified in a controlled way by either a light or electric field, is a way to add additional functionality to an otherwise totally passive device. We examine and model several candidate host materials, and characterize their behavior when used as a SPF overlay. These overlays are found to have spectral responses useful for several passive devices even when undoped.

Side polished fibers were made by standard techniques. Single mode fiber for 820 nm was stripped of the outer coating, glued into grooved quartz blocks with approximately 15 cm radius of curvature, and polished successively on 3 μm, 1 μm and 0.5 μm polishing pads. Films were applied using a "decal deposition" technique: manually applying the film to the SPF overlay region in such a way as to minimize the air gap between the film and SPF surface.

Investigation of two common polymer hosts are reported here: polystyrene (PS, $n_D = 1.59 \sim 1.592$) and polyvinyl carbazole (PVK, $n_D = 1.683$), These polymers were chosen because of their good film forming qualities, low scattering and absorption in the visible and near-infrared, and refractive index values. The basic measurement used to characterize these polymers behavior as overlays, was a white light transmission

measurement. Figure 1a and 2a shows the normalized SPF response to a white light input source, when each film was used as an overlay. These narrow linewidth responses, are desirable for multiwavelength systems, as this linewidth can limit the wavelength density of the system. However, while the PS film shows very little, if any, TE-TM mode splitting, this is not true of the PVK spectrum. This is due to a large refractive index birefringence in the PVK film which results in very noticeable TE-TM mode splitting, even at the higher modes. From a device viewpoint, PS is an appropriate overlay to use for a channel dropping filter, as it results in a polarization independent filter with narrow resonances, while the PVK overlay has the narrow, well separated TE and TM responses required of an SPF polarizer.[2]
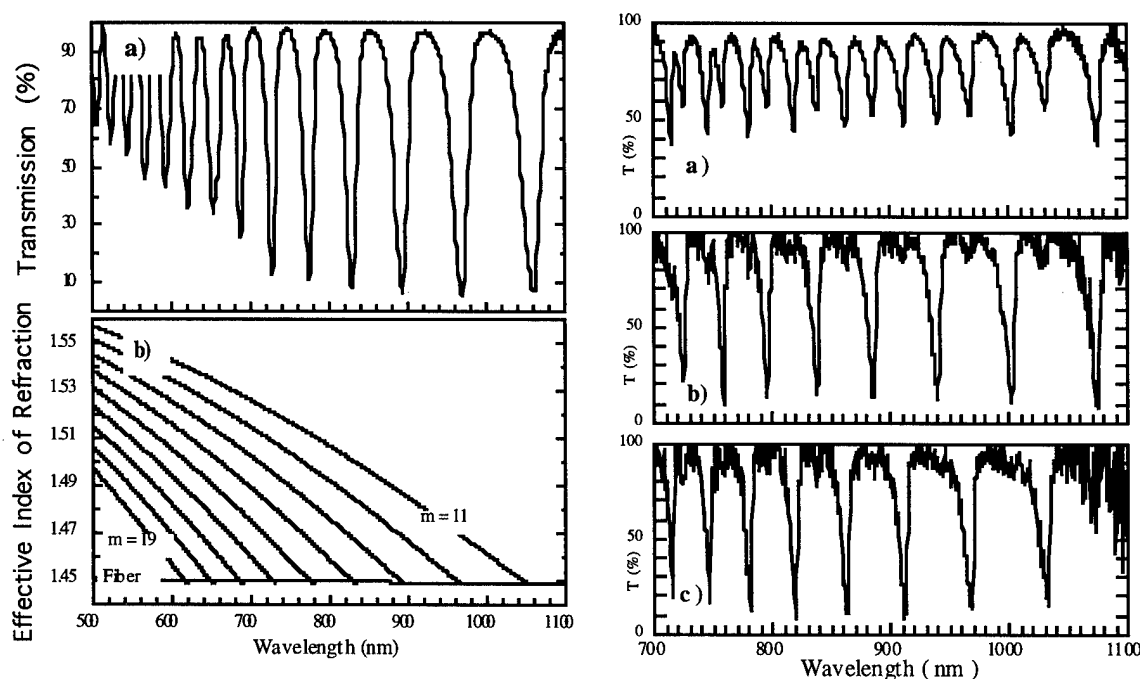
Figure 1: a) Channel dropping response of a SPF with a polystyrene film overlay (9.02 μm). b) the dispersion curves of the "asymmetric slab waveguide" polystyrene film (TE mode), and the single mode fiber (LP$_{01}$ mode). Crossing points represent theoretical channel dropping resonance wavelengths.

Figure 2: Transmission spectra of CD SPF with 8.92 μm thick PVK overlay. a) is the transmission spectrum without an analyzer. b) and c) are the TE and TM mode resonance spectrum, respectively, as selected through an analyzer.

The spectral positions of the CD resonances in figure 1a can be understood by modelling the SPF-overlay system as two weakly coupled waveguides. In this model the overlay is considered a slab waveguide which interacts strongly with the single mode in

the fiber only at wavelengths where the modal effective indices (propagation constants) of these isolated two waveguiding systems are the same. In figure 1b we plot the dispersion curves of the single mode fiber, and a 9.10 μm thick multimode slab waveguide. Coupling of light from the fiber to the planar waveguide occurs at wavelengths where the dispersion curves of the two systems cross. There is good agreement between the resonance wavelengths of figure 1a, and the crossing points in Fig. 1b. Thus the model can be used as a guide in determining what thickness an overlay of given refractive index should be used to position a CD filter at a desired wavelength.

Figures 2b and 2c show the polarizing properties of the PVK film in detail. As the light passes through the SPF certain wavelengths resonantly couple to the overlay film and do not return to the fiber. Light exiting the SPF polarizer at a wavelength resonant with a TE mode of the film is polarized perpendicular to the plane of the film. Setting an analyzer to block this light shows the TE spectrum. Similarly at TM resonant wavelengths exiting light is polarized parallel to the plane of the film, and setting an analyzer to block this light shows the TM spectrum. Polarization contrast ratios exceeding 20 dB, and limited by our measurement setup, were found in this way. By fitting these data to our model we determined in-plane and perpendicular-to-the-plane refractive index values of 1.681 and 1.7037, repectively.

In conclusion, we have demonstrated that several host polymers, fabricated by spin coating and applied using a simple decal deposition technique, can be used as SPF overlays to produce passive devices with good throughputs and high contrast ratios. The main motivation for examining polymer hosts is so that those which function well can be doped with appropriate "guest" molecules and used as the overlay in active devices.

References
1. See references in S.G. Lee, J.P. Sokoloff, B.P. McGinnis, and H. Sasabe, " Polymer Waveguide Overlays for Side-Polished Fiber Devices", submitted for publication, Applied Optics.
2. S.G. Lee, J.P. Sokoloff, B.P. McGinnis, and H. Sasabe, " Fabrication of a SPF Polarizer using a Birefringent Polymer Overlay", Opt. Lett. 22(9), 1 (1997).

Plastic Optical Fibers; Yesterday, Today, and Tomorrow

Toshikuni Kaino

Tohoku University, Institute for Chemical Reaction Science

2-1-1 Katahira, Aoba-ku, Sendai, Miyagi, 980-77 Japan, Tel: +81-22-217-5668

1. Introduction

Plastic optical fibers (POF for short) is one of the attractive optical information transmission medium because of their handling ease with their good ductility, splicing ease to each other and to light sources with their large fiber diameter and high numerical aperture. In this paper, the potential of POFs for practical applications will be discussed.

2. Yesterday: Lowering the optical loss of POF

In the past, lowering the optical loss of POF was main issue and deuteration and/or fluorination technologies were effectively applied. In the mid 1970s, DuPont reported POF using poly(methyl methacrylate) (PMMA) as a core of the fiber with a loss below 300 dB/km at 567 nm wavelength[1]. POF loss was significantly reduced around 1983 and the lowest transmission loss is 55 dB/km at 568 nm[2] and 114 dB/km at 670 nm[3] for PMMA core and PS core POFs, respectively. Up to now, commercially available PMMA core optical fiber losses are around 60 dB/km at 568 nm wavelength.

Among intrinsic loss in the core materials, high harmonics caused by vibrational absorption at the infrared region due to carbon-hydrogen (CH) bonds have the most influence. If the reduced mass of the atom-pair were increased by replacing hydrogen with a more massive atom, the wavelengths of the fundamental vibration and subsequent harmonics would be shifted to longer wavelength region. To lower CH vibrational absorption in the core polymer, deuterium (D) was selected. DuPont showed that the minimum loss could be reduced below 200 dB/km at an increased wavelength of 790 nm by using deuterated PMMA [P(MMA-d8)][1]. The lowest attenuation loss of the P(MMA-d8) core POF fabricated to date, 20 dB/km, was attained from 650 to 680 nm wavelengths[4]. This POF has other optical windows at 780 and 850 nm where 25 dB/km and 50 dB/km losses were attained, respectively.

The possibility had been investigated whether the substitution of hydrogen atoms by fluorine (F) atoms effective to lower attenuation loss for POF. Fluorination is a trivial method to obtain low loss materials. Groh had reported precisely the halogenation effect to shift the absorption wavelength in a longer wavelength region[5]. This shift would allow the use of POF at even longer wavelengths optical windows than that obtained with deuterium substitution. In the first stage, attention has been focused on fluorinated analogues of PMMA. Since it is possible that the polymerization may become difficult if the aliphatic hydrogen of vinyl monomer are replaced by F, it is better to use deuterium D. Thus, pentafluoro-trideutero-styrene, 5F3DSt, polymer was examined as a core for fabricating low loss POF. In 850 nm region, an attenuation loss of 174 dB/km was obtained[6]. Perfluorinated

polymer, perfluoro(alkenyl vinyl ether), CYTOP, was applied as a core of POF[7]. Loss around 60 dB/km at 1.3 μm wavelength was fabricated using the polymer.

Interest in deuterated and/or fluorinated polymers is limited because the raw materials are expensive. For practical applications, problem is the cost of the these polymer core POFs.

3. Today: POF transmission bandwidth

The transmission bandwidth of POFs is important because the application area of POF local area network system or optical interconnection system is influenced by the fiber bandwidth[8]. Signal dispersion of the fiber determines the bandwidth. For step-index (SI) POF, transmission bandwidth is mainly decided by the mode dispersion which result from the difference in propagation time between different modes within the fiber. Considering only the mode dispersion, transmission bandwidth (B) is expressed as follows;

$$B = 0.4 c_0 / L n_1 [(n_2/n_1)-1] \quad \text{(MHz)} \quad \quad (1)$$

where L is the fiber length, c_0 is the vacuum speed of light (m/s), n_1 and n_2 are refractive indices for core polymer and cladding polymer, respectively. By decreasing the NA of the fiber or of the launched light, the dispersion can be reduced. By reducing the POF NA around 0.3, bandwidth of 200 MHz is possible in a commercial base 100 m length POF[9] and over 170 MHz was reported for a 19 multi-core POF with 0.25 NA and 100 m length[10].

In a GI fiber, the refractive index varies radially and hence increases the signal bandwidth. For manufacturing GI-POFs, Ohtsuka's group, Keio University, had fabricated the GI-POF using an interfacial-gel copolymerization technique[11]. In this method, two monomer mixtures, MMA and vinyl phenyl acetate or MMA and vinyl benzoate, for example, with different refractive indices are placed in a transparent PMMA tube and co-polymerized from the tube inner wall to the center axis. A 500 μm-core GI-POF was prepared by heat drawing of the co-polymerized rod and the loss of it at 652 nm was 134 dB/km.

Interests for the use of GI-POF are ignited by reports from Koike's group, Keio University[12]. This GI-POF uses an interfacial-gel polymerization technique. The technique is the method where bromobenzene or other chemicals is used as unreactive component instead of vinyl phenyl acetate or vinyl benzoate in the interfacial-gel copolymerization method. Attenuation loss of 90 dB/km at 572 nm was obtained. MMA-d8 and fluorinated acrylate monomers were also used instead of MMA and an attenuation loss of 113 dB/km and 155 dB/km at 780 nm wavelength were obtained for deuterated POF and fluorinated one, respectively[13]. Recently, perfluoro(alkenyl vinyl ether) was applied as a core of GI-POF[7]. Details of the POF will be discussed in the other presentation of this conference.

The transmission speed of 100-meter length, 420 μm diameter core and 0.21 NA PMMA core GI-POF was revealed to be higher than 2.5 Gbit/s using a 647 nm wavelength laser diode and a Si-PIN photo diode with 400 μm diameter[14]. In this case, sharp eye pattern was detected without detectable noises. For 100-meter PMMA core SI-POF with 980 μm diameter core and 0.5 NA, transmission speed of 250 Mbit/s was too high to detect the eye pattern clearly when the same measurement system was used for bandwidth estimation.

4. Tomorrow: Use of short-wavelength optical windows of POF

In the near-future, the point to open new fields for POF applications will be the use of short-wavelength optical sources. Assuming a maximum transmission length of 400 meters and a system budget of 25 dB with 5 dB margin, we have a target POF attenuation of 50 dB/km, which was already attained using P(MMA-d8). For practical application of POF with realistic material cost and reliability, though, we should use standard polymers, i.e., not the deuterated and/or fluorinated polymers. The 50 dB/km can be achieved using conventional PMMA core POF because 68 dB/km at 518 nm and 60 dB/km at 567 nm have already been attained in a commercially available POF and estimated loss limits are 37 dB/km and 35 dB/km at 516 nm and 567 nm, respectively. The development of optical sources capable of operating in this wavelength optical windows will certainly be stimulated by the prospect of high volume sales. Several research results were reported about the use of optical sources in a 567 nm region. InGaAlP LED was used to transmit optical signal up to 110 meters with 10 Mbit/s operation. Output power of the LED, though, is not sufficient enough to transmit optical signals longer than 150 meters.

We have preliminary examined to use POF optical window near at 518 nm wavelength because there exist several possible optical sources such as InGaN or ZnCdSe LEDs and SHG from nonlinear optical crystals using laser diodes as an optical pump light at around 1.0 μm wavelength. We have used a green laser pointer as a simple optical source which generates about 1 mW output power 532 nm SHG light from LD pumped YAG laser. Measuring several POFs, we can expect to transmit optical signals longer than 200 meters with the minimum detectable optical power of 22 to 23 dBm which permit to transmit optical signals faster than 100 Mbit/s. By reducing the loss of the POF to around 50 dB/km, it is possible to transmit optical signal up to 400 meters using optical sources emitted around 520 nm wavelength region.

5. Conclusion

In this paper, lowering the optical loss of POF through deuteration and/or fluorination of hydrogen, increment of POF bandwidth, and lengthening POF transmission distance using green light are discussed. Considering the realistic application and reliability of POFs including acceptable price and transmission length, we have proposed the use of short wavelength optical window of POF which located near 518 nm wavelength. This region is promising for future POF signal transmission system with distance around 400 meters.

[1] Schleinitz, M. H., , Int. Wire & Cable Symp., 26, 352, 1977   [2] Kaino,T., et al, Appl. Opt., 20, 2886, 1981

[3] Kaino, T., in Polymers for lightwave and integrated optics, Hornak, L. A., Ed., Mercel Dekker, New York, 1992, Chap.1. [4] Kaino,T., et al, Appl. Phys. Lett. 42, 567, 1983   [5] Groh, W., Makromol. Chem., 189, 2861, 1988

[6] Kaino, T., Appl. Phys. Lett., 48, 757, 1986   [7] Koike, Y., Proc. Symp. New trends of Advanced Mat. Polym, Opt. Fiber., p21, 1995   [8] Bates,R., et al, Fiber and Integrated Optics, 12, 199, 1993   [9] Takahashi, S., et al, POF '94 Proceeding, 147, 1994   [10] Munekuni, H., et al, POF '94 Proceeding, 148, 1994   [11] Ohtsuka, Y., et al, Appl. Phys. Lett., 57, 120, 1990   [12] Koike, Y., Polymer., 32, 1737 (1991)   [13] Ishigure, T., et al, CLEO Europe '94, Proceeding, CThD5, 1994   [14] Yamazaki, Y., et al, ECOC '94   Post Deadline Paper, 1994

Electro-Optic Materials

Thursday, October 16, 1997

Carl Dirk, University of Texas at El Paso
Presider

ThC
1:30pm–3:00pm
Seaview A&B

Noncentrosymmetric Ionically Self-Assembled Thin Films
for Second Order Nonlinear Optics

J.R. Heflin[1], Y. Liu[2], C. Figura[1], D. Marciu[1], and R.O. Claus[2]

[1]*Department of Physics, Virginia Tech, Blacksburg, VA 24061-0435*

[2]*Department of Electrical Engineering, Virginia Tech, Blacksburg, VA 24061-0356*

Ionic self-assembled monolayers (ISAMs) are a recently developed [1], revolutionary class of materials that allows detailed structural control at the molecular level combined with ease of manufacturing and low cost. The ISAM method involves the alternate dipping of a charged substrate into an aqueous solution of a cation followed by dipping in an aqueous solution of an anion at room temperature. Since the adsorption is based on the electrostatic attraction of interlayer charges, each layer is self-limiting in thickness and uniform at the molecular level. We have recently demonstrated through second harmonic generation (SHG) measurements with fundamental wavelengths of 1064 and 1200 nm that the ISAM technique can produce a noncentrosymmetric arrangement of NLO chromophores to yield thin films with $\chi^{(2)}$ values comparable to that of quartz. The development of ISAM $\chi^{(2)}$ thin films provides significant advantages over the production of organic $\chi^{(2)}$ thin films by alternative methods. For example, ISAM films can exhibit long-term stability of $\chi^{(2)}$ in contrast to electric field poling of glassy polymers[2], can provide thicker films (upwards of 10 µm) than the Langmuir-Blodgett technique, and can be fabricated much more rapidly than covalent self-assembly[3] methods.

The noncentrosymmetric, ISAM $\chi^{(2)}$ films were produced using the polymeric dye Poly S-119, which consists of a poly(vinylamine) backbone with an ionic azo dye chromophore and was purchased from Sigma. Poly S-119 served as the polyanion for the ISAM fabrication while poly(allylamine) hydrochloride (PAH), which has no $\chi^{(2)}$ response, was used for the polycation. The ISAM fabrication technique simply involves immersion of a charged substrate into an aqueous solution of the opposite charge polyion followed by rinsing and immersion in a polyion solution which has a charge opposite to the first. The formation of the monolayers occurs by electrostatic attraction between the oppositely charged polyions. The process is repeated until a film with the desired number of bilayers has been produced. We have found that the formation of each monolayer occurs in less than one minute of immersion in the polyelectrolyte, thus allowing the rapid buildup of self-assembled, multilayer films. Furthermore, our results have demonstrated that the strong internal electric fields of the ionic layers leads to alignment of polar NLO chromophores, and the resulting noncentrosymmetric films possess a substantial $\chi^{(2)}$.

Figure 1 shows the absorption spectrum of an ISAM film with 68 bilayers of Poly S-119/PAH deposited on a single side of the glass substrate. The film is orange in color and exhibits exceptional homogeneity and lack of scattering. For this study, we have fabricated a Poly S-119/PAH ISAM film with 40 bilayers deposited on both sides of the substrate and films of 28 and 68 bilayers which have had the film removed from one side of the substrate by polishing. (The ISAM films are highly resistant to organic solvents and are extremely robust both mechanically and thermally.) In Figure 2, the absorbance of the three samples at 500 nm is plotted versus the number of bilayers. The linear growth of absorbance with the number of layers illustrates the homogeneous deposition of the polymer dye with each successive layer. We have previously prepared ISAM films of other materials consisting of greater than one thousand bilayers and anticipate no difficulty in scaling to greater than ten thousand bilayers, for a total film thickness of more than ten microns.
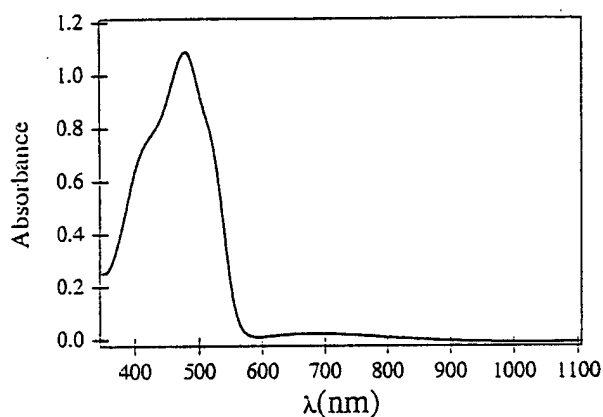
Figure 1. Absorption spectrum of an ISAM film with 68 bilayers deposited on a single side of a glass substrate.
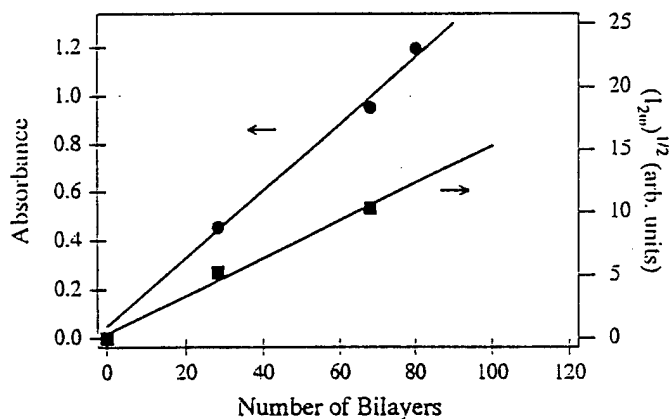
Figure 2. Absorbance at 500 nm (circles) and square root of the second harmonic intensity at 600 nm (squares) for the ISAM films as a function of the number of total bilayers.

The SHG experiments were carried out using both the 1064 nm fundamental wavelength of a Q-switched Nd:YAG laser and the 1200 nm output from a broadband, BBO optical parametric oscillator (OPO). The OPO is pumped by the 355 nm third harmonic of the Nd:YAG and is continuously tunable from 400 to 2500 nm. The 504 nm OPO signal beam is removed from the 1200 nm idler beam using a 700 nm long-pass filter. The incident intensity and polarization on the sample are controlled by a pair of Glan-Laser polarizing prisms. The fundamental beam is weakly focused onto the sample and a 532 or 600 nm spike filter is employed to ensure that the photomultiplier tube measures only the intensity of the second harmonic light. The incident fundamental intensity into the sample is measured using a beamsplitter and photodiode.

Since the films are strongly absorbing at 532 nm, we concentrate here primarily on the measurements using the 1200 nm fundamental wavelength. Figure 3 illustrates the dependence of the SHG signal intensity as a function of the incident fundamental intensity for the single-sided, 68 bilayer ISAM film. The film is rotated 45° away from normal incidence about the vertical axis, and the incident light is p-polarized. The solid curve is a best fit to the data of the form $I_{2\omega} = A(I_\omega)^b$, where $I_{2\omega}$ and I_ω are the second harmonic and fundamental intensities, respectively. The fit yields a value of $b = 2.02$, in excellent agreement with the expected quadratic dependence on fundamental intensity.

When the films are rotated to normal incidence, negligible SHG is observed. This is consistent with the expectation that the alignment of the chromophores occurs perpendicular to the substrate. Furthermore, when the sample is oriented at 45° to normal incidence and the polarization of the fundamental beam is varied, the SHG intensity is observed to smoothly vary from a maximum for horizontal, p-polarized light to a minimum for vertical, s-polarized light. The SHG intensity is 15 times larger for p-polarized light than for s-polarized light, demonstrating that the polar orientation of the chromophores is nearly perpendicular to the substrate.
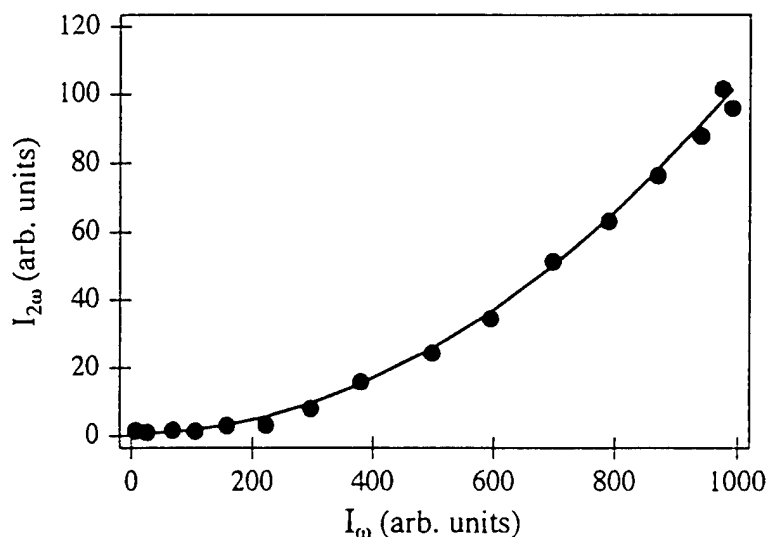
Figure 3. Quadratic dependence of the second harmonic intensity at 600 nm
on the fundamental intensity at 1200 nm for the single-sided 68 bilayer ISAM film.

The ISAM films have been measured by ellipsometry to have a bilayer thickness of 1.3 nm. Since the films studied here are therefore much thinner than the SHG coherence length, the SHG intensity is expected to grow quadratically with the number of bilayers. In Figure 2, $(I_{2\omega})^{1/2}$ is also plotted versus the number of bilayers for the 28 and 68 bilayer films. The data are seen to be consistent with a quadratic dependence. The double-sided, 40 bilayer film is not included here because the films on opposite sides of the substrate are aligned oppositely to one another such that interference occurs between SHG generated on the two sides. By comparison to Maker fringe patterns generated by translation of a quartz wedge across the fundamental beam, and accounting for the thickness of the ISAM films, the $\chi^{(2)}$ value of the ISAM films is found to be 0.70 times the value of quartz, or 0.67×10^{-9} esu. Furthermore, the films have exhibited no measurable decay of $\chi^{(2)}$ over a period of several weeks. We have thus shown that ISAM films can spontaneously assemble into a noncentrosymmetric structure with a substantial and stable $\chi^{(2)}$ value. The process can be applied to a variety of material structures including polymers that possess separate ionic and NLO-active groups as well as to highly nonlinear, nonpolymeric NLO chromophores that have been chemically modified for compatability with the ISAM deposition process. The ISAM technique represents an exciting new approach to the rapid, inexpensive production of $\chi^{(2)}$ thin films for waveguide applications.

References:

[1] G. Decher, J.D. Hong, and J. Schimitt, Thin Solid Films **210/211**, 831 (1992).
[2] K.D. Singer, S.J. Lalama, and J.E. Sohn, Appl. Phys. Lett. **49**, 248 (1986).
[3] W. Lin *et al.*, Angew. Chem. Int. Ed. Engl. **23**, 1497 (1995).

Multifunctional Photoresponses in Carbazole Main-Chain Polymers

Tatsuo Wada, Yadong Zhang, Hiromi Kimura-Suda, Tetsuya Aoyama, Su-An Choi and
Hiroyuki Sasabe

CREST (Core Research for Evolutional Science and Technology), JST, and Frontier Research
Program, The Institute of Physical and Chemical Research (RIKEN), 2-1 Hirosawa, Wako,
Saitama 351-01, Japan, Phone: +81-48-462-1111, Fax: +81-48-462-4695

Introduction

Electronic and optical properties of organic charge-transfer (CT) compounds have attracted a lot of attention from both fundamental science and practical applications. Remarkable progress have been made in development of electroactive CT materials such as organic metals, conducting polymers, and organic photoconductors (OPCs). Among them, OPCs are widely used for electrophotographic applications. Besides photoconductive properties, it has been elucidated experimentally and theoretically that organic inter- and intracharge transfer compounds exhibit large nonlinear optical (NLO) responses. We have investigated the third-order NLO properties of polymeric CT materials based on poly-n-vinylcarbazole (PVK) complexed with 2,4,7-trinitrofluorenone (TNF) in terms of the complex composition.[1] The values of $\chi^{(3)}$ ($-3\omega; \omega,\omega,\omega$) increased linearly with the content of CT complex in the film. Recently large refractive index changes have been demonstrated in organic photorefractive polymers based on PVK/TNF systems.[2] Carbazole compounds play a significant part in electroactive and NLO applications. In order to utilize the unique properties of polymer backbone, acceptor-substituted carbazole moiety was incorporated into the main chain through either 3,6- or 3,9-linkage. In this paper we discuss the multifunctional photoresponses in various carbazole main-chain polymers with shoulder-to-shoulder, head-to-tail, and hyper-branched arrangements as shown in Figure 1.

Multifunctionality of Building Blocks

As a building block for main-chain polymers we selected an acceptor-substituted carbazole. Carbazole derivatives are well-studied as hole-transporting molecules and their photocarrier generation efficiency can be sensitized by the formation of a CT complex. The carbazole molecule has an isoelectronic structure of diphenylamine. Therefore, the introduction of acceptor groups in 3 and/or 6-position induces intracharge transfer. We examined the photocarrier generation properties of acceptor-substituted carbazole derivatives by a xerographic discharge method. Figure 2 shows the typical photocarrier generation sensitivity of carbazole main-chain polymer with a "shoulder-to-shoulder" arrangement at 534 nm. This shoulder-to-shoulder polymer has the same building block as the other polymers. We also examined electro-optic responses using the reflection method at a wavelength of 532 nm. Electro-optic coefficient r_{33} increased linearly as a function of the poling electric field as shown in Figure 2. These results suggest acceptor-substituted carbazole derivatives show both photoconductivity and electro-optic responses which are required for photorefractive applications.

Shoulder-to-Shoulder Polymers

In the shoulder-to-shoulder arrangement, the acceptor-disubstituted carbazoles lie parallel to each other as shown in Figure 1. This arrangement of NLO chromophores provides a new approach to the design of main-chain polymers with large off-diagonal NLO tensor components. In the shoulder-to-shoulder arrangement the dipole alignment can be easily achieved by applying an electric field. The NLO coefficients d_{33} and d_{31} were determined by second-harmonic generation (SHG) measurements at 1064 nm to be 10.6 pm/V and 7.7 pm/V, respectively.[3] The ratio $d_{33}/ d_{31} < 3$ indicated the two-dimensional CT character in shoulder-to-shoulder polymers.

x = 6, 10
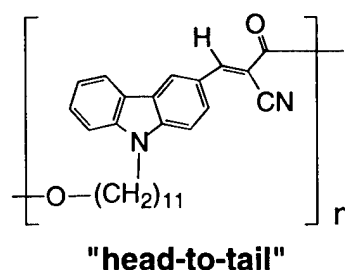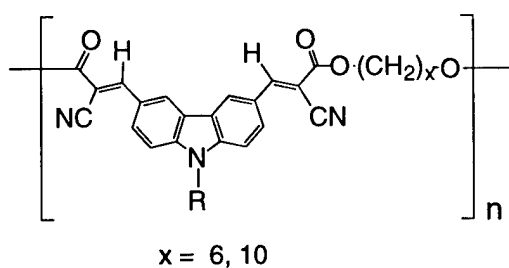
"shoulder-to-shoulder" R: —(CH₂)₁₃Me,

"main- and side-chain" R: —(CH₂)₁₁-N

"head-to-tail"

"hyper-branched"

R: —(CH₂)₁₁—
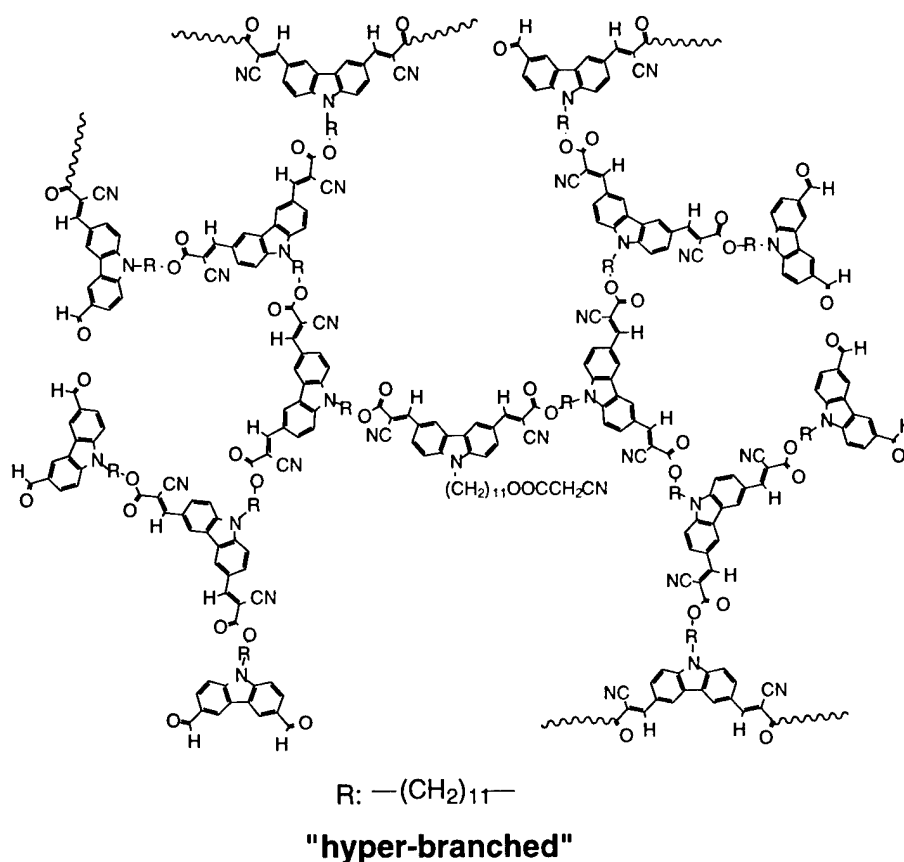
Figure 1 Chemical structures of main-chain polymers.

The photorefractive performance was evaluated by two-beam coupling and four-wave mixing measurements at 532 nm. An asymmetric optical energy exchange in the two beams was observed in the poled thin films as shown in Figure 3. Typical values of two-beam coupling gain and diffraction efficiency are 10 cm^{-1} (15 V/μm) and 1.7 % (23 V/μm). We can apply these carbazole main-chain polymers to obtain monolithic photorefractive materials based on their multifunctional photoresponses.

Figure 2 Electro-optic response as a function of the poling voltage. The insert shows the photo-conductivity as a function of the applied electric field.

Figure 3 Typical two beam coupling response in shoulder-to-shoulder polymer as the grating is translated.

In order to enhance the photoconductivity or NLO performance, additional carbazole moiety or NLO chromophore such as 4-nitro stilbene was introduced int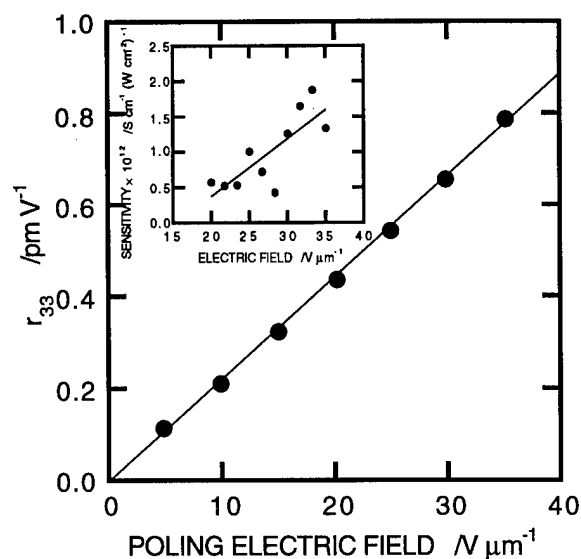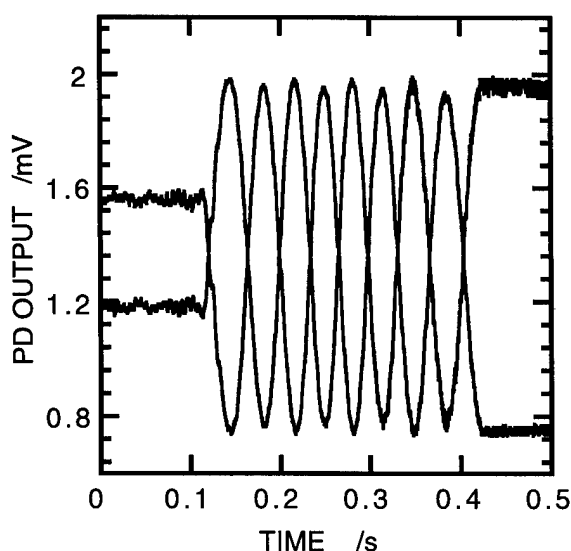o the side chain. The main-chain carbazole polymer with an additional NLO chromophore in the side chain exhibited larger SHG response than that of the original main-chain polymer. The NLO performance could be enhanced by the introduction of additional NLO chromophores into the side chain of the main-chain polymer.

Head-to-Tail and Hyperbranched Polymers

Efficient and stable electric field-induced alignment can be expected in the head-to-tail main-chain polymers due to enhanced dipole moment and molecular hyperpolarizability. However, it is difficult to pole the head-to-tail polymers in the solid state. We have newly synthesized a head-to-tail polymer in which carbazole monomer units were arranged through 9,3-linkage with a long alkyl spacer. The studies on the temporal behavior of SHG signals indicated that head-to-tail polymer has stable polar alignment than those of shoulder-to-shoulder polymers.

The hyperbranched carbazole polymer was prepared from 3,6-diformyl-9-(11-hydroxyundecyl)-carbazole and methyl cyanoacetate by a two-stage Knoevenagel polycondensation with high molecular weights in high yields. Noncentrosymmetric alignment was achieved by corona-poling above glass-transition temperature. The SHG coefficients (d_{33}) could be calculated to be 7 pm/V.[4] Since disubstituted carbazole blocks were linked with head-to-tail arrangement in the hyperbranched polymer, the similar poling and depoling behaviour can be expected with that of the head-to-tail polymer.

REFERENCE
1. S.-Y. Park, T. Wada and H. Sasabe, *Mol. Cryst. Liq. Cryst.*, **227**, 151 (1993).
2. K. Meerholz, B. L. Volodin, Sandalphon, S. Kippelen and N. Peyghambarian, *Nature*, **371**, 497 (1994).
3. Y. Zhang, L. Wang, T. Wada and H. Sasabe, *Macromolecules*, **29**, 1569 (1996).
4. Y. Zhang, L. Wang, T. Wada and H. Sasabe, *Macromol. Chem. Phys.*, **197**, 667 (1996).

"Quadrupoling" for Second Order Nonlinear Optics

K.D. Singer[a], S.F. Hubbard[a], R.G. Petschek[a], N. D'Sidocky[b], C. Hudson[b], L.C. Chien[b],
C.C. Henderson[c], and P.A. Cahill[d]
[a]*Department of Physics,Case Western Reserve University, Cleveland, OH 44106-7079*
[b] *Liquid Crystal Institute, Kent State University, Kent, OH 44242-0001*
[c]*Sandia National Laboratories, Organization 8230, Livermore, CA 94551-0969*
[d]*Sandia National Laboratories, Division 1811, Albuquerque, NM 87185-5800*

Achieving noncentrosymmetric order for second-order nonlinear optical materials has been a continuing focus of research. Monomolecular layer deposition and electric field poling of polymers have been favored approaches to generating noncentrosymmetric polymeric and organic materials.[1] In this case, the alignment exploits the vector part of the molecular hyperpolarizability tensor which is optimized in donor and acceptor substituted conjugated molecules. The principles behind the nonlinearities, both molecular and macroscopic are well-known, and considerable work has been directed at optimizing them. More recently, it has been pointed out that the octupolar hyperpolarizability component is ubiquitous and can be as large or larger than the vector part with appropriate molecular design.[2]

It has been known for a considerable time that even isotropic collections of chiral molecules possess second-order nonlinear optical properties.[3] These derive from the fact that such a material possesses no mirror symmetry and thus is noncentrosymmetric. In this case, however, though parametric mixing is allowed, second harmonic generation and the linear electro-optic effect are not. This is due to the fact that the nonlinear coupling is to the antisymmetric part of the second-order susceptibility tensor. It is straightforward to show that axially aligned collections of chiral molecules do indeed exhibit both second harmonic generation and the linear electro-optic effect. In the uniaxial case, for example, the symmetry operations consist of an infinite-fold rotation about the axial direction, and an infinity of 2-fold axes normal to the axis. Since no mirror planes are present, this belongs to the point group D_∞ or $\infty 22$. For second harmonic generation, the tensor components $d_{14}=-d_{25}$ are nonzero. Examples of such materials are nematic liquid crystals and uniaxially stretched polymers containing chiral molecules. In the case of biaxial alignment, the point group is D_2 or 222 containing three 2-fold axes. In this case, d_{14}, d_{25}, d_{36} are distinct and non-zero. Examples of these materials are biaxially stretched polymers and smectic C liquid crystals containing chiral chromophores. In addition, it may be possible to activate diagonal components of the susceptibility tensor through nonlinear strains.

In all of these cases, the macroscopic susceptibility will couple to the quadrupolar component of molecular hyperpolarizability. This component is revealed by decomposing the hyperpolarizability into its rotationally invariant representations. This decomposition for second harmonic generation leads to 2 vectors, 1 rank-2 pseudotensor, and 1 rank 3 tensor. These are the polar, quadrupolar, and octupolar components. In the case of Kleinman symmetry, only the polar and octupolar parts contribute. The quadrupolar or rank-2 pseudotensor will contribute only in molecular structures and at frequencies where Kleinman symmetry is broken. Thus multidimensional nonlinear optical processes are necessarily involved as would be expected in chiral structures.

The molecular features leading to large quadrupolar hyperpolarizabilities are not known, and, in this paper, we aim to take the first steps in identifying these features. To do this, we have developed a technique to directly measure this specific component of the hyperpolarizability using hyper-Rayleigh scattering.[4] We have also identified a candidate moiety for large quadrupolar optical nonlinearities through quantum chemical calculations which do indeed indicate multidimensional excitation.

Q-NH$_2$
λ_{max}=470 nm

Q-BNH
λ_{max}=520 nm
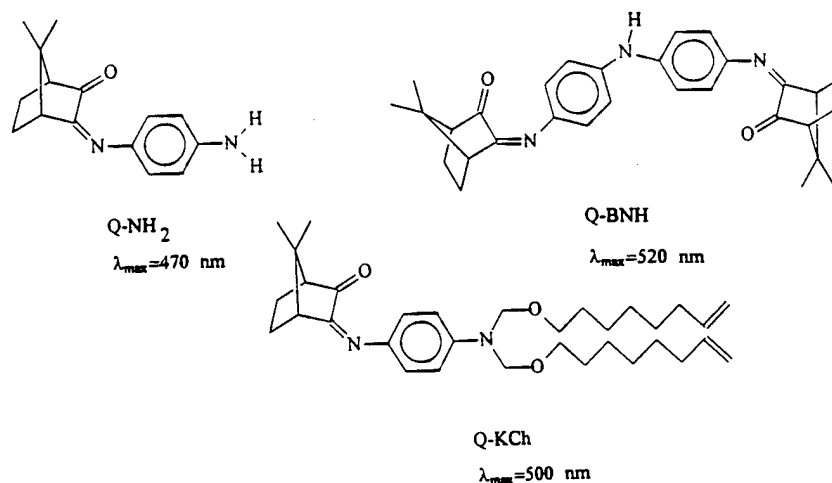
Q-KCh
λ_{max}=500 nm

Figure 1. Compounds used in this study.

The quinone dyes depicted in Fig. 1 were chosen to study the effects of chirality on the first hyperpolarizability. The molecules are rather large and have no point symmetry. As such, there is no obvious distinction between π and σ orbitals. Optical polarization rotation is a strong indication that the π-electron system is delocalized in three dimensions. A solution of Q-NH$_2$ of 1.1% by weight in p-dioxane rotated the linear polarization of a 632.8nm beam by 16° in a 20cm pathlength. Quantum mechanical calculations were carried out, and indicate the largely π-character of the relevant wavefunctions. It is also apparent that the wavefunctions are effectively delocalized in three dimensions over the molecular structure, and that significant charge moves around the camphorquinone upon excitation from the highest occupied to lowest unoccupied molecular orbitals.

Hyper-Rayleigh scattering was carried out using a tunable Nd:YAG based SPOPO source at 1265 nm and 1350 nm fundamental.[5] The sample solution was contained in a triangular cell, and the scattered light detected at 45°. The scattered light was measured as a function of the ellipticity of the incident polarization by rotating a ¼ wave plate with incident p-polarized light. The scattered light polarization state was determined by ¼ waveplate followed by a linear polarizer. The angle of the axes (measured from vertical) of the waveplate and linear polarizer were γ_0 and α_0 respectively. At 1265 nm two experiments were carried out: $\gamma_0 = \alpha_0 = 0°$ and $\gamma_0 = 0°; \alpha_0 = 54.7°$. At 1350 nm two experiments were carried out: $\gamma_0 = \alpha_0 = 54.7°$ and $\gamma_0 = 0°; \alpha_0 = 54.7°$.

Using these geometries, all six rotationally invariant scalars were determined. Of particular interest here are the symmetric vector component usually measured by EFISH

$\beta_{1,ss}$, and the quadrupolar component $\beta_{2,mm}$. Results are listed in Table 1 for the three chiral dyes along with p-nitroaniline (p-NA) and disperse red 1 (DR1) used as references and checks. It is seen that the vector components for pNA and DR1 agree with previous results obtained by both hyper-Rayleigh scattering and EFISH.[5,6] Additionally, the chiral quadrupolar components are negligible within experimental error. The chiral dyes exhibit substantial quadrupolar nonlinearities, some as large at the vector component of pNA. The measurement of Q-BNH at 1265 nm may be confounded by dephasing as the measurement is approaching resonance.

Clearly we have detected quadrupolar second-order optical nonlinearities which may be exploited in axially aligned polymer systems. Results and prospects on these experiments have been discussed. Further, in developing the hyper-Rayleigh technique to measure the six rotationally invariant scalars which measure the various symmetries, we have brought forth a powerful tool to be used in optimizing the molecular quadrupolar nonlinearity through the use of quantum chemistry, synthesis, and measurement. Thus quadrupolar polymers may represent a new approach to nonlinear optical materials.

	λ (nm)	pNA	DR1	Q-KCh	Q-NH$_2$	Q-BNH
$\beta_{1,ss}$	1265	11±2	170±20	39±7	12±5	23±8
$\beta_{1,ss}$	1350	10±2	136±15	32±6	10±4	14±7
$\beta_{2,mm}$	1265	1±2	20±30	10±3	4±1	4±4
$\beta_{2,mm}$	1350	0±2	0±20	9±2	2±2	11±4

Table 1. Values of $\beta_{1,ss}$ and $\beta_{2,mm}$ (10^{-30} esu) at λ=1265nm and 1350nm.

References

[1] K.D. Singer and J.H. Andrews, "Quadratic Nonlinear Optics in Poled Polymer Films: From Physics to Devices," in *Molecular Nonlinear Optics*, edited by J. Zyss (Academic Press, San Diego, 1994), pp. 245.

[2] J. Zyss and I. Ledoux, "Nonlinear Optics in Multipolar Media: Theory and Experiments," *Chem. Rev.* **94**, 77 (1994).

[3] J.A. Giordmaine, "Nonlinear Optical Properties of Liquids," *Phys. Rev.* **138**, 1599 (1965).

[4] R.G. Petschek S.F. Hubbard, K.D. Singer, N. D'Sidocky, C. Hudson, L.C. Chien, C.C. Henderson, and P.A. Cahill, "Measurements of Kleinman-disallowed Hyperpolarizability in Conjugated Chiral Molecules," *J. Opt. Soc. Am. B* (submitted) (1997).

[5] R.G. Petschek S.F. Hubbard, and K.D. Singer, "Spectral Content and Dispersion of Hyper-Rayleigh Scattering," *Opt. Lett.* **21**, 1774 (1996).

[6] J.E. Sohn K.D. Singer, L.A. King, H.M. Gordon, H.E. Katz, and C.W. Dirk, "Second-order Nonlinear Optical Properties of Donor and Acceptor Substituted Aromatic Compounds," *J. Opt. Soc. Am. B* **6**, 1339 (1989).

Thiophene based Nonlinear Optical Chromophore functionalized Epoxy Polymers for Electro-Optic Applications

K. G. Chittibabu and L. Li

Molecular Technologies, Inc., 270 Littleton Road, #29, Westford, MA 01886

X. Wang, J. Kumar and S. K. Tripathy

Departments of Physics and Chemistry, Center for Advanced Materials, University of Massachusetts Lowell, Lowell, MA 01854

Polymeric materials present certain advantages over inorganic crystals for second-order nonlinear optical (NLO) applications because of their low dielectric constant, large optical nonlinearity, low cost, and ease of processability. Stable NLO polymeric materials are potential candidates for electro-optic (EO) devices such as high bandwidth electro-optic modulators [1], optical interconnects [2], and fiber optic gyros [3]. Second-order NLO properties in polymers are present when the chromophores are aligned in a non-centrosymmetric manner. Chromophores with enhanced NLO susceptibilities can be obtained by increasing electron-donating and/or accepting effects [4], by extending the conjugation length between the donor and acceptor groups [5] and by replacing the phenyl moieties in the chromophores with thiophene moieties [6]. Efforts were made by our group [7] and various other groups [6, 8] to synthesize and optimize the properties of the chromophore functionalized polymers with high optical nonlinearity. Jen and coworkers synthesized a variety of thiophene based chromophores with high optical nonlinearity, '$\mu\beta$' [6, 8]. Many of these chromophores, when doped in a polymer matrix exhibited an electro-optic value greater than 20 pm/V. Marder and coworkers studied the effect of strong acceptors in NLO chromophores and have found that an 'r_{33}' value of 55 pm/V at 1.313 μm is realizable with some of these chromophore doped polycarbonate composites. However, most of these systems are of guest-host type, which limit the chromophore solubility as well as temporal stability of the poled order in the NLO chromophore-polymer composites.

We have recently synthesized bisphenol-A based epoxy pre-polymers and subsequently post-functionalized them to obtain donor-acceptor substituted thiophene chromophores in the epoxy polymer. Two polymers, viz., DGEBA-PT-TCV with a 4-(5'-tricyanovinyl-thienyl)aniline chromophore and DGEBA-PAM-NT with a 4-(5'-nitrothienyl-2'-azomethine)aniline chromophore were synthesized.

Epoxy polymer DGEBA-PT-TCV was synthesized as follows: 4-(2-thienyl)aniline was synthesized by reacting 4-bromonitrobenzene with 2-(tributylstannyl)thiophene in the presence of catalytic amounts of tetrakis(triphenylphosphino)palladium (0) followed by the reduction of nitro-group in the resulting compound with tin and hydrochloric acid. The 4-(2-thienyl)aniline is a colorless liquid and reacts readily with diglycidyl-ether of bisphenol-A to give the epoxy prepolymer. The resulting epoxy prepolymer was reacted with tetracyano-ethylene to convert the 4-(2-thienyl) aniline polymer derivative to obtain DGEBA-PT-TCV. The schematic of these chemical reactions is shown in Figure 1. The resulting polymer is deep blue in color and can be cast into thin films with ease. The T_g of this polymer is measured as 132 °C using a Differential Scanning Calorimeter (DSC). DGEBA-PT-TCV polymer is stable upto ca. 300 °C, as determined from Themogravimetric Analysis (TGA). Figure 2 shows the chemical structure of DGEBA-PAM-NT polymer. DGEBA-PAM-NT is pink in color with an absorption maximum of ca. 515 nm in the solid state.
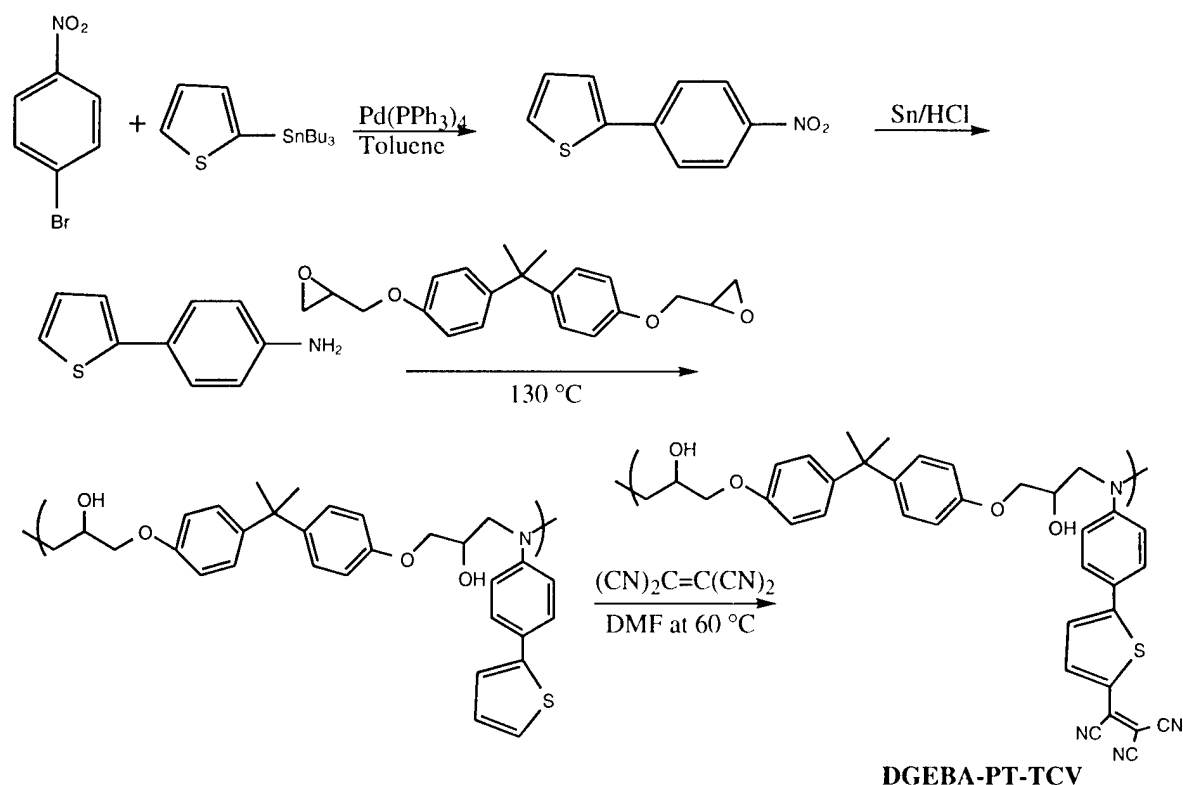
Fig. 1. Synthesis of tricyanovinyl-thienyl functionalized epoxy polymer DGEBA-PT-TCV
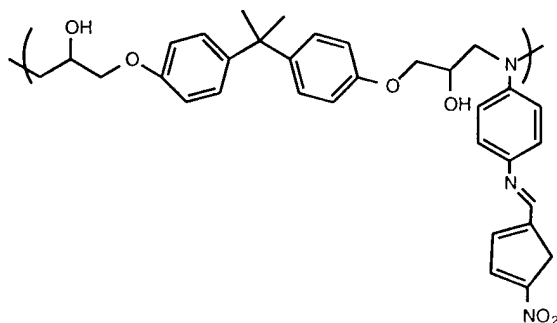

Fig. 2. Chemical Structure of DGEBA-PAM-NT polymer

DGEBA-PT-TCV polymer was processed into thin films (0.2 to 2 μm thick) on glass slides by spin-coating. The linear optical and second order NLO properties of this polymer were investigated. An absorption maximum around 610 nm was measured for this polymer. The samples were poled at 130 °C for 30 min by corona poling technique. The second order NLO characteristics of the poled samples were studied by the Second Harmonic Generation (SHG) method. Large d_{33} value of about 80 pm/V was measured at 1550 nm. The temporal stability of the optical nonlinearities for the poled samples at 80 °C was studied as shown in Figure 3. The NLO properties of the poled samples are relatively stable at 80 °C.

Electro-optic (E-O) coefficient (r_{33}) of the polymer was measured by employing the reflection technique [9]. The polymeric material was processed into thin films (about 1 to 2 μm

thick) on indium-tin-oxide (ITO) coated glass slides by spin-coating. The spin-coated films were dried under vacuum for 48 hours at room temperature. The second order NLO properties in these samples were achieved by the corona poling method in a wire to plane arrangement. The polymer samples were poled at 130 °C for 30 min. After poling, the top gold electrodes were thermally deposited on the poled polymer films in vacuum. The E-O measurements were performed at 1.3 μm with a diode laser. Electro-optic coefficient 'r33' was determined as 12 pm/V for this polymer. However, the measured 'r$_{33}$' is smaller than expected value, and is attributed to ineffective poling of the chromophores in the polymer samples on the ITO coated slide. Experiments on the improvement of poling with the samples coated on ITO slides are in progress and larger 'r$_{33}$' values are anticipated.
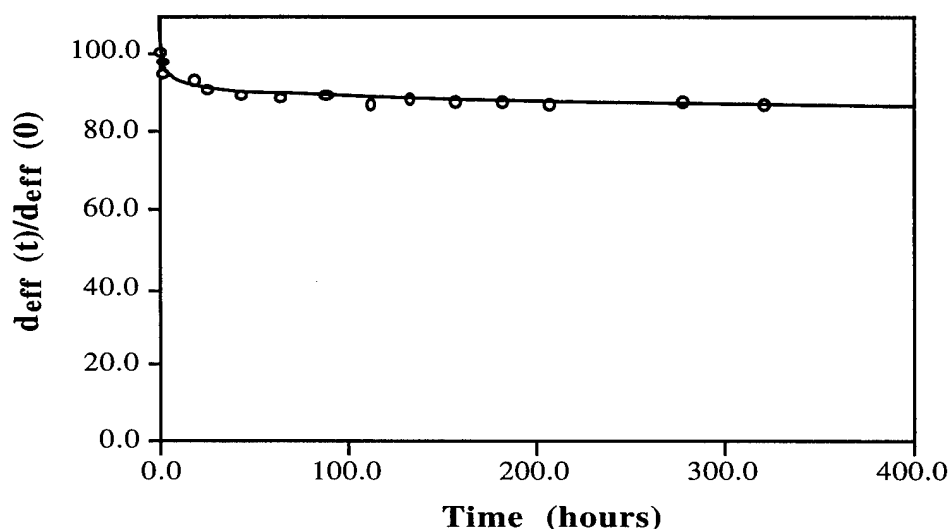

Figure 2. Temporal behavior of the NLO property for a poled sample of the polymer subjected to heat treatment at 80 °C.

REFERENCES

1   D. G. Girton, S. L. Kwiatkowski, G. F. Lipscomb, R. S. Lytel, *Appl. Phys. Lett.*, **58**, 1730 (1991).

2   L. R. Dalton, C. Xu, A. W. Harper, R. Ghosn, B. Wu, Z. Liang, R. Montgomery and A. K-Y. Jen, *Nonlinear Optics*, **10**, 383 (1995).

3   K. Hotate, *Photonics Spectra*, 108 (April 1997).

4   M. Ahlheim, M. Barzoukas, P. V. Bedworth, M. B-Desce, A. Fort, Z. Hu, S. R. Marder, J. W. Perry, C. Runser, M. Staelin, B. Zysset, *Science*, **271**, 335 (1996).

5   D. R. Kanis, M. A. Ratner, T. J. Marks, *Chem. Rev.* **94**, 195 (1994).

6   A. K-Y. Jen, V. P. Rao, K. Y. Wong, and K. J. Drost, *J. Chem. Commun.*, 90 (1993).

7   X. Wang, J. Kumar, S. K. Tripathy, L. Li, J. Chen and S. Martrunkakul, *Macromolecules*, **30**, 219 (1997).

8   T. Chen, A. K-Y. Jen, and Y. Cai, *Chem. Mater.*, **8**, 607 (1996)

9   C. C. Teng and H. T. Man, *Appl. Phys. Lett.*, **56**, 1734 (1990)

Electro-optic Effect and Propagation Loss in Polymer Films Containing Nano-sized Droplets of Liquid Crystal

Shiro Matsumoto, Yasuyuki Sugiyama, Seizou Sakata, and Takayoshi Hayashi
NTT Integrated Information & Energy Systems Laboratories
3-9-11 Midoricho, Musashino, Tokyo 180, Japan
Tel: 81-422-59-2936, Fax: 81-422-59-4065, E-mail: matumoto@ilab.ntt.co.jp

INTRODUCTION

Droplets of liquid crystal (LC) have been energetically investigated during the last ten years.[1] Most of the research has aimed at making use of scattering[2] and diffraction,[3] which occurs either at the surface of individual droplets or at the surface of a layer consisting of many droplets. The droplets were mostly micro-sized. Our aim, however, is to make use of nano-sized LC droplets for active optical devices such as optical switches or tunable filters. The surfaces of nano-sized LC droplets are too small to scatter light, so the total intensity of transmitted light is not changed, but the phase or polarization can be controlled by the birefringence generated by the response of nano-sized LC droplets to an electric field shown in Figure 1. There have been only a few works[4] including ours,[5] which have similar aims. We have already reported the preparation of droplets about 50 nm in diameter and shown they respond to an electric field. In this work, we prepared the polymers containing nano-sized LC droplets by various conditions and measured their electro-optic effect, propagation loss, and response time.

SAMPLE PREPARATION AND OPTICAL MEASUREMENT

The process we used to prepare the small LC droplets is called photo-polymerization induced phase separation.[6] In this technique, a solution of LC and prepolymer is irradiated with UV light; the LC droplets are then phase separated according to the polymerization. We used a combination of nematic LC BL 24 from Merck Industrial Chemicals and UV curable prepolymer NOA 81 from Norland Products. We varied LC concentrations in the prepolymer and UV irradiation strengths.

Figure 2 shows an experimental setup for measuring the electro-optic effect. The sample was a spin-coated film about 20 μm thick sandwiched between two electrodes, a Si substrate, and an Au-deposited layer. The optical path through the polymer was 1 mm. The change in output power due to retardation generated by an applied electric field was measured. Output power I_o is expressed as $I_o = I_i \sin^2 (\phi /2)$, where I_i is input power and ϕ is retardation. The change in birefringence Δn, is calculated
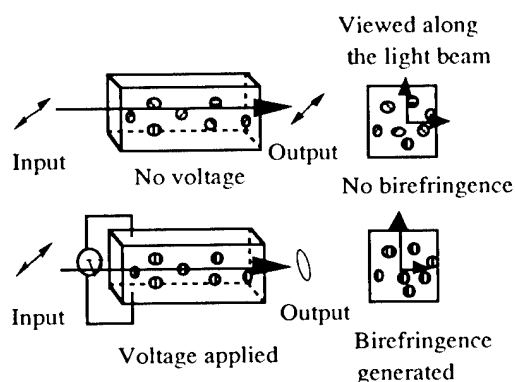

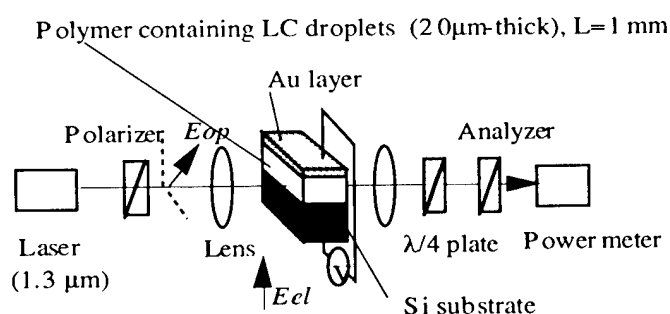Fig. 1. Nano-sized LC droplets and light processing.

Fig. 2. Experimental setup.

from $\phi = 2\pi \cdot \Delta n \cdot L / \lambda$, where L is optical length and λ is wavelength.

Propagation loss was measured from the scattered light. Light with a wavelength of 1.3 μm was coupled through a prism into an about 5-μm-thick polymer film spin-coated onto a glass substrate. The light scattered from the film was detected by an infrared camera. Propagation loss is assumed to be proportional to the attenuation of scattered light along the propagating light beam.
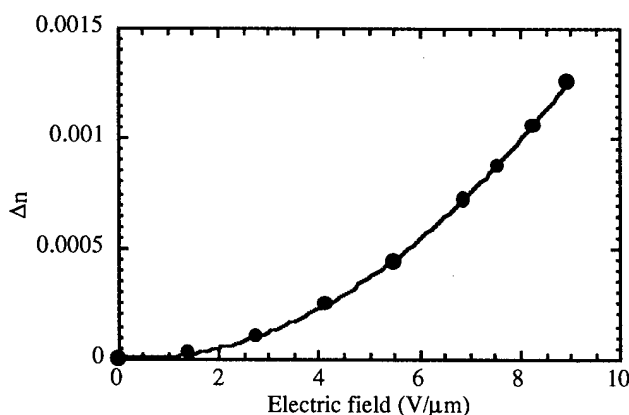

Fig. 3. Change in refractive index depending on electric field.

RESULTS AND DISCUSSION

Figure 3 shows the dependence of Δn on applied electric field for the sample obtained under strong UV irradiation of prepolymer containing LC of 26 wt%. Δn increases almost in proportion to the square of the applied electric field E, that is, $\Delta n = kE^2$, where k is a proportionality constant. This relationship was found for all samples. Figure 4 shows the dependence of k value on LC concentration. At LC concentrations lower than 13 wt%, the k value is zero for both samples obtained under strong and weak UV irradiation, because the LC droplets that respond to applied voltage are not formed at these concentrations. At higher concentrations, k increases linearly with the concentration, probably because the density of droplets increases linearly with the concentration. The k values of samples under strong UV irradiation are smaller than those under weak UV irradiation. This is explained by droplet size being smaller for the polymer under strong UV irradiation,[7] and by smaller droplets needing higher electric fields to produce a response.[8] The largest change in refractive index was 0.001 at 3.5 V/μm.

Figure 5 shows an example of a plot of scattered light intensity against propagation length. The propagation loss was calculated from the slope of the straight line in the figure. The propagation losses between 0.5 dB/cm and 13 dB/cm were obtained in this work. These loss values were plotted vs. their k value, which expresses the
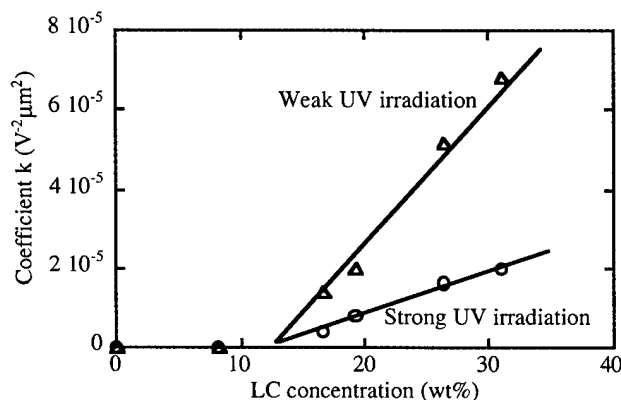

Fig. 4. Dependence of electro-optic effect on LC concentaration.
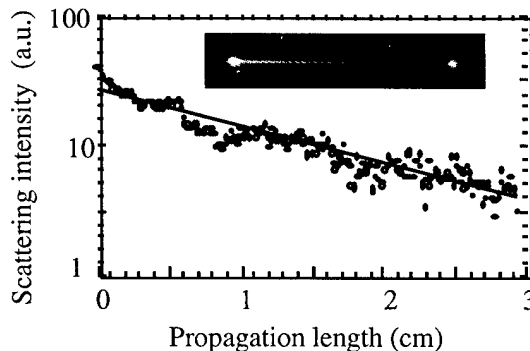
Fig. 5. Scattering intensity vs. propagation length.

magnitude of the electro-optic effect (Figure 6). The larger the electro-optic effect, the larger the propagation loss. This suggests that a larger density of LC droplets brings about a larger propagation loss. The figure also shows propagation loss is much decreased by stronger UV irradiation during sample preparation. This is probably because smaller droplets, which are formed under stronger UV irradiation, lead to smaller scattering loss. The largest change in refractive index among the polymers having low propagation loss (<2.5 dB/cm) was 0.001 at 8 V/μm.

The change in output when a short electric pulse was applied to the sample obtained under strong UV irradiation is shown in Figure 7. The response time is shorter than 10 μs, which is more than two orders of magnitude faster than that in usual bulk nematic LCs. This very fast response also results from using nano-sized LC droplets.

In conclusion, polymer films containing nano-sized droplets of LC have been investigated and polymer materials having a large electro-optic effect (Δn=0.001 at 8 V/μm), low propagation loss (2.5 dB/cm), and very fast response time (10 μs) have been developed. These are expected to be applied to active optical devices.
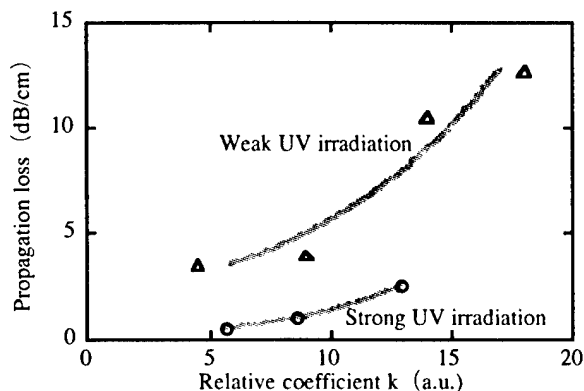
Fig. 6. Electro-optic effect vs. propagation loss.
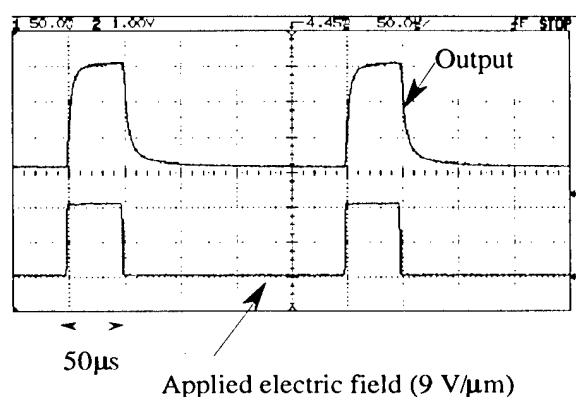
Fig. 7. Response to short electric pulse.
$\tau_{on}=3.8\mu s$, $\tau_{off}=7.8\mu s$

REFERENCES

(1) L. Bouteiller and P. LE Barny, Liquid Crystals, 21, 157(1996).

(2) J. L. Fergason, SID Int. Symp. Dig. Tech. 16, 68 (1985).

(3) R.L. Sutherland, V. P. Tondiglia, L. V. Natarajan, T. J. Bunning, and W. W. Adams, Appl. Phys. Lett., 64, 1074 (1994).

(4) M. J. Sansone, G. Khanarian, T. M. Leslie, M. Stiller, J. Altman, and P. Elizondo, J. Appl. Phys. 67, 4253(1990).

(5) S. Matsumoto, M. Houlbert, T. Hayashi, and K. Kubodera, Appl. Phys. Lett., 69, 1044(1996).

(6) N. A. Vaz, G. W. Smith, and G. P. Montgomery, Jr., Liquid Crystals, 146, 1 (1987).

(7) A. M. Lackner, J. W. Margerum, E. Ramos, and K. -C. Lim, Proc. SPIE Vol. 1080, 53(1989).

(8) P. S. Drzaic, J. Appl. Phys., 60, 2142(1986).

High Glass Transition Temperature Syndioregic Second Order Nonlinear Optical Polymers in Langmuir-Blodgett-Kuhn Films

M. J. Roberts, G. A. Lindsay, J. D. Stenger-Smith, R. A. Hollins, A. P. Chafin, R. G. Gratz[1]

U.S. Navy, Code 4B2200D, NAWCWPNS, China Lake, CA 93555-6001
[1]Department of Chemistry, Mary Washington College, Fredericksburg, VA

Recent progress has been made toward the goal of processing polymers at low temperature to produce all-polymeric nonlinear optical films which may ultimately find application as active waveguides. Our previously reported work [1] has utilized the Langmuir-Blodgett-Kuhn (LBK) technique to produce such films but the noncentrosymmetric order in those films was lost when heated above 80 °C. New polymers were designed to yield ordered films with higher thermal stability by eliminating the long alkyl side chains (Figure 1). The glass transition temperature (T_g) of the bulk polymer is about 240 °C, and the upper limit on short term thermal baking stability is about 320 °C [2].

Many materials intended to utilize the LBK methodology for the fabrication of optical waveguides have suffered from low thermal stability of the noncentrosymmetric order. The low thermal stability is directly correlated with the chemical structure of the previous materials, namely, the presence of low melting alkyl chains. Known strategies to increase the thermal stability of LBK films include interlayer and/or intralayer covalent bonding (ie. crosslinking), incorporation of mesogenic groups to impart liquid crystallinity, removable alkyl groups, and using side-chain chromophores attached to polyimides [3] (high T_g polymer).
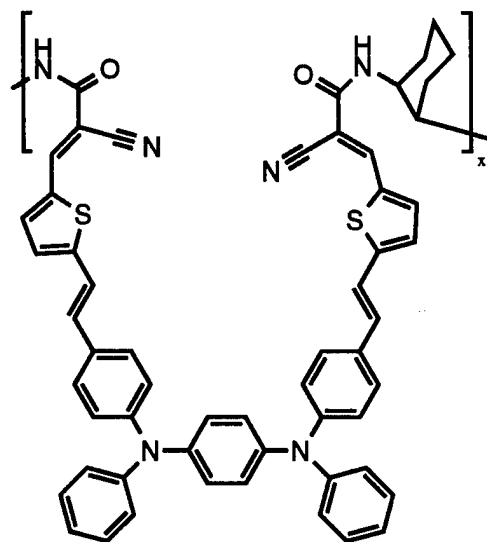

Figure 1. Syndioregic nonlinear optical polymer.

In this study, we are testing the feasibility of LBK processing of a high Tg syndioregic polymer. Film quality is ascertained using plots of peak UV-Vis absorbance and second harmonic generated (SHG) intensity versus the number of deposited layers (film thickness). A linear increase of UV-Vis absorbance and quadratic increase of SHG intensity indicate a high degree of uniformity in chromophore density and alignment layer-to-layer through the thickness of the LBK films. Temporal stability of the noncentrosymmetric ordering of the chromophores is important for most future applications. Particularly, high temperature stability is needed to ensure compatibility with subsequent device fabrication steps.

Films were made using a rectangular LBK trough with symmetrical compression (NIMA, Coventry). The trough was kept in a glove bag (Aldrich, Milwaulkee) continuously purged with nitrogen gas during the film depositions at 24 °C. The substrates were glass slides (Fisher, Cat. # 12-550A) cleaned with H_2SO_4/H_2O_2 and hydrophobicized over refluxing hexamethyldisilazane. A chloroform solution of the polymer was spread at the nitrogen/water interface. The polymer layer was compressed symmetrically at a barrier speed of 10 cm^2/min to a surface pressure of 12 mN/m. The layers were deposited on the downstroke at 3 mm/min (x-type dipping).

The transmission UV-Vis spectra of the films were obtained with a Cary 5 NIR-Vis-UV spectrophotometer. The films were referenced to air and the glass background was subtracted to obtain the film spectra. The SHG signal was generated by transmission of an incident fundamental beam at 54° from normal from a Q-switched Nd:YAG laser (pulse width of 10 ns and repetition rate of 10 Hz). and detected with an intensified Si diode array (Tracor Northern).
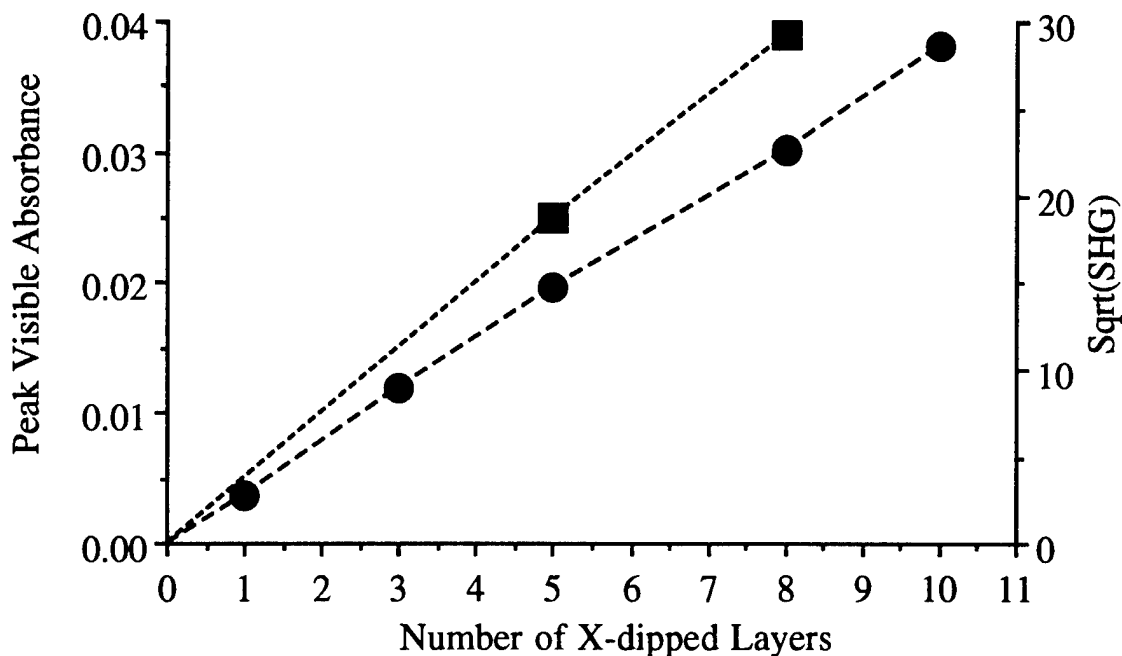
Figure 2. UV-Vis absorbance and SHG as a function of the number of layers.
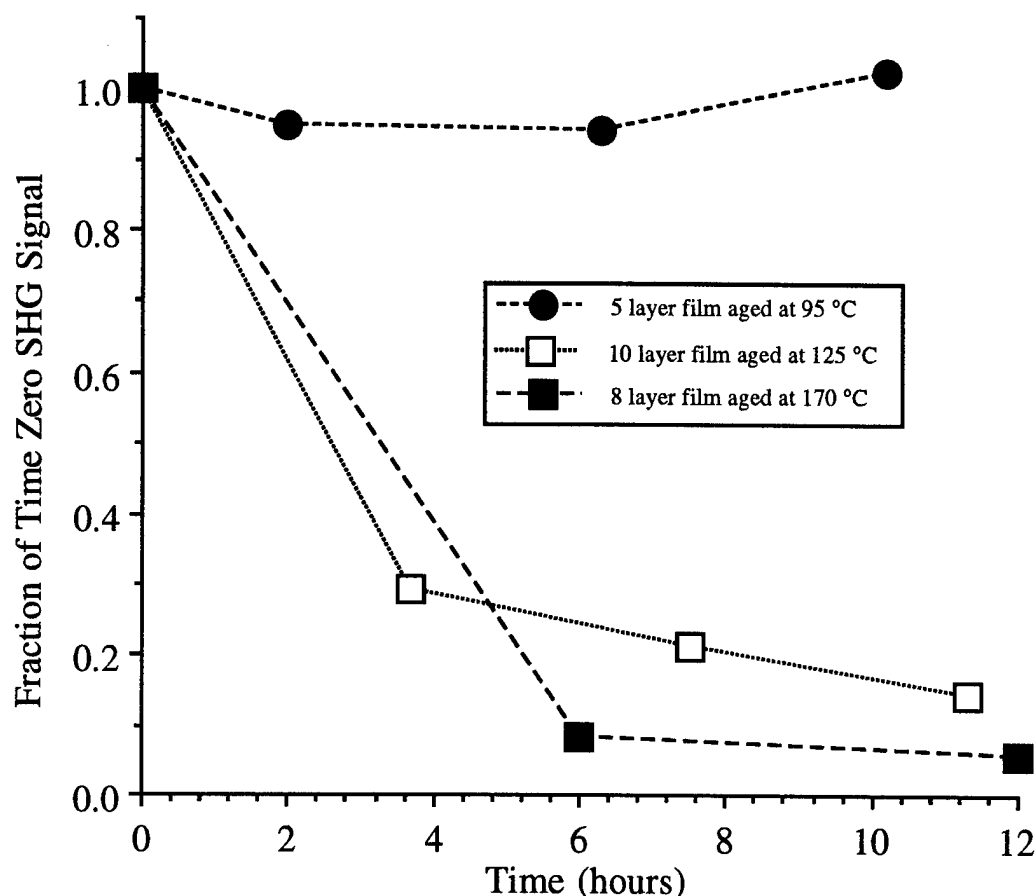
Figure 3. Aging of LBK films at elevated temperatures.

Chemical synthesis of the polymer was achieved though Knoevenagel condensation polymerization [2].

Work thus far has shown that the high T_g syndioregic polymer may be processed with the LBK technique to obtain uniformly deposited films (Figure 2) with stable noncentrosymmetric order to temperatures of 95 °C (Figure 3).

Future work will include attempts to deposit thicker films, extended studies of the temporal stability of the noncentrosymmetric order, and FTIR spectroscopy at elevated temperatures.

References

(1) G. Lindsay, K. Wynne, W. Herman, A. Chafin, R. Hollins, J. Stenger-Smith, J. Hoover, J. Cline, J. Roberts Nonlinear Optics, volume 15, 139-146, 1996.
(2) G. Lindsay, A. Chafin, R. Gratz, R. Hollins, M. Nadler, E. Nickel, J. Stenger-Smith, R. Yee, W. Herman, and P. Ashley, Proceedings of the SPIE, Photonics West, 1997.
(3) T. Yamada, S. Yokoyama, K. Kajikawa, K. Ishikawa, H. Takezoe, A. Fukuda, M. Kakimoto, Y. Imai Langmuir, volume 10, 1160-1163, 1994.

Second-Order Effects

Thursday, October 16, 1997

Joseph Zyss, France Telecom/CNET, France
Presider

ThD
3:30pm–4:30pm
Seaview A&B

NONLINEAR OPTICS OF CHIRAL MEDIA

Thierry Verbiest, Sven Van Elshocht, Gunter Beelen, Carlo Boutton, Martti Kauranen, and André Persoons

Center for Research on Molecular Electronics and Photonics

Department of Chemistry, University of Leuven

Celestijnenlaan 200 D, B-3001 Leuven, Belgium

Chiral media interact differently with left- and right-hand circularly-polarized light. In linear optics this gives rise to optical activity effects like circular dichroism, optical rotation and optical rotatory dispersion. Optical activity effects also occur in nonlinear optics. For example, second-harmonic generation from chiral surfaces is different for left- and right-hand circularly-polarized fundamental excitation.[1,2]

We have studied second-harmonic generation (SHG) from chiral Langmuir-Blodgett films of poly(isocyanide)s and polythiophenes. The key property of these polymers is their helical structure which makes them chiral. We used a recently proposed technique to determine the relative values of all tensor components that describe second-harmonic generation from chiral surfaces up to first order in the magnetic-dipole interaction.[3-5] This technique relies on measuring several second-harmonic signals as functions of the rotation angle of a quarter wave-plate that controls the state of polarization of the fundamental. Only normalized line shapes of p- and s-polarized SHG signals need to be measured.

For all investigated systems we observed large circular-difference effects in the second-harmonic response. The observed second-harmonic signals cannot be explained within the electric-dipole approximation. Since chiral molecules are known to exhibit strong magnetic-dipole transitions, we have

included magnetic-dipole contributions in our formalism to describe the experimental results. The nonlinear polarization is taken to be of the form

$$P_i(2\omega) = \sum_{j,k}\left[\chi_{ijk}^{eee}E_j(\omega)E_k(\omega) + \chi_{ijk}^{eem}E_j(\omega)B_k(\omega)\right]$$

where $E(\omega)$ and $B(\omega)$ are the electric field and magnetic induction field at the fundamental frequency. In addition the medium develops a nonlinear magnetization

$$M_i(2\omega) = \sum_{j,k}\chi_{ijk}^{mee}E_j(\omega)E_k(\omega)$$

The intensity of any component of the second-harmonic field can be expanded as

$$I(2\omega) = \left| fE_p^2(\omega) + gE_s^2(\omega) + hE_s(\omega)E_p(\omega)\right|^2$$

where $E_p(\omega)$ and $E_s(\omega)$ are the p- and s-polarized components of the fundamental field. The coefficients f, g, and h depend linearly on the electric (χ^{eee}) and magnetic (χ^{eem}, χ^{mee}) susceptibility tensors. The second-harmonic technique we use allows an accurate determination of the relative values of f, g, and h. By measuring f, g, and h for different polarizations of the second-harmonic field we were able to determine the relative values of all relevant components of the electric and magnetic susceptibility tensors. This analysis showed that the magnetic-dipole contributions to the nonlinearity of the system can be as high as 20% for the poly(isocyanide)s and of the same order of magnitude as the electric-dipole contributions for the polythiophene. We have also shown that chiral isotropic media can posses an electro-optic response. This is related to the inherently low symmetry of chiral materials:

even isotropic systems composed of chiral molecules are noncentrosymmetric. The predicted effect relies on material damping and occurs within the electric-dipole approximation. It vanishes for a racemic mixture and changes sign between the two mirror image forms of the chiral material. The second-order susceptibility of such a system can be of the order of that of KDP. In addition, the material is thermodynamicly stable and loss of nonlinearity due to relaxation processes (like in poled polymer films) does not occur. Our results also suggest that it is possible to design an axperimental arrangement that could lead to gain for the incident light field. Such an effect would be of considerable importance for the amplification of optical signals in polymeric fibers.

References

[1] T. Petralli-Mallow et al., J. Phys. Chem. 97, 1383 (1993)

[2] M. Kauranen et al., Adv. Mater. 7, 641 (1995)

[3] J.J. Maki et al., J. Chem. Phys. 105, 767 (1996)

[4] J.J. Mali et al., Phys. Rev. B 55, 5021 (1997)

[5] M. Kauranen et al., Phys. Rev. B 55, R1985 (1997)

Thiophene Based Hydrazones: a New Class of Nonlinear Optical Molecular Crystals

Christian Bosshard, Pan Feng, Man Shing Wong, Martin Bösch, Urs Meier, and Peter Günter
Nonlinear Optics Laboratory, Institute of Quantum Electronics
ETH Hönggerberg, CH-8093 Zürich, Switzerland, Phone + 41-1-633 23 29

1. Introduction

Crystalline solids are often regarded as the best choice of material form for practical use as optical frequency converters because of the excellent long-term orientational stability and extremely high density of active components. Such materials can be combined with inexpensive diode lasers for optic parametric generation of a broad range of optical frequencies [1, 2]. We here report on our on-going efforts in the development of novel and highly efficient second-order nonlinear optical crystalline materials for frequency conversion, based on the hydrazone derivatives 5-(methylthio)-thiophenecarboxaldehyde-4-nitrophenylhydrazone (MTTNPH) and 5-nitro-2-thiophene-carboxaldehyde-4-methylphenylhydrazone (NTMPH).

2. Description of thiophene based hydrazones

One of our approaches for the development of molecular crystals with large second-order nonlinearities is to use a non-rod-shaped π-conjugated hydrazone backbone as a highly extended π-conjugated core which shows a high preference for non-centrosymmetric packing and improves the crystal properties relative to the classical counterparts [3, 4]. These chromophores possess a bent hydrazone skeleton, (—CH=N\NH—), due to the non-rigid nitrogen-nitrogen single bond. One of the successful examples in this class is 4-dimethylaminobenzaldehyde-4-nitrophenylhydrazone (DANPH), which was found to have the largest phase-matchable nonlinear optical coefficient $d_{12} = 196\pm40$ pm/V at $\lambda = 1.524$ µm up to now [5, 6].
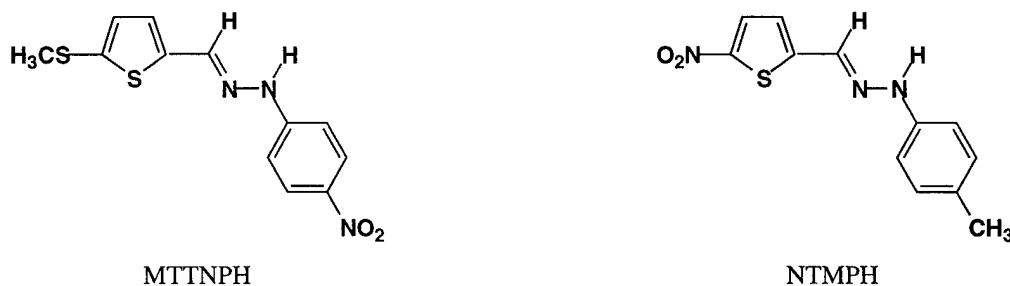
Fig.1 Formula of the hydrazone derivatives MTTNPH and NTMPH.

We have recently shown that thiophene based hydrazone derivatives can considerably enhance the molecular second-order nonlinearities [4]. Two examples of this series with excellent crystal properties are MTTNPH and NTMPH whose macroscopic nonlinear optical properties are here presented for the first time. MTTNPH is a type I hydrazone, whereas NTMPH belongs to the class of type II hydrazones (the difference lies in the position of the donor and the acceptor at opposite ends of the conjugation bridge since the hydrazone backbone is not symmetric). The vector parts of the first-order hyperpolarizabilities, β_z, determined with electric field-induced

second-harmonic generation at the wavelength $\lambda=1.907\mu m$, are $\beta_Z=130 \times 10^{-40}$ m^4/V (MTTNPH) and $\beta_Z=205 \times 10^{-40}$ m^4/V (NTMPH) [4].

3. Nonlinear optical properties

MTTNPH shows a high thermal stability (m.p.=172°C), good crystallinity, and easy crystal growth from solution. Single crystals of MTTNPH were grown from purified synthetic material by the controlled temperature lowering of a seeded saturated acetonitrile solution. By carefully preparing the seed crystals and controlling the supersaturation to develop the facets, typically single crystals of dimensions of about 25x5x5mm^3 were grown with good optical quality checked by polarized microscopy. MTTNPH has a large effective phase-matchable nonlinear optical coefficient, $d_{eff}= 29\pm3$ pm/V at $\lambda=1318$nm [5]. The relevant figure of merit $d^2_{eff}/n^3=126$ pm^2/V^2 is 16 times larger than the one of the highly nonlinear crystal KNbO$_3$ and more than 65 times higher than that of KTiPO$_4$ (KTP). The effective nonlinear optical coefficient d_{eff} is based on the large nonlinear optical coefficient d_{32}. The large off-diagonal nonlinear optical coefficients can be explained with the fact that the chromophores are bent in the crystal lattice and therefore more than one tensor element of the first-order hyperpolarizability β contributes to the macroscopic nonlinearities. Calculations based on the measured dispersion of the refractive indices indicate that MTTNPH crystals are suited for optic parametric oscillation when pumped with e.g. Ti:Sapphire lasers or low power laser diodes. A wavelength range from 1000nm to 2400 nm can be covered by angle tuning for a pump wavelength of $\lambda=800$nm. (Fig.2). For $\Phi = 0$ a large d_{eff} between 24 and 26 pm/V is expected neglecting the wavelength dispersion of the nonlinear optical coefficients [5].
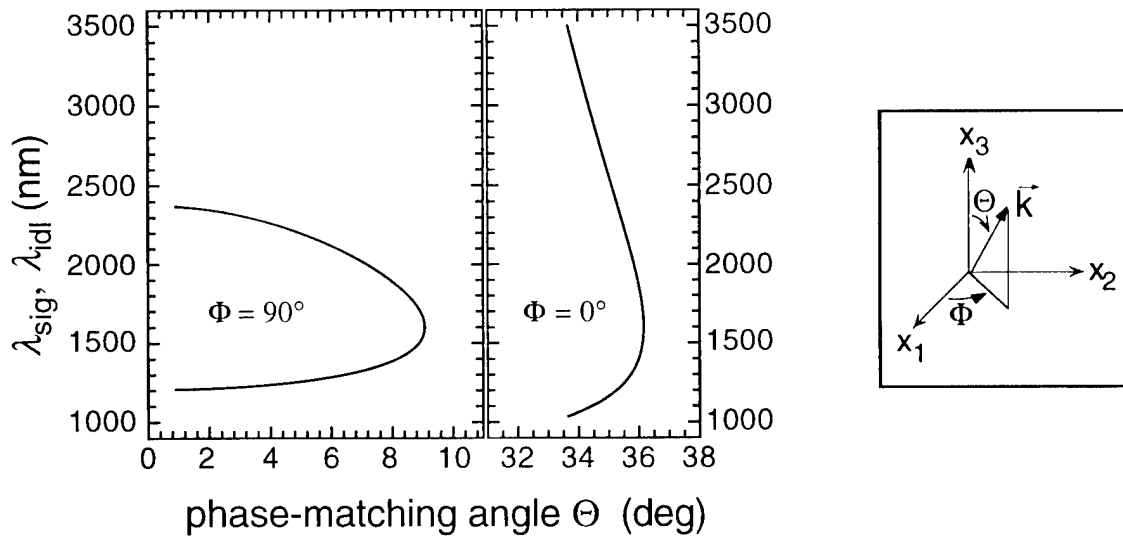
Fig.2 Phase-matching curves for sum-frequency generation or optical parametric oscillation of type I in a MTTNPH crystal. λ_{sig} and λ_{idl} are the signal and idler wavelengths, respectively. Tuning curves for one pump wavelength, $\lambda_3=800$ nm (Ti:Sapphire laser), were calculated based on the Sellmeier coefficients. $\Phi=90°$: polarization of the pump beam in the bc-plane. $\Phi=0°$: polarization of the pump beam in the ac-plane.

Re-crystallization of NTMPH in various solvents under different conditions yielded three crystalline phases, red greenish plates (NTMPH-I) in space group $P2_1/n$, red orange prisms (NTMPH-II) in space group $Pna2_1$, and black needle (NTMPH-III) in space group $P2_1/n$. The crystal structures of NTMPH showed that three different intermolecular forces dominate the stabilization of one- or two-dimensional structures of the three phases of the NTMPH crystals, namely the hydrogen bonding, dipole-dipole interactions, and the van der Waals forces for NTMPH-I, -II and -III crystals, respectively. The polar axes of the molecules in the NTMPH-II crystals are oriented with an optimized orientation for phase matched second-harmonic generation, making it an interesting second order nonlinear optical crystal (Fig.3). Nonlinear optical experiments of these crystals are in progress.

$\vec{\mu}$ = molecular dipole moment
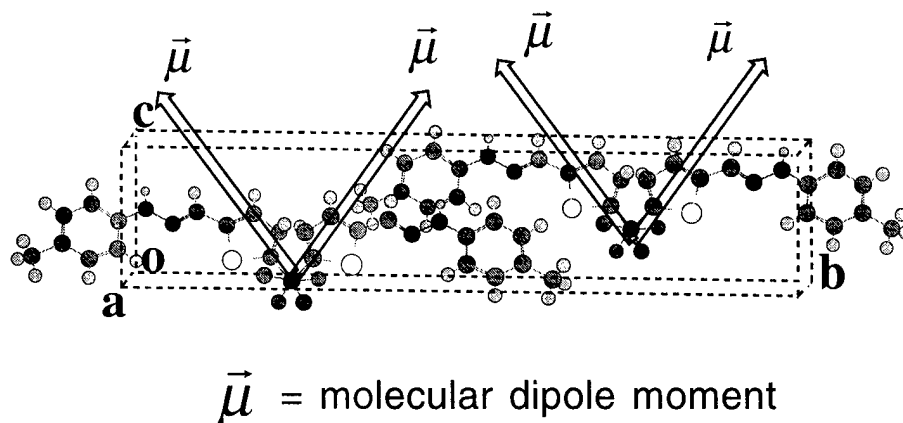
Fig.3   The three dimensional structure of the NTMPH-II crystals showing the direction of the molecular dipoles.

4. References

1.   C. Bosshard, K. Sutter, P. Prêtre, J. Hulliger, M. Flörsheimer, P. Kaatz, and P. Günter, *Organic Nonlinear Optical Materials,* edited by A. F. Garito and F. Kajzar (Gordon and Breach Science Publishers, Amsterdam, 1995)

2.   J. Zyss, Ed.,*Molecular Nonlinear Optics: Materials, Physics, Devices* (Academic Press, Inc., Boston, 1994)

3.   C. Serbutoviez, C. Bosshard, G. Knöpfle, P. Wyss, P. Prêtre, P. Günter, K. Schenk, E. Solari, and G. Chapuis, Chem. Mater. **7**, 1198 (1995).

4.   M. S. Wong, U. Meier, F. Pan, C. Bosshard, V. Gramlich, and P. Günter, Adv. Mater. **8**, 416 (1996).

5.   All nonlinear optical coefficients and hyperpolarizabilities in this text are based on $d_{11}=0.3pm/V$ of quartz at $\lambda=1064nm$ and the Miller-δ for the conversion to other wavelengths.

6.   S. Follonier, C. Bosshard, G. Knöpfle, U. Meier, C. Serbutoviez, F. Pan, and P. Günter, J. Opt. Soc. Am. B **14**, 593 (1997).

Difference in relaxation time between coherent and incoherent second-harmonic generation.

Koen Clays, Geert Olbrechts, David Van Steenwinckel, and André Persoons

Laboratory of Chemical and Biological Dynamics, Center for Molecular Electronics and
Photonics, Celestijnenlaan 200D, B-3001 Leuven, Belgium,
tel.: +321/632.75.08

The experimental technique of generating incoherent second-harmonic, also known as hyper-Rayleigh scattering, has become widely appreciated for the determination of the first hyperpolarizability β of nonlinear optical chromophores in solution. This technique was first demonstrated with nanosecond pulses from Neodymium-YAG lasers,[1] but has also been extended to femtosecond pulses from Titanium-sapphire lasers.[2]

A specific advantage of using femtosecond pulses is the low total energy content in a single pulse, that still delivers enough peak power for nonlinear effects to be observed. This low energy avoids optically induced heating and concomitant damage, especially in solid samples that exhibit slight absorption or point defects. In solutions, where the molecules are allowed to freely rotate, orientational averaging is necessary to deduce an actual value for the molecular hyperpolarizability. In solid samples, where the chromophores are fixed in orientation, knowledge of the orientational distribution of the chromophores is required to deduce this value. In both cases, a reference is necessary to give an absolute value for the molecular nonlinearity.

With femtosecond pulses on solid samples, a second important parameter in second-order nonlinear optics is also accessible, without the need for a reference. This parameter is the degree of spatial orientational correlation between the chromophores.

This correlation is important for the efficient generation of coherent frequency-doubled light or for electro-optic modulation with low driving voltages. The better all the chromophores are aligned in a non-centrosymmetric fashion and the longer the spatial orientational correlation length between aligned chromophores can be maintained, the larger the second-order nonlinear optical effect is. The positive effect of poling nonlinear optical polymer films on the second-order nonlinear optical susceptibility is well known. A positive effect of this poling on the spatial orientational correlation length was recently demonstrated.[3]

The experimental values for this spatial orientational correlation length vary between 50 and 200 μm. This is the case for samples with coherence lengths of the same order of magnitude, as well as for samples with millimeter coherence lengths from modal dispersion mode matching.[4] This difference has been attributed to the fact that a coherence length is solely determined by a first-order linear optical parameter, *i.e.* the linear refractive index, not influenced by symmetry-considerations, while the spatial orientational correlation length is inherently determined by the orientation of the chromophores, and hence is related to non-centrosymmetry. Although for perfectly quasi-phasematched structures, an infinite coherence length should be obtained from phase-matching curves, a finite interaction length is believed to result from this limited spatial orientational correlation length.

Apart from the positive influence of poling on the value of the spatial orientational correlation length, the negative effect of temporal relaxation has also been studied. Correlation lengths have been obtained as a function of time after poling. From these experiments, a temporal relaxation time for the spatial orientational correlation length has been retrieved. These relaxation times have been compared with the relaxation times obtained using more classical coherent second-harmonic generation studies at elevated temperature and extrapolation to room temperature. A significant discrepancy has been observed.[5] The relaxation time for the spatial orientational correlation length, as obtained from incoherent hyper-Rayleigh scattering, is much shorter than the one from coherent second-harmonic generation. This has consistently been observed for different kinds of polymeric thin films.

An explanation for this observation is now proposed. The observed magnitude for the ratio between the relaxation time for the coherent process and that for the incoherent one is 540 days / 3.4 days ≈ 160. This is the same magnitude as the square of the ratio between the coherence length (relevant for the coherent measurement, and for the poly(methylmetacrylate) polymer system in the dispersion-free spectral region approximately equal to 10 μm) and the wavelength (relevant for the incoherent measurement, and for the Titanium-sapphire system equal to 800 nm). This unequivocally points to translational diffusion, as governed by $<x^2> = 2Dt$. The (translational) diffusion coefficient D (in cm^2/s) governs the speed of diffusion. The incoherent measurement will already be affected after diffusion over a distance only equal to the wavelength, while only after diffusion over a whole coherence length will this be so for the coherent measurement. From the dimensions of the diffusion coefficient necessary in this analysis, it follows that translational diffusion should be invoked as the physical mechanism responsible for the relaxation of the non-centrosymmetry. We invoke fast *rotational* relaxation for the *noncentrosymmetric* chromophore when in a free volume pocket in the polymer matrix, combined with *translational* diffusion of the *centrosymmetric* free volume pocket. The chromophore is capable of rotational relaxation only when it is given enough free volume. In this way, the temporal relaxation of non-centrosymmetry can be related to translational diffusion, as suggested by the experimental observations.

references:

1. K. Clays and A. Persoons, "Hyper-Rayleigh Scattering in Solution," Phys. Rev. Lett. **66**, 2980-2983 (1991).
2. K. Clays and A. Persoons, "Hyper-Rayleigh Scattering in Solution with tunable femtosecond continuous-wave laser source," Rev. Sci. Instrum. **65**, 2190-2194 (1994).
3. G. Olbrechts, E. Put, K. Clays, A. Persoons and N. Matsuda, "Probing of spatial orientational correlations between chromophores in polymer films by femtosecond hyper-Rayleigh scattering," Chem. Phys. Lett. **253**, 135-140 (1996).
4. unpublished results,
5. N. Matsuda, G. Olbrechts, E.J.H. Put, K. Clays and A. Persoons, "Comparison between optical nonlinearity relaxation times from coherent second-harmonic generation and from incoherent hyper-Rayleigh scattering," Appl. Phys. Lett. **69**, 4145-4147 (1996).

Poster Session

Thursday, October 16, 1997

ThE
4:30pm–7:00pm
Seaview C

Third-order nonlinear optical property of platinum group metal complexes with square planar configurations.

Takehito Kodzasa, Hirobumi Ushijima, Hiro Matsuda and Toshihide Kamata

Department of Physical Chemistry
National Institute of Materials and Chemical Research
1-1 Higashi, Tsukuba, Ibaraki, 305 **Japan**.
+81-298-544536.

Introduction

The developments of novel materials having large third-order nonlinear optical susceptibility $\chi^{(3)}$ and fast response give a considerable interest as the key subjects for future optoelectronic technology. It was proved in former researches that the large low dimensional delocalization field for optically excited electron is effective for large $\chi^{(3)}$ value. Third-order optical nonlinearities of many materials, mainly inorganic semiconductors or organic conjugated polymers, have been investigated. Many inorganic materials have studied for their large $\chi^{(3)}$ and thermal stability. On the other hands, organic nonlinear optical materials also have been noted, because they have advantages of fast optical response, architectural flexibility and ease of fabrication.

The transition metal complex is greatly promising material, because it is able to combine large optical nonlinearlity and thermal stability of transition metal with fast response and architectural flexibility of organic ligands. It had been thought that the metal complex is not suitable for it because of electrically shielding effect of organic ligands. In the case of the complex with square planar configurations, it has the great possibility to construct a large delocalized field of optically excited electrons through the stacking of complex molecules, because it has two electrically opened sites upon the square plane of the complex. The stacking manner can be divided into three styles: **[type A]** Metal stacked along a normal axis to from linear metal chain (-M-M-).   **[type B]** Metal stacked on a ligand to form one-dimensional metal-ligand chain (-M-L-M-).   **[type C]** Metal stacked to form a small associate by a few molecules.

In this study we prepared the vapor-deposited thin films of square planar platinum complexes with different stacking forms and carried out the measurements of third-order nonlinear optical property of them[1,2]. We discuss these results from a relationship between the stacking manner of planar molecules and intermolecular electrical interaction.

Experiments

Molecular structure of platinum complexes used in this study are shown in Figure 1. [Type A : dionedioxme metal complexes, Type B : dithiolene metal complexes, Type C : Shiff base metal complexes.]   Bis(1,2-disubstituted-1,2-ethylenedithiolato)metal(II) (B) were synthesized by
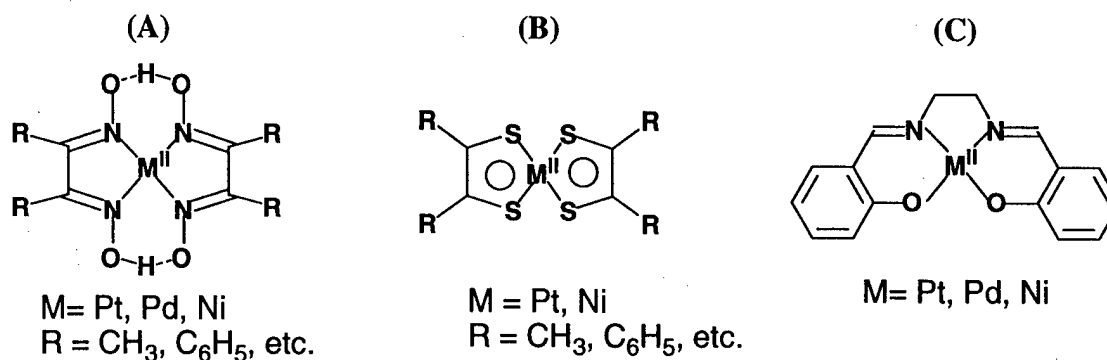
(A)

M= Pt, Pd, Ni
R = CH₃, C₆H₅, etc.

(B)

M = Pt, Ni
R = CH₃, C₆H₅, etc.

(C)

M= Pt, Pd, Ni

Figure 1 Molecular structure of platinum group complexes used in our study

the method of Schrauzer et al.[3]. Other complexes were prepared by reactions of metal chloride with available ligands in water-alcohol solution. Their vapor-deposited thin films were obtained onto quartz substrate at ca. 10^{-4} Torr. Thickness of the thin film measured by Tencor Instruments Alpha-step 300 surface profilometer were ca. $0.1\mu m$. Linear transmission spectra of the film were recorded in the wavelength range between 200-2500 nm. $\chi^{(3)}$ values of films were estimated by the third harmonic generation(THG) Maker-fringe method[4]. They were carried out between 1.5 and 2.1 μm of fundamental wavelength. The value of $\chi_s^{(3)}=1.0 \times 10^{-14}$ esu for fused silica glass was used as the standard reference.

Results and Discussion

[Type A] It is known that some of platinum group metal complexes with dionedioxime ligands form linear metal chain. Linear absorption spectrum of thin film of bis(1,2-dimethyl-1,2-ethylenedione-dioximato) platinum is shown in Figure 2. A strong absorption band appear at around 680nm. The band is assigned to the $5d_{z^2}$-$6p_z$ transition of platinum ions, which arises from d-orbital overlapping between adjacent platinum metals in the stacking planar molecules[5]. $\chi^{(3)}$ values at various third harmonic wavelengths are also plotted in Figure 2. The $\chi^{(3)}$ values are 0.3-2.2 X 10^{-11} esu, which increase with linear absorption coefficients of the film. This shows that their optical nonlinearities are enhanced by three photon resonance on delocalized-electrons of platinum chains. That is to say, a strong interaction in one-dimensional chain consisted from central metal ion of square planar complexes plays important role for their optical nonlinearities.
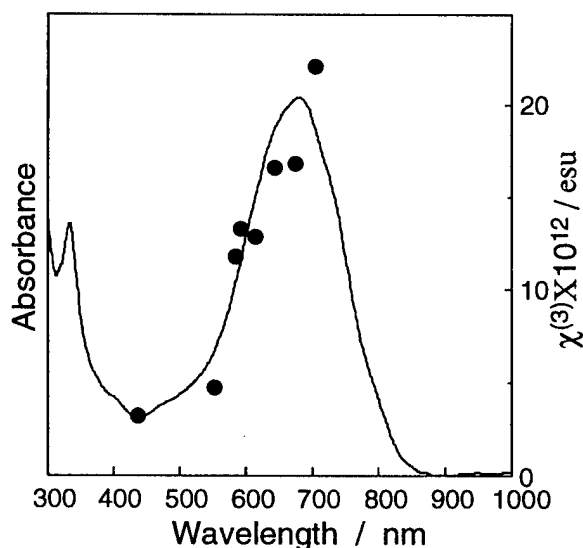
Figure 2   UV-Vis spectrum(solid line) and $\chi^{(3)}$ (●) of thin film of compounds (A) (M=Pt, R=CH₃).

[Type B] Figure 3 shows linear absorption spectrum of thin films of bis(1,2-diphenyl-1,2-ethylenedithiolato) platinum. A large absorption band, appeared at ca. 800nm, is assigned to low energy $\pi-\pi^*$ transition from ligand rings linked through the central metal ion. Transition metals dithiolene complexes with square planar configuration has the delocalized π-d electron system consistent from the central metal ions and sulfur-coordinating ligands, though they do not have direct metal-metal stacking[6]. $\chi^{(3)}$ values at third harmonic wavelength are also plotted in Figure 3. The $\chi^{(3)}$ values ($<5.2\times10^{-12}$esu) are also enhanced by three photon resonance on the

Figure 3 UV-Vis spectrum(solid line) and $\chi^{(3)}$ (●)of thin films of compounds (B) (M=Pt, R=C_6H_5) .

band. This seemed to be lead from the effect of spreading π-d electron system among slidely stacked complexes.

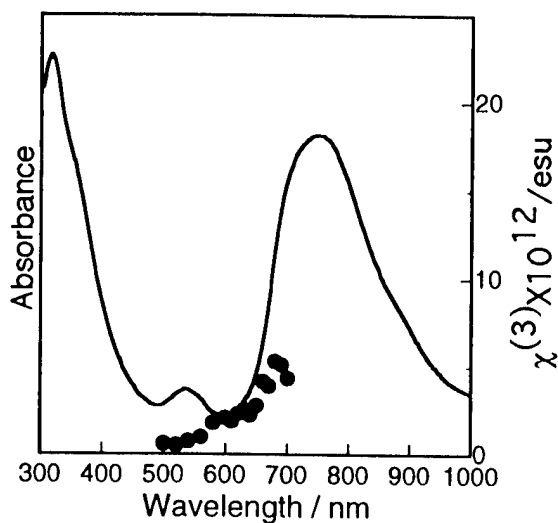[Type C] Bis-(salicylaldehyde) ethylenediimine transition metal(II) complexes forms dimer or trimer through the metal-oxygen stacking in their solid state. This type can not form large delocalized electric field like former complexes. Thus they do not show large absorption bands in the visible-near IR region like former complexes. Their optical nonlinearity was also estimated by THG measurements. However enough strong signal could not be observed. This means $\chi^{(3)}$ values of them are below 10^{-13} esu.

From above results, it is suggested that transition metal complexes with square planar configuration are greatly promising for the nonlinear optical material, because they can have the intermolecular electric correlation between central metals of the stacked molecules. Especially those of forming linear metal chain by stacking along the normal axis of planer complexes are comparatively superior to those of forming metal-ligand chain.

REFERENCE

1. T. Kamata et al. Chemical Physics Letter, 221, 194(1994).
2. H. Ushijima et al. Molecular Crystals & Liquid Crystals, 286, 275(1996).
3. G. N. Schrauzer et al. Journal of American Chemical Society, 78, 1483(1956).
4. T. Kamata et al. Journal of Physical Chemistry, 99, 13239(1995).
5. Y. Ohashi et al. Inorganic Chemistry, 9(11), 2551(1970).
6. D. Sartain et al. Journal of Chemical Society (A), 1264(1967).

Nonlinear absorption in CuPc-SiO$_2$ Composite

E. Blanco[†], R. Litrán and M. Ramírez-del-Solar
Dep. Física de la Materia Condensada. Universidad de Cádiz. SPAIN
F.J. Aranda and D.V.G.L.N. Rao
Physics Department, University of Massachusetts, Boston, MA 02125
D. Narayana Rao[‡][†] , J.A.Akkara and M. Nakashima
US Army Natick Research Development and Engineering Center, Natick, MA
S. Tripathy
Center for Advanced Materials, University of Massachusetts, Lowell, MA

Recently macrocyclic organic dyes have attracted a lot of attention as possible candidates for applications in optical power limiters and pulse shaping devices. The fundamental requirement for power limiting is that the system must exhibit fluence dependent reverse saturable absorption. Copper Pthalocyanines possess a larger excited state absorption cross section than a ground state absorption cross section. They are thus suitable candidates for limiting applications. Most of the nonlinear optical studies have been done for solutions of the dyes[1]. For applications such as intracavity pulse shaping devices a solid material is more attractive than a solution[2]. In this paper we report nonlinear absorption studies of Copper Pthalocyanine, CuPc, in solution in sulfuric acid as well as incorporated in a Silica matrix host. The concentration of the solution was 5.75 x 10^{-4} Molar. The composite had a concentration of 1 x 10^{-4} Molar in the sol. Upon drying of the gel we estimate a similar concentration for the composite as in the solution given the reduction in volume. The thickness of the composite is of 4 mm. The solution was held in 1 mm thick spectroscopic grade glass cuvettes. The CuPc/silica composite was obtained by the Sol-gel method from the hydrolysis of tetramethoxysilane (TMOS). The reaction of TMOS with acidic water (pH=2) was promoted by means of 20 kHz ultrasound energy. The resulting gel was kept drying at room temperature for two weeks. We observe marked differences in the linear absorption spectrum of the solution and the composite. These changes are attributable to aggregation of the Copper Pthalocyanine molecules in the pores of the silica matrix as well as to the interaction between the dye molecules and the matrix. The linear absorption spectrum for both samples is shown in Fig. 1.

[†] Visiting Professor at University of Massachusetts at Boston ; [‡]NRC Fellow
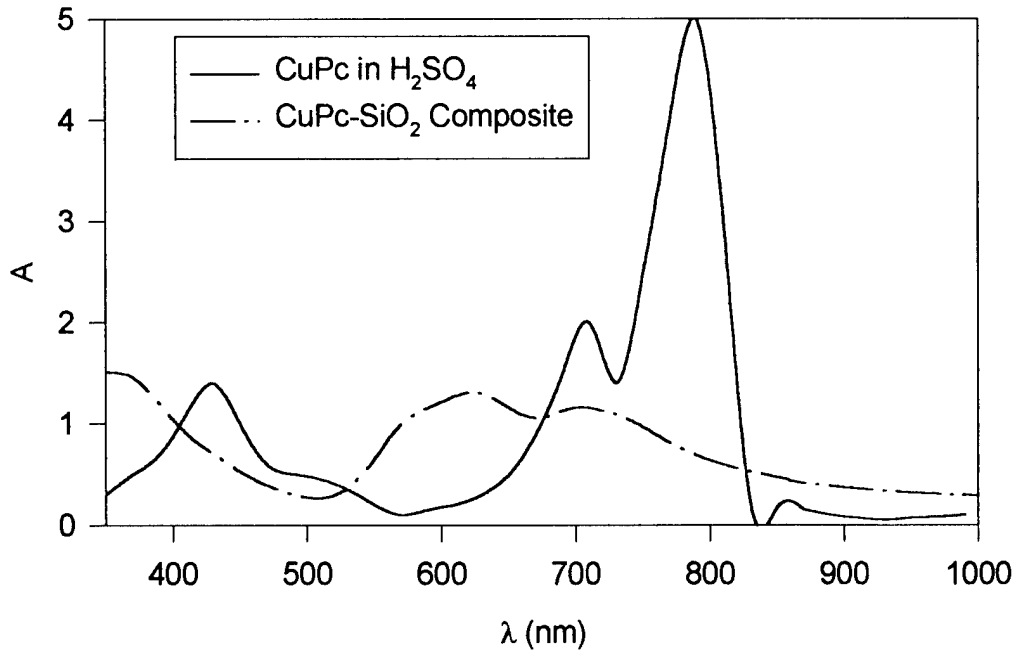
Figure 1. Linear absorption spectrum of the CuPc solution and the composite.

The linear absorption at 530 nanometer wavelength was of 0.2 absorbance units for the solution and of 0.35 absorbance units for the composite. The nonlinear absorption of the samples was studied using the Z-scan technique with 4 nanosecond pulses at 530 nanometer wavelength. The laser source was a repetitively pulsed (10 Hz) Spectra Physics Nd :YAG pumped optical parametric oscillator. Open aperture Z-scans were obtained for both samples, the results are shown in Figs. 2 and 3. The average energy per pulse incident on the samples was of 0.1 mJ for the solution and of 1.2 mJ for the composite. The two samples exhibit reverse saturable absorption. We fitted the data[3] to

$$T = \ln\left(1 + \frac{q_0}{1+x^2}\right)\bigg/\left(\frac{q_0}{1+x^2}\right) \tag{1}$$

where $q_0 = \dfrac{\sigma_{eff}\,\alpha F_0 L_{eff}}{2\hbar\omega}$ and $x = z/z_0$, in order to obtain the effective excited state absorption cross sections. The solution has σ_{eff} of 9.783×10^{-18} and the Pthalocyanine/silica composite has σ_{eff} of 1.097×10^{-18}.
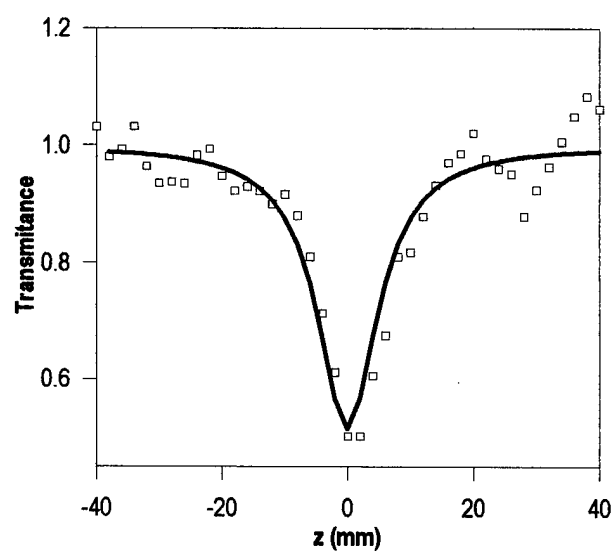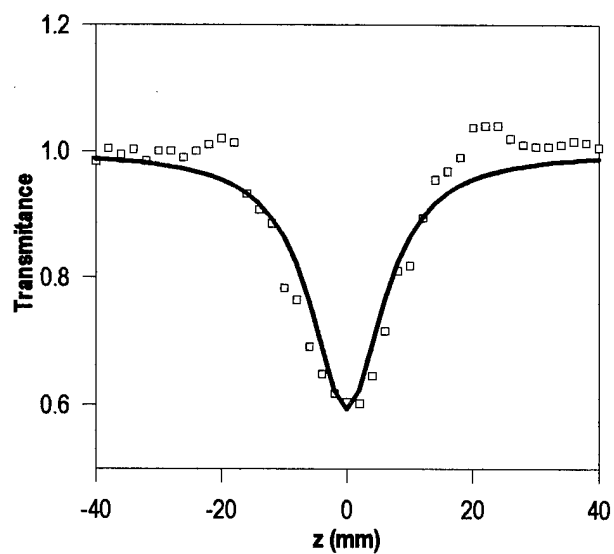
Figures 2 and 3. Open aperture Z-scans for composite (upper trace) and solution (lower trace)

1. T.H. Wei, D.J. Hagan, M.J. Sence, E.W. Van Stryland, J.W. Perry, D.R. Coulter, Appl. Phys. B, **54**, 46 (1992)
2. F. Bentivegna, M. Canva, P. Georges, A. Brun, F. Chaput, L. Malier, J. Boilot, Appl. Phys. Lett., **52**, 1721 (1993)
3. G.L. Wood, M.J. Miller, A.G. Mott, Opt. Lett., **20**, 973 (1995)

Linear Electro-Optic measurements of Dye-Doped Polymers

F. Ghebremichael and R. J. Knize[1]
Laser and Optics Research Center
Physics Department, USAFA, CO 80840
Phone/FAX: 719-333-2483/3182
ghebremichaelf.dfp@usafa.af.mil

INTRODUCTION

The basic Mach-Zehnder interferometer was modified for use in *in-situ* temperature dependent linear electro-optic (LEO) measurements of thin films of 4-dimethylamino-4'-nitrostilbene (DANS) doped into poly(methyl methacrylate) (PMMA). Optimum interferometer phase stability was possible because of an incorporated electronic feedback system. Film thickness variation was compensated for in order to obtain more accurate LEO coefficient measurements and thus the second order susceptibility. Moreover, both the α–relaxation associated with the glass transition, T_g, and β-relaxation associated with the secondary transition occurring below T_g of PMMA + 2%wt.DANS were obtained.

EXPERIMENT

Nonlinear organic chromophores were incorporated into the polymer matrix by dissolving PMMA and 2%wt. DANS. Films were then prepared by spin coating the solution on 1" x 2" indium tin oxide (ITO) coated glass substrate pieces. Two such films were then joined with their polymer sides touching and fused together by raising their temperature to above T_g for an hour under an applied pressure. The ITO-film-ITO sandwich configuration resulted in films of about 5-10 μm thickness.

The samples were subjected to chromophore-aligning electric fields in order to induce bulk asymmetry necessary to observe second-order nonlinear optical effects. The strength of the LEO signal intensity, which is related to the degree of chromophore alignment, was then used to characterize the polymer system. In the *in-situ* experiments, the poling field and the temperature were varied, whereas in the pre-poled-sample experiments, the temperature was varied and the LEO signal monitored without the application of a poling field. The poled films were prepared by maintaining the temperature 10°C above T_g for three hours with a dc voltage of 100 V applied. The temperature was then allowed to reach room temperature with the voltage still on. The electric field induced phase variations in the films resulted from the changes in refractive index and the film thickness variations:[2]

$$\Delta\phi = \frac{2\pi}{\lambda}\left[l\Delta n_s + n_s\Delta l\right]$$

where λ = 632.8 nm is the laser wavelength, *l* is the beam path in the film, and n_s is the refractive index in the film sample. In order to get the proper behavior of the LEO coefficient, which depends solely on the modification of the refractive index, the phase change from the thickness variation must be eliminated. Figure 1 shows the technique used to achieve minimum thickness variation effect. The ITO-polymer-ITO configuration was gold coated covering half of the sample on both sides and mounted on a heating block (not shown in the figure).

QW = λ/4 Retarder
M = Gold Coating
BS = Polarizing Beam Splitter
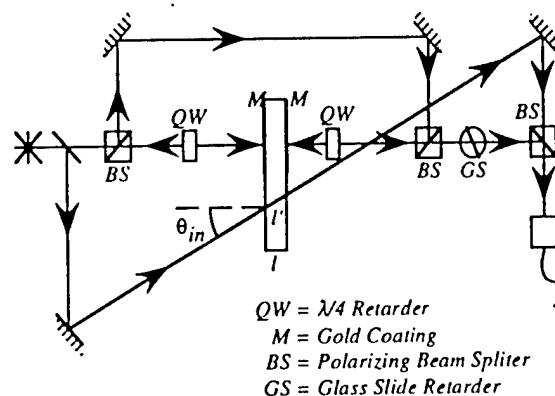GS = Glass Slide Retarder

Figure 1. Modified Mach-Zehnder Set-up

The reference beam was made to reflect off the gold mirrors (on both sides) and then recombine with the beam passing through the sample at an incident angle. A feedback control system compensated for changes in the path lengths of the interferometer arms by proportionally rotating a glass plate placed in one of the arms (GS in Fig. 1.)

RESULTS AND DISCUSSIONS

The results of the modifications is shown in Fig. 2. Contributions from effects such as electrostriction, Coulomb attraction of the electrodes , and piezoelectric are significantly reduced, leaving room for better determination of the electro-optic effect.
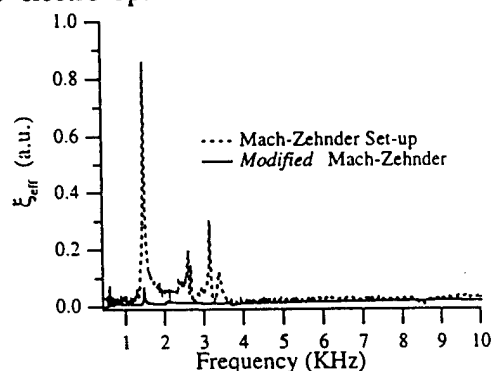

Figure 2. Frequecy spectrum of interferometer output

Figure 3 shows the phase and the intensity outputs of the lock-in amplifier, and the reference signal. The reference and the lock-in amplifier outputs were in phase during the contrast measurement taken using a beam-chopper at 2 kHz. The reference output signal was used in the feedback system which was used to control the relative interferometer phase. The LEO dependent intensity shows two peaks for every cycle of the unmodulated reference output, the bottom curve of Fig. 3
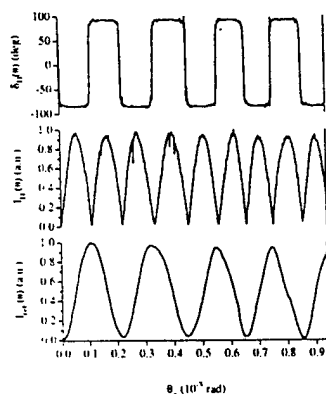

Figure 3. Contrast and optimum output phase determination

The positions of the peaks, corresponding to maximum sensitivity of the interferometer, fall at the maximum slope positions of the reference

trace. The top curve of Fig. 3 shows the relative phase. The electronic, electrostriction, and orientation effects of the polymer have very fast responses (10^{-15}, 10^{-12}, and 10^{-9} seconds, respectively) therefore their relative phases are restricted to 0 or π in the time scales of our experiments.[3] Figure 3 shows the π change (shifted by $\pi/2$ in the figure) associated with the sign of the slope of the reference curve. This information was used by the feedback system in selecting the relative phase of the interferometer. Errors arising from RF pick-up and thermal fluctuations were significantly minimized by measuring the LEO coefficient at several ac amplitudes. In the pre-poled-sample experiments, as the temperature of the poled sample was raised, the LEO coefficient remained virtually constant up to the T_g of the sample, after which it started to decrease until the signal was no more detectable at about $T_g + 20$ °C. This is consistent with the results of Ren et al.[4] As the temperature was raised, the thermal energy gained by the chromophores helped them to agitate into randomness thus diminishing the poling-induced bulk asymmetry necessary for second-order nonlinear effects. Figure 4 shows the result of such an experiment. The curvature of the decay knee is dictated by the breadth of the distribution of relaxation times.
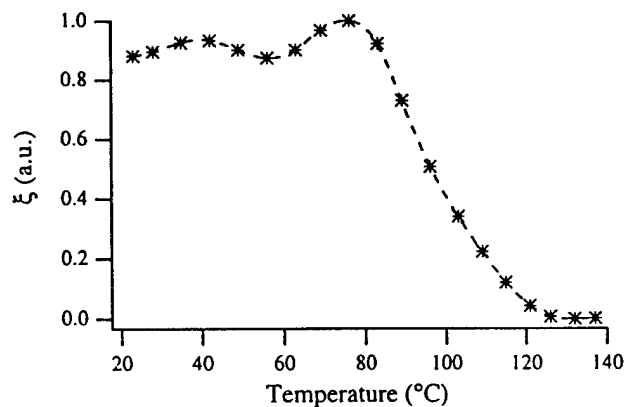

Figure 4. Temperature dependency of a prepoled film

The molecular mobility is greatly influenced by the polymer matrix and reveals the micro-environment of the doped polymer system where the chromophores reside. In Figure 4 there is a slight increase of the LEO coefficient

just before the curve starts its steep decline at T_g. The anomalous maximum occurred at the temperature at which an increased alignment was also observed in the *in-situ* poling measurements. In these experiments a fresh sample was placed in the heating block and the LEO coefficient measured at various temperatures with a poling field of 50 volts applied each time.
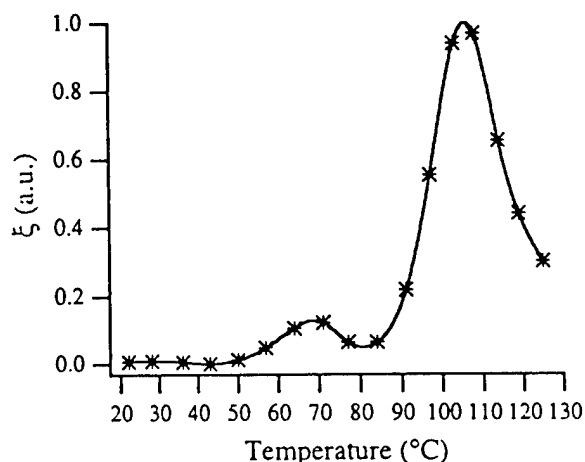

Figure 5. Polymer mobility as a function of temperature

Figure 5 shows a typical data with a large increase in the effective LEO coefficient at T_g (~98 °C) followed by a pronounced peak.

As the polymer becomes soft near or above T_g, the order parameter increases resulting in a better molecular alignment, thus a higher second order parameter and consequently a higher LEO coefficient. It also shows a smaller

secondary peak at about 70 °C. The secondary peak is attributed to the β-transition of the polymer. Experiments on different chromophore concentrations showed the same characteristic shape of the temperature dependence curve, with T_g slightly moving to lower temperatures with increased concentration while the secondary peak remaining virtually the same. The sub-T_g phase transition has been seen in studies of TSD,[5] and dielectric relaxation (DR).[6]

CONCLUSIONS

With this new technique incorporating *in-situ* poling, it was possible to study the electro-optic effect as a function of temperature and poling field. It included a novel idea of eliminating from consideration the thickness variation that arises with the application of the poling fields to thin films. The set-up can be used to quickly determine the mechanical thickness response of a film sample. This technique has displayed its versatility in measuring the LEO effect as a function of several parameters in single experimental set-up. It has also been demonstrated for the first time that optics may be used to study the thermal and temporal characteristics of the secondary mechanical relaxation of polymers. It is important to understand all the mechanical, thermal and temporal behaviors of these device oriented polymer systems for a better commercial feasibility.

REFERENCES

[1] This work is supported by the Air Force Office of Scientific Research.
Part of the work was done at Purdue University with Prof. H. Lackritz.

[2] T. Kobayashi, "A method for measuring electrooptical constants," Nonlinear Optics, 1, 239-252 (1990).

[3] P. N. Butcher and D. Cotter, The Elements of Nonlinear Optics, Cambridge University Press, Cambridge, (1990).

[4] W. Ren, S. Bauer, S. Yilmaz, W. Wirges, and R. Gerhard-Multhaupt, "Optimized poling of nonlinear optical polymers based on dipole-orientation and dipole-relaxation studies," J. Appl. Phys. 75, 7211-7219 (1994).

[5] W. Kohler, D. R. Robello, P. T. Dao, C. S. Willand, and D. J. Williams, "Second harmonic generation and thermally stimulated current measurements: A study of some novel polymers for nonlinear optics," J. Chem. Phys., 93 , 9157-9166 (1990).

[6] N. G. McCrum, and R. E. Read, and G. Williams, Anelastic and dielectric effects in polymeric solids, (Wiley, London, 1967).

Linear and Second- Order Nonlinear Optical Properties of Urethane-Urea Copolymers

Masaaki Tsuchimori, Osamu Watanabe and Akane Okada

Toyota Central Research and Development Laboratories Inc., 41-1 Yokomichi, Nagakute, Nagakutecho, Aichigun, Aichi 480-11, Japan

Nonlinear optical (NLO) polyurethanes have been intensively studied to develop electro-optic devices, because they have not only large second-order NLO coefficients (d_{33}) but also good temporal stability of d_{33} at room temperature [1,2]. We have reported that introducing urea groups into main chains of polyurethanes, namely urethane-urea copolymers, improves the temporal stability at elevated temperatures [3]. The copolymers have many advantages, for example easiness of synthesis, relatively high intrinsic viscosity [η] (molecular weight), easiness of poling process, and applicability of photobleaching method [4]. In the present work, linear and second-order nonlinear optical properties of the copolymers are discussed.

Urethane-urea copolymers were prepared by a two-step reaction scheme as shown in Fig. 1. In this scheme, diol (1) having a NLO-active group reacted with a diisocyanate in the first step to prepare a diisocyanate containing urethane groups, and then the resulting diisocyanate was polymerized with a diamine in the last step to prepare the copolymer. In these reactions, an amount of solvent was found to affect [η] strongly. Polyurethanes were also prepared by polymerizing diol (1) with diisocyanates in order to compare their properties.

Physical, thermal and NLO properties were observed by the same methods described in the references [3,5]. The [η] was measured in N-methyl-2-pyrrolidone (NMP) at 30°C. Refractive indices and propagation losses of slab waveguides at an 830-nm wavelength were measured using a Metricon model 2010 prism coupler. Polymer films spin-coated on slide glasses were used for the measurements.

Fig. 1 Synthesis of urethane-urea copolymers.

Table 1 Physical properties of polymers.

polymers	[η] (dL/g)	T_g (°C)	diol contents (wt%)	λ_{max} (nm)	α [a] (μm^{-1})	refractive indices [b]	
						532 nm	1064 nm
UT1	0.20	135	67	475	9.5	1.98	1.72
UT2	0.32	130	59	476	8.4	1.94	1.72
UU1	0.35	141	53	474	8.0	1.89	1.69
UU2	0.58	141	45	475	6.2	1.91	1.69

[a] The absorption coefficients at 532 nm.

[b] These values were measured for non-poled thin films using an ellipsometer.

Physical properties of four synthesized polymers are listed in Table 1. Monomers of these polymers are listed in Table 2. Copolymers UU1 and UU2 showed higher [η] and T_g than polyurethanes UT1 and UT2. The higher [η] of copolymers is presumably owing to higher reactivity of NH groups as compared with OH groups. In order to form a film 3 μm thick without any clucks, [η] of a urethane-urea copolymer was requested to be higher than ca. 0.3 dL/g. Since introducing urea groups into a main chain of a polyurethane reduces a diol content, magnitude of nonlinearity was also reduced by the introduction (Fig. 2). An optimum poling temperature (T_p^{opt}) was increased by increase of a urea content (Fig. 3). The increase of T_p^{opt} led to improvement of temporal stability of d_{33} (Fig. 4). Observed NLO properties are listed in Table 3.

Slab waveguides of the synthesized polymers were prepared by spin-coating from pyridine solution. Refractive indices (n) and propagation losses of the slab waveguides depended strongly on film preparation and film thickness (Table 4 and Fig. 5). For as spun film, both n and loss of TE mode were larger than those of TM mode. These

Table 2 Monomers.

polymers	monomers		
	diol	diisocyanate	diamine
UT1	(1)	TDI	—
UT2	(1)	MDI	—
UU1	(1)	TDI	DMP
UU2	(1)	MDI	DMP

TDI; toluene-2,4-diisocyanate
MDI; 4,4'-diphenylmethane diisocyanate
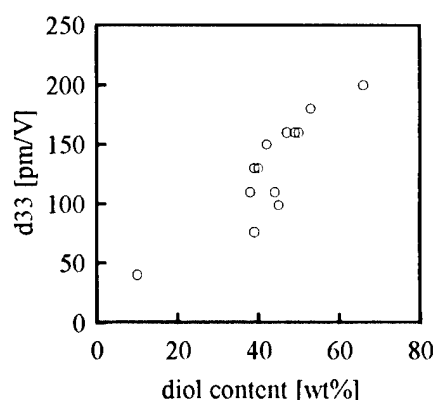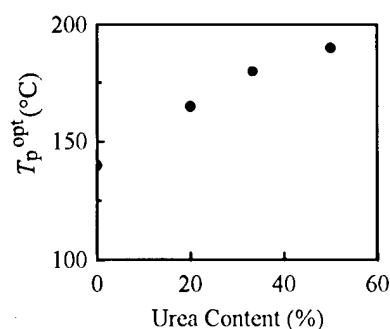DMP; trans-2,5-dimethylpiperazine

Fig. 2 Relation between a diol content and d_{33} for urethane-urea copolymers and polyurethanes.

Fig. 3 Optimum poling temperatures versus urea contents of the polymers synthesized from the same monomers with difference molar ratio.
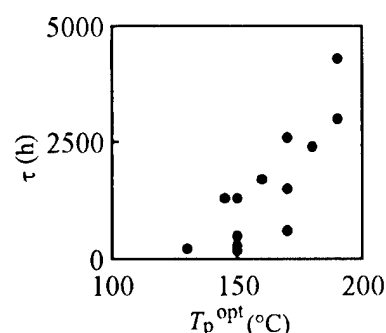

Fig. 4 Relation between an optimum poling temperature and a relaxation time obtained by fitting temporal behaviour of d_{33} at 100°C.

Table 3 Nonlinear optical properties

polymers	$T_p^{opt\ a}$ (°C)	$d_{33}^{max}(0)^{\ b}$ (pm/V)	τ (h)^c 80°C	τ (h)^c 100°C
UT1	140	220	>10000	1300
UT2	140	210	>10000	500
UU1	180	190	>10000	4300
UU2	170	140	>10000	2400

[a] Optimum poling temperatures.

[b] Maximum d_{33} shortly after poling at a 1064-nm fundamental wavelength.

[c] Relaxation times of d_{33} fitted by a stretched exponential function.

Table 4 Refractive indices and propagation losses (dB/cm) at 830 nm of copolymer UU2.

samples	n TE	n TM	loss TE	loss TM
as spun	1.698	1.676	3.9	3.3
annealed [a]	1.697	1.692	4.1	3.7
corona-poled	1.684	1.713	7.0	7.4

[a] 150°C, 2h.

Fig. 5 Propagation losses at an 830-nm wavelength of non-poled UU2 films.

differences between TE and TM modes decreased by annealing a film above T_g. In the case of a corona-poled film, both n and loss of TE mode were smaller than those of TM mode. These results are interpreted as follows. The NLO group used in this study is considered to have larger polarizability and stronger absorption along its dipole moment as compared with those perpendicular to the moment. The anisotropy of n and loss indicates orientation of the NLO groups. In as spun film, the NLO groups are ordered with their dipole moment parallel to the film. The order is fairly randomized by the annealing.

Single mode cannel waveguides were also produced using copolymer UU2 by the photobleaching technique. Optical propagation losses of the cannel waveguides were measured at 13 and 0.5 dB/cm at 830-nm and 1300-nm wavelengths, respectively. The electro-optic (EO) coefficient (r_{33}) at an 830-nm wavelength was estimated from retardation of an EO modulator by 12 pm/V.

In conclusion, we have presented potential of urethane-urea copolymers for photonic application. Though the synthesized copolymers showed large propagation losses at an 830-nm wavelength, they are applicable to waveguide devices at a 1300-nm wavelength. Making such devices is under way.

References

[1] M. Chen, L. Yu, L. R. Dalton, Y. Shi and W. H. Steier: *Macromolecules* **24** (1991) 5421.

[2] R. Meyrueix, J. P. Lecomte and G. Tapolsky: *Proc. SPIE* **1560** (1991) 454.

[3] M. Tsuchimori, O. Watanabe, S. Ogata and A. Okada: *Jpn. J. Appl. Phys.* **35** (1996) L444.

[4] O. Watanabe, M. Tsuchimori and A. Okada: *J. Mater. Chem.* **6** (1996) 1487.

[5] M. Tsuchimori, O. Watanabe and A. Okada: *J. Mater. Chem.* in press.

Orientational Relaxation of NLO Dipole Moments Transversely Aligned to the Main Backbone in the Linear Polyurethane

Naoto Tsutsumi, Osamu Matsumoto and Wataru Sakai
Department of Polymer Science & Engineering, Kyoto Institute of Technology, Matsugasaki, Sakyo, Kyoto 606, Japan
Phone: +81-75-724-7810, Fax: +81-75-724-7800, E-mail: tsutsumi@ipc.kit.ac.jp

Introduction

Recently, we have synthesized a new type of linear polyurethane (T-polymer) with NLO azobenzene chromophore whose dipole moment is aligned transverse to the main chain backbone and another linear urethane polymer (L-polymer) with NLO dipole chromophore incorporated in the main chain backbone.[1] The resultant poled T-polymer shows the large second order nonlinearity of d_{33}=1.6 × 10^{-7} esu (67 pm/V) with good thermal stability at the ambient conditions.[1] This polymer is amorphous with a high density of NLO chromophore moiety and optically transparent thin film, which can be processed by spin-casting or solvent casting.

In this paper, the orientational relaxation of NLO dipole moments in the T-polymer corona-poled at two different temperatures is studied from the time-dependent decay of the SHG activity at the several elevated temperatures. The resultant orientational relaxation of the aligned NLO chromophore is discussed in relation to the structural factor of the effective glass transition temperature for SHG activity due to the smaller free volume.

Figure 1. Molecular structure of T-polymer

Results

Polymer sample investigated is T-polymer prepared with 4-[(2-hydroxyethyl)amino]-2-(hydroxymethyl)-4'-nitroazobenzene (T-AZODIOL) and aromatic diisocyanate 2,4-tolylene diisocyanate (TDI). Chemical structures polymer is shown in Figure 1. NLO chromophore in T-polymer has a feature that one head is embedded in the polymer backbone and the dipole moments extend transverse to the main chain. Reduced specific viscosity of T-polymer was 0.14 dL/g. Differential scanning calorimetry (DSC) measurement gives that T-polymer has the glass transition temperature, T_g, at 57°C.

Figure 2 shows the SHG activity profiles of d_{33} vs. annealing temperature (solid curve in the figure) and d_{33} vs. poling temperature (dashed curve in the figure). In the poling process, the dependence of d_{33} on the poling temperature shows two step increase
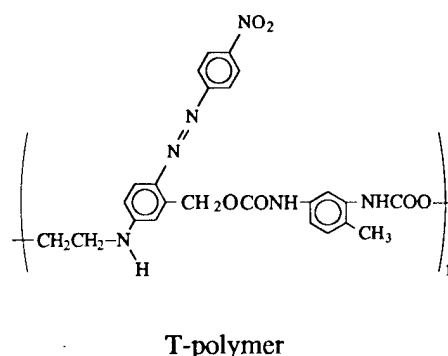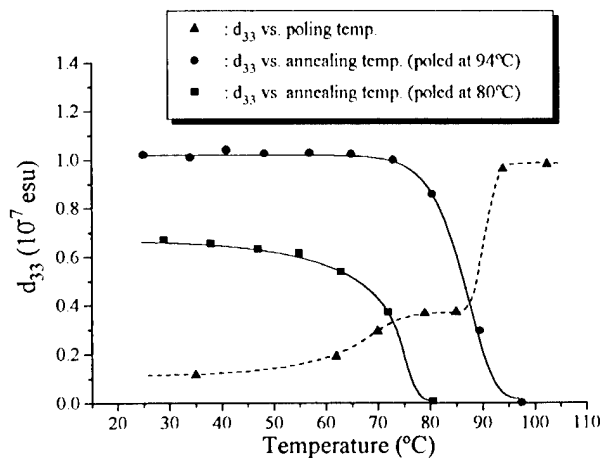

Figure 2. Dependence of d_{33} on poling and annealing temperatures.

of d_{33}, where the first plateau is in the vicinity of 80°C and the second plateau is above 90°C. Value of d_{33} for T-polymer corona-poled at 94°C is approximately two times larger than that poled at 80°C. In the annealing process, T-polymer poled at 94°C (closed circle in the figure) does not show the significant loss of SHG activity until the large activity loss occurs at the temperature around 85°C. Whereas, SHG activity for T-polymer poled at 80°C (closed square in the figure) was significantly lost at the temperature above 70°C.

The time-dependent decay of the second-order nonlinear susceptibilities d_{33} for T-polymer poled at two different temperatures of 80 and 94°C are investigated at various elevated temperatures. The observed time-dependent decay of nonlinear susceptibilities d_{33} was nonexponetial and analyzed by a Kohlrausch-Williams-Watts (KWW) stretched exponential function:

$$d = d_0 \exp(-(t/\tau)^\beta) \quad (0 < \beta \le 1) \tag{1}$$

where τ is the characteristic relaxation time and β is a measure of width of the distribution of relaxation time and the extent of deviation from a single exponential behavior. When $\beta = 1$, the time-dependent decay corresponds to a single exponential decay profile. The characteristic relaxation time τ is that time required for the system to decay to $1/e$ of its initial value. Table 1 summarizes the obtained τ and β values for both samples.

Table 1. Relaxation time τ and β values obtained from the appropriate fitting of KWW stretched exponential function.

(a) Sample poled at 94°C

Temperature (°C)	25	40	50	60	70	80	87	90
τ value (s)	1.62×10^9	2.11×10^7	2.23×10^6	5.04×10^5	1.04×10^5	3.40×10^3	2.7×10^3	6.60×10^2
β value	0.31	0.59	0.60	0.37	0.58	0.71	0.65	0.65

(b) Sample poled at 80°C

Temperature (°C)	40	45	55	63	72	76
τ value (s)	3.00×10^4	3.70×10^3	5.10×10^3	6.90×10^2	3.80×10^1	5.1×10^0
β value	0.33	0.37	0.34	0.52	0.44	0.61

Discussion

Results of the relaxation time exhibit that T-polymer poled at 94°C has long-term thermal stability over 50 years at room temperature. The dependence of the inverse of the relaxation time on the inverse of temperature for T-polymer is described well at all by an single energy-activated Arrhenius expression. It is noted that the relaxation time of T-polymer poled at 94°C is three order of magnitude larger than that poled at 80°C as listed in Table 1. The slope of the Arrhenius relation of the inverse of the relaxation time with the inverse of temperature gives the activation energy for the reorientation of the aligned NLO dipole moments. The activation energy is related to the potential barrier that NLO dipole moments meet when they thermally orient with an assistance of corona-poling. From Arrhenius plot, both relaxation processes have the same activation energy of 195 kJ/mol. Then the question arising is why the orientation of NLO dipole moments for the sample poled at 94°C is more stable than that for the sample poled at 80°C.

Let us think the effect of glass transition temperature on SHG activity. DSC profile gives that T-polymer has T_g at 57°C. It is noted that SHG activity for T-polymer poled at 94°C is stable at temperature beyond T_g and that poled at 80°C is remarkably depressed at temperature above T_g as shown in Figure 2. To our common knowledge, the glass transition temperature is the temperature when the oriented amorphous NLO dipole moments are

usually randomized and the resultant SHG activity is largely depressed. However the present results suggest that T_g value determined by DSC is not necessarily a measure for determining the thermal stability of NLO dipole moments. Therefore, the effective glass transition temperature, T_0, for SHG activity must be introduced to understand the difference of the orientational relaxation between samples poled at 80 and 94°C. Thermally stimulated discharge current (TSC) curve for the sample poled at 94°C gives the sharp and distinct peak at 92°C, and the SHG measurement on annealing as shown in Figure 2 gives that SHG activity is significantly depressed around 85°C. Thus the effective glass transition temperature T_0 for the sample poled at 94°C is to be 85°C. As for the sample poled at 80°C, T_0 is to be 60°C. The effective glass transition temperature for SHG activity is the useful measure for comparing orientation-relaxation of NLO chromophores.

In order to compare the orientation-relaxation of NLO chromophore in polymers with different glass transition temperatures, the scaling relation of

$$\tau(T) = A' \exp(\frac{T_0 - T}{T})$$
(2)

is proposed, where A' is a constant and T_0 is the glass transition temperature of polymers.[2] Figure 3 shows the scaling plot of the relaxation time in the present system using eq. (2) with $T_0 = 85°C$ for the sample poled at 94°C and $T_0 = 60°C$ for the sample poled at 80°C. Logarithmic τ value for the relaxation of NLO chromophore in the present polyurethane is linearly dependent on the $(T_0 - T)/T$. One can understand that the remarkable difference of the relaxation time for the samples poled at different temperatures is ascribed to the difference of effective glass transition temperature for SHG activity between both samples. Next question is what is the origin for the difference of effective glass transition temperature between both samples. One possible explanation is the effect of the free volume of the matrix which provides the free space where the aligned dipole moments can be thermally reoriented. Free volumes estimated from density are $0.171 cm^3/g$ for as-cast film, $0.169 cm^3/g$ for film annealed at 80°C and $0.161 cm^3/g$ for film annealed at 94°C. The smaller free volume for the samples poled at 94°C contributes to the restriction of molecular motion of NLO moiety in the matrix and thus the increase of the effective glass transition temperature. Furthermore, one can say that the hydrogen bonding might be related to the orientational stability of NLO chromophore.
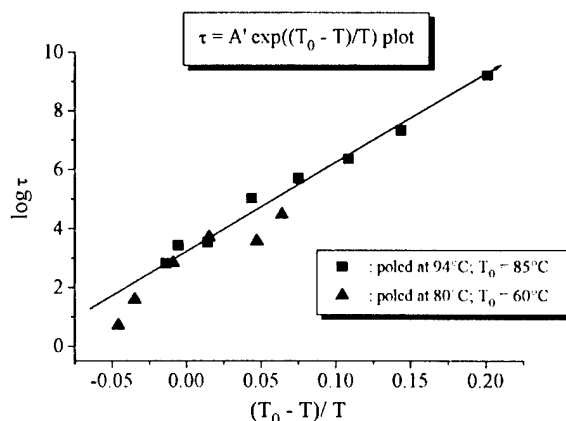

Figure 3. Plots of logarithmic τ vs. $(T - T_0)/T$ for both samples.

References
(1) Tsutsumi, N.; Matsumoto, O.; Sakai, W.; Kiyotsukuri, T. *Appl. Phys. Lett.* **1995**, *67*, 2272; ibid., **1996**, *68*, 2023; *Macromolecules*, **1996**, *29*, 592; ibid., **1996**, *29*, 3338
(2) Prêtre, P.; Kaats, P.; Bohren, A.; Günter, P.; Zysset, B.; Ahlheim, M.; Stähelin M.; Lehr, F. *Macromolecules,* **1994**, *27*, 5476.

Hyper-Rayleigh Scattering and Two-Photon Absorption-Induced Fluorescence of Chromophores with Enhanced Thermal Stability

Chia-Chen Hsu, National Chung Cheng University, Department of Physics, Ming-Hsiung, Chia-Yi, Taiwan, Tel: 886-5-272-0411-6072; Ching-Fong Shu, Tzer-Hsiang Huang, Jiunn-Lih Lin, Yuh-Kai Wang, Yi-Liang Zang, National Chiao Tung University, Taiwan; C.H. Wang, University of Nebraska-Lincoln

Hyper-Rayleigh scattering (HRS) technique has been frequently used to determine chromophore's β values.[1] Comparing with the electric field induced second harmonic generation (EFISH) technique, the HRS technique offers a straightforward method for measuring the first hyperpolarizabilities of organic molecules. Recently, HRS from some molecules excited with the fundamental radiation at 1064 nm wavelength has been found to be accompanied by the two-photon absorption (TPA) induced fluorescence.[2-3] Consequently, the β value determined by the HRS technique without making appropriate corrections for the contribution due to TPA induced fluorescence could be too large. To obtain the correct β value, the TPA induced fluorescence must be discriminated or removed from the HRS signal.

Until recently, the design and synthesis of NLO chromophores has been primarily focused on optimizing the molecular β value. However, the practical application of these NLO chromophores also depends on other E-O properties such as thermal stability. The chromophore must have sufficient thermal stability in order to survive the material processing and device fabrication steps. In this paper, the HRS β values and thermal stability of thiophene incorporated polyene chromophores with and without a configuration locked trans-triene bridge (shown in Fig. 1) are measured and compared.
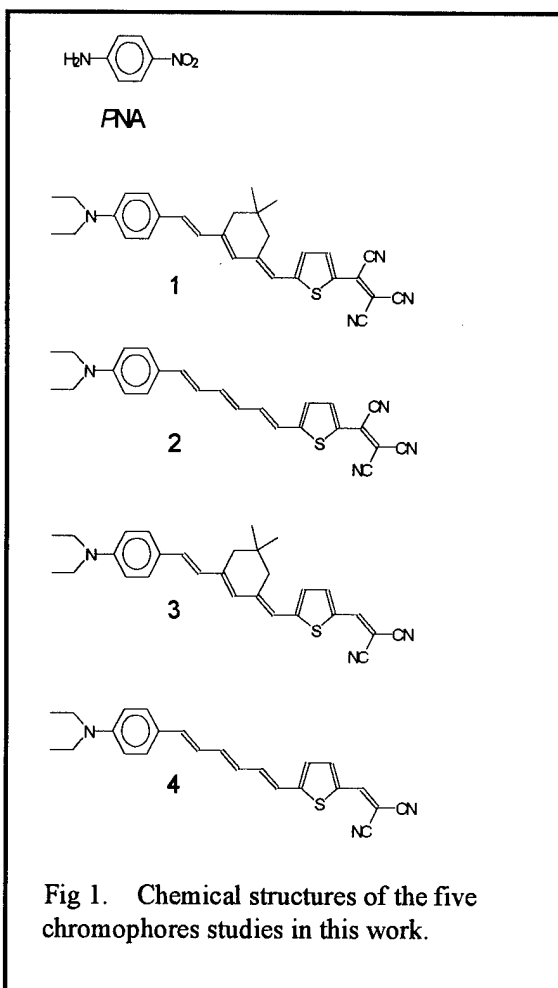
Fig 1. Chemical structures of the five chromophores studies in this work.

Figure 2 shows the HRS and TPA induced fluorescence spectra of pNA and chromophores 1, 2, 3, and 4. As shown in this figure, all samples have clear HRS signal at 532 nm. The β values of these chromophores are obtained by removing their own fluorescence contribution. After removing the TPA induced fluorescence contribution, the corrected β value of chromophores 1, 2, 3, and 4 are found to be 1504×10^{-30} ,1410×10^{-30}, 1125×10^{-30} , and 1500×10^{-30} esu, respectively.

The thermal stability of the chromophores were examined by dissolving the correspondent chromophores in a high temperature polymer (polyquinoline 100), and heating the thin films
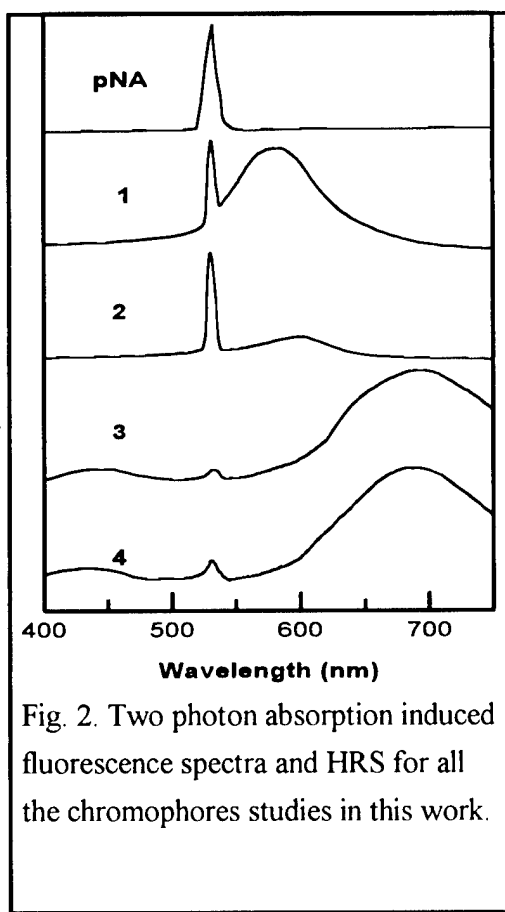
Fig. 2. Two photon absorption induced fluorescence spectra and HRS for all the chromophores studies in this work.

samples isothermally at 150, 170, 190, 210, 230 and 250 ^{0}C for 20 minutes, respectively. The absorption band after each baking was used to monitor the decomposition temperature. Figure 3 shows the temperature dependence of the normalized absorbance of the charge-transfer band for chromophores 1, 2, 3, and 4. As illustrated in this figure, chromophores 1 and 3, with configuration-locked trans-triene bridge, possess much better thermal stability than chromophores 2 and 4
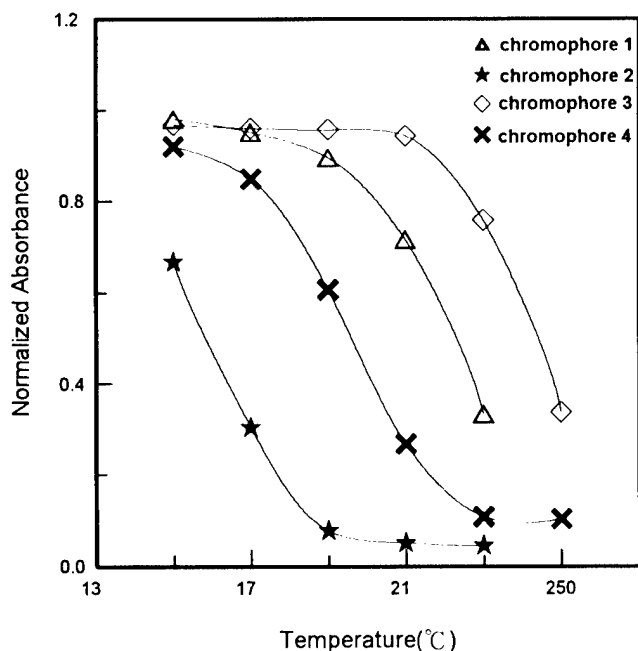
Fig. 3. The temperature dependence of the normalized absorbance for chromophores 1, 2, 3,and 4.

which have a trans-triene bridge. This result indicates that the configuration-locking method provides a dramatic enhancement of molecular thermal stability.

Table 1 summarizes both linear and nonlinear optical properties of all chromophores studied in this paper. The errors of the measured β values are approximately 5%. β_0 is the static (dispersion free) hyperpolarizability obtained from the two level

Table 1 Linear and nonlinear optical properties of chromophores pNA, 1, 2, 3, and 4.

Chromophore	λmax (nm)	β (10^{-30}esu)	β_0 (10^{-30}esu)
pNA	354	16.9	8.4
1	686	1504	582
2	678	1410	523
3	560	1125	88
4	546	1500	59

approximation. λ_{max} is the linear absorption peak wavelength. As shown in Table 1, both λ_{max} and β_0 values of chromophore 1 are larger than those of chromophore 2. This indicates that the configuration locked trans-triene bridge not only enhances the thermal stability but also raises the NLO response of polyene chromophores. This result suggests that incorporating a 6-membered ring to lock the configuration of the π-configuration triene may enhance the planarity and electron delocalization efficiency of the π-configuration system. By the same token, both the λ_{max} and β_0 values of chromophore 3 are much larger than those of chromophore 4. One notes that in Table 1, both the λ_{max} and β_0 values of chromophores 1 and 2 are larger than those of chromophores 3 and 4. This indicates that the strength of the acceptor $(CN)_3$ in chromophores 1 and 2 is larger than those of the acceptor $H(CN)_2$ in chromophores 3 and 4.

References

1. K. Clays and A. Persoons, Phys. Rev. Lett. **66,** 2980 (1991).

2. C. C. Hsu, T. H. Huang, Y. L. Zang, J. L. Lin, Y. Y. Cheng, J. T. Lin, H. H. Wu, C. H. Wang, C. T. Kuo, and C. H. Chen, J. Appl. Phys. **80,** 5996 (1996).

3. M. C. Flipse, R. de Jonge, R. H. Woundenberg, A. W. Marsman, C. van Walree, and L. W. Jenneskens, Chem. Phys. Lett. **245,** 297 (1995).

Nonlinear Optical Films from Pairwise-Deposited Semi-ionomeric Syndioregic Polymers

M. J. Roberts, G. A. Lindsay, J. D. Stenger-Smith, P. Zarras, R. A. Hollins, A. P. Chafin, M. P. Nadler, K. J. Wynne[1]

U.S. Navy, Code 4B2200D, NAWCWPNS, China Lake, CA 93555-6001
[1]Office of Naval Research, Arlington, VA 22217-5000

Processing polymers near room temperature to produce all-polymeric nonlinear optical films has important advantages [1]. For example, the Langmuir-Blodgett-Kuhn (LBK) technique offers control over final film thickness to within one monolayer. Also, materials may be precisely located within the film to control properties for purposes such as phase matching of the fundamental and second harmonic waveguide modes [2].

We have had some success in producing LBK film waveguides and prototype Mach-Zehnder modulators [3]. The long-standing problem of low thermal stability of LBK films has been addressed by using high Tg polymers [4]. However, a serious limitation of LBK technique remains, namely, the long processing time required to build up films of sufficient thickness (>0.5 micrometers) for waveguiding. In principle, the rate of film thickness growth may be increased if two polymer layers could be transferred with each deposition cycle.

New polymers were designed for this LBK deposition scheme (Figure 1). The complimentary polymers, a polycation insoluble in water and a water-soluble polyanion, are used to build up a polar film (Figure 2). The result is an electro-optic (EO) film which uses primarily ionic and hydrogen bonding to maintain noncentrosymmetric order.
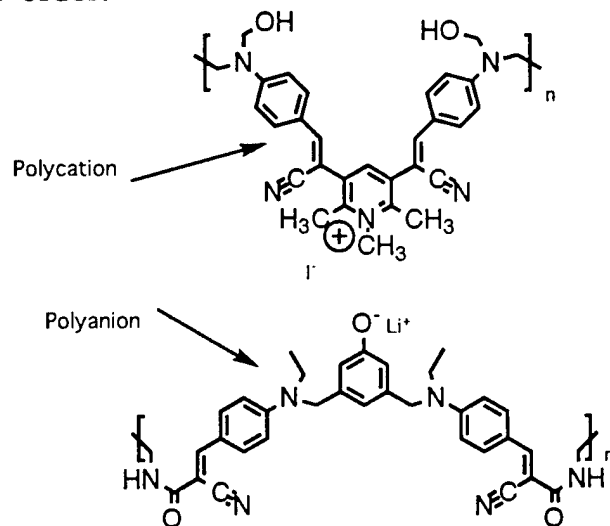
Figure 1. Ionic nonlinear optical polymers.
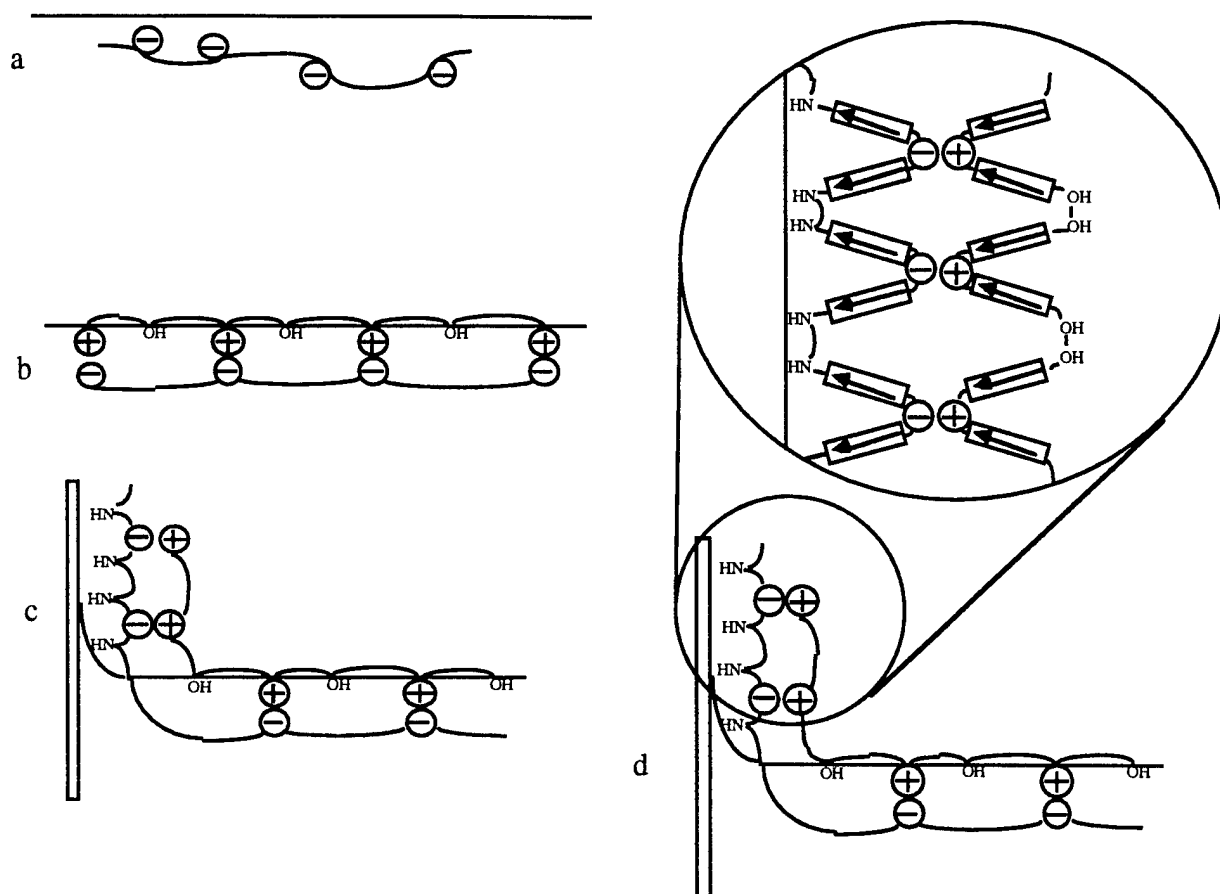
Figure 2. (a) NLO-active polyanion is dissolved in the subphase. (b) NLO-active water-insoluble polycation is spread on the water. The polyanion bonds ionically to the polycation. (c) The polymeric salt is transferred to a substrate. (d) More detailed view of the transferred film.

Films were made using a rectangular LBK minitrough (NIMA, Coventry) kept in a glove bag (Aldrich, Milwaulkee) purged with argon gas at 24 °C. The substrates were glass slides (Fisher, Cat. # 12-550A) cut to 1.5 cm x 2.5 cm and cleaned with H_2SO_4/H_2O_2. Under argon, a 0.026 M solution of the polyanion dissolved in dimethylsulfoxide was diluted to 10^{-4} M with water from a Barnstead Nanopure water purification system (17.9 MΩ resistivity, 0.2 micron filter). The trough was filled with the 10^{-4} M solution of polyanion (pH=9). A chloroform/pyridine (3:1) solution of the polycation was spread at the argon/aqueous solution interface. The system was allowed to equilibrate for 1 hour before the polymer bilayer was compressed symmetrically at a barrier speed of 5 cm^2/min to a surface pressure of 15 mN/m. Once the system reached the target surface pressure, the substrates were moved on the upstroke at 1.5 mm/min through the Ar-water interface. Subsequent bilayers were built up on the substrates by repeating this z-type deposition procedure.

The transmission UV-Vis spectra of the films were obtained with a Cary 5 NIR-Vis-UV spectrophotometer. The films were referenced to air and the glass background was subtracted to obtain the film spectra.

The second harmonic generation (SHG) signal was generated by transmission of a fundamental beam, incident at 54° from normal, from a Q-switched Nd:YAG laser (pulse width of 10 ns and repetition rate of 10 Hz) and detected with an intensified Si diode array (Tracor Northern).

The ATR FTIR spectra were obtained with a Nicolet 60sx with 4 cm^{-1} resolution. Si and ZnSe ATR crystals were used as substrates.

Brewster angle microscopy was performed with a microscope built in-house. An argon laser was used to illuminate the films on the trough.

Chemical synthesis of the polymers was achieved though Knoevenagel condensation polymerization [3].
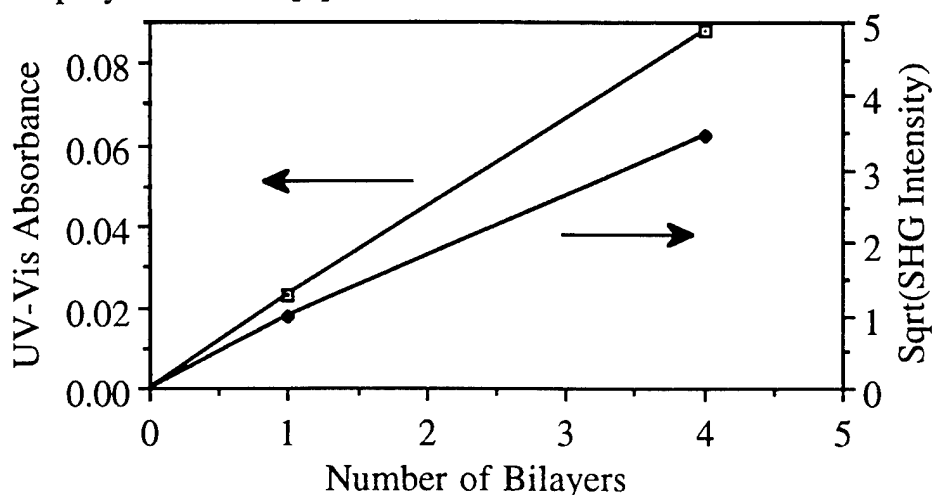
Figure 3. UV-Vis absorbance and SHG plotted versus the number of bilayers

Based on the evidence gathered thus far we conclude that the water soluble polyanion ionically bonds with the water insoluble polycation at the argon-water interface. The polycation/polyanion bilayer can be transferred to hydrophilic substrates such as glass with a high degree of uniformity layer to layer with respect to chromophore concentration and orientation. A noncentrosymmetric oriention of the chromophores is retained in the transferred multilayer film.

References

(1) G. Lindsay, K. Wynne, W. Herman, A. Chafin, R. Hollins, J. Stenger-Smith, J. Hoover, J. Cline, J. Roberts *Nonlinear Optics*, volume 15, 139-146, 1996.
(2) T.L. Penner, H.R. Motschmann, N.J. Armstrong, M.C. Ezenyilimba, D.J. Williams *Nature*, vol 367, 6 January 1994.
(3) G.A. Lindsay, M.J. Roberts, J.D. Stenger-Smith, A.P. Chafin, R.A. Hollins, R.A. Henry, W.N. Herman, P.R. Ashley, K.J. Wynne, submitted *Naval Reviews.*

Nonlinear-Optical Properties of Bacteriorhodopsin in Multilayer Langmuir-Blodgett Films

A.V.Kir'yanov[*], H.Lemmetyinen[**], I.A.Maslyanitsin[*], V.V.Savranskii[*], N.A.Tkachenko[**]

[*]General Physics Institute, Vavilov St.,38, Moscow 117942, Russia.

[**]Technical University of Tampere, Tampere, PO Box 830, Finland.

CORRESPONDING AUTHOR: Dr. Alex V. Kir'yanov, General Physics Institute, Vavilov Str., 38, Moscow 117942, Russian Federation, Phone: (095) 135-0327, Fax: (095) 135-2055, Email: kiryanov@kapella.gpi.ru

Nonlinear optical properties of multilayer Langmuir-Blodgett films (LBF) of bacteriorhodopsin (bR) were studied experimentally. The samples were deposited in Y- and Z-configurations (Z-type bR films up to 50 layers were manufactured at first). The method of second-harmonic generation and the Z-scan technique were used in order to evaluate the elements of susceptibility second-order tensor and to determine the sign and approximate magnitude of refractive index nonlinear part for the samples studied.

MOLECULAR ORIENTATION IN PROTEIN FILMS DEPOSITED ON SUBSTRATES COATED WITH LANGMUIR-BLODGETT AND SELF-ASSEMBLED MONOLAYERS

Paul L. Edmiston, Laurie L. Wood, John E. Lee, and S. Scott Saavedra
Department of Chemistry, University of Arizona, Tucson, Arizona 85721
phone: (520) 621-9761
fax: (520) 621-8407
email: sssaaved@ccit.arizona.edu

Formation and characterization of organic thin film assemblies intended for use in biomolecular devices, such as biosensors, is currently a very active area of research. We have been investigating techniques for creating macroscopically ordered protein films formed by covalent bonding between a unique site on the protein and an appropriately derivatized substrate surface. Assemblies consisting of heme proteins immobilized on substrates coated with self-assembled monolayers and Langmuir-Blodgett are being examined. Macroscopic film order is probed using a combination of total internal reflectance fluorescence and planar integrated optical waveguide-attenuated total reflection spectroscopies, from which the orientation distribution of heme tilt angles in the protein film is determined.

It is well recognized that structure and function in a thin film of protein molecules immobilized on a solid substrate are strongly dependent on the physical and chemical properties of the substrate surface. Developing a more systematic understanding of these relationships is the overall thrust of this project, and is a prerequisite to the rational and effective utilization of protein films in molecular device technologies such as biosensing. Our long-term goal is to determine if (and how) the immobilization process can be controlled to specify the structural and functional properties of the protein film assembly. (Examples of these properties are molecular orientation, packing density, maintenance of native conformation, ligand binding functionality, electron transfer behavior). Advancing the state of knowledge in this research area requires concurrent development of new and powerful analytical capabilites, since conventional approaches are inadequate for studying protein monolayers *in situ*.

Consequently, a recent focus of our research group has been the development of novel spectroscopic techniques designed to characterize interfacial protein films, and use of these techniques to examine structural features of protein monolayers immobilized using a variety of methods. Specifically, we: (*i*) Developed a technique to measure the molecular orientation distribution in a film of fluorescent dipoles coated on a planar dielectric substrate. (*ii*) Extended this approach to the measurement of orientation distributions in hydrated monolayers of heme proteins. (*iii*) Began examining the influences of substrate surface chemistry and molecular assembly technique on molecular orientation in adsorbed and self-assembled protein films. (*iv*) Developed a planar waveguide spectrometer for measuring broadband visible ATR spectra of molecular films, and tested the capability of this device for use in conformational and functional studies of heme protein films.

a. Dipole Orientation Distributions in Langmuir-Blodgett Films.

We developed the IOW-ATR+TIRF method to determine the orientation distribution of fluorescent molecules in a thin, substrate-supported film [1]. Absorbance linear dichroism of is measured in an attenuated total reflection (ATR) by depositing the film on the surface of a planar integrated optical waveguide (IOW). Steady-state anisotropy is measured in a total internal reflection fluorescence (TIRF) geometry on a film deposited on fused silica, but prepared under otherwise identical conditions. The mean dipole tilt angle and angular distribution about the mean are recovered from the tandem measurements by modeling the distribution as a probability density specified by two adjustable parameters. The method was tested on Langmuir-Blodgett (LB) films of arachidic acid doped with linearly and circularly polarized fluorescent amphiphiles. The results showed that dipoles in the headgroup region of arachidic acid LB films are more ordered than dipoles in the alkyl chain region, which is consistent with previous studies of similar film geometries using other techniques. More importantly, the results demonstrated the utility of the IOW-ATR+TIRF method for studying relationships between assembly technique and structure in thin molecular films.

b. Molecular Orientation Distributions in Heme Protein Films.

The geometric orientation of an immobilized protein may determine if the molecule's native function is retained in the interfacial environment. For example, an antibody immobilized with the antigenic sites facing the substrate will be sterically restricted from binding a macromolecular antigen. Numerous laboratories are consequently investigating methods to produce protein film assemblies having a defined macroscopic orientation. However, assessing the success of these efforts has been hampered by the experimental difficulty of measuring the distribution of molecular orientations in a protein monolayer immobilized at a solid-liquid interface. Our successful extension of the IOW-ATR+TIRF method to heme protein films [2,3] provided a solution to this problem,; this work represents the first reported orientation distribution measurements for protein film assemblies (furthermore, the measurements were made on hydrated (not dried) films).

We began by examining films formed by physical adsorption of heme proteins to substrates functionalized with either LB films or silane-based, self-assembled monolayers [2]. (Heme proteins, such as horse cytochrome *c* (hcyt *c*) and myoglobin, are being used for these studies

because the intrinsic porphyrin can be used as a spectral probe of molecular orientation, bioactivity, and conformation). Specifically, we sought to determine if a macroscopically oriented (i.e., liquid crystalline) protein film can be produced via "nonspecific" adsorption. The results show that an adsorbed protein film with a narrow range of orientation distributions is produced when a single, high affinity type of noncovalent binding occurs between the surface of the protein and the substrate surface. For example, electrostatic adsorption of positively charged horse heart cytochrome c (hcyt c) to the negatively charged head groups of a LB film of arachidic acid (at pH 7) produces a narrow orientation distribution. When multiple, competing adsorptive interactions are operative, which is the case when hcyt c adsorbs to a clean, hydrophilic glass surface, a relatively disordered film is produced. The hypothesis of oriented adsorption is well accepted in the interfacial protein community. Due to the asymmetric distribution of amino acids on the surface of a protein, one "face" of the molecule may be preferentially attracted to a given adsorbent material, while other "faces" may be repelled. Thus in retrospect, our results are not surprising; however their observation is unprecedented.

We have also begun to examine site-directed covalent bonding as a strategy for producing oriented protein films. Our initial candidate architecture consisted of yeast cytochrome c (ycyt c) immobilized via disulfide bonding on the thiol tail groups of self-assembled monolayers (SAM) [3]. SAMs were produced by deposition of a thioacetate-capped hexadecyltrichlorosilane onto waveguide and quartz substrates, followed by in situ reduction to generate a thiol-coated surface. Ycyt c, which has a single reduced cysteine at position 102 on the surface of the protein, was then deposited to form a disulfide linked protein film. The results of orientation distribution measurements show that this approach produces a relatively disordered protein film. Very little of the immobilized ycyt c could be removed by dithiothreitol, indicating that very little of the protein was immobilized solely via disulfide bonding. The presence of multiple, nonspecific binding interactions between the protein and the SAM appears to be the primary cause of the broad orientation distribution.
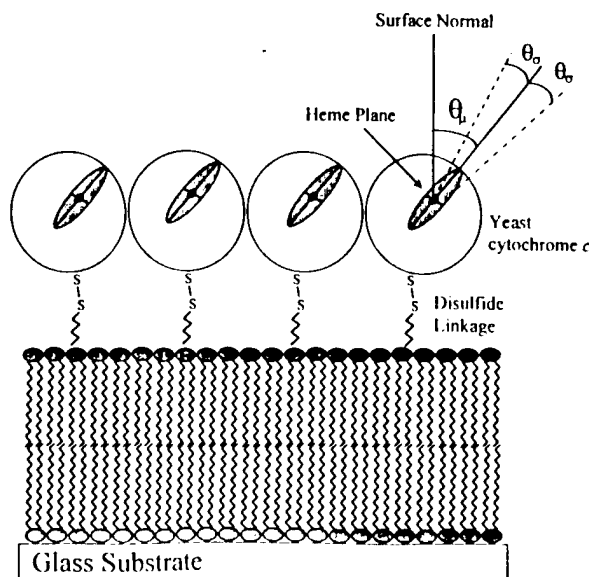
Figure 1. Schematic illustration of a protein film assembly in which ycyt c is disulfide bonded to a LB bilayer of dioleoyl phosphatidylcholine (DOPC) containing 12% (mol/mol) of dioleoyl phosphatidyl-ethanolamine bearing a pyridyl disulfide head group (PDS-DOPE).

More recently, we examined immobilization of ycyt c to a planar supported lipid bilayer, composed of a 1:8 (mol/mol) mixture of DOPE bearing a pyridyl disulfide head group (PDS-DOPE) and DOPC (Fig. 1). The low extent of non-specific protein adsorption to DOPC bilayers is well known, while PDS-DOPE provides the capability for disulfide bond formation with an extrinsic thiol. This molecular architecture does in fact form a well ordered protein monolayer (the orientation distribution, 40±11 degrees, is slightly wider than that measured for hcyt c adsorbed to arachidic acid LB films) [4]. The specific nature of the interaction between ycyt c and PDS-DOPE was established by measuring: i) nearly quantitative protein desorption from the bilayer in the presence of dithiothreitol; and ii) very little non-specific adsorption of ycyt c adsorption to pure

DOPC bilayers. These results, when considered in tandem with those from the SAM immobiliztion experiments, demonstrate that macroscopically oriented protein films can be formed via site-directed covalent bonding *when* non-specific protein-substrate interactions are largely absent. Again, while in retrospect these results are not surprising, their observation is unprecendented.

c. Planar Waveguide ATR Spectrometer.

The inherently high sensitivity of the planar IOW-ATR geometry is well known. The major disadvantage is spectral bandwidth -- at a given launch angle, conventional grating and prism incouplers are efficient only over a narrow (<5 nm) spectral range. Thus all planar waveguide ATR studies reported prior to our recent work utilized a monochromatic source or a narrow spectral band isolated from a polychromatic source. We addressed this limitation by developing an achromatic planar IOW incoupler with a spectral bandwidth of ca. 100 nm [5]. A "second generation" version of this incoupler was subsequently used as the basis for construction of a prototype multichannel planar IOW-ATR spectrometer capable of measuring broadband visible absorbance spectra of a molecular film confined to a waveguide-aqueous interface [6].

We developed the spectrometer specifically to enable spectral studies of structure and function in the immobilized heme protein film assemblies described above. Visible absorbance spectroscopy is a potentially powerful approach, since the position, shape, and intensity of the heme absorption bands are markers of ligand binding, the oxidation state of the central metal ion, and protein conformation in the vicinity of the heme. We tested the prototype spectrometer by measuring spectra, over a 100 nm bandwidth, of a hydrated film of hcyt *c* adsorbed to a hydrophilic glass waveguide surface before and after *in situ* reduction with sodium dithionite [6]. The success of this experiment demonstrated extension of the very high sensitivity of the IOW-ATR geometry to the broadband regime. This capability should have a significant impact in several areas, including spectral characterization of structure-property relationships in thin molecular films, and chemical sensing for multiple analytes that can be spectrally resolved and thus detected simultaneously.

References

1. P.L. Edmiston, L.L. Wood, J.E. Lee, and S.S Saavedra, *J. Phys. Chem.*, **1996**, *100*, 775-784. "Dipole Orientation Distributions in Langmuir-Blodgett Films by Planar Waveguide Linear Dichroism and Fluorescence Anisotropy."

2. P.L. Edmiston, J.E. Lee, S.-S. Cheng, and S.S Saavedra, *J. Amer. Chem. Soc.*, **1997**, *119*, 560-570. "Molecular Orientation Distributions in Protein Films. I. Cytochrome *c* Adsorbed to Substrates of Variable Surface Chemistry."

3. L.L. Wood, S.-S. Cheng, P.L. Edmiston, and S.S Saavedra, *J. Amer. Chem. Soc.*, **1997**, *119*, 571-576. "Molecular Orientation Distributions in Protein Films. II. Site-Directed Immobilization of Yeast Cytochrome *c* on Thiol-Capped, Self-Assembled Monolayers."

4. P.L. Edmiston and S.S Saavedra, manuscript submitted to *Biophys. J.* "Molecular Orientation Distributions in Protein Films. III. Yeast Cytochrome *c* Immobilized on Pyridyl Disulfide Capped Phospholipid Bilayers."

5. S. Mendes, Lifeng Li, J. Burke, J.E. Lee, and S.S. Saavedra, *Appl. Optics*, **1995**, *34*, 6180-6186. "70 Nanometer Bandwidth Achromatic Waveguide Coupler."

6. S. Mendes, L. Li, J. Burke, J.E. Lee, and S.S. Saavedra, *Langmuir*, **1996**, *12*, 3374-3376. "Broad-Band Attenuated Total Reflectance Spectroscopy of a Hydrated Protein Film on a Single Mode Planar Waveguide."

Fabrication of the One-Dimensional Superlattice in the Epitaxially Grown Film of Platinum Dioxime Complexes

Kaoru Yamamoto[†], Toshihide Kamata[‡], Kiyoshi Yase[‡], Yuji Yoshida[‡], F. Mizukami[‡], and T.Ohta[†]

[†] *Department of Chemistry, School of Science, The University of Tokyo,*
7-3-1 Hongo, Bunkyoku, Tokyo 113, JAPAN

[‡] *National Institute of Materials and Chemical Research,*
1-1 Higashi, Tsukubashi, Ibaraki 305, JAPAN

1. Introduction

A large number of studies have been done for multiple quantum wells of inorganic semiconductor, because confined electronic system in a thin layer shows various properties essential for optoelectronic application. Since the quantum size effect increases when the electron system approaches lower dimension, fabrication of higher order confined structures has been attempted to advance the properties. On the other hand, there are many substances having one-dimensional structure in the nature. It can be thought that the one-dimensionality is prospective to realize a higher order confined system.

The series of square-planer d^8 metal complexes with various kind of dioximes is one of the well-known one-dimensional substances; these metal complexes form one-dimensional metal chain structure in the molecular column of the crystal.[1] We have already reported their superior third-order nonlinear optical property due to electron delocalization along the one-dimensional metal chain.[2] Since the metal chain is formed by a stack of the individual molecules, it seem to be relatively easy to arrange the one-dimensional structure obtaining higher order confined system such as one-dimensional superlattice. Namely, one-dimensional superlattice can be prepared by stacking different type of the molecules in a column in a certain order, in the same way as fabricating inorganic multi quantum wells by the alternate deposition.

In order to create a one-dimensional superlattice, the following conditions must be satisfied. First, we must find the suitable combination of two types of metal complexes. In other words, the two types of the molecules could be combined in a column, while they have large difference in their electron states of the metal chain for obtaining the effective electron confinement. Second, for stacking the two types of the molecule in a column by the alternate deposition, the metal chains in the evaporated film are perpendicular to the substrate surface.

In this paper, we first co-evaporated the two types of the metal complexes, bis(dimethylglyoximato) platinum(II) (Pt(dmg)$_2$) and bis(diethylglyoximatlo) platinum(II) (Pt(deg)$_2$) on a glass substrate, and confirmed by means of XRD and UV-vis absorption measurements that the two complexes were mixed in a column. The two types of the metal complexes have large difference in their metal-metal distance in the chain and, thus, in their electronic states. Therefore, the combination is thought to be profitable for producing confined electron systems in the superlattice structure. Secondly, we fabricated the epitaxial film on the cleaved surface of KCl. Transmission electron diffraction (TED) showed that the metal chain of the film was perpendicular to the surface. Finally, we fabricated the multilayered film by the alternate deposition of the metal complexes to demonstrate the preparation of the one-dimensional superlattice. The metal chain structure was investigated by UV-vis absorption. It was confirmed that the elementary one-dimensional superlattice was created in the metal chain of the multilayered film.

2 Results & Discussion

2.1 Co-evaporated film of Pt(dmg)₂ and Pt(deg)₂

The metal-metal distance between the adjacent molecules of the two types of the metal complexes, Pt(dmg)₂ and Pt(deg)₂, are different from each other because of the difference in steric hindrance of their alkyl substituent groups; Pt(dmg)₂ has the orthorhombic crystal system in which metal-metal distance between adjacent molecules is 3.25 Å, and Pt(deg)₂ has the monoclinic structure in witch the metal-metal distance is 3.55 Å.

Figure 1 shows UV-vis spectra of the evaporated films of pure Pt(dmg)₂ and Pt(deg)₂, and of the co-evaporated films. The Pt(dmg)₂ film showed strong absorption band at 681 nm assigned to the d-p

Figure 1. UV-vis absorption spectra of the evaporated films of Pt(dmg)₂, Pt(deg)₂, and the co-evaporated films

transition.[3] The Pt(deg)₂ film showed the corresponding absorption band at 465 nm. The difference in the wavelength of the d-p transition band is attributed to the difference in the metal-metal distance between the two types of the metal complexes.

The d-p transition band of the co-evaporated films varied continuously between the peak wavelengths of the respective pure metal complexes in proportion to the mixing ratio. The energy shift of the d-p transition shows that the two types of the metal complexes mix into one column, in spite of the difference in the crystal lattices of the metal complexes. It is expected that the high miscibility of the two metal complexes make it possible to prepare the super lattice by stacking the two types of the metal complexes in a column.

2.2 Epitaxial film of Pt(dmg)₂

Figure 2 is the TED pattern of the evaporated film of Pt(dmg)₂ removed from the substrate. Since the TED gave the spot pattern, the crystal of the film was found to grow epitaxially with a certain orientation against the substrate surface. The pattern can be assigned as shown in the figure, which indicate that the column (c-axis) in the film is perpendicular to the surface.

It is though that the orientation of the metal chain is in proper to fabricate the one-dimensional superlattice. Since the metal chain is perpendicular to the surface, we could arrange the stacking order of the column by depositing different metal complexes alternately.

Figure 2. Transmission electron diffraction of the Pt(dmg)₂ film removed from the substrate.

2.3 Alternately deposited film

Figure 3 is the UV-vis absorption of the multilayered film of $Pt(dmg)_2$ and $Pt(deg)_2$ on KCl surface. The film was composed of the following three layers: first layer, $Pt(dmg)_2$; second layer, $Pt(deg)_2$; third layer, $Pt(dmg)_2$. The thickness of each layer was 20nm, which is sufficient to prepare a continuous layer. Therefore, the upper layer was surely piled up on the lower layer.

No absorption peaks appeared in the absorption spectrum of normal incidence (Figure 3(a)). On the other hand, the spectrum of oblique incidence showed the two d-p absorption peaks (Figure 3(b)). The two absorption bands are attributed to the d-p transition of $Pt(dmg)_2$ and $Pt(deg)_2$ layers, respectively; the appearance of the two absorption bands indicates that the deposited two types of the metal complexes form the respective layers.

Figure 3. UV-vis absorption spectra of the multilayered films measured by (a) oblique and (b) normal incidence.

The clear dichroism of the d-p absorption illustrates that the metal chain of each layer is kept perpendicular to the surface; the electric field of the incident light crosses the dipole moment of the d-p transition at right angle in the normal incidence. Therefore, it can be considered that the epitaxial growth of the film is kept through the interface between the hetero-layers and the two types of the metal complexes form the three-layered one-dimensional superlattice.

3. Conclusion

We have found that a one-dimensional superlattice is formed in the multilayered film prepared by alternately depositing two types of the d^8 metal dioxime complexes, though the detailed structure of the metal chain has not been found explicitly. There were still several important restrictions for fabricating the superlattice. For example, the layer thickness was rather thick for obtaining the quantum size effect and the number of layers was also limited. To control the layer thickness and to increase the number of the layers are some of the tasks for our future research. Although there remain problems we must settle, we conclude that alternate deposition of the d^8 metal complexes with dioxime ligands would be considered prospective for creating the one-dimensional superlattice.

References

(1) H. Endres, H. J. Keller, R. Lehmann, A. Poveda, H. H. Rupp, H. van de Sand, Z. Naturforsch., 1977, 32b, 516.
(2) T. Kamata, T. Fukaya, M. Mizuno, H. Matsuda, F. Mizukami, Chem. Phys. Lett., 1994, 221, 194; T. Kamata, T. Fukaya, T. Kodzasa, H. Matsuda, F. Mizukami, M. Tachiya, R. Ishikawa, T. Uchida, Y. Yamazaki, Nonlinear Optics, 1995, 13, 31; T. Kamata, T. Fukaya, T. Kodzasa, H. Matsuda, F. Mizukami, Mol. Cryst. Liq. Cryst., 1995, 267, 117.
(3) Y. Ohashi, I. Hanazaki, S. Nagakura, Inorg. Chem., 1970, 9, 2551.
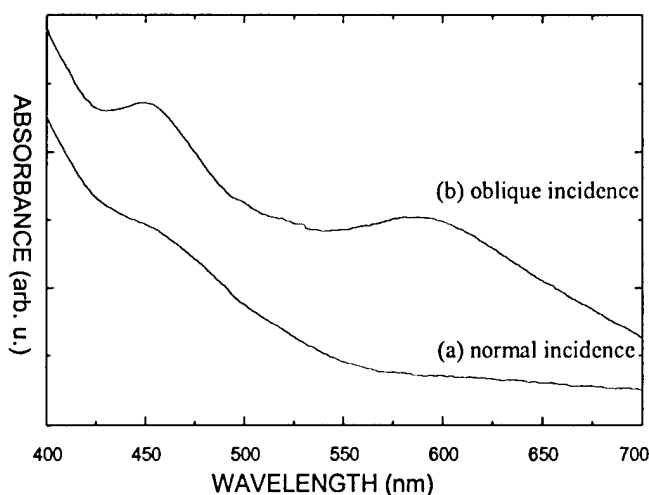
Bacteriorhodopsin Opto-Electronic Synapses

David P. Shelton

Physics Department
University of Nevada Las Vegas
Las Vegas, NV 89154-4002
tel: (702) 895-3564, fax: (702) 895-0804
email: shelton@physics.unlv.edu

In recent years there has been a resurgence of interest in artificial neural networks, and several optical implementations have been investigated [1]. Neural networks are intrinsically parallel computers, and optics can provide the massive parallelism and interconnectivity they require. The key components of neural networks are the synapses between the neurons, which are the locus of signal processing, learning, and memory. Bacteriorhodopsin (BR) has photochromic properties which will enable one to construct functionally complete synapses in the form of a thin-film optically-addressed spatial light modulator. Here we present measurements of properties of bacteriorhodopsin relevant to synaptic functions.

Absorption of a photon at 570 nm converts a bacteriorhodopsin molecule from the yellow-absorbing ground state (B) to the relatively long-lived blue-absorbing state (M). Thermally activated relaxation, or absorption of a blue photon, returns the molecule to the B state, completing the photocycle. The protein part of BR ensures stereoselective and reversible photoisomerization of the retinal chromophore with high quantum yield and without side reactions [2]. A key feature, in the present context, is that the forward (B→M) and reverse (M→B) photoreactions can be switched off by lowering the temperature of the BR film. This allows one to write a pattern on the film with a light beam, and then read out the pattern without erasure using the same light beam.

The temperature dependence of the forward and reverse photoreactions was studied by measuring the changes in the B-state optical absorbance of BR film when illuminated by yellow or blue light [3]. The sample film was mounted in a variable temperature cryostat, and could be illuminated with several light beams. In the first experiment, the sample was prepared in the B state and cooled to the desired temperature. Then the sample was illuminated with a cw dye laser beam at 590 nm with an intensity about 100 mW/cm^2, and the steady state absorbance change at 560 nm was measured. At low temperature, an additional laser beam at 680 nm was used to empty the first long-lived intermediate state (K). In the second experiment, the sample was prepared in the M state using the 590 nm pump beam and cooled to the desired temperature. Then the sample was illuminated with a 3 ns flash of blue light at 410 nm from a pulsed dye laser, and the transient absorbance change seen by a 543.5 nm probe laser beam was measured.

The results of these measurements for a wild-type high-pH BR/polymer film are shown in Figure 1. The film was produced by Bend Research and has peak optical

density 2.0 at 570 nm. At temperatures above 200 K the photoreactions are fully enabled, and the M→B photoreaction is completed in about 200 ns. Below 100 K the photoreactions are disabled. The forward and reverse reactions show approximately the same temperature dependence. The photoreactions involve conformational changes in the protein as well as the chromophore.
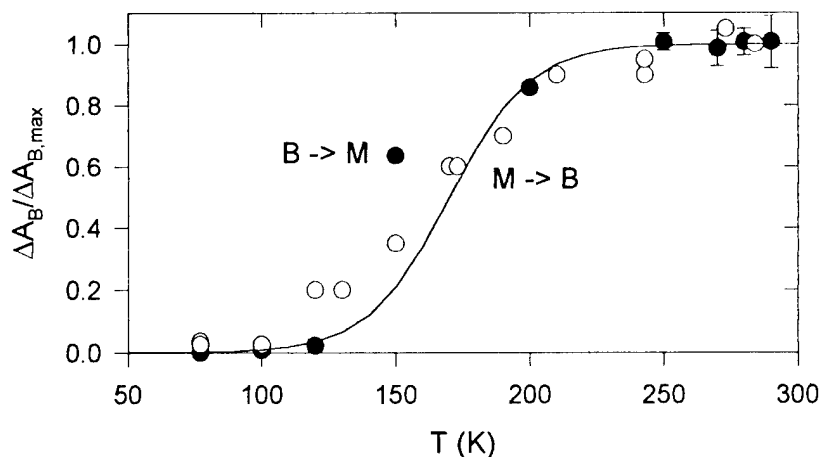

Figure 1. Normalized B-state absorbance change versus temperature measured for wild-type bacteriorhodopsin/polymer film. Filled and open circles show results for the forward (B→M) and reverse (M→B) photoreactions, respectively. The fitted curve is the function $F(T) = [\ 1 + \exp(\ -(T-170)/15\ )\ ]^{-1}$.

One neuron of a neural network which can be constructed using BR synapses is shown in Figure 2. The input light beams pass through the BR film, where the synaptic weights are written as a pattern of light transmittance, and are summed by a photodetector. An electronic circuit processes the detector output and drives a laser output device. The synaptic weights remain fixed while the BR film is maintained at low temperature. Learning in the neural network is enabled when the temperature of the BR film is raised, so that the input light beams can change the transmittance of the BR film. Effective learning rules for modifying the synaptic weights of the network to achieve a desired function are critical to most neural network applications [4].

Bacteriorhodopsin synapses can efficiently implement an associative learning rule, as well as recording the updated synaptic weights [5]. To do this, a heater for the BR thin-film synapses on a neuron is driven with the output signal from that neuron. Figure 3 shows the response of a simple model neuron using BR synapses with properties as measured in Figure 1. In this model, the temperature and blue light intensity falling on the BR film increases in proportion to the neuron activation. As a result, the effect of a yellow input light beam depends on the degree of neuron activation. When the neuron is weakly activated (U=0.2), an input light beam is unable to alter the synaptic weight. When the neuron is strongly activated, the synaptic weight will increase or decrease according to whether the synapse sees a strong or a weak input. Synapses with correlated activity are reinforced, while synapses with uncorrelated activity are weakened.

Thus, simple BR synapses are able to store analog weights and perform complex signal processing functions.
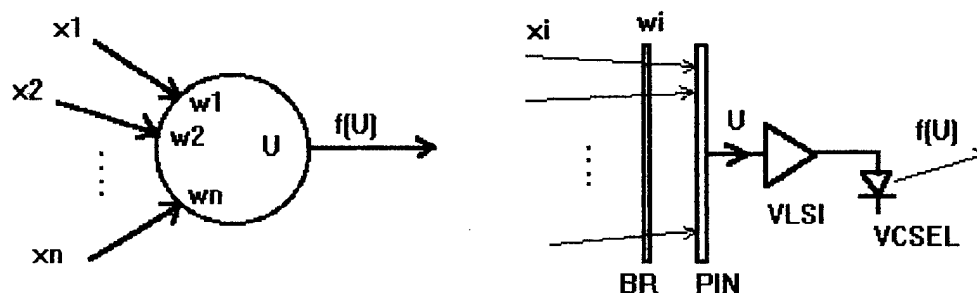
Figure 2. Schematic diagrams of an opto-electronic neuron, with optical inputs x_i, synaptic weights w_i, neuron electrical activation $U \propto \Sigma_i \, w_i \, x_i$, and neuron optical output $f(U)$. The synapses are implemented with a bacteriorhodopsin film (BR) and photodiode (PIN), whose output goes to an integrated circuit (VLSI) which drives a laser (VCSEL).
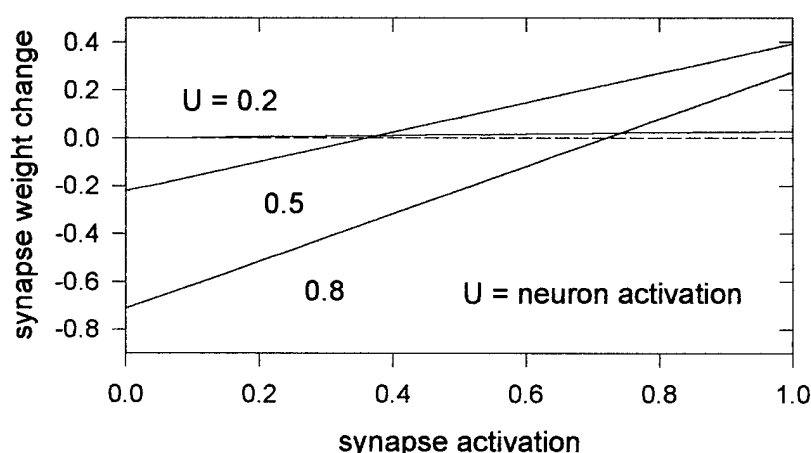

Figure 3. "Learning rate" versus "synaptic input" for various fixed values of "neuron activation", calculated for a simple model neuron using bacteriorhodopsin synapses.

References

1.   M. Balberg, M. Razvag, S. Vidro, E. Rafaeli, A.J. Agranat, Opt. Lett. **21**, 1544 (1996); Applied Optics **32**, (10 March 1993) Feature Issue on Optical Implementation of Neural Networks; D. Psaltis, D. Brady, X.G. Gu, S. Lin, Nature **343**, 325 (1990).

2.   D. Oesterhelt, C. Brauchle, N. Hampp, Quarterly Reviews of Biophysics **24**, 425 (1991); R.R. Birge, Annu. Rev. Phys. Chem. **41**, 683 (1990).

3.   M. Bacon, C.H. Wang, A.K. Kar, R.L. Baxter, B.S. Wherrett, Opt. Commun. **124**, 175 (1996).

4.   S. Haykin, *Neural Networks* (Macmillan, Englewood Cliffs, 1994).

5.   T.H. Brown, S. Chattrji, *Hebbian Synaptic Plasticity*, Ch. 8, p.287, in E. Domany, J.L. van Hemmen, K. Schulten, eds., *Models of Neural Networks II* (Springer, New York, 1994).

Beam Splitting in Nonlinear Polymeric Waveguide Induced by Photobleaching

Aaron Wilkosz, Nichols Research Corporation, 4040 S. Memorial Parkway, Huntsville, Alabama 35815, (205) 883-1170 ext. 1648

Sergey Sarkisov, Alabama A&M University, Normal, Alabama 35762
(205) 851-5305

INTRODUCTION

Optical beam splitting has been first reported for photorefractive waveguides built by titanium diffusion in $LiNbO_3$ [1,2]. The effect has been qualitatively explained as an appearance of spatial dark solitons in self-defocusing nonlinear medium [3]. Optical splitting has also been observed in pure self-defocusing Kerr media in a two dimensional configuration [4,5] similar to that of a slab waveguide. The splitting effect in this case is apparently associated with dark spatial solitons. This paper presents theoretical and experimental data and discusses a theoretical model developed to study optical beam splitting induced by photobleaching a dye-doped polymeric waveguide, where instant refractive index reaction to light intensity redistribution is replaced by permanent index decrease associated with dye photobleaching.

MODEL THEORY

The index response to an optical field amplitude E is given by the rate equation

$$\frac{\partial \tilde{n}(E)}{\partial t} = -C \frac{|E|^2}{2}(\tilde{n}(E) - \tilde{n}_s) \qquad (1)$$

for $\tilde{n} = 0$ at $t = 0$, where $\tilde{n}(E)$ is the electric field dependent component of the refractive index $\tilde{n}(E) = n(E) - n_0$, where n_0 is the initial unperturbed refractive index; E is the electrical component of a TE mode propagating in a single mode slab waveguide; C is the efficiency of light induced index modification; and $\tilde{n}_s$ is the saturation index change. Equation (1) applies to nonstationary and nonuniform optical fields. According to experimental data the absorption coefficient and dependent on it propagation loss rate remain constant. The light propagation in a single mode slab waveguide is given by a two dimensional nonlinear Schrödinger type equation

$$-2i\beta \frac{\partial E}{\partial x} + \frac{\partial^2 E}{\partial y^2} - i\gamma\beta E + \frac{\beta^2 \tilde{n}(E)}{n_0} = 0 \qquad (2)$$

where x and y are coordinates in the plane of the waveguide along and across the propagation direction respectively; β is the mode wave number; and γ is the propagation loss factor. The light beam injected into the waveguide was assumed to have a uniform phase plane wavefront and a Gaussian profile of the optical field given by $E = E_0 \exp(-y^2/2\sigma^2)$ at $x = 0$, where E_0 is the beam amplitude, and σ is the beam width. Equations 1 and 2 were solved numerically by integrating along the dimension

x and time t using central difference method for the second order partial derivative in the y direction.

RESULTS

Figure 1 shows results obtained from numerical simulations of light propagating in the waveguide at various times after the light was launched. The time scale shown in Figure 1 is based on a normalized time parameter given by $\tau = t/C|E_0|^2/n_0$. One can see apparent primary beam splitting into two secondary beams with separation between them growing in time. This process can be understood qualitatively in terms of light escaping out of bleached regions with low refractive index to unbleached regions with high index of refraction.
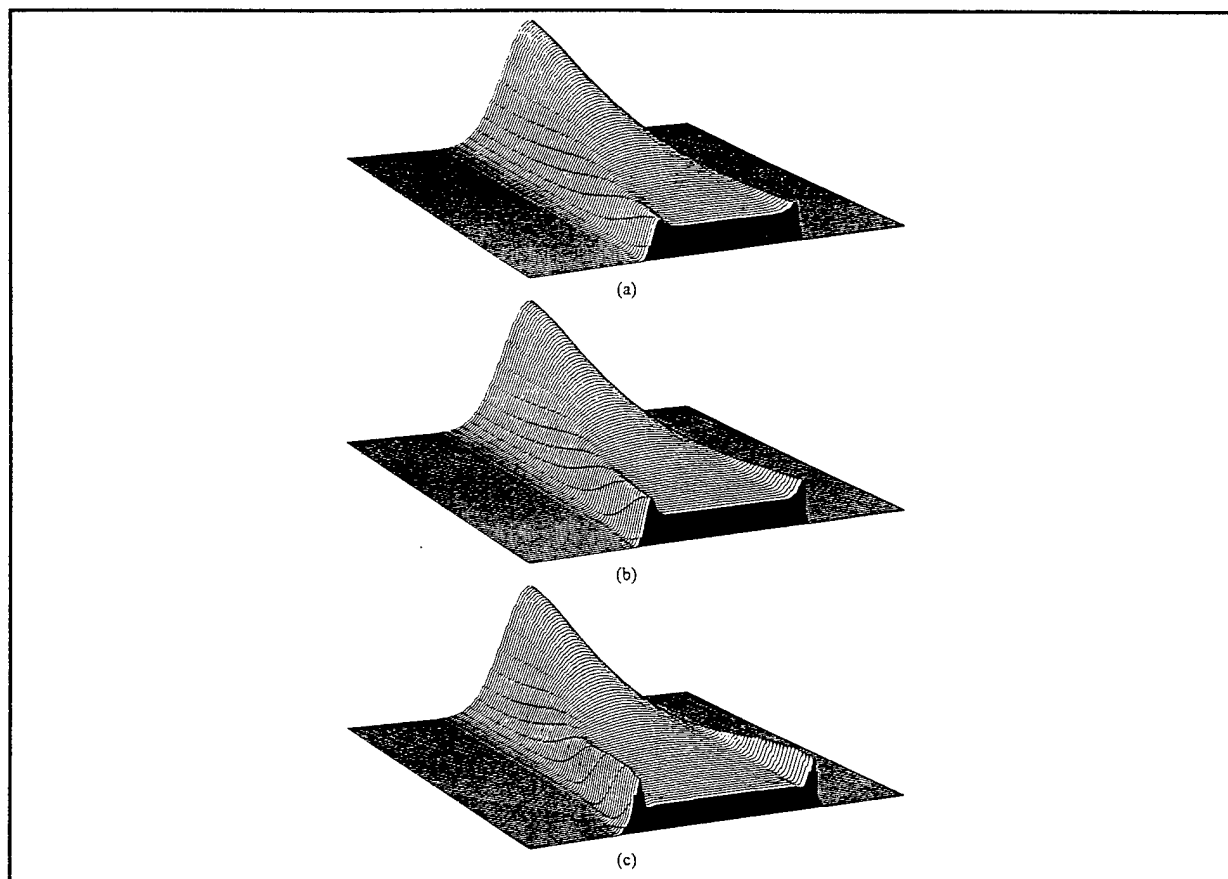
Figure 1. Numerical simulation of the evolution of the beam intensity profile along the propagation direction at a) $\tau = 1.5$, b) $\tau = 2.0$, and c) $\tau = 3.0$.

The experimental waveguide was fabricated by spin-coating preoxidized silicon wafer with SiO_2 layer with a thickness of 1.5 μm and a refractive index of 1.46. The coat was made of poly(methyl methacrylate) (PMMA) solution in chlorobenzene doped with the dye 4-(Dicyanomethylene)-2-methyl-6-(p-dimethylaminostyryl)4H-pyran (DCM) and spin coated. This produced a dual mode slab waveguide with thickness of 1.2 μm and a refractive index of 1.496 at 633 nm. The Gaussian beam width of 0.35 mm from a He-Ne cw laser (633 nm) with TE polarization was injected into the waveguide using a

prism coupler. Figure 2 shows the transverse intensity profiles of experimental results taken at different times. The features of the branch structures are similar to those predicted by the computer model. The appearance of the central branch at 323 seconds in Figure 2 coincides with simulation results shown in Figure 1. In conclusion, optical branching has been modeled and experimentally observed with very close agreement between theory and experiment.
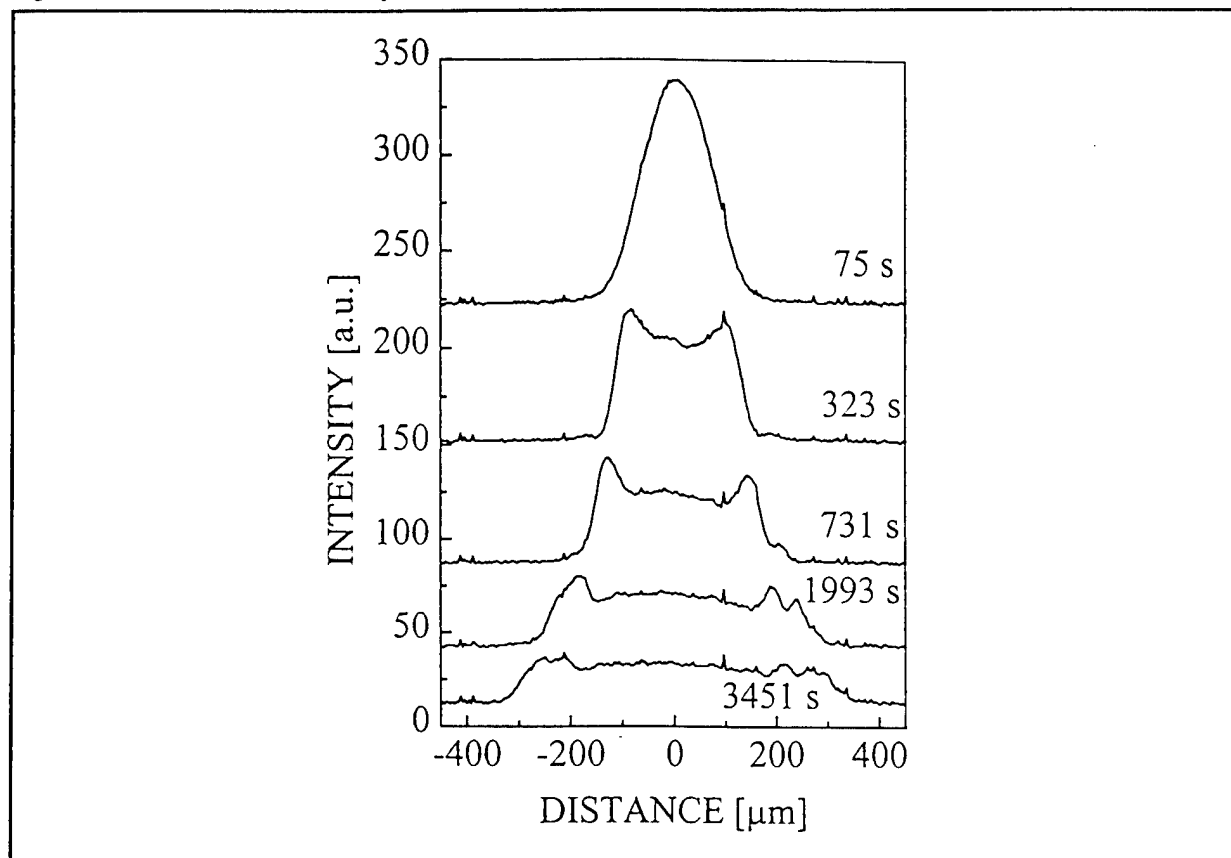
Figure 2. Experimental measurements showing the evolution of the light beam profile at various times after beam injection.

REFERENCES

1.   H. Jerominek, R. Tremblay, and C. Delisle, "Optical branching effect in photorefractive sensitive Ti:LiNbO3 slab waveguides", IEEE J. Lightwave Technol. Vol. LT-3, p. 1105, 1985.
2.   H. Jerominek, C. Delisle, and R. Tremblay, "Optical branching effect in Ti:LiNbO3 waveguides: near-field pattern studies", Appl. Opt. Vol. 25, pp. 732-736, March 1986.
3.   P.A. Belander, and P. Mathieu, "Dark solitons in a Kerr defocussing medium", Appl. Opt. Vol. 26, pp. 111-113, January 1987.
4.   G.R. Allan, S.R. Skinner, D.R. Andersen, and A.L. Smirl, "Observation of fundamental dark spatial solitons in semiconductors using picosecond pulses", Opt. Lett. Vol. 16, pp. 156-158, Febr. 1991.
5.   B. Luther-Davies, and X. Yang, "Waveguides and Y junctions formed in bulk media by using dark spatial solitons", Opt. Lett. Vol. 17., pp. 496-498, April 1992.

Field-Induced Spatial Deformations in Chiral Smectic A Liquid Crystals

F. J. Bartoli, J. R. Lindle, S. R. Flom, B. R. Ratna, R. Shashidhar
Naval Research Lab
Washington, DC 20375
202-404-7374

The application of an electric field to an electroclinic liquid crystal (ELC) causes the molecules to tilt, permitting efficient modulation of an optical signal. This electroclinic tilt also leads to a reduction of the smectic layer thickness, thus introducing strain and causing the planes to deform in order to accommodate the change in the layer thickness. When the ELC is viewed under a polarizing microscope, a spatial modulation of the transmission is observed.[1-5] The resulting stripe texture is generally depicted as a triangular deformation of the smectic layer, where a deformation angle equal to the electroclinic (EC) tilt angle preserves the interlayer spacing.[5] In this paper, the relationship of the deformation angle and the EC tilt angle is investigated by measuring the field dependence of the transmission of an ELC placed between crossed polarizers. The measured extinction is sensitive to the molecular alignment and is therefore a useful probe of the field induced deformation.

The transmitted intensity of a birefringent material placed between crossed-polarizers is given by [6]

$$I = I_0 \sin^2(2\phi) \sin^2(\delta/2) \tag{1}$$

where I_0 is incident intensity, ϕ is the angle of the molecular axis of the liquid crystal relative to the orientation of the polarizer, and δ is the phase angle introduced by the sample birefringence, Δn. ($\delta = 2\pi \Delta n \, d/\lambda$, where d is the sample thickness and λ is the wavelength.)

Fig. 1 displays the measured crossed-polarized transmission as a function of polarization angle at several values of applied field for an organosiloxane liquid crystal denoted TSiKN65.[7] The data in Fig. 1 is plotted on a semi-log scale to emphasize the transmission minimum and is normalized to the transmission maximum in order to remove the phase contribution [see Eqn.(1)]. The angular shift in the position of the minima with field is due to the electroclinic tilt, whereas the change in the amplitude of the transmission minimum with field is associated with the deformation of the SmA planes. The molecular tilt angle, the birefringence and the extinction are determined as a function of field using Eqn.1 to fit the data in Fig. 1.

Fig. 2 is a plot of the field dependence of the extinction for a 10.8 μm thick TSiKN65 sample as the field is varied from 0 to 10 V/μm. The sample is maintained at 300K where it is in the Sm A phase. At low fields, the deformation angle is small and does not appear to depend on the applied field. As the field is increased, a threshold is reached where the extinction increases monotonically with field.

The maximum and minimum of transmitted intensity can be calculated by integrating Eqn. (1) over a stripe period, Λ, that is,

$$I_\perp(\gamma) = I_0 \sin^2(\delta/2) \frac{1}{\Lambda} \int_0^\Lambda \sin^2[2\gamma + 2\psi(x) + 2\theta] \, dx \tag{2}$$

where γ is the polarizer angle, ψ is the deformation angle, and θ is the EC tilt angle. The minimum in Eqn. (2) occurs at $\gamma+\theta=0$, the maximum occurs at $\gamma+\theta=\pi/4$, and for small angles $\sin(2\psi)\approx 2\psi$ and $\sin(2\psi+\pi/2)\approx 1$. Thus, the extinction is related to the deformation angle by

$$\frac{I_{min}}{I_{max}} \approx \frac{1}{\Lambda} \int_0^\Lambda [2\psi(x)]^2 dx \approx [2\psi_{eff}]^2 \quad , \tag{3}$$

where ψ_{eff} is the rms deformation angle. The deformation angles calculated from Eqn. (3) are plotted in Fig. 3 as a function of the measured tilt angle. The deformation angle is not linearly dependent on the EC tilt angle as one might expect on the basis of the simple triangular deformation model. At small applied fields, the deformation angle appears to be independent of the EC tilt angle. For tilt angles greater than 5^0 the deformation angle begins to increase monotonically with the tilt angle. This behavior is probably due in part to the fact that TSiKN65 does not rotate as a rigid rod molecule.

The extinction has also been investigated in a related liquid crystal KN125 which is known to rotate as a rigid rod.[1] KN125 contains no siloxane groups. The extinction was measured as a function of electric field for a 2 μm sample thickness. The induced deformation progressively spoils the extinction as the field increases. Unlike TSiKN65, KN125 exhibited a linear dependence of the deformation angle on tilt angle. For both samples studied, this process appears to be entirely reversible and the extinction returns to its initial value after the field is removed. This suggests that under these conditions the deformation takes place within the elastic limit. The implications of these findings will be discussed.

REFERENCES:
1. G. P. Crawford, R. E. Geer, J. Naciri, R. Shashidhar and B. R. Ratna, Appl. Phys. Lett. 65, 2937 (1994).
2. A. G. Rappaport, P. A. Williams, B. N. Thomas, N. A. Clark, M. B. Ros, D. M. Walba, Appl. Phys. Lett. 67, 17 (1995).
3. R.F. Shao, P.C. Willis and N.A. Clark, Ferroelectrics 121, 127 (1991); R. Shao, Z. Zhuang and N.A. Clark, Liq. Cryst. 14, 1079 (1993).
4. J. Fünfschilling and M. Schadt, Jpn. J. Appl. Phys. 30, 741 (1991).
5. J. Pavel and M. Glogarová, Liq. Cryst. 9, 87 (1991
6. M. Born and E. Wolf, Principles of Optics, 5nd Ed. (Pergamon Press, New York, 1975) p 695.
7. J. Naciri, J. Ruth, G. Crawford, R. Shashidhar, and B. R. Ratna, Chem. Mater. 7, 1397 (1995).
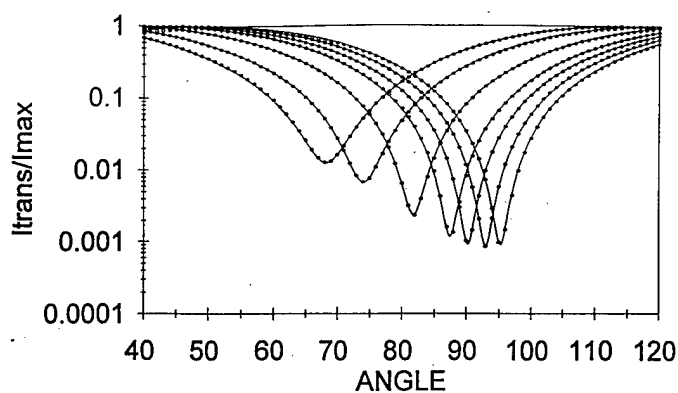
Figure 1. Angular dependence of the transmission of a 10.8 μm thick TSiKN65 sample placed between crossed polarizers for fields of 0 V/μm (right most curve), 1 V/μm, 1.9 V/μm, 2.8 V/μm, 4.7 V/μm, 7.0 V/μm, and 9.4 V/μm (left most curve). The lines drawn through the data are the calculated best fits. The sample temperature was 300K and the laser wavelength was 543.5 nm.
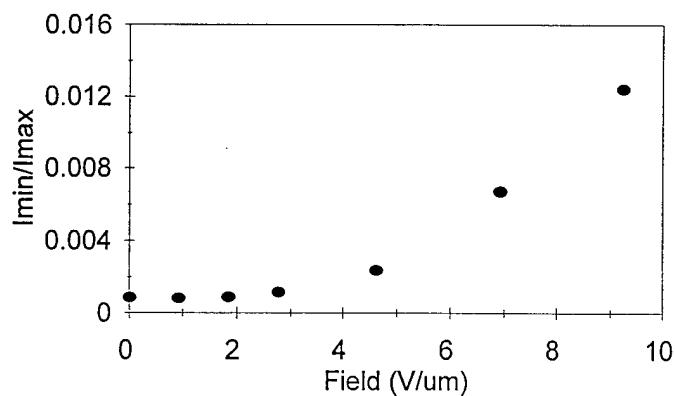
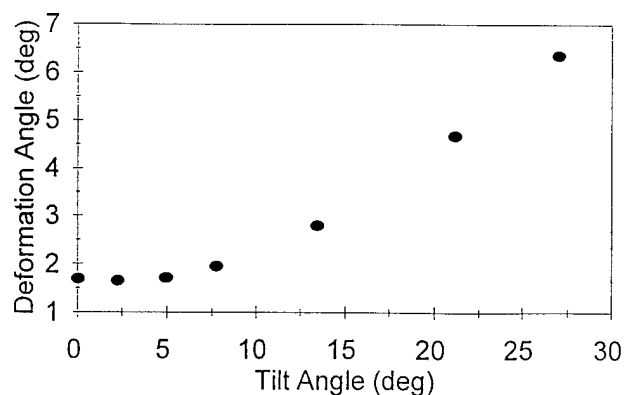Figure 2. The field dependence of I_{min}/I_{max} determined from the data in Fig. 1.

Figure 3. The relationship of the deformation angle and the electroclinic tilt angle.

Electro-optic Modulation in Waveguides Based on
Single Crystal Films of Organic Materials

Jianjun Xu and M. Thakur

Auburn University, AL 36849

Optical amplitude modulators are important components for optical signal processing and telecommunication. Organic single crystal materials have excellent stability, and high figures of merit for electro-optic applications. In this work, two different methods of electro-optic modulation have been studied: i) using direct fabrication of organic single crystal waveguides and end-fire coupling and ii) using evanescent coupling from fiber to organic single crystal film overlay.

Shear method has been successful in preparing single crystal films of organic second order optical materials. Modifying the shear method utilizing patterned lines (SiO_2 ridges) on one of the substrates a guided crystal growth method has been developed which enables control of the dimensions of the crystal film within the confines of a patterned line. Channel waveguides of NPP single crystal were grown by this method. Repeating the growth process with metal deposited alongside the SiO_2 lines amplitude modulators with a transverse geometry were obtained. Light was coupled using end-fire coupling into these waveguides and about 10% modulation was observed for a low applied field (0.5V/μm, dc).

Evanescent coupling from fiber to electro-optic overlay was recently used to realize modulator using lithium niobate[1] and electro-optic polymer films[2]. Using single crystal film of COANP (2-cyclooctylamino-5-nitropyridine) prepared by the shear method, as an overlay on a fiber half-coupler, a modulator was constructed (Fig. 1). In the modulator metal electrodes were deposited on the organic crystal film, so that electric field could be applied in the transverse configuration to change the refractive index. A fiber half-coupler made from a single mode fiber (at 790nm) was used. An index matching liquid was used between the fiber half-coupler and the electro-optic thin film to ensure good coupling. A laser beam with electric field

parallel to the film surface was coupled into the fiber half-coupler. The output of the half-coupler depends on several parameters including thickness of the film, the refractive index of the thin film, the wavelength of the laser beam and the interaction length between fiber half-coupler and the electro-optic thin film. The measured electro-optic modulation as a function of wavelength is shown in Fig.2. About 1% modulation was observed for a low ac field (1V/μm). While this modulation depth is not very large substantially larger modulation is expected using an optimum device configuration. The results are highly promising in terms of electro-optic applications of organic single crystal films.
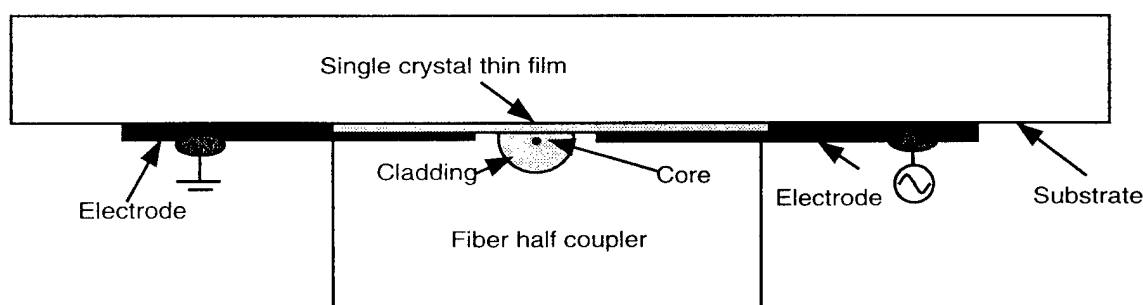
Fig. 1. Schematic diagram of an in-line fiber modulator with a single crystal film overlay
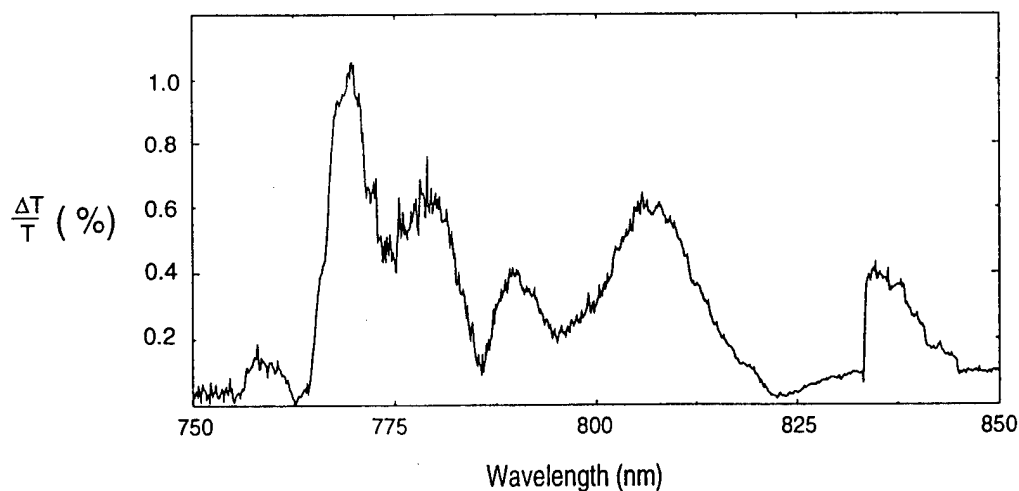
Fig. 2. Observed electro-optic modulation as a function of wavelength

References:

1. Johnstone, W., Murray, S., Thursby, G., Gill, M., McDonach, A., Moodie, D. Culshaw, B., "Fibre optic modulators using active multimode waveguide overlays", Electron. Lett., 27 894--896 (1991).

2. Wilkinson, M., Hill, J. R., Cassidy, S. A., "Optical fiber modulator using electro-optic polymer overlay", Electron. Lett., 27 979-981(1991).

Enhanced Degenerate Four-Wave Mixing in an Endohedral Metallofullerene Through Metal-to-Cage Charge-Transfer

D. Marciu, C. Figura, S. Wang, and J.R. Heflin

Department of Physics, Virginia Tech, Blacksburg, VA 24061-0435

P. Burbank, S. Stevenson, and H.C. Dorn

Department of Chemistry, Virginia Tech, Blacksburg, VA 24061-0212

Since the initial discovery and development of a technique for macroscopic preparation of the archetypal and most abundant fullerene C_{60}, a wealth of fullerene-based structures have been produced including higher fullerenes, charge-transfer complexes, fullerene derivatives, superconducting exohedral-doped fullerenes, and carbon nanotubes. One of the most intriguing fullerene classes is the endohedral fullerene in which the spheroidal molecular structure is employed to encapsulate a small number of atoms (one to four) internal to the cage.[1,2] Until recently, the difficult separation process of endohedral fullerenes had limited their availability to submilligram levels. Consequently, initial studies of these materials had primarily been restricted to electron paramagnetic resonance (EPR) and linear spectroscopy. EPR measurements demonstrated that, for the case of $La@C_{82}$, the La atom transfers three electrons to the fullerene cage and resides in the +3 oxidation state.[2] Metal-to-cage charge transfer appears to be a common feature of transition metal-containing endohedral metallofullerenes. Meanwhile, nonlinear optical studies of empty-cage C_{60} and C_{70} have shown that these materials possess both large third order susceptibilities $\chi^{(3)}(-\omega_4;\omega_1,\omega_2,\omega_3)$[3] ($\sim 10^{-11}$ esu) and strong optical limiting behavior.[4,5] We report here the first nonlinear optical measurements of an endohedral metallofullerene and find a dramatic enhancement in the third order nonlinear optical response. Degenerate four-wave mixing (DFWM) experiments on solutions of the endohedral metallofullerene $Er_2@C_{82}$ show that the metal-to-cage charge transfer provides a mechanism for increasing $\chi^{(3)}(-\omega_4;\omega_1,\omega_2,\omega_3)$ by orders of magnitude relative to empty-cage fullerenes.

The $Er_2@C_{82}$ sample was separated and purified using an automated high performance liquid chromatography (HPLC) apparatus that yields multi-milligram quantities of pure endohedral metallofullerenes.[6] Separation of $Er_2@C_{82}$ is achieved in a multi-step automated HPLC procedure that utilizes Buckyclutcher and Pentabromobenzyl (PBB) derivatized silica gel columns. The inclusion of the PBB chromatographic phase in the separation protocol allows the entire separation process to be automated in contrast with previous procedures. The absorption spectrum of $Er_2@C_{82}$ (isomer III) is compared to that of C_{82} in Figure 1. The endohedral fullerene shows enhanced absorption features near 650 and 900 nm that result from the charge transfer from the metal to the fullerene cage. The endohedral fullerene also possesses an absorption tail to longer wavelengths than in the empty-cage structure. There is therefore a very weak absorption at 1064 nm, the wavelength at which the DFWM measurements are made.

The DFWM experiments are made in the standard, phase-conjugate geometry using the 1064 nm fundamental wavelength of a Q-switched Nd:YAG laser. The three incident beams are focused to e^{-2} radii of 550 μm, and the probe beam is at an angle of 5° with respect to the forward pump beam. The maximum energy of the pump beams is 3 mJ, corresponding to an intensity of 20 MW/cm^2. The sample solutions, with a maximum concentration of 0.32 mg $Er_2@C_{82}$ in 0.8 ml of CS_2 (2.9×10^{-4} mol/l), are contained in 5 mm path length spectrophotometer cells. For even the most concentrated solutions, the internal (reflection-corrected) transmittance was greater than 93% at 1064 nm. In our measurements, the counter-propagating pump beams are vertically polarized
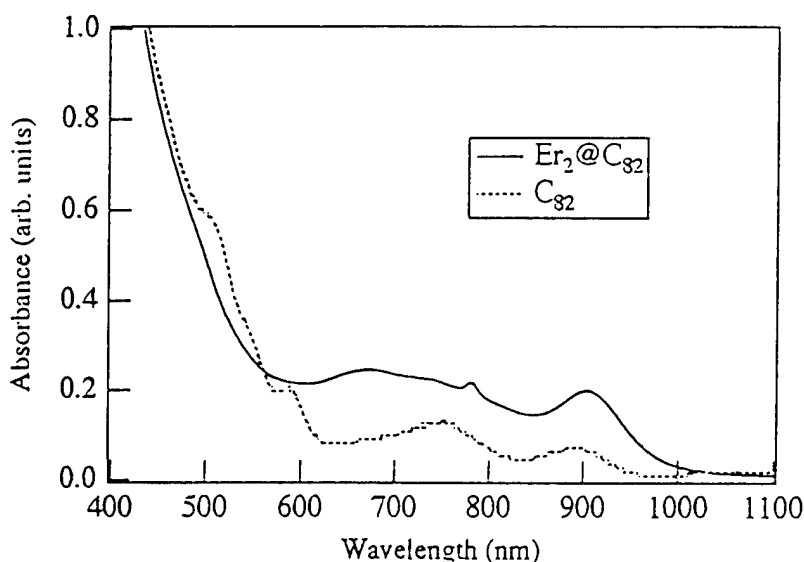
Figure 1. Absorption spectra of $Er_2@C_{82}$ and the corresponding empty-cage structure C_{82} in CS_2.

while the probe and signal beams are horizontally polarized (thus measuring $\chi^{(3)}_{xyyx}(-\omega;\omega,\omega,-\omega)$). This configuration ensures that neither thermal nor population gratings contribute to the DFWM signal, since we are interested in the electronic contribution to $\chi^{(3)}_{ijkl}(-\omega;\omega,\omega,-\omega)$. This is particularly important since the samples have a small absorption at 1064 nm corresponding to a molar extinction coefficient ε of 221 M^{-1} cm^{-1} and an absorptivity α of 0.15 cm^{-1} at the highest concentration.

Figure 2 shows the DFWM signal intensity observed for the CS_2 reference and the 2.4×10^{-4} mol/l $Er_2@C_{82}$ solution together with fits to the data of the form AI^3, where I is the incident intensity. A signal dependence on the incident intensity with an alternate exponent would be an indication of undesired mechanisms in the DFWM process, such as two-photon absorption. The DFWM signal (proportional to $|\chi^{(3)}_{xyyx}(-\omega;\omega,\omega,-\omega)|^2$) of the most concentrated solutions decreases by as much as 50% relative to pure CS_2 solvent indicating a very large, negative molecular susceptibility $\gamma(-\omega;\omega,\omega,-\omega)$ for $Er_2@C_{82}$. For a large number of concentrations, the signal is measured as a function of the incident intensity and is fit to a cubic to obtain the $\chi^{(3)}_{xyyx}(-\omega;\omega,\omega,-\omega)$ value of the solution. Figure 3 illustrates the linear decrease of the solution $\chi^{(3)}_{xyyx}(-\omega;\omega,\omega,-\omega)$ with increased concentration. From this linear dependence, we obtain a value for the molecular susceptibility, $\gamma_{xyyx}(-\omega;\omega,\omega,-\omega)$, for $Er_2@C_{82}$ of -8.7×10^{-32} esu. Using an estimated density of 1.7 gm/cm^3, this corresponds to a $\chi^{(3)}_{xyyx}(-\omega;\omega,\omega,-\omega)$ for a pure $Er_2@C_{82}$ film of -1.1×10^{-9} esu. For comparison, in measurements with all beams parallel polarized, values of $\chi^{(3)}_{xxxx}(-\omega;\omega,\omega,-\omega)=7 \times 10^{-12}$ and 12×10^{-12} esu have been previously reported for C_{60} and C_{70} films, respectively, at 1064 nm, while a value of $\chi^{(3)}_{xyyx}(-\omega;\omega,\omega,-\omega)=1 \times 10^{-12}$ esu was measured for both films.[3]

DFWM was also measured in CS_2 solutions of the empty-cage fullerenes C_{60}, C_{82}, and C_{84} at concentrations equal to or larger than that of the $Er_2@C_{82}$ solution. In each case, the DFWM signal was indistinguishable from that of the pure solvent demonstrating the substantially smaller values of $\gamma_{xyyx}(-\omega;\omega,\omega,-\omega)$ in those materials. As an example, the data for C_{82} at a similar concentration to that of $Er_2@C_{82}$ are shown on Figure 2.

The dramatic enhancement in $\chi^{(3)}$ that we have observed in $Er_2@C_{82}$ establishes the endohedral metallofullerenes as a new potential class of materials for nonlinear optical devices. Specifically, a factor of two to three orders of magnitude higher value for $\chi^{(3)}$ is predicted for a
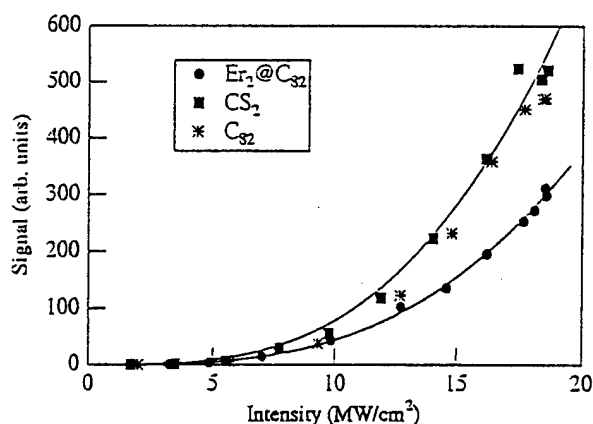
Figure 2. DFWM signal as a function of incident intensity for 2.4×10^{-4} M $Er_2@C_{82}$ in CS_2, C_{82} in CS_2, and pure CS_2 solvent. The solid curves are cubic fits for the $Er_2@C_{82}$ and CS_2 data.

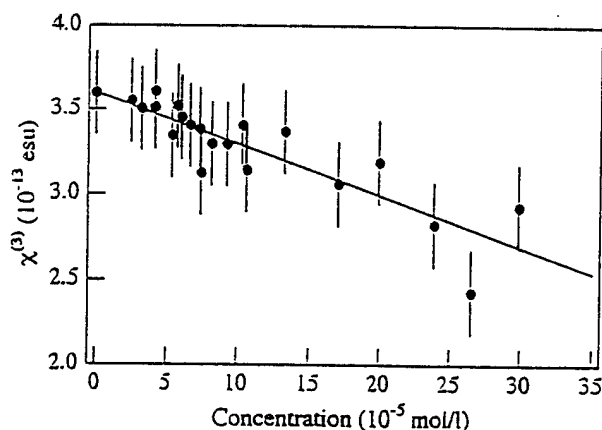Figure 3. Concentration dependence of $\chi^{(3)}_{xyyx} (-\omega;\omega,\omega,-\omega)$ for $Er_2@C_{82}$ in CS_2.

pure film of $Er_2@C_{82}$ relative to thin films of C_{60} and C_{70} illustrating the importance of metal-to-cage charge transfer. A standard figure of merit for the applicability of materials for nonlinear optical switching and modulation devices is $\chi^{(3)}/\alpha$ where α is the linear absorptivity. As described above, the enhanced $\chi^{(3)}$ observed in $Er_2@C_{82}$ at 1064 nm is accompanied by some residual absorption. The absorption is substantially reduced in the 1300 to 1500 nm optical telecommunications window. Experiments are currently underway to measure the nonlinear optical response at these wavelengths in both solutions and pure $Er_2@C_{82}$ films as well as in other endohedral metallofullerenes.

References:

1. Y. Chai *et al.*, J. Phys. Chem. **95**, 7564 (1991).

2. R.D. Johnson, M.S. de Vries, J. Salem, D.S. Bethune, and C.S. Yannoni, Nature **355**, 239 (1992).

3. Z. H. Kafafi *et al.*, Chem. Phys. Lett. **188**, 492 (1992).

4. L. W. Tutt and A. Kost, Nature **356**, 225 (1992).

5. J. R. Heflin, S. Wang, D. Marciu, C. Figura, and R. Yordanov, Proc. SPIE **2530**, 176 (1995).

6. H. C. Dorn *et al.*, Proc. of Mater. Res. Soc. Vol. **359**, 123 (1995).

Fabrication of vertical tapers in polymer thin films by oxygen reactive ion etching with a shadow mask for photonic device applications

Antao Chen, Felix Ignacio Marti-Carrera, Sean Garner, Vadim Chuyanov, and William H. Steier

Department of Electrical Engineering-Electrophysics
University of Southern California, Los Angeles, CA 90089-0483, (213) 740 8781

The taper structure is the key component of an on-chip mode size transformer for efficient fiber coupling. The taper provides a smooth transition between two waveguide sections with different mode sizes with minimum radiation loss. The tapered mode size transformer has become a standard approach for efficient fiber coupling with semiconductor lasers and amplifiers[1]. Various taper fabrication techniques are developed for semiconductor and LiNbO$_3$ devices[2-5], but most of them are not applicable to polymer waveguides. Oxygen reactive ion etching is the primary method to etch a polymer film. For most polymer waveguides, the major part of fiber coupling loss is due to the mode size mismatch between the waveguide and fiber in the vertical direction, therefore a vertical taper is needed to reduce the fiber coupling loss. In this paper, a reactive ion etching (RIE) technique with a shadow mask is demonstrated. A similar technique has been reported for etching submicron tapers in InP with methane plasma[5]. Our approach can effectively create tapers several microns deep and a few millimeters long with oxygen plasma which is required for multilayer polymer waveguide structures.

The etching technique is schematically shown in Fig. 1. The shadow mask is made of a piece of 0.25 mm glass slide. It is attached with UV epoxy to a glass spacer which serves as a support and determines the height of the shadow mask. The mask with spacer is placed on the sample to be etched, and the oxygen plasma etching is carried out in a standard parallel plate etcher. No adhesive is used to hold the shadow mask on the sample. The shadow mask partially shields the sample underneath and also deflects the ion flux during the etching, causing a position dependent etch rate in the vicinity of the end of the shadow mask. An example of measured surface profile of an etched taper is given in Fig. 2. The taper has a smooth S-shape and fits well into the function

$$y = \frac{h}{1 + e^{8\frac{x-c}{l}}} + d,$$

where the physical meanings of parameters l, h, c and d are shown in Fig. 2.
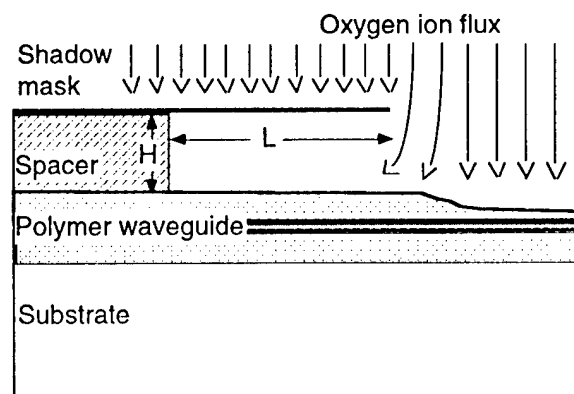
Fig. 1 Taper etching with a shadow mask in oxygen plasma.

For a given RIE condition, namely pressure, power and flow rate, the length of the taper, l, is determined predominantly by the height of the shadow mask. The relationships between the taper length and etching parameters such as pressure, power, and etch time have been investigated in detail. Fig. 3 shows the taper length obtained with various mask heights and oxygen pressures. Etching with high pressure produces a longer taper, and the taper length is more sensitive to the shadow mask height because the ion flux is less directional. The length of the taper is independent of the length of the shadow mask L, as long as L is larger than 2 mm.
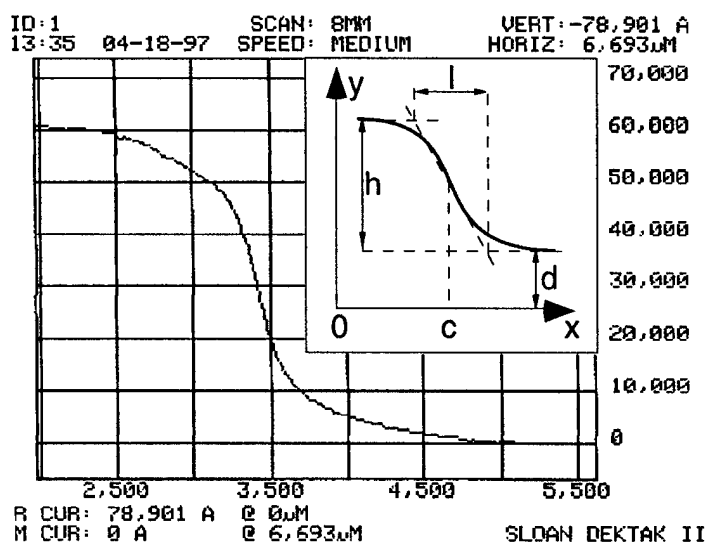
Fig 2 An actual surface profile of a taper etched in the polymer waveguide cladding film. The horizontal scale is in μm and the vertical scale is in Å.
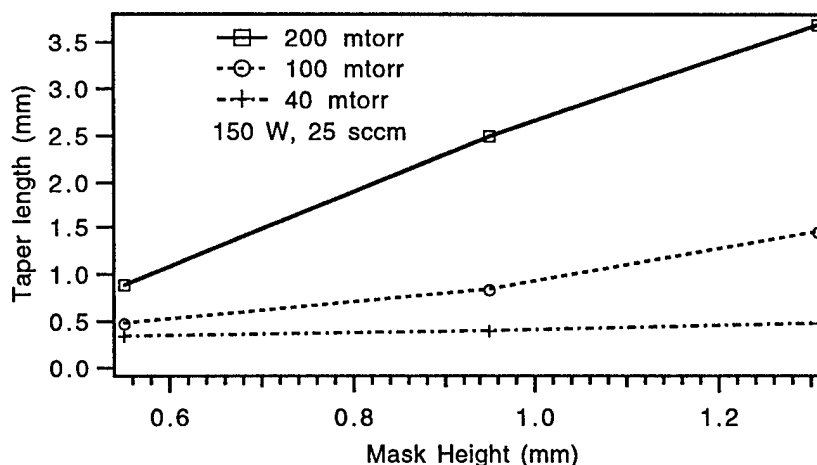
Fig. 3 Taper length as a function of shadow mask height with various etching pressure.

Another consideration of selecting etching parameters is the scattering loss due to the roughness of the etched surface[6], which depends strongly on the plasma etching parameters. It is found that high pressure and low power etching produces not only a longer taper, but also a smooth surface, as shown in Fig. 4.

We also experimented with a shadow mask and spacer made of aluminum sheets of similar thickness to that of the glass shadow mask. No significant difference in the etching results was observed. This phenomenon suggests that the taper etching is mostly due to the physical shielding of ions instead of deflection of ion flux by disturbing the electric field distribution near the sample surface.

| 50mTorr-0.32W/cm^2 | 400mTorr-0.05W/cm^2 |
| 0.93dB/cm | 0.05dB/cm |
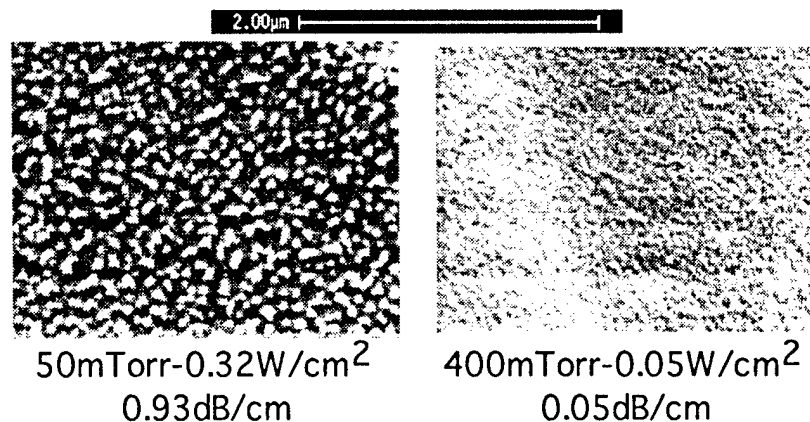
Fig. 4 Surface roughness and the measured scattering loss at 1.3 μm after various oxygen RIE.

A very simple approach to fabricate vertical tapers with the length and depth suitable for multilayer polymer waveguide devices is demonstrated. The etching is done in one step, and no other processing such as photolithography is required. The shadow mask is made of commonly available glass slides. Because oxygen plasma does not etch glass, the shadow mask can be used repeatedly. This taper etching technique has been successfully used in a mode size transformer which effectively expands the mode of polymer waveguide for improved coupling with optical fiber[7].

References

[1]   I. Moerman, G. Vermeire, M. Dhondt, W. Vanderbauwhede, J. Blondelle, G. Coudenys, P. Vandaele, and P. Demeester, "III-V semiconductor wave-guiding devices using adiabatic tapers," *Microelectronics Journal*, vol. 25, pp. 675-690, 1994.
[2]   I. Moerman, M. D'Hondt, W. Vanderbauwhede, P. V. Daele, P. Demeester, and W. Hunziker, "InGaAsP/InP strained MQW laser with integrated mode size converter using the shadow masked growth technique," *Electronics Letters*, vol. 31, pp. 452-454, 1995.
[3]   H. S. Kim and R. V. Ramaswamy, "Tapered, both in dimension and in index, velocity coupler: theory and experiment," *IEEE Journal of Quantum Electronics*, vol. 29, pp. 1158-1167, 1993.
[4]   O. Mitomi, K. Kasaya, Y. Tohmori, Y. Suzaki, H. Fukano, Y. Sakai, M. Okamoto, and S. Matsumoto, "Optical spot-size converters for low-loss coupling between fibers and optoelectronic semiconductor devices," *Journal of Lightwave Technology*, vol. 14, pp. 1714-1719, 1996.
[5]   B. Jacobs, R. Zengerle, K. Faltin, and W. Weiershausen, "Vertically tapered spot size transformers fabricated by a simple masking technique," *Electronics Letters*, vol. 31, pp. 794-796, 1995.
[6]   A. Chen, K. Kaviani, A. W. Rempel, S. Kalluri, and W. H. Steier, "Optimized oxygen plasma etching of polyurethane-based electro-optic polymer for low loss optical waveguide fabrication," *Journal of Electrochemical Society*, vol. 143, pp. 3648-3651, 1996.
[7]   A. Chen, V. Chuyanov, F. I. Marti-Carrera, S. Garner, W. H. Steier, J. Chen, S. Sun, and L. R. Dalton, "Integrated polymer waveguide mode size transformer with a vertical taper for improved fiber coupling," *Proceedings of SPIE*, vol. 3005, paper 11, in press, 1997.

Spontaneously Self-Assembled Polar Multilayers With High Second-Order Optical Nonlinearity

M. S. Johal, L. Smilowitz[1], J. M. Robinson, D. W. McBranch, D.Q. Li, [2]W. [2]S. Yang, [2]Y. W. Cao, [2]X. D. Chai, [2]Y. S. Jiang, and [2]T. J. Li

Chemical Science & Technology Division, Los Alamos National Laboratory, Los Alamos, NM 87545 (505-665-6186), [1]Physics Department, Boston University, 590 Commonwealth Ave, Boston, MA 02215, [2]Chemistry Department Jilin University, Changchun, Jilin P. R. China

INTRODUCTION

Ordered molecular assemblies can lead to materials with extremely high second-order non-linear optical (NLO) properties [1] with applications in technologies such as optoelectronics [2] and permanent magnetism [3]. Although organic molecules with high nonlinearities are well known, it has been difficult to design bulk materials in which the molecules are highly ordered with the same orientation. In this work, we use second harmonic generation (SHG) to determine the second-order nonlinear coefficient (d_{33}) of a spontananeously self-assembled, polar multilayer film (Figure 1) grown by drop casting on a silica substrate. Using ellipsometry to measure film thickness, the average molecular orientation of the chromophores is also determined.
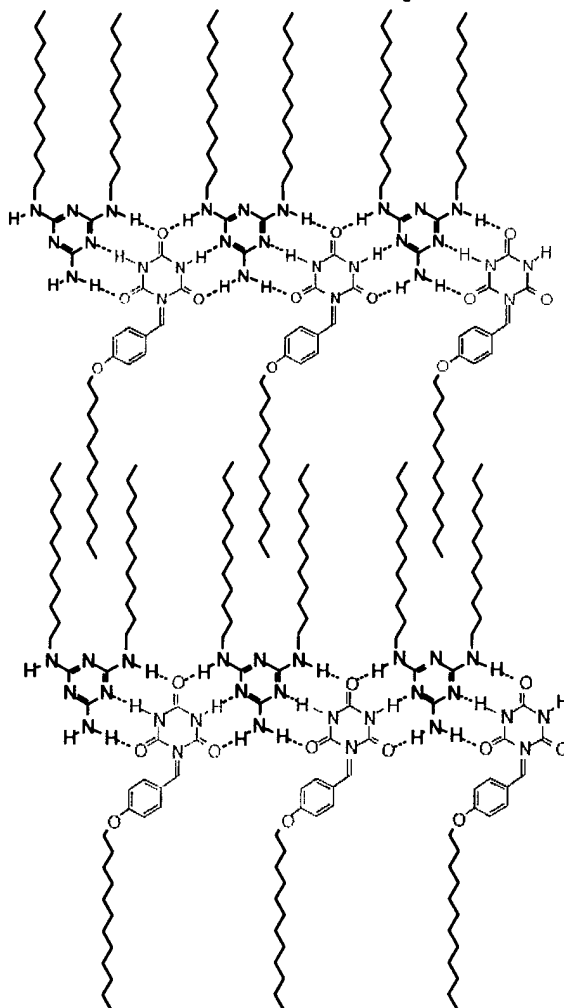
Figure 1. Schematic representation of multilayer supramolecular systems (shown 2 layers) assembled into asymmetric structures through highly organized hydrogen bonds and hydrophobic interactions. NLO-active units are shown in grey scale.

EXPERIMENTAL DETAILS

SHG measurements were carried out in transmission geometry under non-resonant conditions. A Nd:YAG laser provided ~50 psec pulses for fundamental excitation at 1064 nm. The energy density at the sample was 2mJ/mm². The transmitted SHG signal at 532nm was measured as a function of the incident angle from normal (0°) to 60° [4]. The transmitted SHG signal was separated from the fundamental beam using a 532 nm notch filter and color filters, passed through a polarizing analyzer, and detected using a PMT and gated boxcar integrator. The SH data points were averaged over 100 laser pulses.

DISCUSSION

The transmitted p-polarized SH intensity from a multilayer film grown on one side of a silica substrate for both s- and p-polarized incident excitation is shown in Figure 2. No appreciable s-polarized SH signal was observed using either p- or s-polarized excitation.
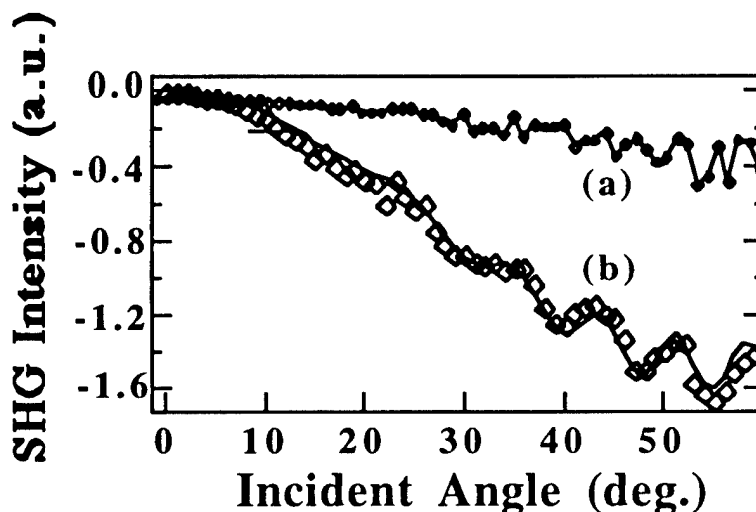
Figure 2. The p-polarized SH data for M12PB12. (a) s-polarized incident excitation. (b) p-polarized incident excitation. The solid line is a theoretical fit to the data points discussed in the text.

Two major features are observed in the data in Figure 2: the increase in SH signal at high angles of incidence and the weak interference fringes. These fringes arise from the interaction of the SH waves from the multilayer and the opposite surface of the silica substrate [5,6]. The absence of azimuthal orientation dependence observed within the plane of the self-assemblies indicate that the films possess uniaxial symmetry about the surface normal [7]. Thus only two independent tensor elements (X_{zzz} and $X_{zxx}=X_{zyy}$) of the second-order nonlinear susceptibility are nonzero. The fit to the p-polarized fundamental and second harmonic generation from the film to the theoretical model described by Katz *et al.* [8] is shown by the solid line though the data of Figure 2(b). The data were referenced to the X_{xxx} tensor component of quartz using the SH response from a y-cut quartz crystal under the same experimental conditions. With the film thickness determined to be 300Å by ellipsometry (assuming a refractive index of 1.55 for the multilayer), the magnitude of the non-linear optical coefficient is $d_{33}=3.2$ pmV^{-1} and the average angle of the chromophores is approximately 45° with respect to the surface normal. The relatively large magnitude of d_{33} ($d_{33}=19$ for multilayer azo polymers [9]), can be attributed to the combination of polarizable, delocalised π-electrons associated with the phenylene-carbon double bond linkage as well as the spontaneous assembly into a relatively ordered, polar structure. Modification of the chemical structure of the multilayers is currently being pursued.

CONCLUSION

We have shown that drop cast films of a nonlinear chromophore spontaneously self assemble into ordered NLO active multilayers. The relatively large SHG response from the multilayer can be attributed to the partially delocalised π-electrons in the phenyl groups of the multilayer film and a bulk polar structure.

REFERENCES

[1]   A. Ulaman, *An Introduction to Ultrathin Organic Films from Langmuir-Blodgett to Self-Assembly*, Academic Press Inc., San Diego, 1991.

[2]   D. Li, T.J. Marks, C. Zhang, G.K. Wang *Snth. Methods* **(1991)**, 41-43, 3157.

[3]   S. Aldrovandi, F. Borsa, A. Lascialfari, V.J. Tongnetti *J. Appl. Phys.* **(1991)**, 67(9,2A), 5914.

[4]   P.D. Maker, R.W. Terhune, N. Nisenoff, C.M. Savage *Phys. Rev. Lett.* **(1962)**, 8, 21.

[5]   D. Li, B.I. Swanson, J.M. Robinson, M.A. Hoffbauer *J. Am. Chem. Soc.* **(1993)**, 115, 6975.

[6]   D. Li, B.I. Swanson, J.M. Robinson, M.A. Hoffbauer *Nonlinear Optics III* **(1992)**, 1626, 424.

[7]   D. Li, M.A. Ratner, T.J. Marks, C. Zhang, J. Yang, G.K. Wang *J. Am. Chem. Soc.* **(1990)**, 112, 7389.

[8]   H.E. Katz, G. Scheller, T.M. Putvinski, M.L. Schilling, W.L. Wilson, C.E.D. Chidsey *Science* **(1991)**, 254, 1485.

[9]   X. Wang, S. Balasubramanian, L. Li, D. Sandman, M. Rubner, S. Tripathy *submitted.*

Modified attenuated total reflection for the fast and routine electrooptic measurements of nonlinear optical polymer thin films

Antao Chen, Vadim Chuyanov, Sean Garner, and William H. Steier
Department of Electrical Engineering - Electrophysics, University of Southern California
Los Angeles, CA 90089-0483, (213) 740 8781

Larry R. Dalton
Department of Chemistry, University of Southern California
Los Angeles, CA 90089-1062, (213) 740 8768

In the course of developing EO polymers, a convenient and fast method to obtain the electrooptic (EO) coefficients, r_{33} and r_{13}, is highly desirable. Some of the existing EO measurement techniques such as Fabry-Perot interferometry(1) and ellipsometry(2) require metal deposition and electrode processing for each test sample. Therefore, they are not suited for daily sample testing. Second harmonic generation (SHG) is an indirect method to measure the EO coefficients(3). It is usually performed with 1.064 Nd:YAG laser and encounters difficulties with polymers that contain high $\mu\beta$ chromophores because these chromophores usually have red-shifted absorption peaks that causes the Kleiman symmetry, a fundamental assumption of this technique, to break down. Attenuated total reflection (ATR) can directly measure the EO coefficients with no restriction on the wavelength of the absorption peak. One measurement scan provides the refractive index, the thickness, and an EO coefficient. Typically, the thin film electrode in contact with the test sample is made of Au or Ag in conventional ATR techniques(4). These metal thin films are soft and not durable for repeated measurements. The curve fitting algorithm for data processing(4, 5) is also inconvenient for fast sample evaluation. In this paper, a modified ATR technique for routine EO measurement is presented which does not require electrode preparation for each test sample and uses a simple algorithm for data processing.

The ATR measurement is based on the change of prism coupling angles of the polymer film due to the EO effect. The setup is schematically shown in Fig. 1. The polymer thin film is spun on a commercially available ITO coated glass slide. The ITO functions as both the ground electrode during corona poling and the modulation electrode in the measurement. The setup is built in such a way that the contact point between the test sample and the prism is kept on the rotation axis of the stage. The EO polymer sample is held against the thin film coated prism by a pneumatic plunge. Mounting the sample is by simply flipping a switch, and no alignment is needed for each measurement.

Conventional ATR uses Au or Ag as the modulating electrode between the prism and sample surface. These metals have low optical loss and give sharp reflection minima that corresponds to each waveguide mode of the polymer film. But Au and Ag films are soft and can be easily damaged if they are used for repeated measurements. We chose Cr as the material of the electrode coated on the prism. Cr is extremely scratch resistant due to its hardness and its superior adhesion to glass prism.

An interesting phenomenon observed in ATR with Cr electrode film is the distortion of the reflection spectrum. Instead of sharp reflection minima observed with Au or Ag electrodes, the mode dips are broadened and more asymmetric, as shown in Fig. 2. Simulations of the multilayer structure were made with the Fresnel's formulae(6) and this phenomenon was attributed to the large imaginary part of the dielectric constant of Cr and the roughness of the metal film(7). The roughness is caused by the laser monitored chemical etching which is the method we used to reduce the film thickness. It is proven that such distortion does not affect the accuracy of the EO measurement.
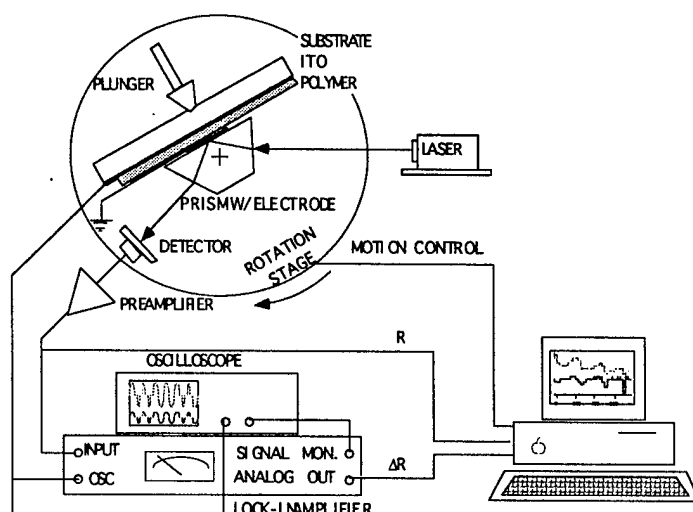
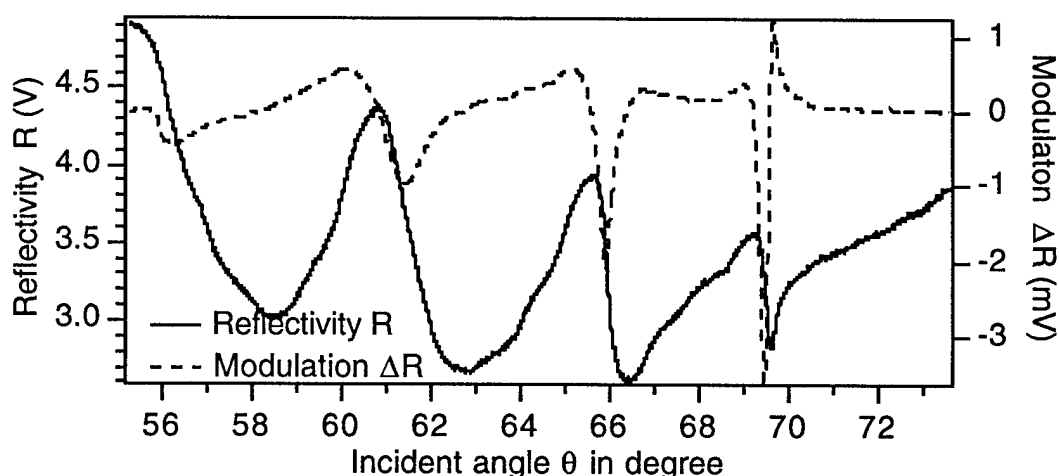Fig. 1. Setup of the EO measurement.

Fig. 2. Measurement data from a typical ATR scan. Cr electrode produces broad reflection minima. Each reflection minimum corresponds a waveguide mode. Measurement is made with TM polarization.

The standard method to get results from an ATR measurement(5) is by adjusting the parameters to be measured to fit the theoretical curve to the measurement data. Because the index change due to the electrooptic effect is only on the order of 10^{-5} for EO polymers, and the mode dips are very broad with Cr electrode, the angular modulation of the mode dips are in the order of 1% of the width of the mode dips, we use a simplified formulae based on the linear approximation:

$$r_{13} = \frac{2d\Delta R}{n_{TE}^3 V} \frac{\partial n_{eff}}{\partial \theta} / (\frac{\partial R}{\partial \theta} \frac{\partial n_{eff}}{\partial n_{TE}})$$ (1a)

$$r_{33} = \frac{2d\Delta R}{n_{TM}^3 V} \frac{\partial n_{eff}}{\partial \theta} / (\frac{\partial R}{\partial \theta} \frac{\partial n_{eff}}{\partial n_{TM}})$$ (1b)

where n_{TE} and n_{TM} are the refractive indices of the polymer film for the TE and TM polarizations, respectively. d is the thickness of the polymer film. θ is the angle of incidence in the prism at the prism-sample interface. The DC part of the reflectivity, R, and the AC part of the reflectivity due to the index modulation, ΔR, are measured as the output voltage of the detector. V is the modulating voltage across the polymer film. $n_{eff}=n_p \sin\theta$, where n_p is the refractive index of the prism. All the variables in the formulae, and therefore r_{33} and r_{13}, are obtained by one test scan. r_{33} and r_{13} are measured independently by different polarizations of the incident beam. The piezoelectric (PE) effect is neglected in this algorithm. Firstly, we have never observed the inversion of the sign of the lock-in signal in our measurements, which is commonly considered as an evidence of negligible piezoelectric effect(4). Secondly, our simulation showed that the PE effect basically affects only the angular changes of higher modes. The angular position of the 0th order mode is far less dependent on the thickness change than on the index change from the EO effect. The calculation is usually made with the measurement data of the 0th order mode. By using a slightly more complex algorithm, piezoelectric coefficients can be calculated from the measurement data of two modes(5). The differences between the results obtained with the above approximated formulae using the lowest 3 modes and from the rigorous model of the surface plasma in multilayer medium are within 5%.

To further verify the accuracy of our technique, a comparison of the EO measurement results obtained by this modified ATR technique, the ellipsometry and SHG has been made. Identically processed thin films of the same EO polymer were used for the comparison. Furthermore, the same sample was used for ATR and ellipsometry. The r_{33} values obtained by the ATR, ellipsometry, and SHG are 9.9±1.5, 10.4±0.8, and 9.9±0.6 pm/V, respectively. These results show a good agreement among the three measurement techniques.

In conclusion, we have developed a modified ATR technique suitable for the routine evaluation of poled EO polymer thin films. Scratch resistant metal electrode and a simplified algorithm have been successfully used. We have a Cr thin film electrode coated on a prism that has withstood three years of daily use and more than a thousand measurements without damage. The broadening of the mode dips does not seriously affect the sensitivity of the measurement because the modulation signal ΔR is in the mV range for typical measurements, much higher than the detection limit of a lock-in amplifier. With this technique, the measurement and data processing take only about 10-15 minutes to complete. The good accuracy of this technique is verified by comparison with the results obtained with other EO measurement techniques and also by the rigorous theoretical modeling.

References

1.   N. P. Wang, T. M. Leslie, S. Wang, S. T. Kowel, *Chemical Materials* **7**, 185-191 (1995).
2.   Y. Levy, P. A. Chollet, G. Gadret, F. Kajzar, *Proceedings of SPIE* **1775**, 299-310 (1992).
3.   D. M. Burland, R. D. Miller, C. A. Walsh, *Chemical Reviews* **94**, 31-75 (1994).
4.   D. Morichere, et al., *Journal of the Optical Society of America B* **10**, 1894-1900 (1993).
5.   D. Dentan, Y. Levy, M. Dumont, P. Robin, E. Chastaing, *Optics Communications* **69**, 379-383 (1989).
6.   S. Herminghaus, B. A. Smith, J. D. Swalen, *Journal of the Optical Society of America B* **8**, 2311-2317 (1991).
7.   R. Russjager, H. A. Macleod, *Journal of Modern Optics* **42**, 1335-1360 (1995).

Return Loss Measurements for the Determination of Critical Materials Parameters for Polymer Optical Waveguides

R. A. Norwood, AlliedSignal, Inc., 101 Columbia Rd., Morristown, NJ 07962-1021, (201) 455-3450

There is a significant amount commercial and research activity currently centered around the deployment of various optical networks, including wavelength division multiplexing systems[1] and passive optical networks. Recently, there has been increased effort devoted to investigating the use of polymers as the materials for passive components in these systems, such as wavelength division multiplexers[2] and splitters. Low loss polymer single-mode waveguides have been demonstrated in a number of systems to this point[3,4] and it is likely that components with sufficiently low insertion loss will be available in the near future.

However, for most applications it is also important to know how the component's performance varies with temperature, humidity and optical wavelength. Measurements of these effects can be difficult and time consuming. An elegant approach to measuring quantities such as dn/dT, humidity effects, and $dn/d\lambda$ is to measure the return loss from the interface between the material to be measured and an optical fiber,[5] as shown in Figure 1. If the fiber optical properties are well-known, then by simply measuring the change in return loss upon heating, for example, the dn/dT of the material can be determined.
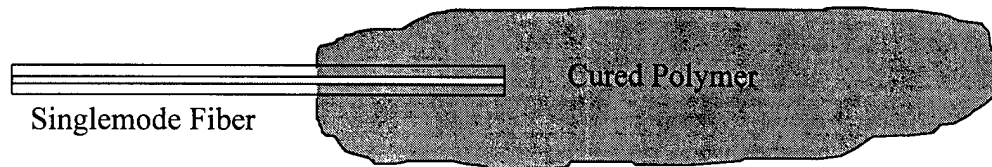
Figure 1. Sample geometry for return loss measurements.

Straightforward calculation using Fresnel's equations yields the following relationship between $dn_{polymer}/dT$ and $d(Return\ Loss)/dT$

$$\frac{dn_{polymer}}{dT} = \frac{n_{fiber}^2 - n_{polymer}^2}{17.4 n_{fiber}} \frac{d(\text{Return Loss})}{dT} \tag{1}$$

where the return loss is measured in dB and we have neglected the dn/dT of the fiber itself; this is justified since it is an order magnitude less than that of the polymer. (1) indicates that to determine $dn_{polymer}/dT$ it is only necessary to determine the slope of the return loss with temperature; absolute measurements

of the refractive index can be performed if necessary with very careful measurements of the return loss. A similar analysis would obtain for determining $dn/d\lambda$, although in this case the fiber dependence would also have to be included, especially in the 1.3 μm and 1.55 μm regions that are of interest for telecommunications.

Experiments were performed using a commercially available return loss meter (Rifocs 585RL) with a light source at 1.3 μm and 1.55 μm. The fiber cable used had an angle-polished connector on one end, which can give very low return loss (70 dB), and a bare fiber pigtail on the other end. To prepare the samples, a good fiber cleave was obtained on the pigtail end, which was then immersed in photomonomer and then cured. The polymer is a photocurable acrylate that exhibits a high degree of three-dimensional crosslinking and is known to have optical transmission with excellent thermal stability.[6] The sample was then immersed in an environmental chamber that had control over both humidity and temperature. For temperature dependence measurements the humidity is held constant at 50% RH and the temperature is taken between set points; measurements are taken once the temperature has stabilized at a set point.
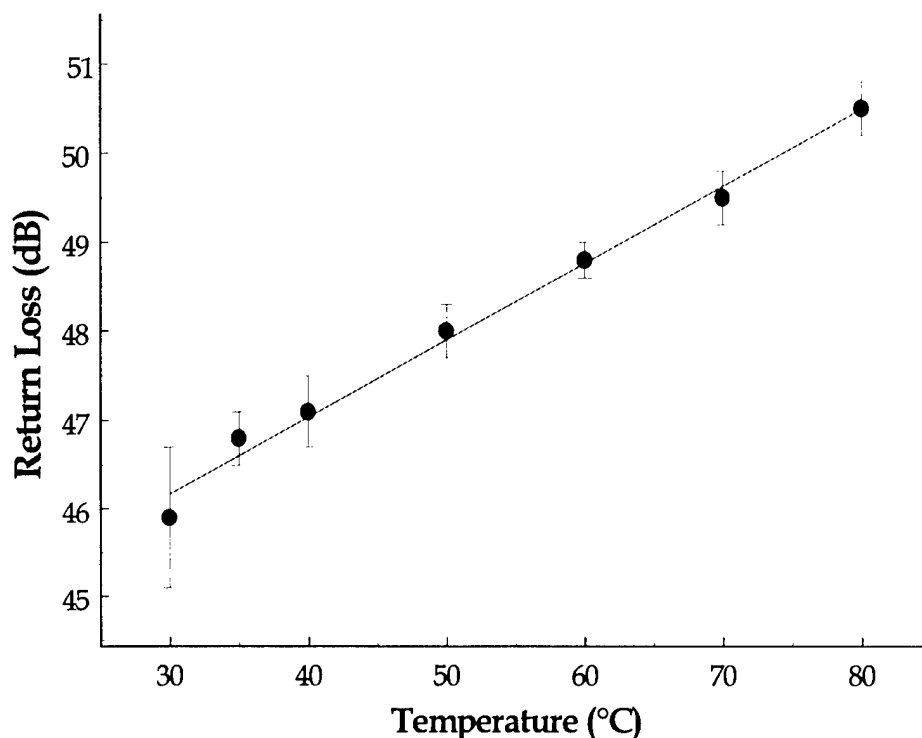
Figure 2. Measurement of return loss vs. temperature for fiber terminated by photocurable acrylate polymer.

The results of the measurement are shown in Figure 2 where we plot return loss vs. temperature. Note that the vertical scale is only accurate to a small additive constant that can vary based on the quality of the referencing procedure; however, only the slope of the line is necessary for extracting $dn_{polymer}/dT$. Taking n_{fiber} = 1.462 and $n_{polymer}$ = 1.491 (@ 1.3 µm), we can use (1) to find that $dn_{polymer}/dT$ is - 3.0 ± 0.3 x 10⁻⁴/°C, a typical number for a polymer. We also looked at the effects of humidity on the return loss. The sample was held at 60°C and allowed to stabilize for 30 minutes at relative humidities of 20, 40, 60, and 80%. We observed a decrease in return loss from 40.5 dB in the 20-40% RH range to 42 dB in the 60-80% range. This translates into a drop in the refractive index of 0.0045 in going from low to high humidity. Changes of this order would effect singlemode waveguide performance if core and cladding changes were different; they would also effect return loss of the device if index matching were used as the method to reduce return loss.

We will present further measurements using this method, including measurements of $dn/d\lambda$, a number which is of importance for wavelength division multiplexers. Accurate knowledge of these parameters aids greatly in device design, testing, and packaging, all of which significantly impact the utility of polymeric integrated optical devices in telecommunications applications.

1. I. P. Kaminow, C. R. Doerr, C. Dragone, T. Koch, U. Koren, A. A. M. Saleh, A. J. Kirby, C. .M. Ozveren, B. Schofield, R. E. Thomas, R. A. Barry, D.M. Castagnozzi, V. W. S. Chan, B. R. Hemenway, Jr., D. Marquis, S. A. Parikh, M. L. Stevens, E. A. Swanson, S. G. Finn, and R. G. Gallager, "A Wideband All-Optical WDM Network," *IEEE J. on Selected Areas in Comm.* **14**, 780 (1996).

2. Y. Hida, Y. Inoue and S. Imamura, "Polymeric arrayed-waveguide grating multiplexer operating around 1.3 µm," *Electronics Letters* **30**, 959 (1994).

3. Th. Knoche, L. Müller, R. Klein and A. Neyer, "Low loss polymer waveguides at 1300 and 1550 nm using halogenated acrylates," *Electronics Letters* **32**, 1284 (1996).

4. L. Eldada, C. Xu, K. M. T. Stengel, L. W. Shacklette, and J. T. Yardley, "Laser-fabricated low-loss single-mode raised-rib waveguiding devices in polymers," *J. Lightwave Tech.* **14**, 1704 (1996).

5. M. Kihara, S. Nagasawa, and T. Tanifuji, "Return loss characteristics of optical fiber connectors," *J. Lightwave Tech.* **14**, 1986 (1996).

6. R. A. Norwood, L. Eldada, S. Emo, J. Gustus, R. Rapoport, K. M. T. Stengel, L. W. Shacklette, C. Wu, C. Xu, and J. T. Yardley, "Polymer optical interconnection technololgy: toward WDM applications," *Proc. SPIE* **2690**, 151 (1996).

Optical Measurement of the Glass Transition Temperature of Polymer Waveguides for Integrated Optics

Harald Bock[1], Stefan Christian[1], Wolfgang Knoll[1,2]

1) *Max-Planck-Institut für Polymerforschung, 55128 Mainz, Germany*

2) *Frontier Research Program, The Institute of Physical and Chemical Research (RIKEN), 2-1 Hirosawa, Wako, Saitama 351-01, Japan*

Jan Vydra

Institut für Angewandte Physik, Technische Hochschule Darmstadt, 64289 Darmstadt, Germany

The development of polymeric devices for integrated optical applications has recently received much attention [1]. The thermodynamic properties of the waveguiding materials are of vital interest in this field. In particular the fabrication of active components based on poled nonlinear chromophore functionalized polymers requires knowledge of the materials' glass transition temperature T_g, since the relaxation of noncentrosymmetric orientational order is strongly related to the glass transition.

The choice of important processing parameters (i.e. temperatures for electric field poling or annealing conditions) depends on a film's or more specifically a waveguide's T_g. On the other hand processing steps can in turn change a material's T_g significantly. It can be reduced by residual solvent in the film after spin-casting or by degradation due to processing.

The conventional method to find out about these effects is to carefully scrape the film off its substrate and perform a differential scanning calorimetry (DSC) measurement on the material. One major drawback of this technique is that one needs to destroy several samples in order to obtain enough material for the DSC experiment. Due to the still quite small amount of material (<1mg) the resulting curves are noisy [2].

Non-destructive and thus more convenient methods to measure T_g in a planar waveguide are based on detecting the abrupt change at T_g of the polymer's expansion coefficient, which is the derivative of the film's volume versus temperature T: $\beta_V = \partial V/(V\partial T)$. In a thin film geometry the expansivity β is confined to a change in thickness t: $\beta = \partial t/t\partial T$. Thus, determination of the temperature dependence of a sample's thickness t is a possibility to characterize the glass transition of a polymer. This can easily be done in a film geometry by optical techniques, i.e. by ellipsometry [3] or attenuated total reflection spectroscopy (ATR) [4].

Additionally the increase in volume with increasing temperature causes a dilution of polarizable molecules in the material and thus a decrease in refractive index n. Thus, the derivative $\partial n/\partial T$ also shows a discontinuity at T_g.

Change of n and t due to thermal expansion partially compensate for each other when looking at a total optical thickness $(n \cdot t)$ of a film. It is thus desirable to determine refractive index and thickness independently which was done here by ATR measurements on multimode waveguides [5].

Measurements of refractive indices and thicknesses were performed in an attenuated total reflection setup in Kretschmann configuration (Fig. 1a). Polarized laser light ($\lambda = 633$ nm) passes through a prism and the sample's substrate to be reflected by a thin gold layer carrying a polymer waveguide. The reflected light is detected by a silicon photodiode using lock-in technique. Sample and detector are mounted on a high precision $\theta/2\theta$-goniometer in order to be able to vary the angle of incidence accurately.

At certain resonance angles light can propagate in the thin polymer film and the reflected intensity is drastically reduced. Using a Fresnel formalism, both the corresponding thickness and refractive index are determined from the angular dependence of reflectivity (Fig. 1b).

The sample is mounted on a temperature controlled brass plate which is used for heating. All waveguides are first heated to a temperature well above their T_g ($T > T_g + 30$ °C). After annealing at this temperature for 20 min they are cooled down to room temperature with a well defined ramp of 5 K/min.

Angular reflectivity curves are recorded at discrete temperatures ($\Delta T \approx 10$ °C) and both $n(T)$ and $t(T)$ are calculated from a Fresnel formalism. β and $\partial n/\partial T$ can then readily be determined by linear fits (see Fig.2) well below and above T_g. The intersection points of the fitted lines provide T_g. For materials sensitive to water uptake measurements are performed in a cuvette that was purged with dried Argon.
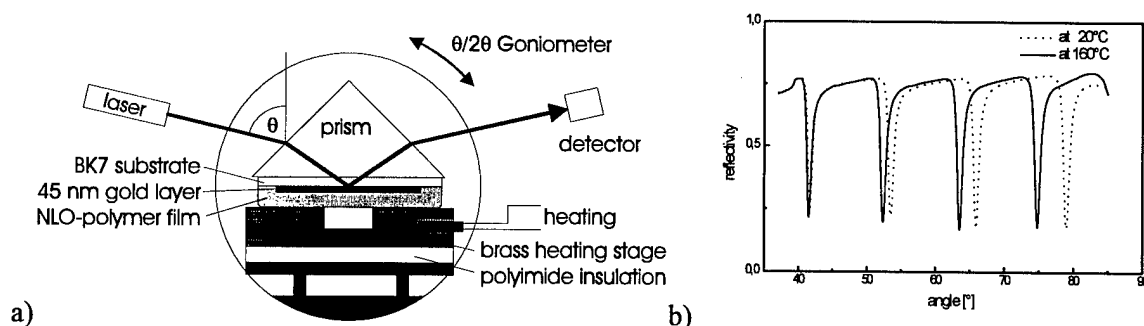
FIG. 1: a) ATR experimental setup for the determination of refractive index and thickness of polymer waveguides as a function of temperature

b) Angular reflectivity scans at room temperature (T = 25°C) and at T = 160 °C of a sample of PMMA/DRMA 10 %. Thickness changes from 2000 nm (n = 1.599) at room temperature to 2095 nm (n = 1.559) at 160 °C.
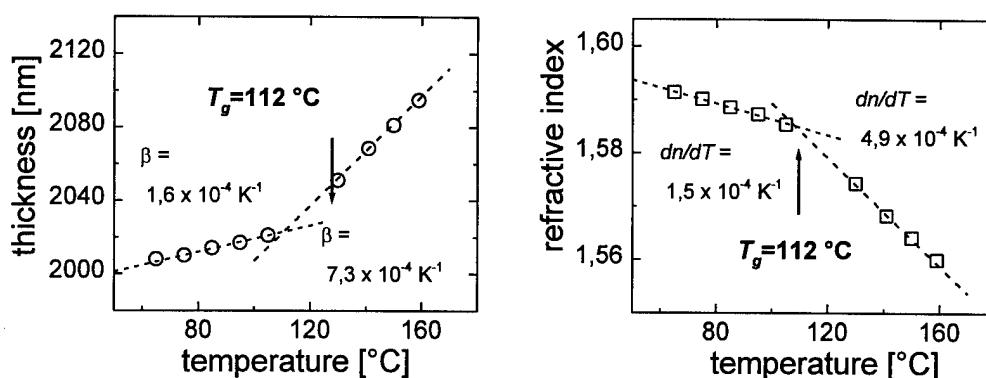

FIG 2: Thickness and refractive index determined from measured reflectivity scans are plotted versus temperature. At T_g the derivatives $\beta = \partial t/(t\partial T)$ and $\partial n/\partial T$ change discontinuously.

The ATR-experiments were carried out on three NLO side-chain polymers: the test polymer P1 a polymethacrylate copolymer of 90 mol% methyl methacrylate and 10 mol% Disperse Red 1 (DR1) methacrylate (24 weight% chromophore content, $T_{g,\ bulk}$ = 123 °C) and P2 the same copolymeric system as P1 with a different dye content of 20 mol% DR1 methacrylate ($T_{g,\ bulk}$ = 123 °C). The high glass transition polyimide P3 is composed of alkylmaleimides carrying the DR1 chromophore (62 weigth% chromophore content, $T_{g,\ bulk}$ = 172 °C) [6]. 1-2 μm thick films of the NLO-polymers were spin cast from diethyleneglycol-dimethylether and cyclohexanone solutions, respectively, on BK7 substrates precoated with a 45 nm gold layer. Subsequently, the films were baked in vacuum at $T_{g,\ bulk}$ + 20°C for 12 h to remove traces of the solvent. For the investigation of the anticipated T_g decrease due to photolysis by photobleaching, films of polymer P1 were fully bleached by a high pressure mercury lamp (λ_{bleach} > 295 nm) [7].

The passive waveguiding materials investigated were polymethylmethacrylate (PMMA) and a polymethacrylate copolymer of 60 mol% methylmethacrylate and 40 mol% adamantyl methacrylate. Decrease of T_g due to photobleaching was investigated after different exposure times.

Comparison of the T_g values measured by the ATR technique with corresponding values from DSC measurements of the bulk material show differences of several °C (Table 1). The ATR experiment results in slightly reduced values which are probably due to several reasons: The temperature ramp used was 5 K/min in contrast to the DSC cooling rate of 10 K/min which explains a reduction of T_g. Additionally the measurements should be done in a vacuum chamber in future to reduce water uptake or other environmental influences and the accuracy of the temperature measurement (ΔT = 4 °C) should be improved.

	T_g^{ATR} [°C]	T_g^{DSC} [°C]
1		
. cured at 110°C, 24h nd 170°C, 2h all in acuum	112	123
. UV-bleached and nnealed at 160°C, 24h n vacuum	105	122
2		
. cured at 110°C, 24h nd 170°C, 2h all in acuum	117	123
3		
. cured at 150°C, 24h nd 180°C, 2h - vacuum	166	172

Table 1: T_g values measured by ATR spectroscopy agree well with DSC results. The DSC values for P1 were determined from scraped off films, all other DSC values were measured on non-processed bulk materials.

FIG 3: T_g versus dosage of UV-irradiation of passive waveguiding materials. A significant decrease of 50 °C is observed.
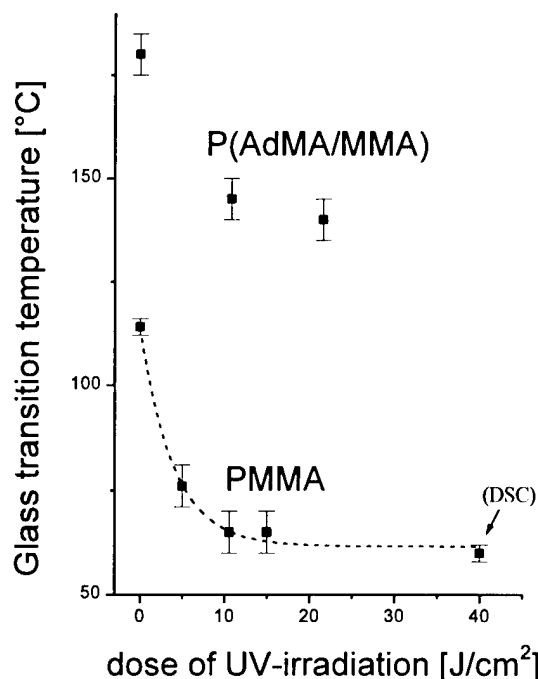
Both passive waveguiding materials show a significant decrease of T_g of up to 50 °C due to photobleaching that was also confirmed by a DSC-measurement on a fully bleached material (Fig. 3). This change is so drastic, that its knowledge really is vital for additional processing steps. Characterization of bleaching kinetics through this method may even help in further understanding of the mechanisms involved in this important structuring step.

This novel non-destructive method to measure T_g by ATR spectroscopy in a planar waveguide geometry has proven its advantages over conventional techniques. Routine characterization of the influence processing steps have on the thermodynamic properties of polymeric materials for waveguiding applications is possible with this technique. Especially in the field of electro-optics this could provide better understanding of the influence of processing parameters (i.e. annealing, UV-bleaching etc.) on the stability of glassy polymers. This nondestructive optical method to measure T_g in polymeric planar waveguides could become an important tool for characterization of materials for integrated optics.

References

[1] D.M. Burland, R.D. Miller, C.A. Walsh, Chem. Rev., **94**, 31 (1994)

[2] J. Vydra, H. Beisinghoff, H. Feix, M. Eckl, P. Strohriegl, W. Görtz, M. Eich, SPIE Proc. **2527**, 171 (1995)

[3] J.L. Keddie, R.A.L. Jones, R.A. Cory, Faraday Discuss., **98**, 219 (1994)

[4] O. Prucker, S. Christian, H. Bock, C.W. Frank, W. Knoll, submitted ACS

[5] W. Knoll, Encyclopedia of Applied Physics, **14**, 596 (1996)

[6] M.Ahlheim, F. Lehr, Macromol. Chem. Phys., **195**, 361 (1994)

[7] J.Vydra, H. Beisinghoff, T.Tschudi, M.Eich, Appl. Phys. Lett., **69**, 1035 (1996)

Passive alignment of optic fiber array using silicon V-grooves monolithically integrated with polymer waveguide devices

Antao Chen, Mehrdad Ziari, and William H. Steier

Department of Electrical Engineering - Electrophysics, University of Southern California
Los Angeles, CA 90089-0483, (213) 740 8781

Packaging is the crucial link between a laboratory demonstrated device and a reliable component in a practical system. To achieve and maintain the sub-micron alignment tolerances between fiber and waveguide is the major factor that makes the packaging of photonic devices labor intensive, time consuming, and costly[1, 2]. Fiber arrays are important in WDM multiplexers and demultiplexers where multiple fiber attachment is essential. To avoid the complexity of the active alignment and attachment of individual fiber to each waveguide, we experimented with the passive alignment of fiber arrays with silicon V-grooves. The V-grooves are made on the same substrate that the polymer device is built on. The waveguide channels aligned to the center of the V-grooves are also processed together with the V-grooves using the same photolithography and etching technology. This technique is fundamentally different from the use of silicon V-grooves as fiber carrier for $LiNbO_3$ and semiconductor devices, in which V-groove and devices are made on different substrate and bonded together later[3, 4]. The width and the position of V-grooves can be fabricated in submicron precision with mature microelectronics technology. The fiber placed in the V-groove is entirely self-aligned in both vertical and lateral directions. The idea and some fabrication results of this approach have been presented earlier[5]. In this paper, our recent results of fiber coupling experiments are reported.

The V-grooves and the waveguide channels aligned with them are fabricated on a silicon wafer that has a 4 μm thermally grown SiO_2 layer which is used as both the etch mask for the V-grooves and the lower chadding of polymer waveguides. Fig. 1a shows a processed substrate ready for fiber placement and the fabrication of polymer waveguides. The overhang structure at the end of the V-grooves are used to enable the contact between the fiber and waveguide.

The cleaved fiber is placed in the V-groove and bonded by UV-curable epoxy. The height of the center of each fiber can be measured with Lloyd mirror fringe technique. A height range from 0 to 4 μm above the wafer surface is obtained by using V-grooves with different width. The polymer waveguide layer is spin-cast on the substrate with an array of fibers already attached. This is an unique process impossible for $LiNbO_3$ and semiconductor devices. A special chuck for the spinning is built which keeps the fiber intact up to a spin rate of 5000 rpm, much faster than the spin rate usually used in the fabrication of waveguide layers. Fig. 1b is a scanning electron microscope picture of a finished sample.

Spinning waveguide with fiber in the V-groove produces a vertical taper profile in front of the fiber facet. A complete beam propagation analysis of the effects of the taper on the coupling is in progress and it is believed that the taper can function as a mode size transformer between the optic fiber and polymer waveguide to improve the coupling efficiency. Optimization of the taper shape and fiber position to take advantage of this natural taper will be investigated. Various taper profiles are obtainable by adjusting the spin rate and the viscosity of polymer solution, as shown in Fig. 2.

To test this idea, we first tried coupling 830 nm single mode fiber into a PMMA planar waveguide. If this fiber is directly butt coupled with the waveguide, the minimum coupling loss obtained is 5.9±0.2 dB experimentally. This value is very close to the theoretical prediction of 5.8

dB using overlapping integrals. With our V-groove self-alignment approach, the average loss from an array of 7 fibers is 6.0±1.5 dB. The distribution of the coupling loss of the fiber array is given in Fig. 3. This average coupling loss is basically the same as the lowest butt coupling loss achievable. Furthermore, a few fibers have coupling loss as low as 3 to 4 dB, which is much lower that the theoretical limit of direct butt coupling. These low loss values indicate that the taper did improve the fiber coupling in these cases.
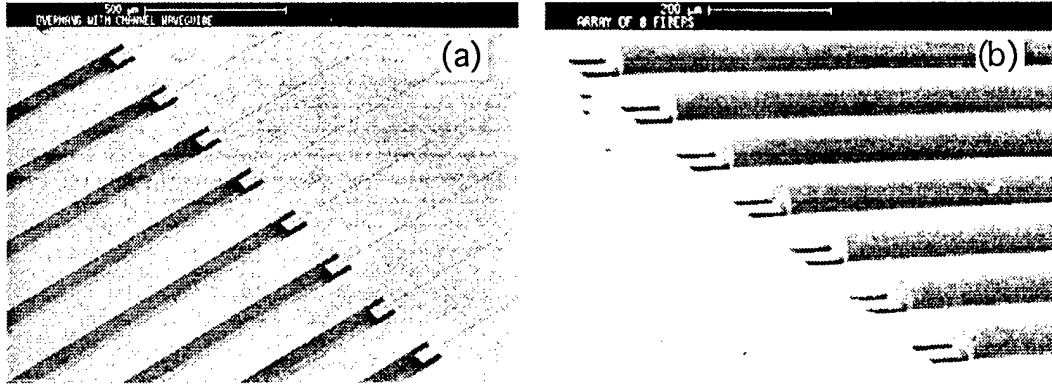
Fig. 1. (a) V-grooves aligned waveguide channels fabricated on Si/SiO$_2$ substrate. (b) The sample after fiber placement and spin casting of polymer waveguide layer.
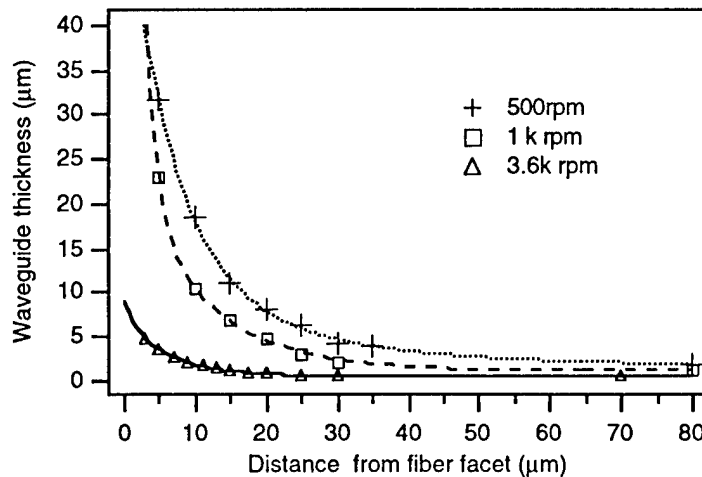
Fig. 2. Taper profiles obtained with different spin rate. The polymer solution is 10% PMMA in chloroform.

Fiber array coupling with single mode channel waveguide array was also investigated. The waveguide channels etched in the SiO$_2$ are 4 μm wide and 0.2 μm deep. The waveguides are 10 mm long with fibers attached at both ends of the sample in the V-grooves. The polymer waveguide layer has the same thickness as the previously tested planar waveguides. The lowest insertion observed in our preliminary experiment is 16 dB, which includes fiber coupling losses at two ends and waveguide propagation loss. The cross talk between adjacent waveguides is from -29 to -44 dB. Improvement is expected by further optimization of design and processing.
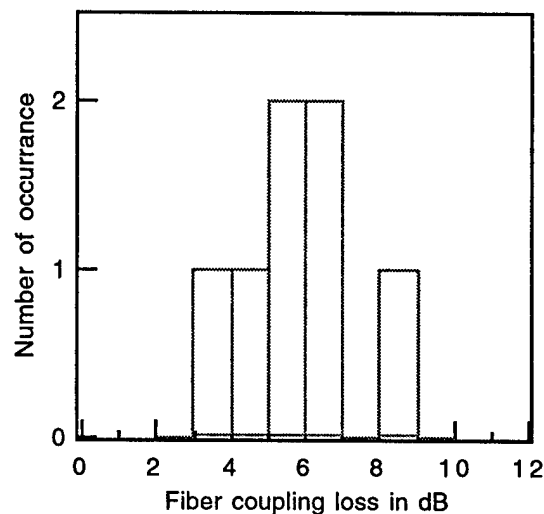
Fig. 3 Distribution of the fiber coupling loss of an array of 7 fibers.

A passive and self-aligned coupling between fiber and polymer waveguide is demonstrated as an attempt for a cost effective approach of the packaging of polymer waveguide devices. The experiment results indicate that the coupling can be more efficient than direct butt coupling. The V-grooves and the waveguide channels aligned with them are fabricated with standard VLSI technology, such as photolithography, plasma etching, and wet etching. This technique can be applied to the future monolithic integration of fiber coupled polymer waveguide devices with VLSI circuitry.

References

[1]   T. Kato, F. Yuki, K. Tanaka, T. Habu, Y. Akiyama, T. Shimura, A. Takai, K. Mizuishi, T. Teraoka, and Y. Motegi, "A new assembly architecture for multichannel single mode-fiber-pigtail LD/PD modules," *IEEE Transactions on Components, Hybrids, and Manufacturing Technology*, vol. 16, pp. 89-93, 1993.
[2]   M. R. Matthews, B. M. MacDonald, and K. R. Preston, "Optical components-the new challenge in packaging," *IEEE Transaction on Components, Hybrids, and Manufacturing Technology*, vol. 13, pp. 798-806, 1990.
[3]   C. A. Armiento, A. J. Negri, M. J. Tabasky, R. A. Boudreau, M. A. Rothman, T. W. Fitzgerald, and P. O. Haugsjaa, "Gigabit transmitter array modules on silicon waferboard," *IEEE Transactions on Components, Hybrids, and Manufacturing Technology*, vol. 15, pp. 1072-1079, 1992.
[4]   M. S. Cohen, M. F. Cina, E. Bassous, M. M. Opyrsko, J. L. Speidell, F. J. Canora, and M. J. DeFranza, "Packaging of high-density fiber/laser modules using passing alignment techniques," *IEEE Transactions on Components, Hybrids, and Manufacturing Technology*, vol. 15, pp. 944-955, 1992.
[5]   M. Ziari, A. Chen, S. Kalluri, W. H. Steier, Y. Shi, W. Wang, D. Chen, and H. R. Fetterman, "Polymer electrooptic waveguide fabrication," in *Polymers for Second-Order Nonlinear Optics*, vol. 601, G. A. Lindsay and K. D. Singer, Eds. Washington, DC: American Chemical Society, 1995, pp. 420-435.

Ionization-assisted Deposition of Polyurea Thin Films for NLO Applications

H. Usui, H. Kikuchi, K. Tanaka, S. Miyata, T. Watanabe, W. Knoll* and H. Bock*

Tokyo University of Agriculture and Technology, *Max-Planck-Institut für Polymerforschung
Naka-cho, Koganei, Tokyo 184, Japan   Phone +81-423-88-7055   usui@cc.tuat.ac.jp

Introduction

Polymeric material needs a poling process to align the dipole moment for activating optical nonlinearity.   The major problem is the relaxation of dipole orientation, which is to be solved by designing a molecular structure of higher rigidity.   However, it leads to a contradiction that the thermally stable polymer, like the linear main-chain NLO polymer, is difficult to align the dipole orientation by the poling procedure.   This paper will propose a new concept in film formation of NLO polymer, integrating the dipole orientation process with the polymerization and film deposition.   The authors have investigated the film formation of organic materials by using the ionization-assisted deposition method.   It is a unique method that involves the ionization of evaporated material in the course of vacuum deposition, and grows the films with an assistance of the ionized particles that are accelerated toward the substrate.   It is reported that polymeric thin films can be synthesized on the substrate surface by co-deposition of bifunctional monomers.   If the polymerization proceeds under an electric field, the dipole orientation could take place much effectively, because the electric field influences the highly mobile monomers.   Our objective is to control the dipole orientation in the film formation process by utilizing the electric field that is generated by the substrate bias voltage and by the electric charge carried by the deposition ions.   Polyurea (PU) was chosen for the film material because of its thermal stability and optical transparency.   Moreover, its dipole moment is built in the backbone, making this material attractive as a stable optical nonlinear material.

Deposition Process

Figure 1 shows the two monomers, i.e. the deposition source material, and the expected product.   The ionization-assisted deposition apparatus is schematically shown in Fig. 2.

4,4'-diphenylmethane-diisocyanate (MDI)

1,3-di(4-piperidyl)propane (PIP)
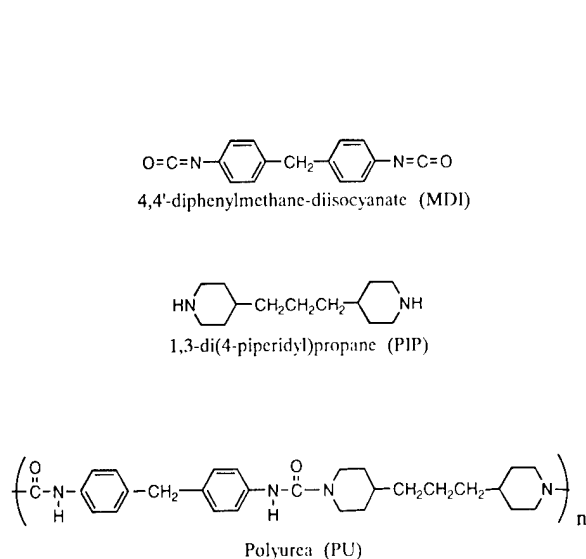
Polyurea (PU)

Fig. 1   Monomeric source materials and the expected product polymer.
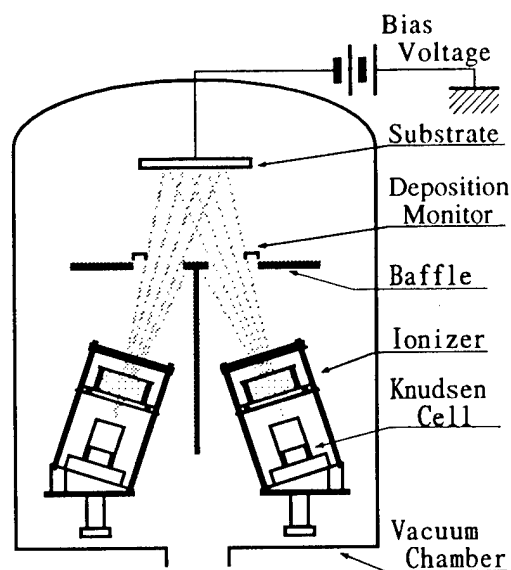
Fig. 2   Schematic diagram of the ionization-assisted deposition system.

Each monomer was evaporated from individual Knudsen cell, and was ionized by electrons in a Bayard-Alpert gauge type ionizer. The electron energy for ionization was 50 eV, and the emission current was 2 mA. The substrate was given a negative potential with respect to the ionizer to extract and accelerate the positive ions. The typical ion current read at the substrate was tens of microamperes. The substrate was not heated intentionally. The film growth rate was about 15 nm/min.

In general, polyaddition reaction requires the monomers to be supplied in equal molar ratio, which means that a deliberate control of the evaporation temperature of each monomer is important. For this reason, the deposition rate of each monomer was monitored by quartz microbalance, and the evaporation temperature of PIP and MDI was stabilized at 100℃ and 140℃, respectively. Figure 3 shows the IR absorption spectra of the films together with those of source monomers. Under the proper deposition condition, the end group of isocyanate at 2290 cm^{-1} and that of PIP at 3227 cm^{-1} were not detected in the spectra of the films. On the other hand, the appearance of C=O absorption at 1640 cm^{-1} and N-H absorption at around 3330 cm^{-1} implies the formation of urea bonds. This result suggests that the co-deposition of MDI and PIP leads to the formation of PU thin films by the polyaddition reaction.

NLO Characteristics

SHG characteristics of the PU films were investigated by the Maker fringe method. PU films of 0.6 to 1 μm were deposited on glass substrates at different bias voltage Va. Figure 4 indicates the Maker fringe patterns of the as-deposited films. The primary beam was Nd-YAG laser, and both the primary and the secondary beams were p-polarized. It is evident that the films are SHG active, indicating that the ionization-assisted method is capable of influencing the dipole orientation in the course of film deposition. The fringe patterns of Fig. 4 are suggestive of a film whose dipole moments are uniaxially oriented normal to the film surface. However, the nonlinear optical coefficient d_{31} of these films was estimated to be 0.1 to 0.2 pm/V, and the relation $d_{33} = 3d_{31}$ did not hold for these films. It is probable that the dipole alignment is not complete, or has a peculiar orientation different from the common poled films.
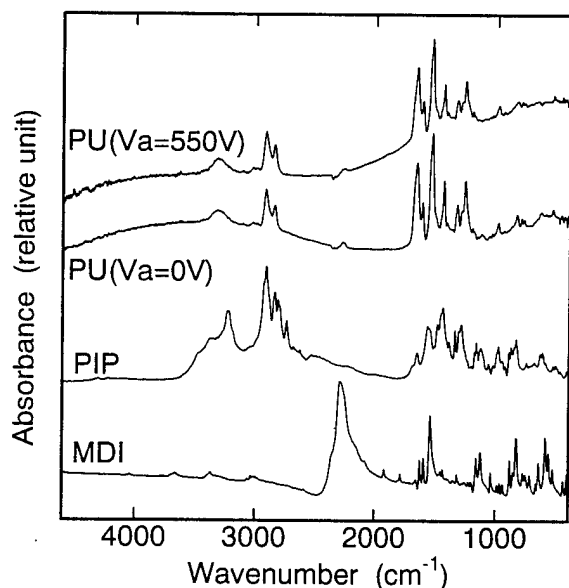
Fig. 3   IR absorption spectra of the deposited films and the source monomers.
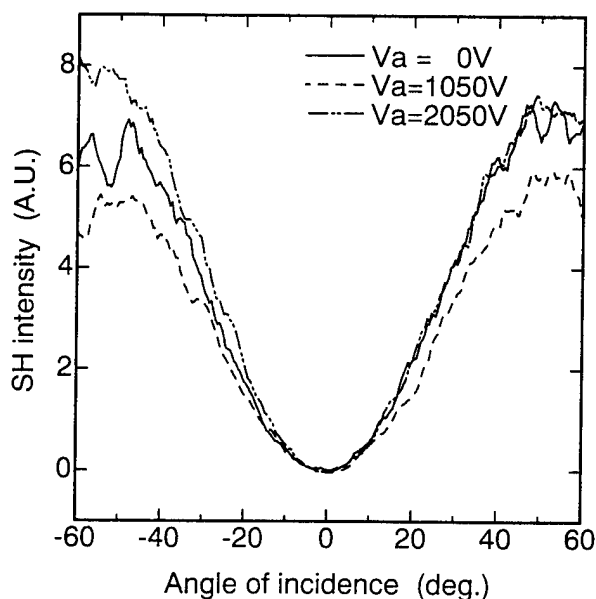
Fig. 4   Maker fringe patterns of the PU films deposited with different bias voltage.

Reflectivity signal

Lock-in Amplifier

He-Ne Laser

Detector

Prism

Chopper

Lock-in Amplifier

θ

Polarizer

Modulated signal

Glass substrate

Au
PU
Au

1kHz 20Vp-p

400

—— Va= 0V
······ Va= 550V
----- Va=1050V

200

Modulated signal (A.U.)

0

-200

-400

20   40   60   80

Angle of incidence (deg.)
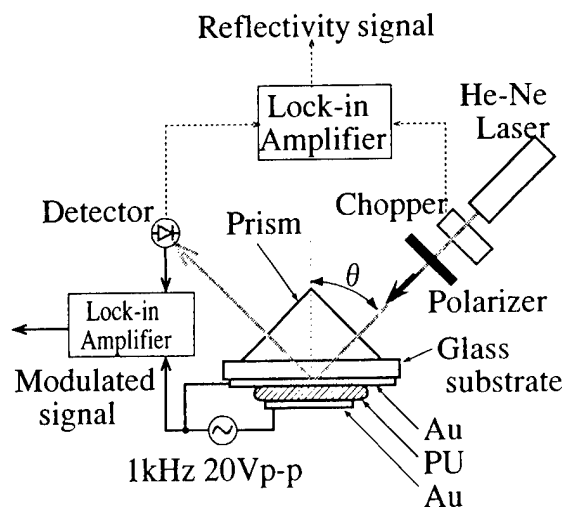
Fig. 5 Schematic diagram of field-modulated ATR measurement.
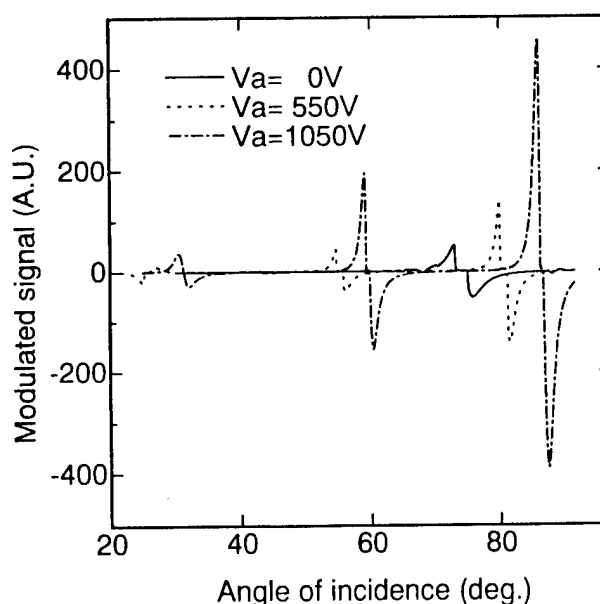
Fig. 6 Modulated signal of reflectivity by the ATR measurement for the films deposited at different bias voltage.

The electrooptic (EO) effect was characterized by a field-modulated attenuated total reflection (ATR) measurement. The measurement system is illustrated in Fig. 5. The glass substrate was coated with 46 nm thick Au, on which the PU films of 0.6 to 1 μm was deposited by the ionization-assisted method, followed by Au deposition of 40 nm. Reflection of HeNe laser beam was measured from the back of the substrate through a coupling prism as a function of the incidence angle. 1 kHz AC voltage of 20 V was applied between the Au films, which caused the modulation of reflectivity at those incident angles that excite the waveguide modes in the PU film. Figure 6 shows the modulation in reflectivity for the films deposited with different bias voltage on the substrate. The film deposited at higher bias voltage yielded larger modulation signal, suggesting the enhancement of nonlinearity by the electric field applied in the course of polymerization. A detailed analysis revealed that the modulation is caused by the concurrent effects of EO and electrostriction. The EO coefficient r_{33} was 0.12 pm/V for the film deposited with the bias voltage of 550 V, and 0.68 pm/V for 1050 V.

The result of ATR measurement was in consistency with our intention that the dipole orientation can be controlled by the electric field in the film deposition process. The SHG measurement revealed that the film has NLO activity in the as-deposited state, but did not indicate an evident dependence of the SHG coefficient on the substrate bias voltage. This is probably because the films for the SHG measurement were deposited on glass substrates, while those for the ATR measurement were formed on the conductive Au surface, which assured the substrate potential to be controlled by the bias voltage.

Conclusion

Our results suggests that the ionization-assisted deposition method enables to align the dipole orientation normal to the film surface in the process of polymerization and film growth. Although the detailed alignment factors, such as the surface potential and field strength, have not yet been clarified, this method has a high potential as a new technique of polymeric film formation for NLO applications. It can be applied to various types of insulating NLO materials, including side-chain or host-guest polymer systems.

Characterization of electrooptic polymers with high μβ chromophores for photonic device applications

Antao Chen, Sean Garner, Araz Yacoubian, and William H.Steier
Department of Electrical Engineering-Electrophysics
University of Southern California, Los Angeles, CA 90089-0483, (213) 740 8781

Jinghong Chen, Aaron Harper, Jingsong Zhu, Mingqian He, Shajing Sun, Fang Wang,
Younsoo Ra, Shane S. H. Mao, Cheng Zhang, and Larry R. Dalton
Department of Chemistry, University of Southern California, Los Angeles, CA 90089-1062,
(213)740 8659

Datong Chen, and Harold R. Fetterman
Department of Electrical Engineering, University of California at Los Angeles
Los Angeles, CA 90095, (310) 206 9457

For electrooptic (EO) polymer devices to be accepted in high speed fiber communication systems, the operation voltage of these devices must be reduced to a level compatible with the high speed electronics that drives the polymer devices. A low operation voltage, or V_π in the case of modulators, requires EO polymers with high electrooptic coefficients. The electrooptic effect comes from the nonlinear chromophores in the polymer and the alignment of these chromophores by poling. High electrooptic coefficients calls for chromophores with large nonlinearity, i.e., high μβ. The synthesis and characterization of EO polymers with high μβ chromophores[1] have been the focus of recent research in the field of nonlinear optic polymers.

Previous studies on the relationship between the macroscopic nonlinear optic properties of an EO polymer and the microscopic nonlinear properties of the nonlinear chromophores are based on the assumptions of small μβ and low poling field. These studies predict that the EO coefficients of a poled EO polymer should scale linearly with the μβ of the chromophore and the chromophore number density[2-4]. However, with high μβ chromophores, experimental results deviate greatly from the linear relationship. Aggregation due to strong chromophore-chromophore interaction further complicates the problem. EFISH[5] technique can measure the μ and β of a chromophore in solvent, but chromophores may behave differently in a solid polymer matrix. It is necessary to determine if a chromophore has the potential to give high EO coefficients in a solid state polymer matrix before investing large effort to covalantly attach them to a polymer backbone to make device material.

To evaluate the behavior of a new chromophore in a polymer matrix, we first dope the chromophore into a thermoplastic host polymer such as PMMA and polycarbonate at various weight percentages. An *in situ* poling is performed by monitoring the second harmonic signal of a 1.06 μm Nd:YAG laser while poling with the temperature ramping up from 20 °C. At low temperature, the poling is inefficient because the polymer matrix is still rigid. At a temperature higher than the T_g of the composite polymer, the combined effect of the increased conductivity of the polymer film and the thermal randomization of chromophore orientation also reduces the poling efficiency. There exists an optimum poling temperature which depends on the polymer host and the chromophore weight percent. This temperature is typically between 40 and 110 °C for the host materials used. The EO coefficient, r_{33}, of a sample poled at this optimum temperature is measured by an ATR technique modified for the routine measurement of corona poled EO polymer films on ITO coated glass slides, and the results are obtained in about 15 minutes after poling, after the fast decay of the unusable nonlinearity resulting from the surface charge. The above described

procedure provides valuable information on the chromophore such as what level of r_{33} can be expected, and the optimal weight percent of this chromophore in the host polymer matrix, as shown in Fig. 1. A high optimal weight percent is desirable because it indicates weaker interaction between the chromophores in the polymer host and lower tendency of aggregation. *In situ* poling with intermittent illumination of the sample by visible light also reveals whether the chromophore has undesirable photoconductivity, which is sometimes seen with high $\mu\beta$ chromophores. The second harmonic signal as a function of poling voltage and how fast the SHG signal reaches its saturation level tell us whether this chromophore can be efficiently poled with moderate poling voltage.

A special concern of EO polymers with high $\mu\beta$ chromophores is the optical loss. As the $\mu\beta$ value of chromophores increases, the absorption peak is usually shifted to longer wavelengths and some chromophores have a slow decay of the absorption tail that extends to the device operation wavelength of 1.3 μm. From the device point of view an optical loss of a poled film higher than 5 dB/cm is hardly acceptable. Both chromophore absorption and scattering from the aggregation of chromophores and other components of the polymer are sources of optical loss. Since the scattering loss due to aggregation may be suppressed when chromophores are covalently attached to polymer matrix in the thermosetting and side-chain EO polymer, we are focused on the intrinsic absorption loss of the chromophores. We found that the absorption tail seen in NIR absorption spectrum is in strong correlation to the material loss, as shown in Fig. 2, and therefore a simple absorption scan of the chromophore solution or a thick piece of the composite polymer with a spectrophotometer reveals the loss property of the chromophore. The scattering loss is indicated in the nonlinear relationship between the optical loss and chromophore weight percent in the polymer. Severe aggregation is detectable with a scanning electron microscope or even with an optical microscope. High optical loss can be induced during the electric poling process[6,7]. This is believed due to the aggravation of aggregation at elevated poling temperature and the surface damage during poling. Through the optimization of the poling protocol, good results have been obtained of reducing the poling induced loss without compromising the EO coefficients.
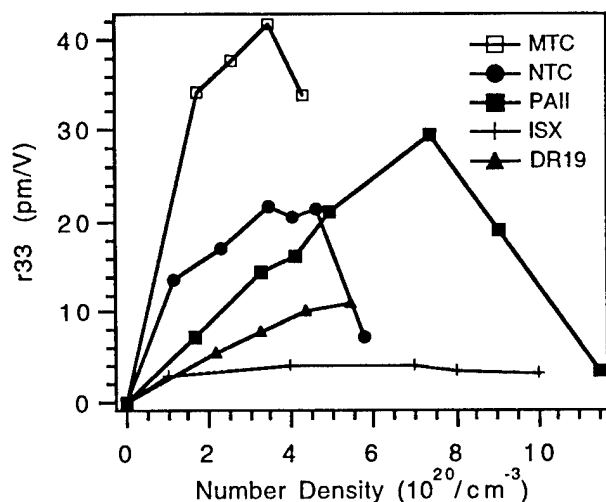
Fig. 1 Measured r33 of various chromophores as functions of chromophore number density in polymer host.
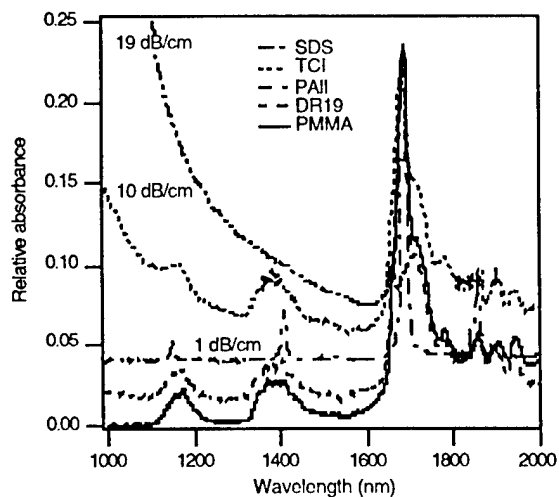
Fig. 2 The correlation between the absorption tail and optical loss at the wavelength of 1.3 μm. The curves are vertically offset for clarity.

Conductivity of the polymer thin film seriously affects the poling efficiency of EO polymer. During poling, the nonlinearity of the polymer drops sharply at the temperature at which the conductivity of the film begin to increase. Since many high $\mu\beta$ chromophores are the final products of many steps of chemical reactions, care must be taken to prevent any contamination of ionic impurities. Photoconductivity in visible light is also observed with some high $\mu\beta$ chromophores. These chromophores need to be poled in the dark.

The chemical and optical properties of EO polymers with high $\mu\beta$ chromophores are drastically different from their small $\mu\beta$ counterparts such as DANS and disperse red based materials. Encouraging progress in both synthesis[8,9] and theory[10] has been achieved in this challenging field after years of intensive research. Guest-host polymers with r33 in the range of 30 to 40 pm/V and optical loss approximately 1 dB/cm at the wavelength of 1.3 μm are obtained[9,11]. Current efforts are focused on covalantly attaching these chromophores to thermosetting crosslinkable polymer matrix to make EO polymers with good thermal and temporal stability for practical photonic devices.

References

[1] S. R. Marder and J. W. Perry, "Nonlinear optical polymers: discovery to market in 10 years?," Science **263**, 1706-7 (1994).

[2] D. M. Burland, R. D. Miller, and C. A. Walsh, "Second-order nonlinearity in poled-polymer systems," Chemical Reviews **94**, 31-75 (1994).

[3] K. D. Singer, J. E. Sohn, and S. J. Lalama, "Second harmonic generation in poled polymer films," Applied Physics Letters **49** (5), 248-250 (1986).

[4] J. L. Oudar, D. S. Chemla, and E. Batifol, "Optical nonlinearities of various substituted benzene molecules in the liquid state, and comparison with solid state nonlinear susceptibilities," Journal of Chemical Physics **67** (4), 1626-35 (1977).

[5] L.-T. Cheng, W. Tam, G. R. Meredeith *et al.*, "Nonresonant EFISH and THG studies of nonlinear optical properties and molecular structure relations of benzene, stilbene, and other arene derivatives," Proceedings of SPIE **1147**, 61-73 (1990).

[6] Jr. T. A. Tumolillo and P. R. Ashley, "A novel pulse-poling technique for EO polymer waveguide devices using device electrode poling," IEEE Photonics Technology Letters **4** (2), 142-145 (1992).

[7] C. C. Teng, M. A. Mortazavi, and G. K. Boudoughian, "Origin of the poling-induced optical loss in a nonlinear optical polymeric waveguide," Applied Physics Letters **66** (6), 667-669 (1995).

[8] Jingsong Zhu, Minqian He, A. W. Harper *et al.*, "Progress towards the translation of large microscopic nonlinearities to large macroscopic nonlinearities in high $\mu\beta$ materials," Polymer Preprints **38**, 973-974 (1997).

[9] F. Wang, A. W. Harper, M. He *et al.*, "Design and synthesis of a perfluoroalkyldicyano-vinyl-based NLO material for electrooptic applications," Polymer Preprints **38**, 971-972 (1997).

[10] A. W. Harper, S. Sun, M. He *et al.*, "translating microscopic optical nonlinearity to macroscopic nonlinearity: The role of chromophore-chromophore electrostatic interactions," Journal of Optical Society of American B , in press (1997).

[11] Jinghong Chen, Jingsong Zhu, Aaron W. Harper *et al.*, "Synthesis and characterization of a high-$\mu\beta$ chromophore containing the isophorone moiety for electro-optic applications," Polymer Reprints **38** (2), in press (1997).

Electro-optic Modulation Based on Channel Waveguide of Organic Single Crystal Material

Jianjun Xu, Ligui Zhou and M. Thakur
Auburn University, AL 36849

Channel waveguide is the basic element in fabrication of electro-optic modulator for external electro-optic modulation. Using polymer electro-optic materials, channel waveguide device can be comparative easily fabricated, but the main problem for polymer materials is their stability. On the other hand, organic single crystal has excellent stability, the disadvantage of them is the difficulty in processing which limited their application potential. Recently, channel waveguide has been fabricated by direct growth inside the hollow fiber, but those channel waveguides proved to be difficult to fabricate electrode besides the crystal [1]. By combining ideas of growth of crystal from hollow fibre and shear method [2], a new method able to fabricate raised-up channel waveguide of organic crystal was initiated. In this method, solution of organic molecule was introduced between two substrates, one of them has patterned lines on it. Due to the polar interaction between the substrate materials and molecules of the solution, Single crystal channel waveguides were grown along the patterned line on the substrate, the dimension and direction of the crystal materials were controlled by these patterned lines. Fig.1 illustrated the diagram of this method.
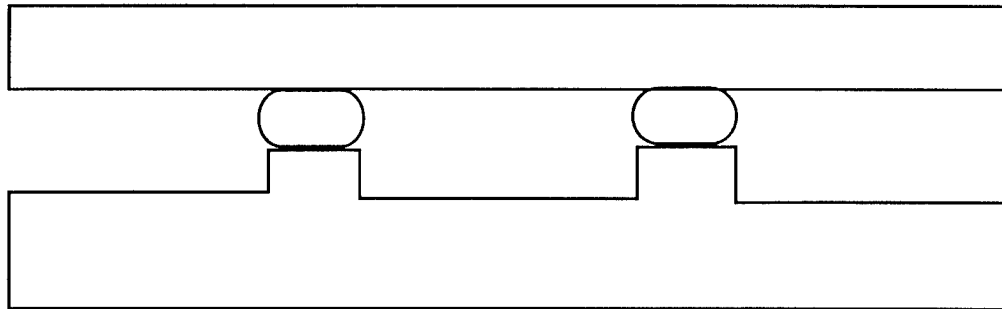
Fig.1 The schematic diagram for growing channel wave guide

The picture of grown crystal channel waveguide of NPP taken under the microscope is show in Fig.2.
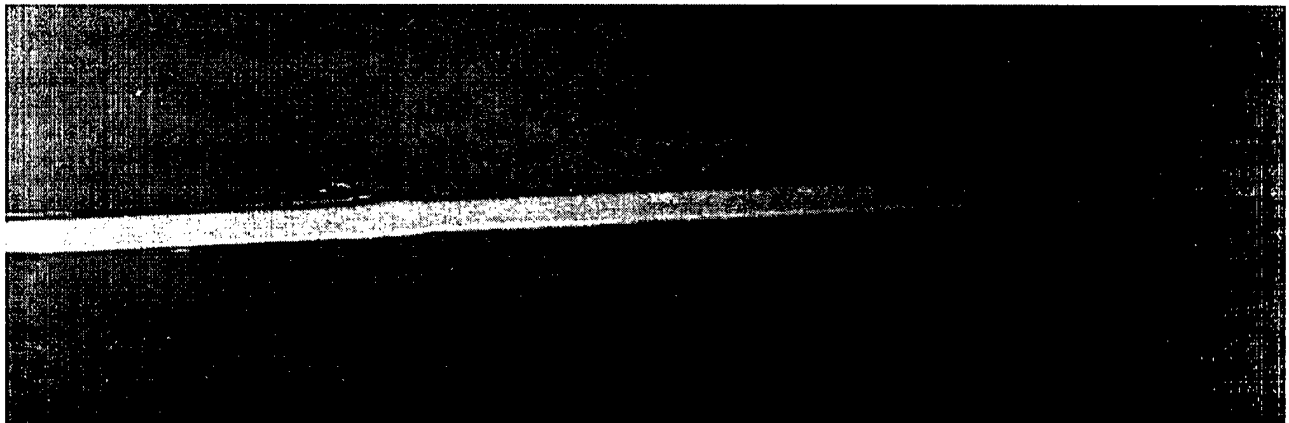
Fig2. NPP channel waveguide grown from guided growth method.

The dimension of the channel waveguides is about 2μm×30μm×5mm. By using of cross polarized configuration of transmission microscope, in most cases, it is found that the cleavage surface which has an angle with waveguide boundary was parallel to one of the principal axis of refractive index.
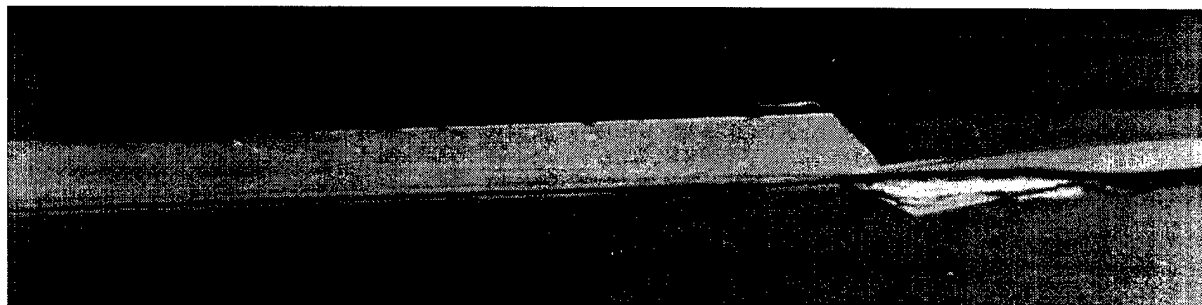
Fig. 3 A channel waveguide with a cleavage surface on its end

Fig. 3 shows a channel waveguide with a cleavage surface on its end . In these cases , if there is an electric field applied perpendicularly to the waveguide direction, there are components of electric field along both principal axes. By fabricating metal electrode on one of the substrates, and cutting the substrate perpendicular to the waveguide direction, a section about 1mm of waveguide, a phase modulator is obtained. End-fire coupling was used to couple laser beam into the channel waveguide. Clear guiding of laser beam through the waveguide was observed using infrared camera. Using cross polarized configuration, electro-optic modulation measurement was made. As shown in Fig.4, by applying 20 volts DC voltage on the electrodes, about 10% change in intensity of the output was observed
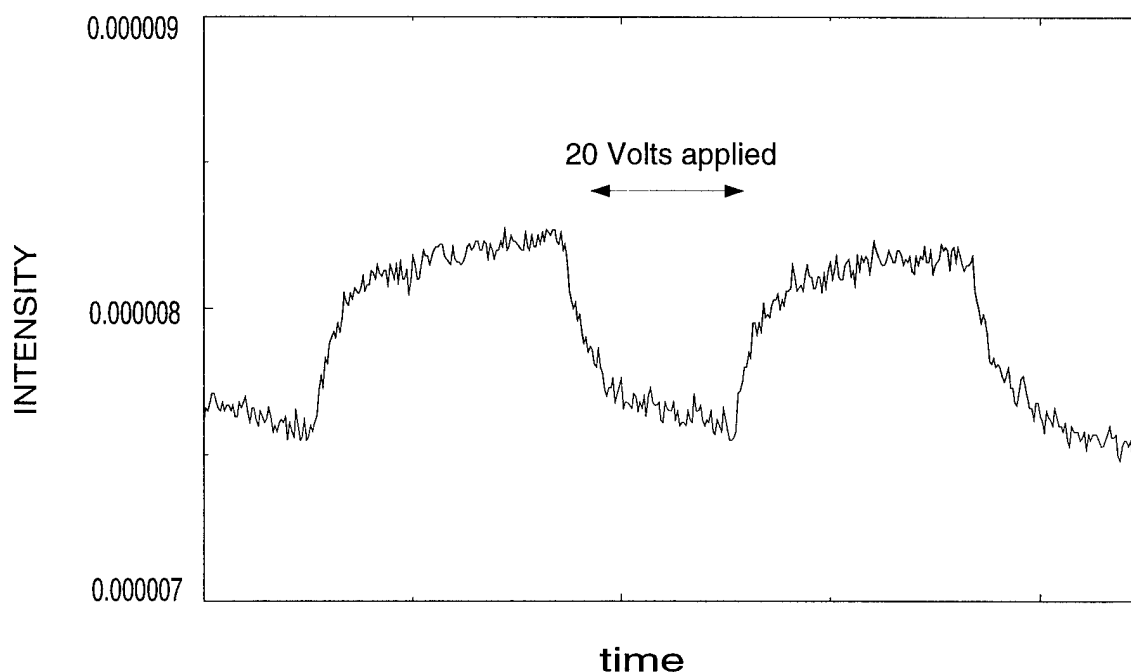
Fig.4 Light output change due to applied voltage

References:

1. P. Kerkoc, Ch. Bosshard, H. Arend, and P. Gunter. Growth and characterization of 4-(N,N-dimethylammino)-3-acetamidonitrobenzene single crystal core fibers", Appl. Phys. Lett., Vol. 54, 1535-1537 (1991)

2. M. Thakur and S. Meyler, " Growth of large-area thin film single crystal of poly(diacetylenes)" Macromolecules Vol. 18, 2341(1985)

Transient Photoconductivity in Thin Films of Ferrocene Carboxylic Acid

Chandra S. Prayaga and Carl E. Mungan
Department of Physics, The University of West Florida, Pensacola, FL 32514

and Lee Chow
Department of Physics, University of Central Florida, Orlando, FL 32816

Introduction

Organic thin films have been actively studied since the early 1980s for photonic applications, due to their large, ultrafast nonlinear optical and electro-optic coefficients, as well as their stability and their ability to be molecularly engineered. Many of the most interesting applications depend on charge transport of the delocalized π electrons in the medium, and hence are influenced by the electronic mobility and the presence of optically active traps [1]. The incorporation of metal ions into the organic compounds enhances their optical nonlinearities. Photoconductivity is also directly related to the mobility of photo-excited charge carriers, their lifetimes, and the recombination mechanisms, and has applications such as in optoelectronic switching and optical detection [2].

Historically, photoconductivity has been of greatest interest in the study of semiconductors. In these materials, the conductivity is due to excitation of electrons across a bandgap or from in-gap impurities. On the other hand, in organic materials, charge generation takes place through transitions in molecular orbitals, and the recombination and transport mechanisms are entirely different than in semiconductors. Organometallics are typically found to have negligible conductivities up to quite high incident optical intensities [3]. In consequence, it is necessary to investigate the transient photoconductivity of a sample by illuminating it with short laser pulses, both because of the high peak optical powers involved and because it permits one to time resolve the origin and recombination kinetics of the charge carriers.

Organic metallocenes are of interest for their photoconductive behavior [4]. In this paper, we report preliminary results of studies on transient photoconductivity in thin films of ferrocene carboxylic acid (carboxycyclopentadienyl-cyclopentadienyliron), hereafter referred to as FeCA.

Experiment

The films were made by evaporation of solutions of pure FeCA and of FeCA codissolved with poly(methyl methacrylate), abbreviated here as PMMA, in acetone in two different manners. In one case, a few drops of the solution were sandwiched between standard glass slides and allowed to dry. Thin strips of copper foil were also placed between the glass slides, providing electrical contacts. The gap between the electrodes was about 0.5 mm. The resulting films were estimated to be 80 μm thick. In the other case, the film was spin-coated onto a glass slide which had 1000-Å-thick vacuum-evaporated gold electrodes. This gave films having a thickness of approximately 1 μm. A high-voltage dc power supply was connected across the gap in both cases, in series with a 1-MΩ current-limiting and a 1-kΩ current-to-voltage-converting resistor. The thin, yellow film had a dc resistance of approximately 5×10^{10} Ω, in ambient light.

Photo-excitation was provided by a pulsed optical parametric oscillator (Spectra Physics MOPO 710) pumped by a Q-switched, frequency-tripled Nd^{3+}:YAG laser (Spectra Physics GCR-170). The beam was incident on the sample transverse to the plane of the film. The laser pulse width was 3 ns. Average laser powers ranging from 30 to 100 mW were used, and the measurements of conductivities were made at several wavelengths in the blue and green regions, spanning the 450-nm absorption peak of FeCA shown in Fig. 1.

The conductivity appeared to follow the absorption lineshape. The laser beam was focused to a 1.2-mm diameter spot extending across the
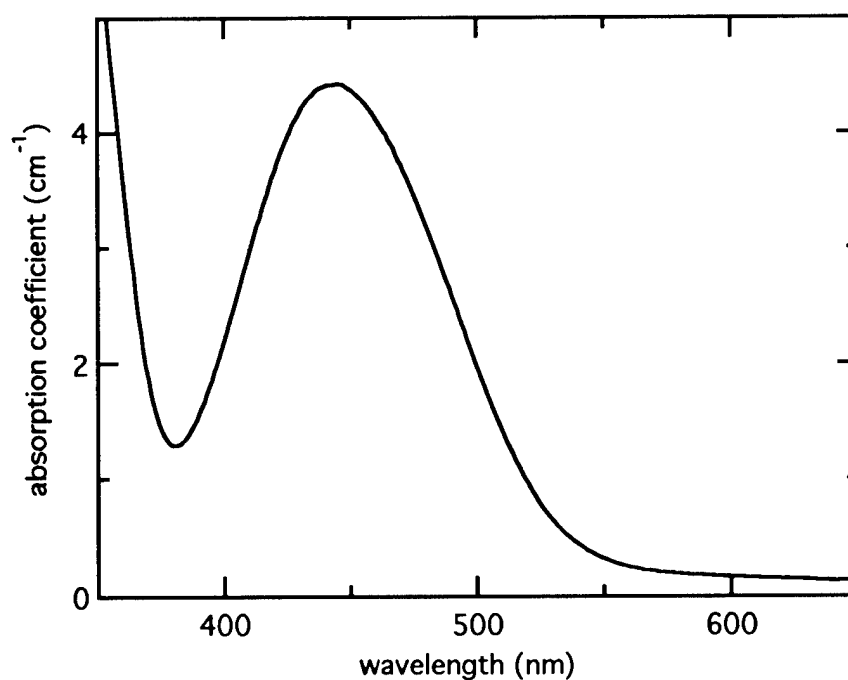
Fig. 1. Absorption spectrum of a solution of ferrocene carboxylic acid in acetone with 1 nm resolution at room temperature.
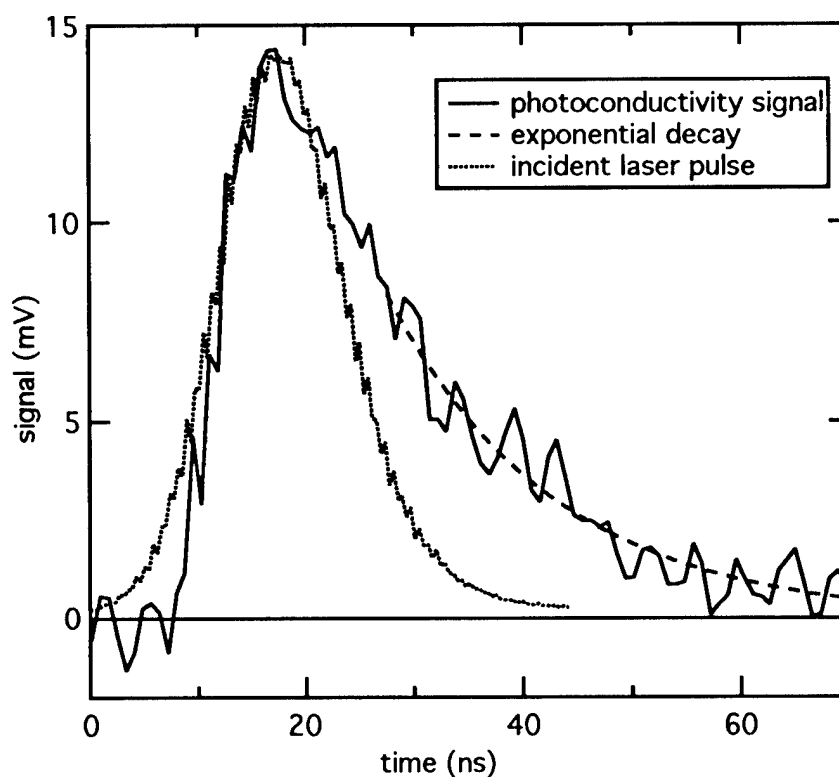
Fig. 2. Photoconductivity of FeCA thin film excited at 532 nm with 95 mW at a bias voltage of 1100 V.

gap between the electrodes. Bias voltages of between 500 and 1500 V dc were used to drive the current generated by the excited charge carriers. The resulting voltage across the 1-kΩ resistor was measured with a 20-GHz digitizing oscilloscope (Hewlett-Packard 54750A). Measurements were also made by exciting the samples with the second harmonic of the YAG laser at 532 nm, where the pulse width was 12 ns. Figure 2 shows a representative signal in this configuration, plotted together with the laser pulse for comparison. The photoconductive response has a tail, which appears to be exponential with a time constant on the order of 10 ns which did not noticeably depend on the excitation wavelength. The fact that the conductivity signal rises more sharply than the laser pulse indicates a threshold behavior.

Summary

The transient photoconductivity of thin films of ferrocene carboxylic acid has been measured. The main features observed in the results are the following:
(1) The photoconductive signal follows the shape of the absorption spectrum.
(2) There is a threshold in the photocurrent as a function of the light intensity.
(3) The signal decays exponentially on a nanosecond timescale.

References

[1] J.C. Scott, L. Th. Pautmeier, and W.E. Moerner, J. Opt. Soc. Am. B **9**, 2059 (1992).
[2] G. Yu, S.D. Phillips, H. Tomozawa, and A.J. Heeger, Phys. Rev. B **42**, 3004 (1990).
[3] S. Ambily and C.S. Menon, Solid State Commun. **94**, 485 (1995).
[4] A.K. Chakraborty and B. Mallik, Synthetic Materials **73**, 239 (1995).

PRECISE DETERMINATION OF ELECTRO-OPTIC COEFFICIENTS FOR POLED POLYMERIC FILMS WITH ELLIPSOMETRIC TECHNIQUE

M. H. Lee, H. J. Lee, W.-Y. Hwang. M.-C. Oh, J.-H. Ahn, S. G. Han, and Y. H. Won.

Photonic Switching Section,
Electronics and Telecommunications Research Institute,
P.O.Box 106, Yusong, Taejon 305-600, Republic of Korea
Tel ; +82-42-860-5243
E-mail ; mhl@etri.re.kr

Introduction

The electro-optic (EO) effect was the earliest nonlinear optical(NLO) phenomenon discovered. The EO effects are the change in the refractive index resulting from the application of a dc or a low frequency electric field. NLO polymeric materials have been of great interest because of their potential use for optical devices. Poled polymers are one of the promising materials for EO applications. Our purpose is to measure the linear EO effects of poled polymeric films precisely. In this paper, the determination of the linear EO coefficients of poled polymeric films with the ellipsometric reflection technique has been discussed in detail. The interference effects were introduced with the spurious signal. The magnitude and phase retardation of the spurious signal were obtained empirically. We have analyzed and demonstrated experimentally with DANS and DR1 side chain poled polymer.

Experimental

For our experiments, we used several side chain polymers with 4 - dimethylamino-4'-nitro-stilbene (DANS) and disperse red 1 (DR1) chromophores. A thin film with a thickness range of 1 ~ 3 μm was spun on an indium tin oxide (ITO) coated glass and dried for 2 hr at 160 °C in an oven under flowing nitrogen. Then a thin layer of gold was deposited onto the polymeric film using a thermal evaporator. Electrode contact poling was performed at its glass transition temperature.

In the measurement of the linear EO coefficients, we used an ellipsometric technique to measure the changes in the refractive index of the poled polymeric films under the influence of an applied electric field. An experimental setup is the simple reflection technique, proposed by Teng and Man[1] and Schildkraut[2] at the same time. A He-Ne laser and 3 semiconductor lasers were used with the wavelengths of 632.8 nm, 830 nm, 1300 nm and 1550 nm. A laser beam is incident on the back of the glass substrate at the fixed angle $\theta = 45°$. We detected the output intensity and the modulated intensity as a function of compensator retardation using a Soleil-Babinet compensator, a photo detector, a lock-in amplifier, and a function generator.

Results and Discussion

In figure 1 (a), we show a result obtained from one of our samples in which the intensities of the modulated EO signals biased at the compensator retardation $\pi/2$ and $3\pi/2$ are nearly equal and

the intensity of the modulated EO signal biased at the compensator retardation π is nearly zero. In addition, the phase (lock-in angle) difference of the modulated EO signals biased at the compensator retardation π/2 and 3π/2 is 180°(π). It means there is no other modulation effect except the pure EO modulation. However, this result is the ideal case but atypical. In figure 1 (b), we show a typical result obtained from one of our samples in which the intensities of the modulated EO signals biased at the compensator retardation π/2 and 3π/2 are not equal and the intensity of the modulated EO signal biased at the compensator retardation π is non-zero.
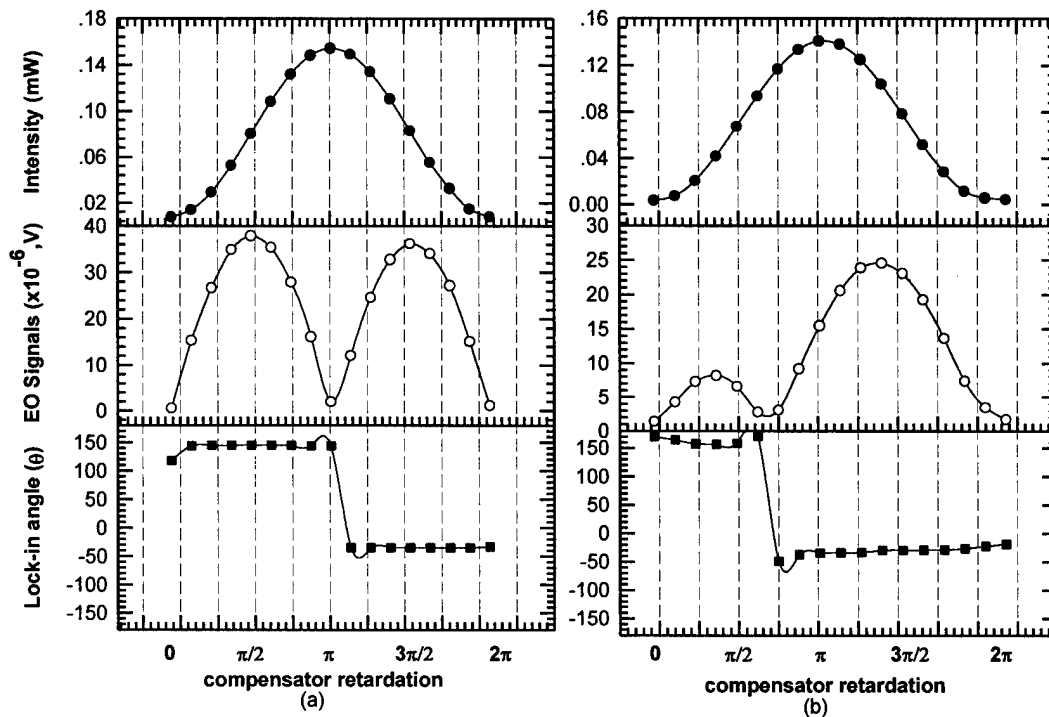
Figure 1. The output intensity, modulated EO signal, and lock-in angle as a function of compensator retardation ; (a) ideal case, taken from PMMA-DR1 side-chain system in which the film thickness is 1.55 μm, the applied poling field is 100 V/μm, and the measured wavelength is 830 nm. ; (b) typical case, taken from Polyester-DR1 side-chain system in which the film thickness is 1.74 μm, the applied poling field is 100 V/μm, and the measured wavelength is 1300 nm.

The degree of asymmetry is directly related to the changing position of the lock-in angle. The degree of asymmetry is getting large as the changing position of the lock-in angle approaches to π/2 or 3π/2 from π. Also, the degree of asymmetry and the shift of the lock-in angle are related to the film thickness. For instances, we found that the degree of asymmetry is getting large and the changing position of the lock-in angle is approaching to π/2 or 3π/2 from π with increasing or decreasing the film thickness from 1.55 μm as shown in figure 1 (a). The degree of asymmetry is not related to the wavelength in the off-resonance range of wavelengths. However, the results measured at 632.8 nm and 1300 nm have similar trend with the variation of the thickness.

We analyze the empirical results and introduce the interference effects between the reflected

beams (r_{gp}, r_{pg}) of the glass-polymer and the polymer-gold interfaces.[1,3] Also, there is the phase retardation between r_{gp} and r_{pg} due to their different optical path lengths. From the empirical data taken from figure 1(b), we can deduce the true EO signals as shown in figure 2. In reality, we can infer the true EO signals in the peaks of figure 1 (b), like the EO signals biased at the compensator retardation $\pi/2$ and $3\pi/2$ in figure 1(a). The relative intensity of the EO signal in one of two peaks of figure 1 (b) divided by the corresponding output intensity is the same as that in another.
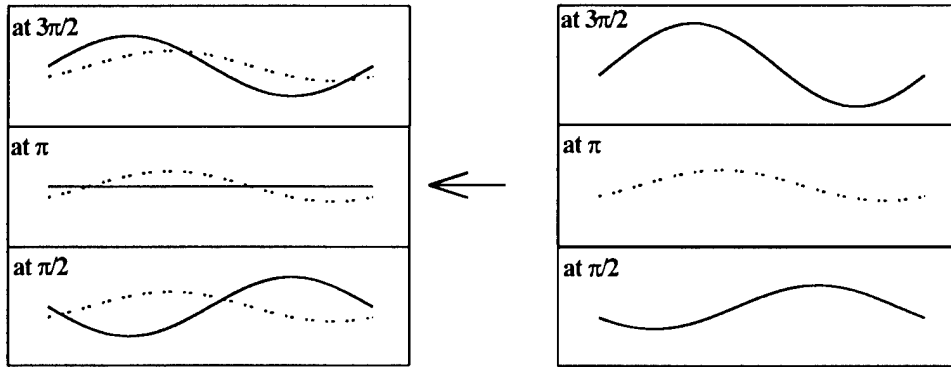
Figure 2. True EO signals (left ; solid lines) are deduced from the measured EO signals (right ; solid lines) and the spurious signal (dotted line). The spurious signal is phase-retarded to $\pi/4$.

Conclusion

To avoid the interference effects due to the phase-retarded spurious signal, we suggest that the deduced true EO signal is used in below equation.[1]

$$r_{333} = \left(\frac{3\lambda}{4\pi n^2}\right)\left(\frac{I_m}{I_c}\right)\left(\frac{1}{V_m}\right)\left[\frac{(n^2 - \sin^2 \theta)^{1/2}}{\sin^2 \theta}\right].$$

where the value of I_m/I_c is taken from the intensity of the EO signal in one of two peaks of figure 1 (b) divided by the corresponding output intensity, instead of the value of the modulated intensity divided by the half intensity biased at the compensator retardation $\pi/2$ or $3\pi/2$.

References
1) C. C. Teng and H. T. Man: Appl. Phys. Lett. 56 (1990) 1734.
2) S. Schildkraut: Appl. Opt. 29 (1990) 2839.
3) G. Khanarian, J. Sounik, D. Allen, S. F. Shu, C. Walton, H. Goldberg, and J. B. Stamatoff: J. Opt. Soc. Am. 13(9) (1996) 1927.

High Performance Electro-Optic Polymer Waveguide Modulator

W.-Y. Hwang , H.-M. Lee*, M.-C. Oh, H. Park,
H.-J. Lee, M.H. Lee, J.H. Ahn, S.G. Han, and Y.H. Won

*Photonic Switching Section, Electronics and Telecommunications Research Institute
P. O. Box 106, Yusong, Taejon, 305-600, South Korea*

**Research Department, Electronics and Telecommunications Research Institute
P. O. Box 106, Yusong, Taejon, 305-600, South Korea*

Tel) 82-42-860-5377, Fax) 82-42-860-6858

I. INTRODUCTION

Electro-optic (EO) polymers have been utilized to fabricate many waveguide devices such as modulators, switches, and polarization control devices [1]-[3]. Up to now, most of the research activities have been focused on electro-optically active materials to improve the device performances. In contrast, less attention has been paid on cladding materials.

Two important factors as well as the refractive index condition should be considered when selecting a proper cladding, i) electrical properties, ii) dimensional stability at elevated temperature and high electric field. Electrical properties are related to poling efficiency and dc drift phenomenon. The conductivity of the cladding layer must be larger than the guiding layer to pole the EO polymer effectively [4]. Recently we have reported that the dc drift in the EO polymer devices is closely related to the dielectric relaxation times of the consisting layers [5]. The analysis indicates that the device can be free from the dc drift when the dielectric relaxation times are the same for each layer, or at least the conductivities of the cladding layers should be higher than the guiding layer to be traceable by the external feedback loop. Dimensional stability affect the poling-induced optical scattering loss. Even very minor inhomogeneity in the cladding layers as well as

in the guiding layer will be amplified during the poling process, which increases the optical loss significantly [6]. Some UV curable polymers used as the cladding layer exhibit it. In order to avoid this scattering loss, the cladding must have a high dimensional stability even at the elevated temperature and very high electric field.

In this paper, we demonstrate that the performances of the EO polymer device can be significantly improved by the proper selection of the cladding polymers. The device characteristics include the half-wave modulation voltage, dc drift, and optical insertion loss.

II. EXPERIMENTALS

We have fabricated a Mach-Zehnder modulator as a test device. The EO polymer used in this work is the P2ANS/MMA (50/50) [2]. A thermally curable phenolic polymer is used as the lower cladding and upper cladding layers. The cladding polymer after curing at 180 °C has high curing conversion of about 90% and cross-linking density of 15 mole/dm^3, and shows good thermal and mechanical properties. Its resistivity is one order of magnitude lower than the EO polymer at the room and the poling temperatures. The thicknesses of the core and the cladding layer

are 3.4 and 1.3 μm, respectively. 4 μm wide channel waveguides are defined using the photobleaching technique. Top electrode are formed by thermal evaporation of Au. The waveguides are poled at 135 °C over the whole waveguide region with the poling field of 200 V/μm. Most waveguides are alive under such a very high electric field. Finally the modulation and the bias electrodes are patterned by lithographic technique followed by cleaving for the performance test. The electrode length is 1.5 cm and the total length of the device is 3.6 cm.

III. RESULTS AND DISSUSIONS

TM polarized lights are coupled into the device using 20x objectives. It shows the modulation extinction better than 20 dB for both of 1.3 and 1.55 μm. The lateral and vertical 1/e mode diameters of 8.3 and 3.6 μm for 1.3 μm and 9.8 and 4.6 μm for 1.55 μm are obtained, respectively. Half-wave modulation voltages are 3.7 and 4.8 V at 500 Hz for 1.3 and 1.55 μm, respectively.

DC-drift behavior after applying a dc bias is characterized by observing the change of the phase shift with time from the initial value. In the measurement, dc bias of 4.3 V is applied to one arm and 100 Hz triangular electrical signal is applied to the other arm to monitor the phase change from the initial value. The details of the technique is described in the paper [5]. The result is shown in Fig. 1. The phase change is normalized from the initial value after applying a dc bias. The phase increases gradually to saturate after 10 min. The phase shift from the initial values are 17 and 4 % for 1.3 and 1.55 μm, respectively. The direction of the dc-drift indicates that the resistivity of the cladding layer is smaller than the guiding layer. And the small amount of the phase shift means that dielectric relaxation times between the guiding and the cladding layers are nearly matched [5].

The propagation loss through the poled straight waveguide with the same poling field is measured by the cut-back method and is shown in Fig. 2. The straight waveguide is located just by the modulator. The measured propagation losses are 2 and 3 dB/cm for 1.3 and 1.55 μm lights, respectively.
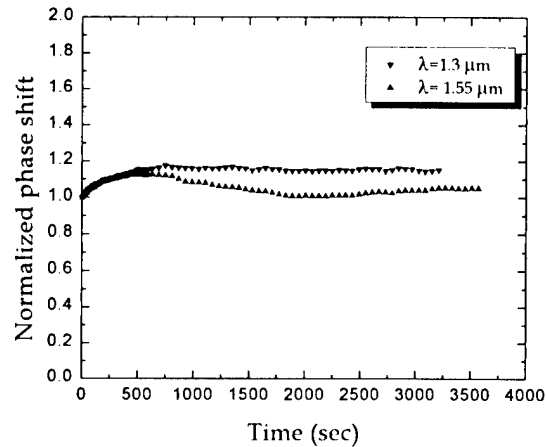
Fig. 1 The recorded phase shift after dc bias is
applied to one arm of the modulator for
the wavelengths of 1.3 and 1.55 μm.

Since the propagation loss in the channel waveguide made of the same EO polymer without poling is about 1 dB/cm at 1.3 μm, the poling-induced optical loss in our device is about 1 dB/cm. The loss is much smaller than the reported one of about 5 dB/cm in the same EO polymer waveguide [6]. When we fabricated the devices using the UV curable polymer like NOA61 or UV15 as the cladding layers, the propagation losses were much higher than the present one even at the lower poling field of 150 V/μm.

IV. CONCLUSIONS

In conclusion, high performance electro-optic polymer modulator is demonstrated by utilizing a proper cladding polymer. Half-wave modulation voltages as low as 3.7 and 4.8 V at 500 Hz are obtained with 1.5 cm long electrode at the wavelengths of 1.3 and 1.5 μm, respectively. The modulator also shows a dc

drift characteristics to be traceable and low poling-induced optical scattering loss.
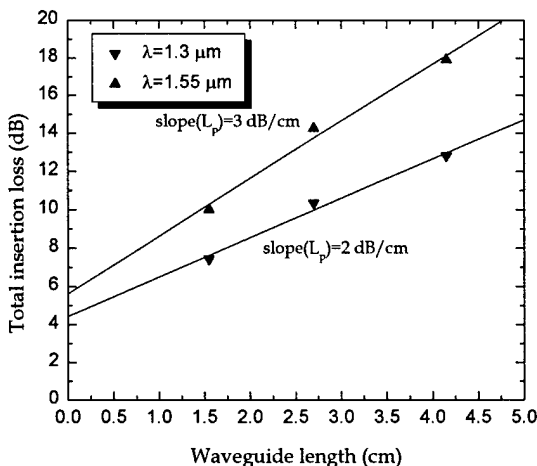
Fig.2 Total insertion loss versus waveguide length determined by the cut-back method in a poled straight channel waveguide for the wavelengths of 1.3 and 1.55 μm.

REFERENCES

[1] Y. Shi, W. Wang, D.J. Olson, W. Lin and J.H. Bechtel, "Electro-optic polymer modulators: manufacturing, packaging, and testing," *Nonlinear optical properties of organic materials IX*, Denver, Colorado, *Proceedings SPIE*, vol. 2852, pp. 258-269, 1996.

[2] W.-Y. Hwang, M.-C. Oh, H.-M. Lee, H. Park and J.-J. Kim, "Polymeric 2×2 electro-optic switch consisting of asymmetric Y junctions and Mach-Zehnder interferometer," *IEEE Photonics Technology Letters*, in press, 1997.

[3] M.-C. Oh, W.-Y. Hwang and J.-J. Kim, "Integrated-optic polarization controlling devices using electro-optic polymers," *ETRI Journal* 18, pp. 287-299, 1997.

[4] P.R. Ashley and E.A. Sornsin, "Doped optical claddings for waveguide devices with electrooptical polymers," *IEEE Photon. Technol. Lett.*, vol. 4, pp. 1026-1028, Sep. 1992.

[5] H. Park, W.-Y. Hwang and J.-J. Kim, "Origin of DC drift in electro-optic polymer waveguide," *Appl. Phys. Lett.*, in press, 1997.

[6] C.C. Teng, M.A. Mortazavi and G.K. Boudoughian, "Origin of the poling-induced optical loss in a nonlinear optical polymeric waveguide," *Appl. Phys. Lett.*, vol. 66, pp. 667-669, Feb. 1995.

Polarization-Independent Electro-Optic Polymer Devices
with Twisted Optic-Axis Waveguide Polarization Converters

M.-C. Oh, W.-Y. Hwang, H. J. Lee, M. H. Lee,

J.-H. Ahn, H. Park, S. G. Han, and Y.-H. Won

Electronics and Telecommunications Research Institute

161 Kajong-dong, Yusong, Taejon, 305-350, Korea

(Phone) +82-42-860-5706, (Fax) +82-42-860-6858, (E-mail) mcoh@nice.etri.re.kr

I. Introduction

Electro-optic waveguide devices are essential components for the high-speed photonic signal processings and broadband optical communications. In the lightwave signal transmission, the polarization state of the light is not maintained when a standard single-mode fibers are used. Hence, polarization independent EO devices are preferred to reduce the system complexity caused by an adaptive polarization controlling circuit. In lithium niobate substrates, there have been various investigations for the polarization-independent switches such as mode-evolution type digital switches [1], directional coupler switches with coincident coupling length for TE and TM modes [2], Mach-Zehnder (MZ) switches on x-cut, z-propagating orientation providing degenerated TE and TM modes [3]. The switching voltages of these devices are 17 ~ 60 V. In this work, we propose a polarization-independent polymer waveguide modulator [4] which can be realized by integrating a polymeric polarization converters [5] in the middle of the MZ modulator. The optic-axis of the polarization converting waveguide is twisted 90 degree by poling it with specially designed electrodes.

II. Twisted optic-axis waveguide polarization converter

In order to slowly twist the poled optic axis of the polymer waveguide, we have employed four electrode structures for the poling of the channel waveguide. A schematic diagram of the modified TOW polarization converter is shown in Fig. 1. Three polymer layers are formed on a substrate together with the four pieces of poling electrodes, and the channel waveguide is fabricated by RIE. At the end of the device fabrication, the channel waveguide

is poled by using the four electrodes with polarities as denoted in Fig. 1. This results in a horizontal electric field at the front end, a slowly rotating electric field in the rotator section, and a vertical electric field at the back end, as shown in the cross-sections of Fig. 1. After the poling, the refractive index parallel to the poling field direction is enhanced so as to produce a positive uniaxial medium. Hence, the optic axis direction is horizontal at the front end and vertical at the back end. In the rotator section, the azimuth angle of the optic axis is slowly twisted along the channel waveguide from the horizontal to the vertical directions.
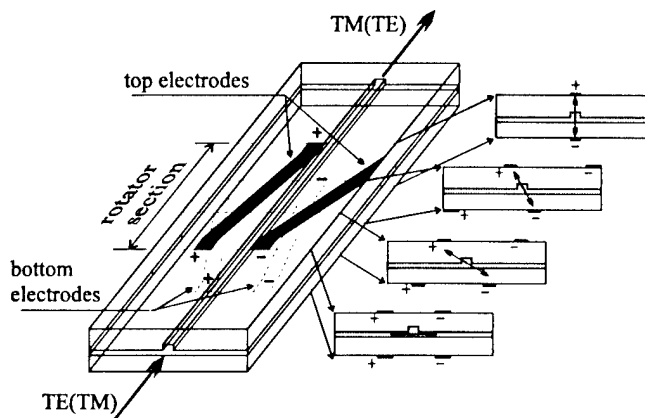
Fig. 1. Schematic diagram of the TOW polarization converter. A channel waveguide is fabricated on a substrate together with four pieces of poling electrodes. The cross-sections are indicating the poled optic axis twisted by the given electrodes.

When the optic axis is formed as stated above, the guided light experiences a polarization conversion by following the twisted optic axis. TE mode at the front end

is coupled to the extraordinary wave in the rotator section, and finally changed to TM mode at the back end. TM mode at the front end is converted to TE mode at the back end via the ordinary wave in the rotator section. When the product of the birefringence and the rotator length is sufficiently large, the polarization coupling between the local orthogonal components is negligible and the light will remain linearly polarized in the device.

For the fabrication of the device, we used 3-inch Si wafers with 1.5 μm thermally oxidized layer. The bottom electrodes were constructed with Ti-Au by a photolithography and a lift-off process. As the lower cladding layer a UV curable optical adhesive (NOA61) was spin-coated and baked to be 1.5 μm thick. For the core layer, we used a PMMA based copolymer with a stilbene derivative as a side chain (poly ((4 - dimethylamino - 4' - nitrostilbene methylmethacrylate)$_{0.5}$ - co - (methylmethacrylate)$_{0.5}$); P2ANS). It was coated and baked to be 3.5 μm thick. Then a rib waveguide was formed in the core layer by O_2 RIE. Over the etched layer, the NOA61 was coated as an upper cladding layer. The top surface was nearly planarized and the effective cladding thickness over the channel waveguide was adjusted to be over 1.5 μm. The top electrodes were formed and patterned with Au. Finally the device was poled on a hot plate at 135 °C by applying an appropriate poling voltage. Then the sample was cleaved for the light coupling. The thickness of the rib waveguide formed by RIE was carefully controlled so as to keep the input and output waveguides single mode and to make a highly confined waveguide at the polarization converter section. Detailed description about the confinement-enhanced single-mode waveguide structure will be appeared elsewhere [6].

The polarization of the 1.3 μm input light was carefully adjusted to TE or TM modes by using a polarizer and a half-wave plate. Then the output light from the device was passed through another polarizer. Single mode operation of the device was confirmed by inspecting the output mode imaged on a CCD. The two polarization conversions following both the ordinary axis (fast axis) and the extraordinary axis (slow axis) were observed. To find the poling voltage for the optimized birefringence, we

fabricated several samples with different poling voltages. When the devices were poled by 200 and 240 V, good conversions were observed. In each sample, there are 4 devices with different dimensions which are defined and summarized in Fig. 3. W_g and W_e are the widths of waveguides and poling electrodes, respectively. W_d is the width of the gap between the electrodes at the front end where the four electrodes are aligned. The length of rotator section is 3 mm and the total device length including the single mode channel waveguide is ~ 12 mm.

The measured polarization extinction ratio indicating the conversion efficiency of the TOW polarization converter is summarized in Fig. 2. For the wide range of the device dimension, the conversion efficiency was better than 20 dB in the two conversions. The conversion efficiency was not degraded during one month of measurements at room temperature. The total insertion loss was measured to be ~ 12 dB and the excess loss was found to be less than 1 dB. Because the insertion loss of the device may depend on the guided light polarization, we measured the insertion loss for each polarization. Most of the devices have exhibited low polarization dependent loss less than 0.5 dB.
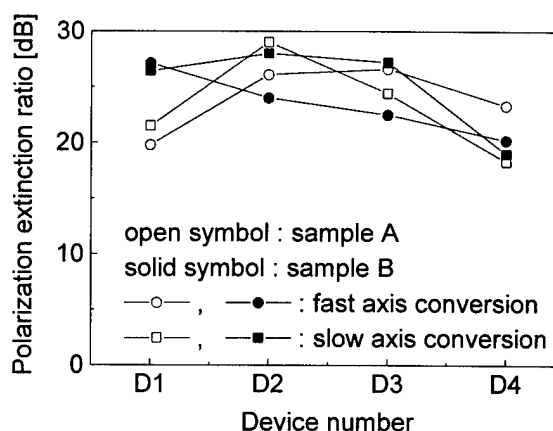
Fig. 2. The measured polarization extinction ratio of the TOW polarization converter. Solid symbol indicates the results of sample A and open symbol indicates those of sample B. The samples A and B are poled by 200 V and 240 V, respectively. On each sample, there are 4 devices whose dimensions are different.

III. Polymeric polarization-independent modulator

A schematic diagram of the proposed polarization-independent polymer waveguide modulator is shown in Fig. 3. By integrating the modified TOW polarization converters and two identical phase modulators (PMs) in the middle of MZ modulator arms, it is possible to obtain polarization independent modulation. Without an additional fabrication process, the two PMs may be fabricated together with the modified TOW polarization converter. The waveguide of PM should be designed to guide both TE and TM polarization modes after the strong poling to induce the large EO effect. The PMs are driven by a single voltage source for the optical intensity modulation. Each PM induces a phase shift of $\Delta\phi$ for TM mode and $\Delta\phi/\alpha$ for TE mode, because the EO coefficients satisfies $r_{33} = \alpha r_{13}$ and $\alpha \approx 3$ in EO polymers [10]. When a TE mode is launched at the input plane of the right arm, it experiences a phase shift of $\Delta\phi/\alpha$ in the PM1 and a phase shift of $\Delta\phi$ in the PM2 since the input TE polarization is converted to TM polarization by the modified TOW polarization converter. For a TM polarization input, a similar process occurs. Therefore, the total phase shift of the device is $(1+\alpha)\Delta\phi/\alpha$ regardless of the input polarization state.

The modulation efficiencies of the proposed modulator and the conventional polarization-dependent MZ modulator are compared as follows. The turn-off state of the proposed modulator is achieved when the driving voltage of V_1 is applied to induce $\Delta\phi_1 = \alpha\pi/(1+\alpha)$ in each phase modulator with length L_1, while the conventional MZ modulator without the TOW polarization converter needs a driving voltage of V_2 to induce $\Delta\phi_2 = \pi$ in the phase modulator with length L_2. Thus, the driving voltages of the proposed modulator and the conventional polarization sensitive modulator satisfy $V_1L_1/V_2L_2 = \Delta\phi_1/\Delta\phi_2 = \alpha/(1+\alpha)$. Therefore, the ratio V_1/V_2 becomes 3/2 when the total length of the phase modulation section is the same, i.e. $L_2 = 2L_1$. The proposed modulator has low driving voltage less than 9 V which is 1.5 times that of the polarization-dependent polymeric MZ modulator [6].
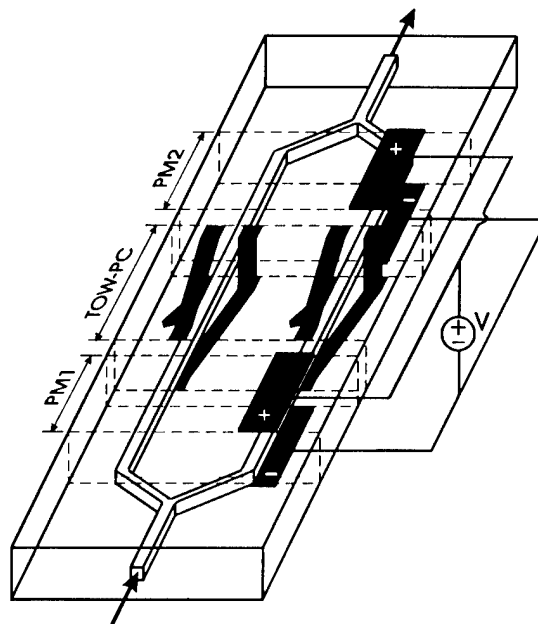
Fig. 3. Schematic diagram of the polarization independent intensity modulator incorporating the twisted optic-axis waveguide polarization converter.

References

[1] A. C. O'Donnell, "Polarisation independent 1 x 16 and 1 x 32 lithium niobate optical switch matrices," *Electron. Lett.*, vol. 27, pp. 2349-2350, 1991.

[2] M. Kondo, Y. Ohta, Y. Tanisawa, T. Aoyama, R. Ishikawa, "Low-drive-voltage and low-loss polarisation-independent LiNbO3 optical waveguide devices," *Electron. Lett.*, vol. 23, pp. 1167-1169, 1987.

[3] J. L. Nightingale, J. S. Vrhel, and T. E. Salac, "Low-voltage, polarization-independent optical switch in Ti-indiffused lithium niobate," Technical digest of Integrated and Guided-Wave Optics, Feb. 6-8, 1989, Houston, TX, paper MAA3-1.

[4] M.-C. Oh and S.-Y. Shin, "Polymeric polarization-independent modulator incorporating twisted optic-axis waveguide polarization converter," *IEEE Photon. Technol. Lett.*, Vol. 8, pp. 1483-1485, 1996.

[5] M.-C. Oh, W.-Y. Hwang, and K. Kim, "TE/TM polarization converter using twisted optic-axis waveguides in poled polymers," *Appl. Phys. Lett.*, Vol. 70, pp. 2227-2229, 1997.

[6] M.-C. Oh, W.-Y. Hwang, H.-M. Lee, S.-G. Han, and Y.-H. Won, "Electro-optic polymer modulators operating in both TE and TM modes incorporating a vertically tapered cladding," *IEEE Photon. Technol. Lett.*, Scheduled for the September 1997 issue.

Polarization-Insensitive Digital Optical Switch Using an Electro-Optic Polymer Rib Waveguide

Sang-Shin Lee* and Sang-Yung Shin

Department of Electrical Engineering
Korea Advanced Institute of Science and Technology
373-1, Kusong-Dong, Yusong-Gu, Taejon 305-701, Korea

*Current address: Department of Electrical Engineering-Electrophysics
University of Southern California, Los Angeles, CA 90089-0483

The digital optical switch (DOS) based on lithium niobate, semiconductors, and thermo-optic polymers [1,2] has attracted much attention as a promising guided-wave switching device. Its advantages include wavelength-insensitive operation and relaxed fabrication tolerance. The guided-wave device in electro-optic (EO) polymers [3] has a small velocity mismatch and a low dielectric constant that are favorable for high-speed operation and small coupling loss to the fiber. Recently, we fabricated an EO polymer DOS with photobleached waveguides [4]. Though the DOS operates independent of the wavelength, but it is not polarization independent since the waveguide fabricated by using photobleaching (PB) method can not support TE modes [3].

The reactive ion etching (RIE) method [5] has been used for the fabrication of a polymeric rib waveguide in preference to the PB method because of the following advantages. First, the excess UV illumination that may degrade the nonlinearity for a poled polymer is not required. Second, the polymeric waveguide formed by RIE may be designed to support both TE and TM modes, since the effective refractive index change for the TE mode resulting from the physical etching of the polymer layers can overcome the poling-induced birefringence. In this paper, a wavelength- and polarization-insensitive DOS is designed by using the beam propagation method, and it is fabricated by employing rib waveguides formed by RIE. The rib waveguide has been carefully designed to have good guiding properties for the TE and TM polarizations, by controlling the RIE etching depth and its aspect ratio, i.e., the ratio of the core thickness and the waveguide width. Especially the etching depth is controlled to change the guided mode profiles of the rib waveguide and thus to achieve an optimum coupling in the branch [6]. The proposed DOS is composed of a linear Y-branch waveguide and a switching electrode. Its schematic configuration is shown in Fig. 1. The waveguide width w is 6 μm and the branch angle θ_B is 0.06°. Its operation is based on the modal evolution effect [6].

In order to realize a polarization-independent DOS, the propagation characteristics of the polymeric waveguide are studied. There are two types of waveguides formed by RIE: a buried type waveguide and a rib waveguide. For the buried-type waveguide with a completely etched core, the wave-guiding properties for TE and TM modes are inevitably different from each other due to the poling-induced birefringence. That is, the poling-induced birefringence reduces the confinement factor of TE mode while it enhances that of TM mode. Unlike the buried-type waveguide, the rib waveguide with an incompletely etched core can provide an identical wave-guiding property for the two polarizations by changing the etching depth for given waveguide width and thickness. For the device reported in ref. 5, the rib waveguide was formed by etching the poled polymer for the core, after poling the two lower layers instead of the entire three layers. This method is sensitive to the thermal property of the polymer material. Consequently, the polymeric rib waveguide poled across the entire three polymer layers is adopted here.

Since for efficient poling the resistivity of the cladding layer of the rib waveguide is small compared to the core, the poling field applied to the core layer is stronger than the average applied field calculated by considering the total thickness. Therefore, the poling field is stronger in the side cladding region than in the guiding region due to its reduced core thickness. The poling-induced birefringence reduces the confinement of TM mode slightly, while it hardly changes the confinement of TE mode. Thus the structure of the rib waveguide can be modified to satisfy equal
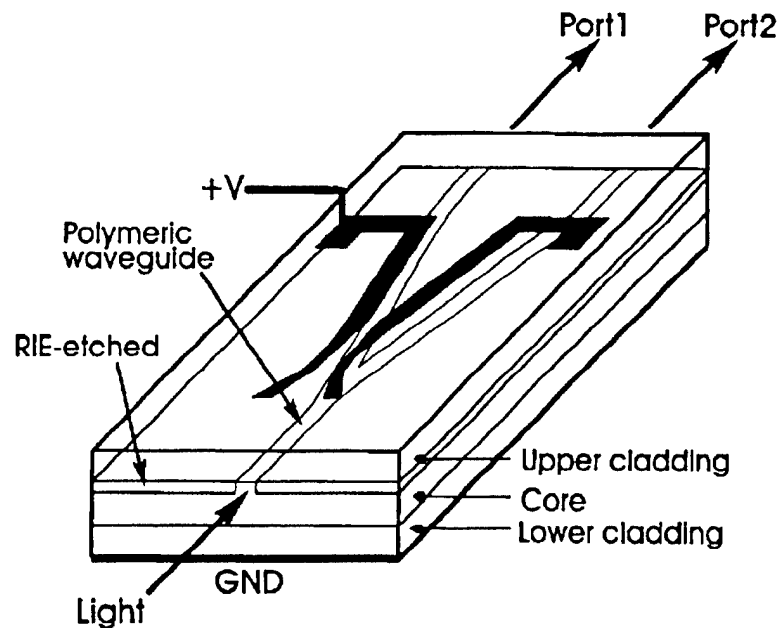
Fig. 1. Configuration of the polymeric DOS with a rib waveguide.

and good single mode condition for two polarizations simultaneously, even though the poling-induced birefringence is included. This has been experimentally confirmed in this work. The lateral guided mode pofiles of the rib waveguide with an etching depth of 0.54 μm have been measured for the TM and TE polarizations, respectively. The $1/e^2$ guided mode sizes for TM and TE modes are 8.4 μm and 8.2 μm, respectively. The propagation losses for the two modes are also comparable within about 3 dB.

The fabrication procedure for the proposed DOS is as follows. On a thermally oxidized Si wafer, the bottom electrode is formed by vacuum evaporation of Au-Ti. The EO polymer used for the core layer is the PMMA backbone side-chained to a Disperse Red 1 dye (poly(disperse red 1 methacrylate-co-methyl methacrylate); PMMA-DR1) from IBM-Almaden Research. For the lower cladding layer, a uv-curable epoxy (UV-15 available from Master Bond Inc.) is spin-coated to be 3.1 μm thick, and cured in vacuum by exposing under UV light. For the core layer, PMMA-DR1 is spin-coated to be 2.7 μm thick. And a standard photolithography and a RIE in oxygen are carried out to form a core rib of the EO polymer. The RIE etching depth is 0.54 μm. Then, the upper cladding layer of 2.6 μm thickness is also formed by spin-coating UV-15. After each spin-coating the polymer is baked sufficiently. The top poling electrode is formed by thermal evaporation of Au. To induce the EO effect, the device is poled in a convection oven at 113 °C by applying 900 V across the three polymer layers. A switching electrode is produced by aligning the rib waveguide pattern with the electrode mask pattern. Finally, for light coupling endfaces are made by cleaving the substrate.

To measure the transfer characteristics of the fabricated device, TE or TM polarized light from a diode laser is launched into the input end, with voltages applied to one of the two top electrodes and the bottom ground electrode. We have measured the transfer characteristics at the

wavelengths of 1.3 μm and 1.55 μm for the TM polarization. The switching characteristics are nearly the same at the two wavelengths. Similar results have been obtained for the TE polarization.

Fig. 2 shows the transfer curves for TM and TE polarizations at 1.3 μm, when voltages are applied to achieve a polarization-insensitive operation. As expected, for the two polarizations the DOS exhibits a digital response with respect to the applied voltage. The switching voltages are about +- 35 V and +- 110 V for TM and TE polarizations, respectively. The crosstalks and extinctions ratios for the switching voltage of +- 110 V are as follows. The crosstalks are about -16 dB for the TE mode and -21 dB for the TM mode. The extinction ratios of each output port are also greater than 16dB. It is experimentally confirmed that the fabricated DOS is wavelength insensitive at least from 1.32 μm to 1.55 μm, with small crosstalk variations of about 1dB. The switching voltage is reduced to less than +- 55 V provided that the device is operated by using the push-pull type electrode. It may be further reduced by more than a factor of 5 by using better polymer material like DANS [3].
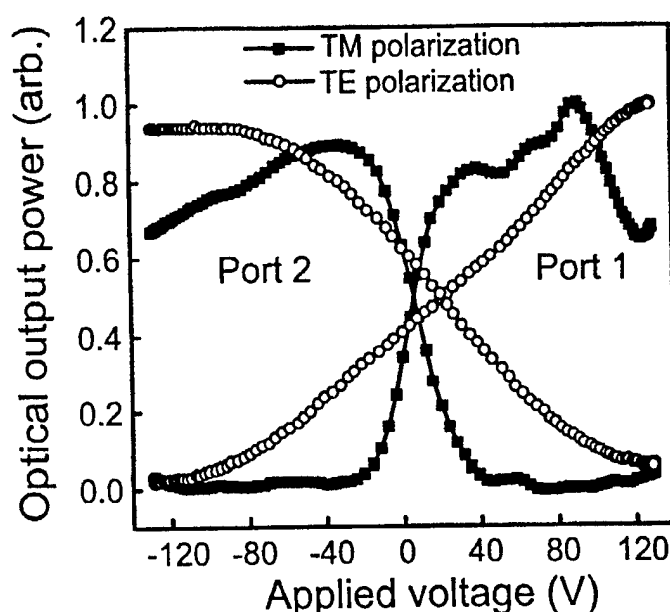
Fig. 2. Measured transfer characteristics for TE and TM polarizations at 1.3 μm.

References

[1] Y. Silberberg, P. Perlmutter, and J. E. Baran, Appl. Phys. Lett., vol. 51, pp. 1230-1232, 1987
[2] N. Keil, H. H. Yao, and C. Zawadzki, Electron. Lett., vol. 32, pp. 1470-1471, 1996.
[3] E. V. Tomme, P. P. V. Daele, R. G. Baets, and P. E. Lagasse, IEEE J. Quantum Electron., vol. 27, pp. 778-787, 1991.
[4] Sang-Shin Lee, Seh-Won Ahn, and Sang-Yung Shin, to be publication, Optics Communications, 1997.
[5] W. Wang, D. Chen, H. R. Fetterman, Y. Shi, W. H. Steier, and L. R. Dalton, IEEE Photon. Technol. Lett., vol. 7, pp. 638-640, 1995.
[6] W. K. Burns, M. M. Howerton, and R. P. Moeller, J. Lightwave Technol., vol. 10, pp. 1403-1408, 1992.

EO Devices I

Friday, October 17, 1997

William H. Steier, University of Southern California
Presider

FA
8:30am–10:00am
Seaview A&B

EO Polymer Devices for Fiber Optics Gyros and Other Applications

Paul R. Ashley
U.S. Army missile Command
AMSMI-RD-WS-CM
Redstone Arsenal, AL 35898-5248

Jeffrey S. Cites
Aegis Research Corporation
6703 Odyssey Dr., Suite 200
Huntsville, AL 35806

ABSTRACT

Integrated photonic components based on polymeric materials have been developed which enhance the integration of fiber optic gyroscopes. New active and passive polymeric materials, device designs, and component integration on optoelectronic substrates are reviewed.

Aside from the potentially lower cost, higher speeds, and greater efficiencies anticipated with polymeric materials, other advantages include the flexibility of design and fabrication as well as the potential hybridization with electronic and optoelectronic devices on silicon or III-V semiconductor substrates. This higher level of integration makes possible the combination of multiport couplers, sources, and detectors together with the power splitter and phase modulators common to the interferometric fiber optic gyroscope (IFOG) system, as well as the supporting control and signal processing electronics. This integration reduces the number of fiber pigtails, splices, and the total number of off-chip components.

Electro-optic (EO) polymer materials have been developed in recent years for use in a variety of devices. Activities exceeding 30 pm/V and temperature stabilities over 150° C have been demonstrated in device structures. In addition, complementary optical cladding materials have been developed to enhance device performance and producibility. Active waveguide modulators using EO polymers have been previously demonstrated using a variety of materials and fabrication techniques. An IFOG which utilizes

an EO polymer based power splitter / phase modulator integrated optical circuit has been demonstrated which exhibited a Vp of 11V at a wavelength of 1.3 mm.[1] This particular IFOG was configured as a single mode, open loop system employing analog reciprocal phase biasing for static and dynamic testing. Detector integration with an active polymer waveguide has been previously demonstrated. An InGaAs p-i-n photodetector was coupled through a transition region to an overlaid polymer waveguide to achieve a coupling efficiency of over 99% and responsivity of 0.84 A/W.[2] The IFOG system requires integrated photonic waveguide components and devices with performance matched requirements, namely insertion loss (includes fiber coupling, Fresnel reflection, propagation, and scattering losses), EO efficiency, and spatial mode properties. New polymeric materials, both active core materials as well as passive upper and lower cladding materials have been investigated with emphasis placed on enhancing overall performance by matching the properties of the waveguide stack layers, specifically refractive index, electrical conductivity, chemical and thermal compatibility, planarization, and overall processability. Also, fabrication techniques employing reactive ion etching have been broadened for specific material properties. Source integration through Z-fold coupling of edge emitting lasers or superluminescent LEDs to single spatial mode polymer waveguides is also currently under investigation. Waveguide, component, and material technologies will be reviewed in comparison to requirements for IFOG and other applications.

---

[1] P.R. Ashley and R.J. Gulotty, *ACS National Meeting*, paper POLY0346, (1994).
[2] J.S. Cites, P.R. Ashley, and R.P. Leavitt, *Appl. Phys. Lett.*, 68, 1452 (1996).

Push-pull Polymer Integrated Mach-Zehnder Modulators

Wenshen Wang, Yongqiang Shi, Weiping Lin, David J. Olson, and James H. Bechtel

TACAN Corporation, 2330 Faraday Ave., Carlsbad, CA 92008

Tel: (760)438-1010, Fax: (760)438-2412

Nonlinear optical (NLO) polymers have been used to demonstrate broadband electro-optic (E-O) modulators in laboratories [1-3]. Because of the small and nondispersive dielectric constants of polymer materials, over 100 GHz modulation can be achieved with a simple integrated microstrip line circuit [3]. However, in order for these polymer modulators to be usable in commercial fiber-optic data links, several other device performance figures have to be improved. In addition to the often-discussed thermal stability issue, the halfwave voltage, optical insertion loss, optical power handling capability, and bias control stability are all of vital importance to the commercial application of polymer E-O modulators. Future polymer photonic devices must have a balanced overall performance, with a much lower cost, broader bandwidth, and competitive thermal, photochemical and bias control stability. We have reported our fabrication and testing of integrated Mach-Zehnder modulators using a double-end-crosslinked NLO polymer LD-3 [4-5]. The LD-3 based modulators have exhibited higher thermal stability, photochemical stability and low optical insertion loss compared to the E-O modulators based on the PUR-DR19 polymer [2]. However, because the LD-3 polymer has a lower E-O coefficient r_{33}, and the corona poling schedule was not optimized, our LD-3 modulators exhibited a higher halfwave voltage which is not acceptable in most applications. In this paper, we report our new device fabrication technique that effectively reduced the halfwave voltage by one-half using an optical push-pull structure in M-Z modulators.

A traditional polymer E-O modulator consists of an integrated M-Z waveguide structure with the same direction of poling and a microstrip line circuit that covers one arm of the M-Z interferometer. In such a device configuration, one has the effective E-O coefficient $r_{eff} = r_{33}$. The effective E-O coefficient can be doubled using a push-pull scheme where the other arm of the M-Z interferometer is modulated simultaneously but 180° out of phase, so that $r_{eff} = 2\, r_{33}$. Push-pull operation can be realized using two electrodes with out of phase RF signals driving each arm of the modulator, which we call electrical push-pull. Electrical push-pull can reduce the halfwave voltage, but could limit the frequency response of the modulator because it requires a broadband phase inverter and two nearby microstrip lines may cause parasitic coupling.

In addition, push-pull operation can be achieved with broad frequency response if one reverses the electrical field poling direction in one of the modulator arms and uses the same electrode to drive both arms. The sign of the electric field induced index change Δn is a function of the relative directions between the driving field and the poling field. With the two arms poled in the opposite directions, the same microstrip line can be used to drive both arms of the modulator, achieving the push-pull operation while maintaining the wideband response of microstrip line electrode. The principle of such device configuration, which we call optical push-pull, is shown in Figure 1 with a microstrip line circuit. Optical push-pull can also be achieved with a coplanar waveguide (CPW) circuit structure, in which the driving electrodes also are used as the poling electrodes.

The broadband operation in a microstrip line structure requires a smaller separation between two arms of the M-Z modulator than the width of the microstrip line. For a film thickness about 10-12

μm, the width of microstrip lines are about 30-40 μm for a 50 Ω impedance. This, in turn, requires a poling electrode gap less than 30 μm. Such a small electrode gap can cause breakdown in air on top of the sample when a high poling electrical field is applied. We have introduced a top clamping piece to modify the field distribution and inert gas to suppress air breakdown, and a sufficient poling field was achieved.
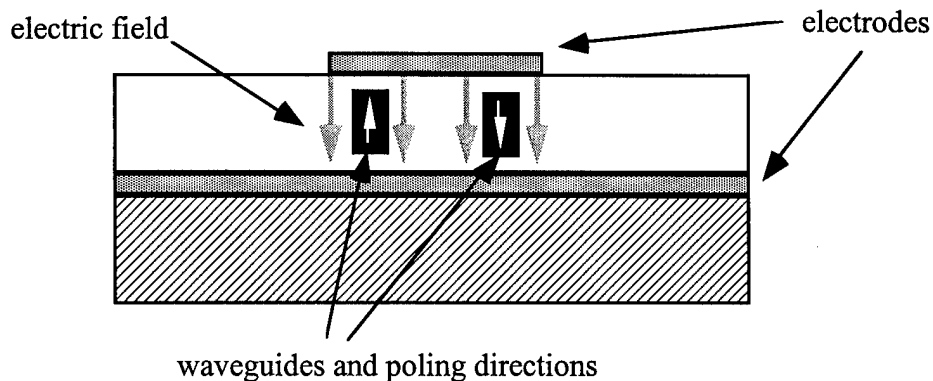
Figure 1: Optical push-pull operation in a polymer E-O M-Z interferometer modulator (cross section).

The device fabrication started with a gold/chromium coated fused silica substrate. For the lower cladding material, a commercial polyurethane, was prepared and spin-cast onto the ground surface with a thickness of 4 μm. The active material LD-3 was then spun on the cured lower cladding layer with a thickness of 3 μm, and pre-dried overnight. A poling electrode made of chromium pattern was then fabricated on the pre-cured LD-3 polymer film. An electric field was applied to the polymer film by applying a voltage across the electrodes. The applied electric field has opposite directions in the regions where the two arms of the M-Z modulator will be fabricated. The poling electrodes had a gap of 30 μm, making it possible to use a single microstrip line driving circuit to cover both modulator arms possible. The temperature ramping schedule was similar to that for corona poling [5], and the peak temperature was about 160°C. The poling voltage applied was about 800V, which gave an estimated electrical field about 140V/μm inside the LD-3 polymer film.

The M-Z waveguide pattern was prepared with photoresist, and the ridge waveguide structure was formed by oxygen reactive ion etching. The top cladding film of 3.5 μm was then applied and driving electrodes covering both M-Z modulator arms were fabricated. The total polymer film thickness was 10.5 μm. Clamping pieces of fused silica were glued on top of the both ends of the modulator before dicing cut and polish.

The modulator was tested using a diode pumped Nd:YAG laser at 1319 nm. The light was coupled into the modulator by direct fiber butt coupling. We have fabricated modulators with built-in optical push-pull and without push-pull on the same device chip, and the halfwave voltages for both cases were measured and compared. For the non-push-pull case, the halfwave voltage was measured to be 40V, as shown in Figure 2(a). The halfwave voltage was reduced to about 20V when the device has the optical push-pull structure, as shown in Fig. 2(b), indicating an expected 50% reduction in the halfwave voltage.

Based on the waveguide dimensions and the indices of refraction of polymer materials used, we have calculated the effective E-O coefficient from the halfwave voltage measurement. The derived E-O coefficient r_{33} was about 7 pm/V, smaller than what is expected from second harmonic generation measurement [4]. We attribute this discrepancy to the poling temperature and time duration, as well as the poling field strength. When the poling schedule is optimized, we expect our current optical push-pull device structure can achieve about 12V halfwave voltage using LD-3 polymer. Currently, we are working towards the optimized poling condition and characterize the device for frequency response.

(a)   (b)
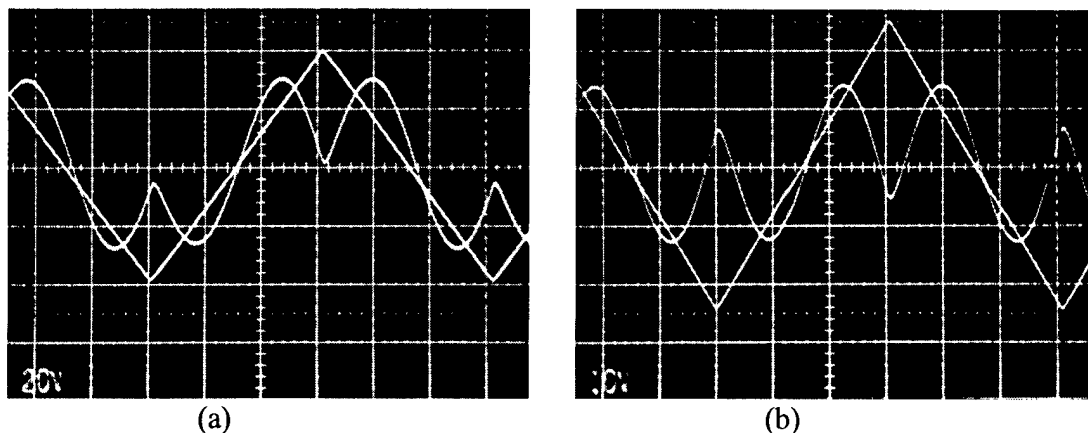
Fig. 2:   (a) Halfwave voltage measurement for non-push-pull M-Z modulator. The applied triangular voltage has a 20V/div. scale, and the measured halfwave voltage was 40V. (b) Halfwave voltage measurement for push-pull M-Z modulator with 10V/div. vertical scale. The measured value was 20V, only one half of the non-push-pull halfwave voltage.

In conclusion, we have successfully demonstrated integrated M-Z modulators with an optical push-pull structure. Efficient electrical field poling has been achieved with a narrow gap to accommodate a single microstrip line circuit. The modulator exhibited a 50% reduction in the halfwave voltage compared to the non-push-pull case, representing a doubled effective E-O coefficient. This work was supported in part by Air Force Rome Laboratory and by the Air Force Office of Scientific Research. The authors would like to thank Professor H. R. Fetterman's group at UCLA and Professor W. Steier's group at USC for the access to their fabrication facilities.

References:
[1]   Y. Shi, et al., *IEEE J. Selected Topics in Quantum Electron.,* **2**, 289 (1996).
[2]   R.S. Moshrefzadeh, et al., in *Organic Thin Films for Photonic Applications, OSA Technical Digest Series,* (Optical Society of America), Washington DC, vol. 17, 1993, pp. 325-327.
[3]   D. Chen, et al., *Proc. SPIE,* **3006**, 314 (1997).
[4]   P. M. Ranon, Ph.D. dissertation, University of Southern California, 1993.
[5]   Y. Shi, et al., *Appl Phys. Lett.,* **70**, 1342 (1997).

Nonlinear Optical Chromophores Containing Fused Terthiophene As A New Type of Electron Relay

O.-K. Kim[1,2] A. Fort[3], M. Barzoukas[3] and J.-M. Lehn[2]

[1]Naval Research Laboratory, Washington, DC 20375-5342
[2]Chimie des Interactions Moléculaires, Collège de France
11 Place Marcellin Berthelot, 75005 Paris, France
[3]IPCMS, Groupe d'Optique Nonlinéaire et d'Optoélectronique
23 Rue du Loess, UM 046 CNRS, 67037 Strasbourg, France

Thiophene-based D-A molecules have been actively sought recently, exploiting interesting results indicating that the incorporation of a thiophene unit or the replacement of a phenylene moiety by thienylene in the relay of a D-A molecule enhanced the molecular hyperpolarizability ($\mu\beta(0)$) significantly (1-3). Accordingly, it is expected that oligothiophenes give a larger contribution to the $\mu\beta(0)$ compared to oligophenylenes. As in the case of polyenes, the rigidification of thiophenes (by cyclization) has also been known to enhance charge-transfer in push-pull D-A molecules, as indicated by a bathochromic shift of absorption bands and a stronger solvatochromism compared to the flexible counterpart (4,5). A further indication for the effectiveness of fused thiophenes as relay is demonstrated by the fact that their absorption maxima increase linearly with the number of rings up to five (6). Aside from the electronic features, another merit of thiophenes is their inherent thermal stability from which thiophene-containing chromophores will benefit (2,3).

We have become interested in a **fused terthiophene, dithieno[3,2-b:2',3'-d]thiophene (DTT)**, anticipating that it could be a particularly efficient relay component, probably more so than terthiophene and fused thienothiophene. However, it is very difficult to make a direct comparison because oligothiophene-based D-A chromophores have been known so far with a very limited number of DA variations and at present, no published results (7) are available in the literature regarding the NLO properties of DTT-containing D-A chromophores. We herewith describe the synthesis and characterization of DTT-containing chromophores bearing various acceptors and a fixed donor, their anomalous solvatochromism and the determination of their $\mu\beta(0)$ values.

General procedure for material synthesis is outlined in the ## Reaction Scheme (Below).
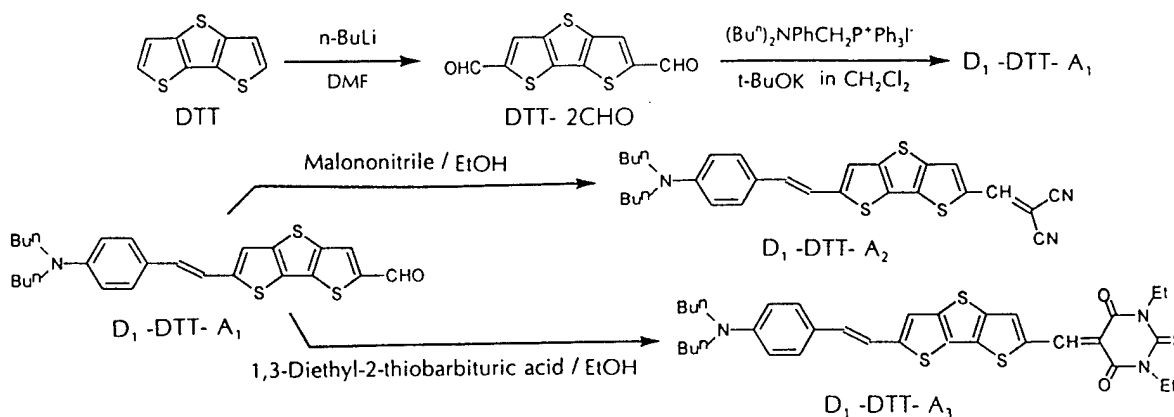
UV-vis spectra were recorded on a Beckman DU-640 spectrophotometer, in various solvents. **Fluorescence spectra** of the compounds were recorded (in chloroform) by using a SPEX FluoroMax. Among the D-A chromophores, only D_1-DTT-A_1 exhibited fluorescence. **Quadratic hyperpolarizabilities** of the DTT-containing chromophores were determined using an electric field-induced second harmonic generation (EFISH) technique described elsewhere (8). The EFISH $\mu\beta(0)$ products were obtained in dichloromethane solution at a fundamental wavelength of 1.907 μm. **Thermogravimetric analysis** was carried out using a Perkin Elmer 7 Series Thermal Analysis System at a heating rate, 10 °C/min.

Table I. **UV/VIS, Molecular Polarizability and Thermal Stability of DTT-containing NLO Chromophores**

Compound	λ_{max}(nm) in CH_2Cl_2	$\mu\beta(2\omega)$ (esu) at $\lambda = 1.907$ mm	$\mu\beta(0)$ (esu)[b]	T_d(°C)[c]
D_1-DTT-A_1	465	950×10^{-48}	680×10^{-48}	348
D_1-DTT-A_2	562	$4,000 \times 10^{-48}$	$2,350 \times 10^{-48}$	344
	558^a	$3,900 \times 10^{-48}$	$2,300 \times 10^{-48}$	
D_1-DTT-A_3	616	$5,000 \times 10^{-48}$	$2,600 \times 10^{-48}$	252

[a] Measured in chloroform. [b] The zero-frequency values were derived from the experimental $\mu\beta(2\omega)$ data by use of the two-level model dispersion factor. Experimental accuracy on $\mu\beta(0)$ is ± 10%. [c] Onset of decomposition temperature was determined from the TGA thermogram taken at a heating rate of 10 °C min⁻¹.

As expected, absorption maxima, λ_{max}, of DTT-containing D-A chromophores in dichloromethane (the best solvent) are shifted to lower energy with increasing acceptor strength ($A_3 > A_2 > A_1$). However, when solvents were varied, a quite anomalous solvatochromic behavior was noted (9), depending sensitively on the solvent polarity ($E_T(30)$) (10). In a solvent of low polarity such as dioxane ($E_T(30) = 36.0$) to dichloromethane ($E_T(30) = 40.7$), the λ_{max} is always red-shifted with an increase of solvent polarity, whereas in a solvent of higher polarity, going from DMF ($E_T(30) = 43.2$) to acetonitrile ($E_T(30) = 45.6$), the λ_{max} is blue-shifted (relative to that in dichloromethane) with increasing solvent polarity. This tendency becomes more pronounced with an increase of the acceptor strength in the chromophores. A somewhat similar behavior was reported with long-conjugated push-pull polyenes (11) with strong DA pairs while it is less likely to occur with a weak DA pair. This is reminiscent of a so-called "inverse solvatochromism" well known for a merocyanine dye, 4-[2-(1-methyl-4-pyridino)ethenyl]- phenolate. Such a reverse solvatochromic behavior does not seem to be the direct consequence of the DA pair strength but is more likely to be associated with the relay character. These results seem to suggest that the solvatochromic behavior of D-A chromophore is strongly influenced by conjugated relays in combination with DA pair strength, and that the positive solvatochromism is not necessarily the measure of molecular nonlinearity.

The $\mu\beta(0)$ products of the DTT containing chromophores are given in Table I, indicating DTT as a highly efficient relay. The magnitude of the $\mu\beta(0)$ products clearly corresponds to the acceptor strength; D_1-DTT-A_3 exhibits the largest value, whereas D_1-DTT-A_1 presents the smallest. This can be anticipated from the absorption spectra. The efficiency of

relays can be assessed by comparing the $\mu\beta$ values among chromophores bearing the same or a similar DA pair, and also by considering the number of π-electrons involved in the relays. Although it is difficult at present to make a direct comparison of relay efficiency between DTT and oligothiophenes due to limited availability in the literature, a rough evaluation can be made based on the $\mu\beta$ values reported for the structurally related chromophores containing bithiophene, fused thienothiophene and thienylvinylene unit(s). While the effectiveness of DTT as relay appears to be smaller compared with that of a polyenic linker with the same number of π-electrons (8), it is likely to be significantly larger than that of terthiophene, judging from the published results (3,12,13). Indeed, i) fused thienothiophene is slightly more effective than bithiophene (12,13), ii) dimeric thienylvinylene is far more efficient compared to bithiophene (3,13), iii) the present fused terthiophene, DTT presents an efficiency similar to or slightly larger than that of the trimeric thienylvinylene (3). The implication of iii) is particularly noticeable when considering the total number of double bond involved in the relays. Since the relay efficiency increases proportionally to the conjugation length, terthiophene should be a better relay than bithiophene and so is trimeric thienylvinylene compared to terthiophene. Accordingly, DTT appears to be a more effective (among oligothiophenes) and uniquely efficient relay unit; while somewhat less efficient than a polyene, it has a significantly higher stability.

As shown in Table I, DTT-containing chromophores present a high thermal stability which is clearly due to the presence of DTT moiety. Both D_1-DTT-A_1 and D_1-DTT-A_2 exhibit a remarkably high decomposition temperature (T_d) compared with D_1-DTT-A_3. The reason for this difference is unclear but attributable to the thiobarbituric moiety. Such a thermally-stable NLO chromophore can be of use for developing solid film-forming materials by making polymeric composites. The $\chi^{(2)}$ measurement of poled thin films of such polymer composites is under way.

In conclusion, we have synthesized advanced NLO chromophores based on fused terthiophene (DTT) as electron relay, studied their anomalous solvatochromism for which DTT is mainly responsible and determined their quadratic hyperpolarizability by EFISH measurements. It was found that their $\mu\beta(0)$ values are remarkably high, depending stronglyly on the acceptor strength. Their results suggest that DTT is a superior electron relay compared to terthiophene and fused thienothiophene. Also, these DTT-containing chromophores are thermally stable so that they can be incorporated into poled polymeric systems to develop various efficient NLO materials.

References

(1) Wuerthner, F.; Effenberger, F. *Chem. Phys.* **1993**, *173*, 305.

(2) Gilmore, S.; Marder, S. R.; Perry, J. W.; Cheng, L.-T. *Adv. Mater.* **1994**, *61*, 494.
(3) Jen, A. K.-J.; Rao, V. P.; Wong, K. Y.; Drost, K. J. *J. Chem. Soc. Chem. Commun.* **1993**, 90.
(4) Brisset, H.; Tobie-Gautier, C.; Jubault, M.; Gorgues, A.; Roncali, J. *J. Chem. Soc. Chem. Commun.* **1994**, 1305.
(5) Gilat, S. L.; Kawai, S. H.; Lehn, J.-M. *J. Chem. Soc. Chem. Commun.* **1993**, 1439.
(6) Masaki, Y.; Kobayashi, K.; *Tetrahedron Lett.* **1989**, *30*, 3315.
(7) One of the reviewers on this paper brought to our attention a poster presented by M. Blenkle, J. Wichem, P. Boldt, et al. at ISOCS 94 (Merseburg): "D-A Substituted Thieno-Acenes ; New Chromophores for Nonlinear Optics".
(8) M. Blanchard-Desce, M.; J.-M. Lehn, J.-M.; Barzoukas, M.; Ledoux, M.; Zyss, J. *Chem. Phys.* **1994**, *181*, 281.
(9) Kim, O.-K.; Lehn, J.-M. *Chem. Phys. Lett.* **1996**, *255*, 147.
(10) Reichart, C. *Chem. Rev.* **1994**, *94*, 2139.
(11) Slama-Schwok, A.; Blanchard-Desce, M.; Lehn, J.-M. *J. Phys. Chem.* **1988**, *94*, 3894.
(12) Rao, V. P.; Wong, K. Y.; Jen, A. K.-Y,; Drost, K. *J. Chem. Mater.* **1994**, *6*, 2210.
(13) Jen, A. K.-Y.; Rao, V. P.; Drost, K. J. et al. *SPIE Proceedings*, **1994**, *2285*, 49.

Thermooptic switches using fluorinated polyimide waveguides

Junya Kobayashi and Tohru Maruno
NTT Opto-electronics Laboratories
3-9-11 Midori-cho, Musashino, Tokyo 180, Japan
Tel: +81-422-59-2474, Fax: +81-422-59-4490, E-mail: junya@ilab.ntt.co.jp

Yasuhiro Hida
NTT Opto-electronics Laboratories
Tokai, Naka-gun, Ibaraki 319-11, Japan

Tohru Matsuura and Shigekuni Sasaki
NTT Science and Core Technology Laboratory Group
3-9-11 Midori-cho, Musashino-shi, Tokyo 180, Japan

1. Introduction

Thermooptic (TO) switches using polymer optical waveguides have attracted much attention because the TO effect of polymers is ten times that of silica. Therefore, using polymers instead of silica [1-2] significantly reduces the required switching power. Moreover, fabricating polymer optical waveguides is easier than fabricating silica-based ones, so large optical devices can be made more easily.

Polymer optical waveguides have been produced from several types of polymers, including poly(methylmethacrylate) (PMMA), polystyrene, poly(organosiloxane), epoxy resin, crosslinked acrylate polymer, and crosslinked benzocyclobutene (BCB). Keil et al. [3] fabricated 4x4 TO switches that operate at a wavelength of 1.55 μm by using PMMA optical waveguides. Y-branching-type 1x2 TO switches have been also fabricated using PMMA waveguides [4] and using BCB polymer waveguides [5].

Polymer optical waveguides applied to TO switches require high thermal stability because the switching is controlled by heating. We previously fabricated channel optical waveguides with high thermal stability above 380°C by using fluorinated polyimides [6]. These waveguides operate in single-mode and have an optical loss of less than 0.3 dB/cm for TE polarization at a wavelength of 1.3 μm. We applied these fluorinated optical waveguides to directional couplers [7].

We have now fabricated optical waveguides by using novel fluorinated co-polyimides with constant birefringence that have low polarization-dependent loss (PDL). The PDL is the change in the optical loss when the polarization of the incident light changes. We have applied these optical waveguides to Y-branching-type TO switches.

2. Fabrication and characterization of optical waveguides

We used 6FDA/TFDB and 6FDA/ODA co-polyimides (Fig. 1) as the cladding and core materials for the waveguides. These polyimides have glass transition temperatures higher than 335°C and 308°C, respectively. Figure 2 shows the refractive indices of the fluorinated co-polyimides for TE and TM polarizations at a wavelength of 1.3 μm. The refractive indices can be precisely controlled by changing the copolymerization ratio (6FDA/TFDB
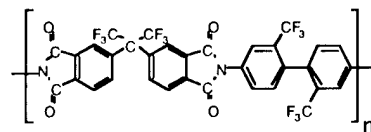
6FDA/TFDB
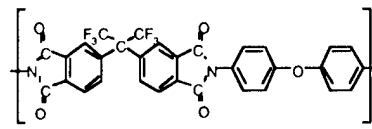
6FDA/ODA

Figure 1 Chemical structure of fluorinated polyimides

content). The birefringences of the co-polyimides were almost constant, with low values of 0.007-0.008 at every 6FDA/TFDB content.

We fabricated the fluorinated polyimide optical waveguides as follows. First, the under-cladding and core layers were formed on a Si substrate by spin-casting and curing. Next, the core ridge of the waveguide was fabricated by photolithographic patterning and reactive ion etching using oxygen. Finally, the over-cladding layer was formed by spin-casting and curing.

The near field patterns observed from the fabricated waveguides had a Gaussian intensity distribution for both TE and TM polarizations at a wavelength of 1.3 μm, indicating that the waveguides operated in single-mode. Figure 3 shows the loss spectrum of the waveguides for both polarizations. The loss values include the connection loss between the fiber and the waveguides. The spectra coincide closely with each other. There is no peak for either polarization at the optical communication wavelengths of 1.3 and 1.55 μm. The propagation loss measured by the cut-back method was 0.3 dB/cm at 1.3 μm and 0.5 dB/cm at 1.55 μm for both polarizations. The PDL was reduced to less than 0.1 dB/cm by using fluorinated polyimides with constant birefringence.
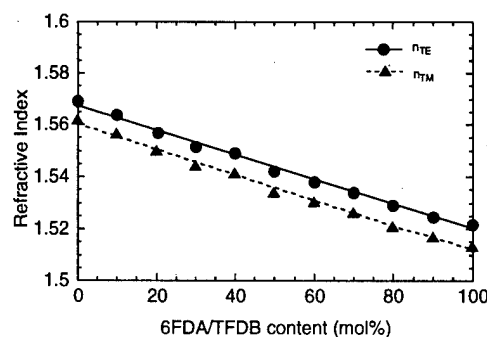
Figure 2 Refractive index dependence on polymerization ratio of fluorinated co-polyimide for TE and TM polarizations
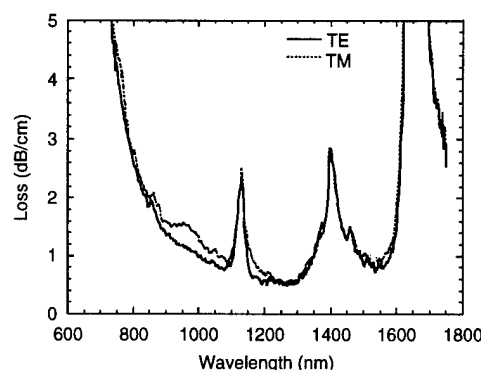
Figure 3 Loss spectrum of fluorinated polyimide optical waveguides for TE and TM polarizations

3. Application to thermooptic switches

We fabricated TO switches by using these fluorinated polyimide optical waveguides. Figure 4(a) shows the structure of the TO switch. The switch consists of a Y-branching waveguide with a shallow opening angle and thin film heaters placed on each branch. In this switch, the optical path is switched by heating one of the branches as shown in Fig. 4(b). When no driving power is applied, the switch acts as a 1x2 splitter. When power is applied to heater 1, the refractive index of port 1 decreases, and the input optical power is directed to port 2. In the same manner, when power is applied to heater 2, the refractive index of port 2 decreases, and the optical power switches to port 1.

Figure 5 shows the output response for both output ports of
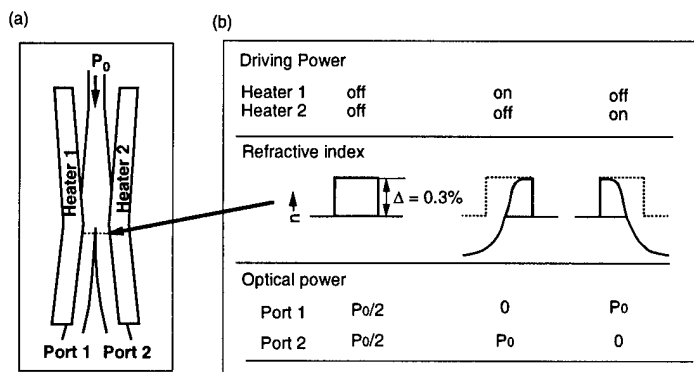
Figure 4(a) Structure of Y-branching-type thermooptic switch. (b) Principle of switching operation.

a Y-branching-type TO switch as a function of the applied driving power at a wavelength of 1.3 μm for TE polarization. The optical output power in unheated port 2 increased as the driving power increased. The extinction ratio was larger than 20 dB when the driving power was above 160 mW at a wavelength of 1.3 μm. The total insertion loss and PDL were less than 1.5 and 0.4 dB, respectively.

Figure 6 shows the pulse response at port 2 when a square-wave pulsed voltage with a 20-ms-wide pulse was applied. It shows that the switching speed was faster than 8 ms.

Figure 7 shows the switching characteristics of the long-term response at relative humidities of 13%, 30%, and 70%, at a temperature of 25°C. The characteristics at 30% RH coincided with those at 70% RH. This implies that the dependence of the switching characteristic on humidity between 30% and 70% RH is small, suggesting that Y-branching-type TO switches fabricated from fluorinated polyimides have good moisture stability.

4. Conclusion

We have fabricated channel optical waveguides by using fluorinated polyimides with constant birefringence. These waveguides operated in single-mode and had a loss of less than 0.3 dB/cm at a wavelength of 1.3 μm, and of 0.5 dB/cm at a wavelength of 1.55 μm for both TE and TM polarizations. We have also fabricated Y-branching-type TO switches using these fluorinated polyimide waveguides. The extinction ratio was larger than 20 dB for driving powers above 160 mW, and the polarization-dependent loss was smaller than 0.4 dB. The switching speed was faster than 8 ms. These fabricated TO switches demonstrated good moisture stability.

Figure 5 Output response for Y-branching-type TO switches at a wavelength of 1.3 μm.
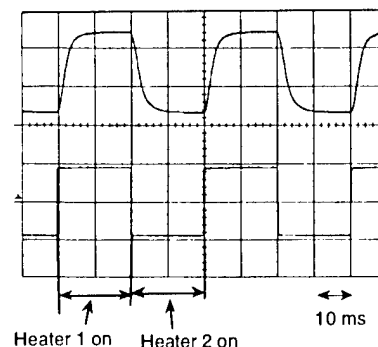
Figure 6 Pulse response at port 2 when a voltage of 9 V was applied.
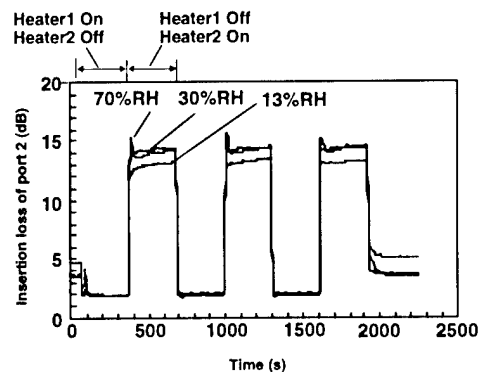
Figure 7 switching characteristics of long-term response for Y-branching-type TO switch.

References

[1] M. N. J. Diemeer et al., J. Lightwave Technol., 7, 449 (1989).
[2] Y. Hida et al., IEEE Photon. Technol. Lett., 5, 782 (1993).
[3] N. Keil et al., Electron Lett. 30, 639-640 (1994).
[4] Ooba et al., Proc. ACS/PMSE, 75, 362-363 (1996).
[5] R. Moosburger et al., Proc. ACS/PMSE, 75, 373-374 (1996).
[6] J. Kobayashi et al., Appl. Opt., to be published.
[7] J. Kobayashi et al., Proc. ACS/PMSE, 75, 371-372 (1996).

Organic Thin Films for Photonics Applications

Polymer Integrated Optics

Friday, October 17, 1997

Yasuhiro Koike, Keio University, Japan
Presider

FB
10:30am-12:00m
Seaview A&B

CONTROL OF THE PHOTOINDUCED MICRO-PATTERNING OF NONLINEAR ORGANIC THIN FILMS: FROM MOLECULAR TO PHOTONIC ENGINEERING

Sophie BRASSELET and Joseph ZYSS

France Telecom - Centre National d'Etudes des Télécommunications

Laboratoire de Bagneux (UA CNRS 250)

Departement d'Electronique Quantique et Moléculaire

196 av. H. Ravera

92225 BAGNEUX, FRANCE

e-mail: zyss@bagneux.cnet.fr

The development of electrooptic polymers now stands at the onset of technological fruition as a result of almost two decades of intense molecular engineering studies and of the more recent maturing of semiconductor compatible integrated optics fabrication processes. Nevertheless, the full potential of organic systems for nonlinear optics[1] and related applications may not have been fully exploited so-far within the paradigmatic orientational scheme of a dipolar *molecular diode* structure coupled with an externally applied poling electric field at thermal equilibrium. In particular, such a configuration makes it difficult to implement (quasi)-phase matched gratings for (cascaded) quadratic NLO, guarantee polarization independant telecom device behaviour or engineer other propagative (e.g. soliton generation) or QED (e.g. microcavity) configurations. A different approach, whereby all-optical photoinduced processes are called-upon instead of thermally equilibrated ones and traditional 1-D systems are traded for more general 3-D multipolar molecules (e.g. octupolar, dipolar or a combination of these) opens-up new possibilities to adress these issues. It permits indeed to micro-pattern and control with subwavelength accuracy a continuous or pixellised spatial $\chi^{(2)}$ tensorial distribution whereby the magnitude and ratios of macroscopic tensorial coefficients are balanced at will by phase and ellipsometric adjustment of the writing beams[2].

From a conceptual point of view, this approach is based on the recognition of the correspondance between an optical "write" multiple beam electromagnetic field tensor and the attached material susceptibility tensor: general coupling rules applying to the irreducible multipolar rotational spectra of the corresponding electromagnetic and material tensors are provided and illustrated in the case of single or cascaded quadratic processes. Indeed, the three-photon transition probability as well as the resulting photoinduced $\chi^{(2)}$ tensor can be expressed as:

$$\chi^{(2)} = N \sum_{J=0,1,2,3} \frac{1}{2J+1} \left\| \beta^J \right\|^2 E^J \qquad (1)$$

where J labels the rotational components (J=1 for the dipolar and J=3 for the octupolar coment with J=0 and 2 pseudo-tensors in the case of resonant processes), $E = E^{2\omega^*} \otimes E^\omega \otimes E^\omega$ representing the *write* field tensor in a deggenerate case and β standing for the quadratic

molecular hyperpolarizability which scales, within a resonnant two level *write* scheme, with the underlying joint one- and two-photon absorption cross-section.

This expression evidences in a specific case the general possibility to monitor and control the magnitude and moreover the irreducible rotational spectrum and nonlinear anisotropy of the $\chi^{(2)}$ tensor distribution by playing on the write field tensor via its irreducible E^J coefficients. Figure 1 below furthermore illustrates the possibility to implement such monitoring by adjustment of the E tensor nonlinear anisotropy via adequate choice of the (ω, 2ω) write beam polarizations. Exp. (1) represents "tensorial filtering" of the write field anisotropy by the molecular hyperpolarizability leading to any desired $\chi^{(2)}$ tensorial pattern.
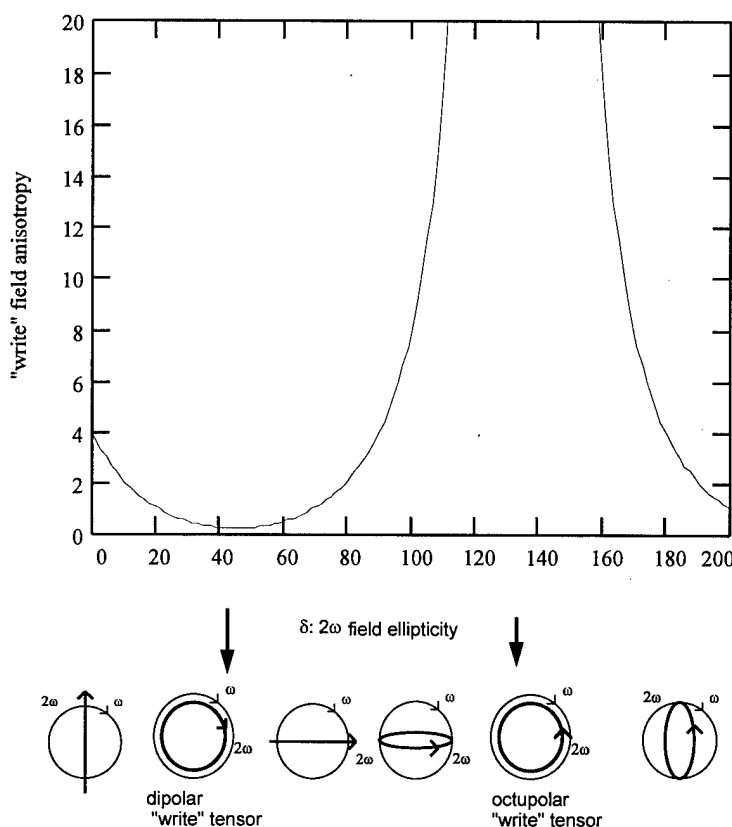
Figure 1: *In practice, any desired nonlinear "write" field anisotropy can be reached by adequate choice of the 2ω "write" beam ellipticity with a circulary polarized ω "write" beam.*

This approach has been implemented and experimentally demonstrated in Fig.2 for a special case. Figure 2 corresponds to a "scissor"-like configuration whereby both *write* fields are linearly polarized at an intermediary angle θ which can be continuously varied. The $\chi^{(2)}$ pattern is then *read* by SHG with an incoming linearly polarized beam at a variable polarization angle ϕ. Purely octupolar (resp. dipolar) configurations have also been generated, based on co-(resp. counter-) clockwise circular polarizations at ω and 2ω, the more general intermediate case corresponding to a circular ω and elliptic 2ω beam.
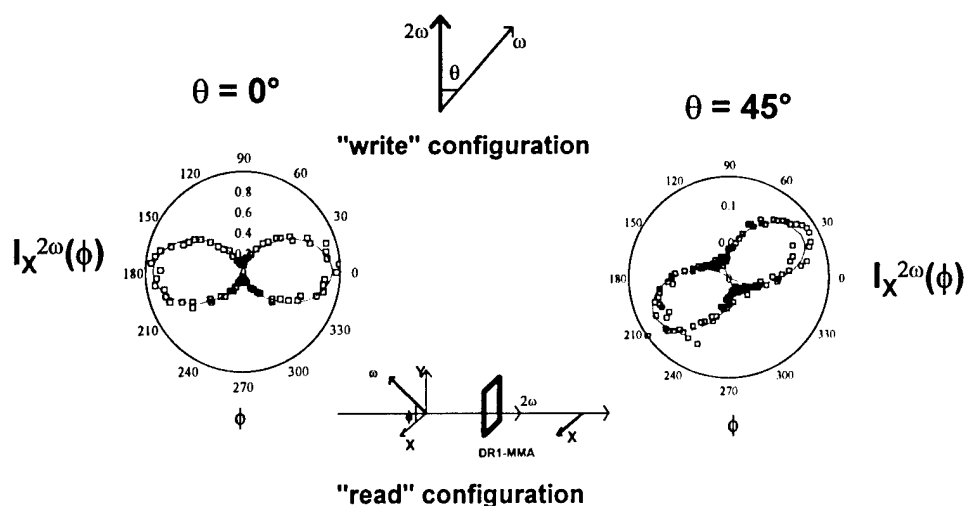
Figure 2: *All-optical phoitoinduced micro-patterning with linearly polarized write beams.*

We have shown in particular that a polarization independant $\chi^{(2)}$ structure can be shaped by use of an octupolar write configuration shining a quasi 1-D DR1 guest-host polymer film. This apparently "orthogonal" and hence forbidden coupling is in fact made possible by the recognition that 1-D systems (e.g. with a β tensor ultimately reduced to a single β_{xxx} coefficient along the main molecular axis) still sustain a significant J=3 component. Tensorial considerations show indeed that, in such case, $\left\|\beta^{J=3}\right\| = \sqrt{2/3}\left\|\beta^{J=1}\right\| = \sqrt{2/5}\beta_{xxx}$, whereas octupolar molecules remain of course ideally tailored candidates for such a scheme with $\left\|\beta^{J=3}\right\| = \beta_{xxx}$.

Moreover, a general theory of orientational processes in nonlinear media encompassing both weak and strong field cases, and accounting for both isotropic (e.g. amorphous) and anisotropic (e.g. such as in liquid crystalline host media) local potentials is being proposed. This model applies to both thermally equilibrated (e.g. "classical" electrically poled polymers) as well as to photoinduced partially optical or all-optical processes in resonnant and non-resonnant cases. It consistently exploits the full 3-D tensorial nature of the orienting fields, via their polarizations, and of the active molecular systems, via more elaborate multipolar chemical design rules. This approach opens the way, beyond the molecular engineering of homogeneously oriented media, towards a full-fledged polymer based photonic engineering with the potential of tailoring at a relevant scale the spatial distribution of NLO properties of relevance for propagative and QED properties.

References

(1) I.Ledoux and J.Zyss, in *Novel Optical Materials and Applications*, I.C.Khoo, F.Simoni and C.Umeton Eds., Chapter I, PP.1-48(1997)

(2) S. Brasselet and J. Zyss, *"multipolar molecules and multipolar fields: probing and controlling the tensorial nature of nonlinear molecular media"*, to be published in J. Opt. Soc. Am. B (1997, feature issue on *Organic and Polymeric Nonlinear Optical Materials*)

In situ trimming of polymer optical waveguides by rapid photobleaching for tuning device specifications

Antao Chen, Felix Ignacio Marti-Carrera, Vadim Chuyanov, Sean Garner, and William H. Steier
Department of Electrical Engineering-Electrophysics
University of Southern California, Los Angeles, CA 90089-0483, (213) 740 8781

Shane S. H. Mao, Younsoo Ra, and Larry R. Dalton
Department of Chemistry
University of Southern California, Los Angeles, CA 90089-1062, (213) 740 8659

Yongqiang Shi
Tacan Corporation, 2330 Faraday Ave., Carlsbad, CA 92008, (619) 438 1010

Electrooptic (EO) polymer is very attractive for ultrahigh speed optical waveguide modulators and switches because of its good speed match between the traveling microwave and optical wave. High-speed EO polymer modulators that operate at frequencies as high as 113 GHz have been demonstrated(1). Besides such advantages as high frequency response, flexible processing capability, low cost, and ease of integration with VLSI circuitry, we will demonstrate an additional advantage of EO polymer - the ability of post-fabrication device trimming.

For waveguide devices, imperfection of fabrication processing can seriously affect the device performance such as the splitting ratio of Y-junction splitters, the extinction ratio of Mach-Zehnder modulators, and the coupling constant of directional coupler switches. A trimming technique that can tune the device specifications will reduce the device cost, improve device performance and increase fabrication yield. In this paper, a technique of fast and *in situ* trimming of already fabricated devices is presented.

The nonlinear optical property of an EO polymer comes from the chromophores contained in the polymer matrix. These chromophores are photobleachable, therefore the refractive index of the polymer changes upon irradiation with ultraviolet or visible light(2). This property has been used for making channel waveguides in EO polymers(3, 4), and it forms the basis of our device trimming technique.

Fig. 1 shows the principle of our trimming technique with a Mach-Zehnder modulator as an example. Suppose that the fabricated power splitting Y-junction has imbalanced output powers due to the defects in the waveguide. This power imbalance causes a lower extinction ratio. By photobleaching the side of the waveguide branch which receives more power immediately before the splitting point or after the recombining point, the refractive index of that area is reduced. This index change shifts the mode peak away from the trimmed side, which is equivalent to a horizontal realignment of the waveguide mode before the splitting. The power in the two arms of the modulator can be balanced without introducing high excess loss. Since the trimming is made outside the waveguide section used for EO modulation, the EO property of the device is not affected by the trimming. For *in situ* trimming, the device should be operated, and the on-off ratio be monitored during the process. A tentative trimming of an arbitrary branch is necessary to determine which arm needs to be trimmed by observing the change of the on-off ratio. Then a trimming of the determined branch is performed to maximize this ratio.

The trimming only requires a modified binocular microscope and it is very easy to perform. The setup is shown in Fig. 2. Light from a 488 nm Ar+ laser is delivered by a multimode fiber. One eyepiece of the microscope is removed, and the output end of the fiber is placed in the image plane of the objective lens. The microscope objective reduces the output pattern of the fiber and projects the reduced image onto the sample. The size of the spot is determined by the fiber core

size, the magnifying power of the microscope objective lens, and the axial position of the tip of the fiber. A spot size from 1 μm to >1 mm on the waveguide sample is obtainable. The position of the spot on the sample is observed through the other eyepiece or by a video camera on the microscope. Because the fiber tip is fixed to the microscope, its image always appears at the same place in the observation field of view when moving the microscope. This arrangement makes it very simple to position the beam spot to where photobleaching should be performed. The device is operated during the trimming and specifications to be optimized such as the splitting ratio, the extinction ratio, and the output state, are monitored *in-situ* and used as the feed back signal for the processing control.
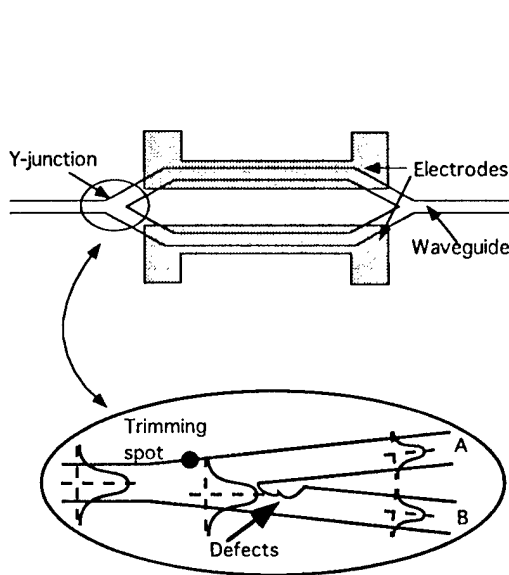
Fig. 1 Principle of trimming a Mach-Zehnder modulator for high extinction ratio.
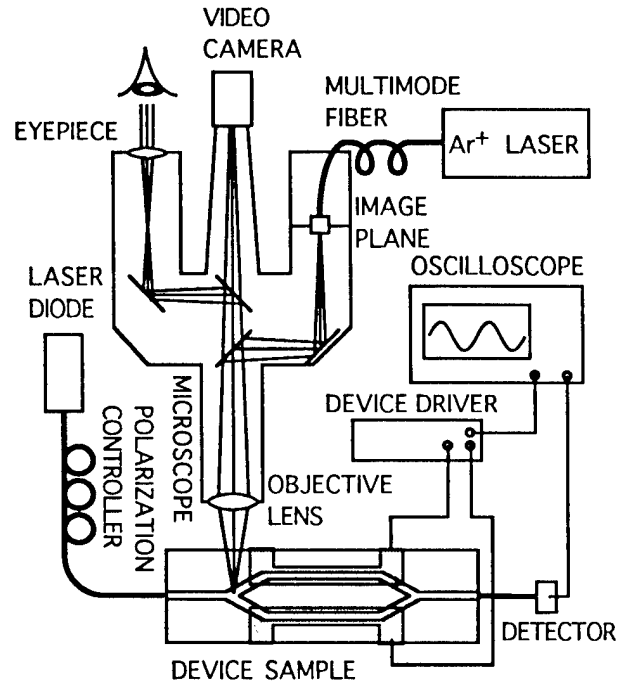
Fig. 2 A schematic diagram of the trimming setup.

To demonstrate this trimming concept, the trimming of waveguide Y-junctions was performed. The single mode channel waveguides are made in a thermally crosslinked PU-DR 19 EO polymer(5, 6) by oxygen reactive ion etching (RIE). The waveguide core is cladded by 5 μm thick polyurethane layers which are transparent to the trimming beam. Fig. 3 shows the typical change of the power output from the two branches of a Y-junction under trimming. The branch which is being photobleached loses power due to a reduced refractive index and the other branch gains power. The splitting ratio is, therefore, changed. Trimming the other branch changes the ratio in the opposite direction. This error correction makes this technique fault tolerant. In our experiment, the splitting ratio could be tuned ±20% for the TE mode and ±10% for the TM mode. The change of the total output power from the two branches is less than 0.2 dB after repeated trimming of the two branches. The fast partial recovery of the splitting ratio after the trimming light is turned off can be explained by the fast relaxation of the cis-trans isomerization and the thermo-optical effect. Over-trimming and multiple trimming sessions can be used to compensate this partial recovery and to reach the required splitting ratio. The power of the unpolarized trimming beam incident on the sample is only a few μW. Since the power is focused on a small spot, the power density in the trimming spot is still very high. The time required to trim a device is only on the

order of 10 seconds. Compared with the conventional masked photobleaching trimming(7) which takes a few hours to complete, our focused photobleaching trimming is very rapid.
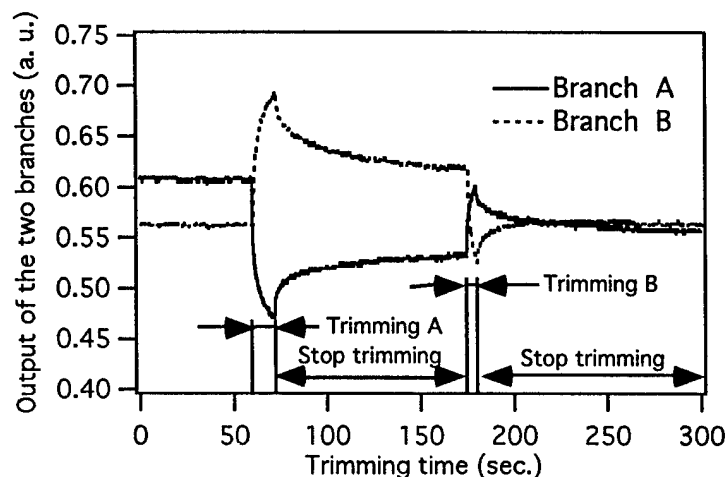
Fig. 3 Output intensities of the two branches during trimming. TE mode is launched in the waveguide.

From a thin film of this polymer, photobleached with the same energy density as used for the typical device trimming, the induced index change at the device working wavelength of 1.3 μm is in the range of 0.025-0.03. Previous investigation in the mechanism of photobleaching has proved that the dominant process in photobleaching is the irreversible photodecomposition of the chromophores(8). This conclusion is confirmed by our FT-IR and UV-VIS absorption scans. The FT-IR signature peaks of the $N=N$ and $C-NO_2$ bonds that only exist in the DR 19 chromophores decrease after photobleaching. As a result, the index change of the photobleached polymer is stable after the initial fast decay process caused by the previously mentioned non-dominant mechanisms. We have observed no further change in the monitored index of a photobleached sample for over 1000 hours at room temperature and exposed to room light. Therefore the performance of a trimmed device is expected to have the same thermal and temporal stability as the original EO polymer device. Our experiment is effective on waveguides made by both RIE and photobleaching.

References

1.   D. Chen, et al., *Proceedings of SPIE* **3006**, 314-317 (1997).
2.   J. Ma, et al., *Applied Optics* **34**, 5352-5360 (1995).
3.   G. R. Mohlmann, *Synthetic Metals* **67**, 77-80 (1994).
4.   J.-J. Kim, W.-Y. Hwang, T. Zyung, *Molecular Crystals and Liquid Crystals* **267**, 353-363 (1995).
5.   M. Chen, L. R. Dalton, L. P. Yu, Y. Q. Shi, W. H. Steier, *Macromolecules*, **25**, 4032-4035 (1992).
6.   Y. Q. Shi, W. H. Steier, M. Chen, L. Yu, L. R. Dalton, *Applied Physics Letters* **60**, 2577-9 (1992).
7.   W.-Y. Hwang, J.-J. Kim, T. Zyung, M.-C. Oh, S.-Y. Shin, *Applied Physics Letters* **67**, 763-765 (1995).
8.   J. Vydra, H. Beisinghoff, T. Tschudi, M. Eich, *Applied Physics Letters* **69**, 1035-1037 (1996).

Application of Surface Relief Gratings
Created on Azobenzene Functionalized Polymer Films as Phase Masks

Lian Li
Molecular Technologies Inc., 270 Littleton Road, Westford, MA 01886
Phone: (508) 392-1304

Xin Li Jiang, Dong-Yu Kim, Jayant Kumar, and Sukant Tripathy
Center for Advanced Materials, Departments of Physics and Chemistry
University of Massachusetts Lowell, Lowell, MA 01854
Phone: (508) 934-3687

Introduction

Holographic recording of surface relief gratings has recently been reported in side chain azo containing polymers by Kumar, Tripathy and coworkers [1-10] and Rochon, Natansohn and coworkers [11-13] It has been demonstrated that large surface modulation (>3000Å) could be inscribed in thin films of these polymers when an Argon ion laser radiation at 488 nm with a modest intensity (a few tens of mW/cm^2) is used to record the gratings. This grating formation process strongly depends on the polarization states of the recording beams [4]. The gratings appear to be almost sinusoidal and recording of crossed gratings has been demonstrated[1]. These gratings are very stable when they are kept below the glass transition temperature (Tg) of the polymer. The gratings can be erased by either heating the grating sample above Tg or exposing it to a single laser beam at appropriate wavelength and with appropriate polarization [10]. This process allows a one step fabrication of complicated surface profile without the need of any pre or post processing of the polymer samples. Complex surface profiles, for example, well defined beat structures and blazed gratings have been recorded on these polymer films [8]. Since this surface relief grating formation process provides the one step processing and large surface modulation on the polymer films, such process is expected to have significant potential applications for various optical devices including diffractive optical elements.

Phase masks [14,15] have been widely used to create periodic intensity modulation of light. They have been employed to fabricate not only fiber gratings [14,15], but also thin-film gratings [16] and surface relief gratings on glass [17]. In this paper, we report on the use of a holographic surface relief grating fabricated with an azobenzene polymer as phase mask. A large surface relief grating was transferred on an azobenzene polymer film with this phase mask.

Experimental Results and Discussions

An epoxy based azobenzene functionalized polymer (PDO3, which has been shown to be able to record large surface relief gratings [1-4]) was used for the present studies. The PDO3 polymer was dissolved in a mixture of propylene glycol methyl ether acetate and dioxane (volume ratio of 3:1) with a weight ratio of

1:10. The filtered polymer solution was spin-coated on glass slides to form good optical quality films. These films were then baked at 70 °C under vacuum overnight. Thin (about 400 nm) and thick (about 1000 nm) films were prepared. Thin samples were used to fabricate phase masks. The phase masks will have lower absorbance at the wavelength they will be utilized.

A phase mask on a thin PDO3 film was created with the experimental set-up as described in ref. 4. The polarization of the recording beams from an Argon ion laser was chosen to be 45° with respect to the s-polarization. This optimal recording condition will not only give rise to large surface modulation on the poplymer film [8, 10], but also prevent from optical erasure of the phase mask grating when a single laser beam with polarization perpendicular to the grating grooves is used to transfer the pattern [10]. The phase mask with a spacing of 900 nm was fabricated at 488 nm with an intensity of 90 mW/cm^2 for 30 min. Large surface relief structure (130 nm) was characterized with an atomic force microscope (AFM) as shown in Fig. 1 (a).

This phase mask was then used to record surface relief gratings on thick samples. The phase mask and a thick polymer film sample were brought together with a 100 μm Teflon spacer placed in between. Laser radiation at 514.5 nm with an intensity of 150 mW/cm^2 was used for recording. At this wavelength, the thin sample will have a transmission loss of about 50% and the phase mask has about 10% diffraction efficiency in either +1 order or -1 order after loss correction. The polarization of the laser beam was selected to be perpendicular to the grating groove of the phase mask. Total recording time was 50 min. A good surface relief grating (> 100 nm of surface modulation) having the same period as that of the phase mask was successfully fabricated on the thick PDO3 sample by using the phase mask. Fig. 1 (b) shows a two-dimensional AFM view of the grating.

(a)   (b)
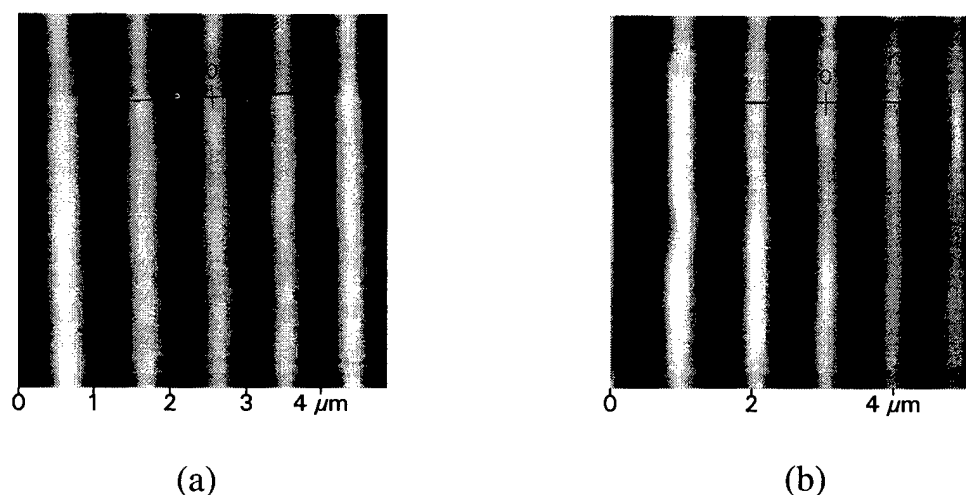
Fig. 1. AFM two-dimensional views of (a) the phase mask
and (b) the grating fabricated with the phase mask.

Conclusions

In conclusion, holographic surface relief gratings on azobenzene polymer films have been successfully employed as phase masks. Surface relief gratings were transferred onto azobenzene polymer films with the phase mask. Large surface modulations were created on the polymer films as a consequence of the transfer pattern.

References

1. D. Y. Kim, L. Li, J. Kumar, and S. K. Tripathy, Appl. Phys. Lett. **66**, 1166 (1995).
2. D. Y. Kim, L. Li, X. L. Jiang, V. Shivshankar, J. Kumar, and S. K. Tripathy, Macromolecules, **28**, 8835 (1995).
3. D. Y. Kim, L. Li, J. Kumar, and S. K. Tripathy, Technical Digest, Optical Society of America, Washington DC, **21**, 361 (1995).
4. X. L. Jiang, L. Li, J. Kumar, D. Y. Kim, V. Shivshankar, and S. K. Tripathy, Appl. Phys. Lett. **68**, 2618 (1996).
5. S. K. Tripathy, D. Y. Kim, T. S. Lee, X. L. Jiang, L. Li, and J. Kumar, ACS polymer preprints, **37**, 123 (1996).
6. D. Y. Kim, X. L. Jiang, L. Li, J. Kumar, and S. K. Tripathy, ACS symposium series on Polymers for Advanced Optical Applications (to be published).
7. D. Y. Kim, X. L. Jiang, T. S. Lee, L. Li, J. Kumar, and S. K. Tripathy, Macromolecular Symposia (to be published).
8. D. Y. Kim, T. S. Lee, X. Wang, X. L. Jiang, L. Li, J. Kumar, and S. K. Tripathy, Proc. SPIE, **2998**, 195 (1997).
9. S. K. Tripathy, D. Y. Kim, X. L. Jiang, L. Li, T. S. Lee, X. Wang, and J. Kumar, Proceedings Paper for the Conference of First International Symposium on Interactive Paper (to be published).
10. X. L. Jiang, L. Li, D. Y. Kim, V. Shivshankar, J. Kumar, and S. K. Tripathy (manuscript under preparation).
11. P. Rochon, E. Batalla, and A. Natansohn, Appl. Phys. Lett. **66**, 136 (1995).
12. C. Barrett, A. Natansohn, and P. Rochon, J. Phys. Chem. **100**, 8836 (1996).
13. M. S. Ho, C. Barrett, J. Paterson, M. Esteghamatian, A. Natansohn, and P. Rochon, Macromolecules, **29**, 4613 (1996).
14. K. O . Hill, B. Malo, F. Bilodeau, D. C. Johnson, and J. Albert, Appl. Phys. Lett. **62**, 1035 (1993).
15. B. Malo, D. C. Johnson, F. Bilodeau, J. Albert, and K. O . Hill, Opt. Lett. **18**, 1277 (1993).
16. J. Nishii, H. Yamanaka, H. Hosono, and H. Kawazoe, Opt. Lett. **21**, 1360 (1996).
17. K. Tsunetomo and T. Koyama, Opt. Lett. **22**, 411 (1997).

Self-Imaging Holographic Optical Waveguides

H. Grebel, J. L. Graziani and S. Vijayalakshmi

Optical Waveguide Laboratory, ECE Department, New Jersey Institute of Technology, Newark, NJ 07102. Tel: (201) 596-3533. E-mail: grebel@admin.njit.edu

L.W. Shacklette, K. M. T. Stengel, L. Eldada, R. Norwood and J. T. Yardley

AlliedSignal, 101 Columbia Road, Morristown, NJ 07962

Periodic structures exhibit an effect known as self-imaging[1-3]. The complex, amplitude distribution of the field, $u(x,y,z)$ is self-similar such that, $u(x,y,z) = u(x,y,z+L_s)$. Here we address self-imaging by use of transverse gratings which extend throughout the entire waveguide (Figure 1). By use of photolithographic techniques in photopolymers, one has a simple means to match waves having dissimilar propagation constants without much loss.
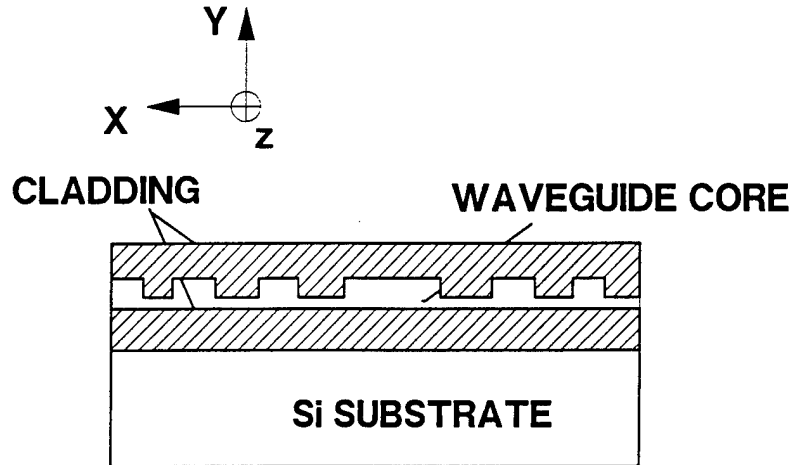
A self-imaging distance L_s is defined as the distance for which an object is imaged onto itself[1]. In waveguides, this condition requires that the mode phase separation at distance L_s will be multiples of 2π (or a multiple of π for inverse images to be included). For a one-dimensional, step-index waveguide of width D, we get, $L_s = s \cdot (8n(0)D^2 / \lambda)$ with $s = 1,2,3...$ For comparison, the self-imaging distance for a one-dimensional grating in free-space with a pitch of Λ, is $L_s = s2\Lambda^2/\lambda$ which is also known as the Talbot distance. This distance is four times smaller if a chirped structure is used, such as, a Fresnel lens; there, $L_s = s2d^2/\lambda$ where d is the width of the central channel. Similarly, the self-imaging distance for a holographic, periodic waveguide is $L_s = s \cdot (4n(0)\Lambda^2 / \lambda)$, with Λ being the transverse pitch of the pattern[2].

The refractive index profile of a chirp structure is taken as, $n^2(x) = n^2(0)(1 + A\cos\alpha x^2)$. When A<<1 and in the paraxial approximation, we get,

$$L_s = 8d^2 n(0) / \lambda_0 . \qquad (1)$$

This result is two times smaller than the corresponding value for periodic stucture.

One can simulate the modal distribution in a patterned slab waveguide by use of a matrix form when the refractive index changes are not small. The computer simulation for a slab waveguide, patterned with a transverse chirp structure, is shown in Figure 2. The central channel was d=31.5μm and the overall transverse dimension was 135μm. The wavelength was λ=0.633μm. The refractive index difference between the core's layers was, $\Delta n = n_2 - n_1 = 10^{-3}$. Only even TE modes are shown here to ease comparison with the experiment. As can be seen from the curve, the modes tend to localize as compared to the "empty slab. In Figure 3 we show the first few self-imaging distances for the chirp-patterned waveguide. It seems that the imaging distance is greatly reduced as compared to the weak modulation case of Eq. 1. Based on this equation the calculated self-imaging lengths are, L_s = 8.6 mm for λ=0.633μm and L_s = 10.1 mm for λ=0.543μm.
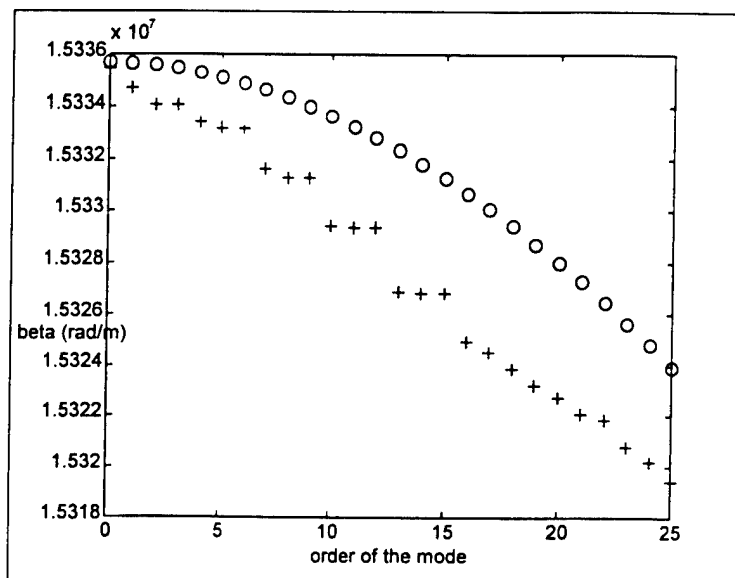
first modes of the Fresnel waveguide (Δn=0.001) (+) compares to the slab of same entire width (135μm) (o)
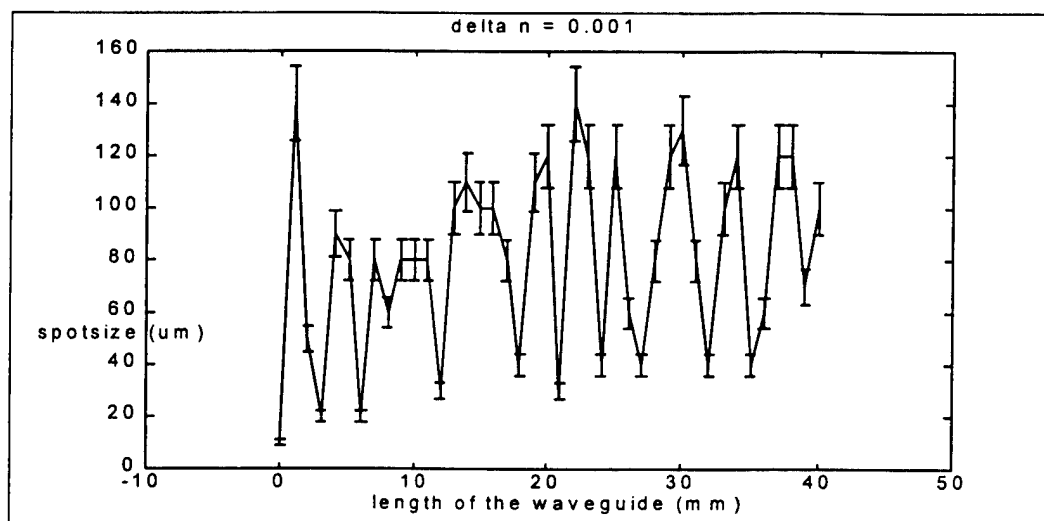
Variation of the light spotsize as a function of z for the Fresnel waveguide (Δn = 1.10^{-3}). The first 50 even modes are considered.

In our experiments, various holographic patterns have been recorded in multi-mode polymeric, waveguides. The waveguides have been fabricated in photo-polymers[4] by use of an optical mask. A cladding layer with a refractive index n_{cl} = 1.517 and of thickness of 8 μm was first spun on a <100> Si wafer. The near field pattern of each cleaved waveguide was measured. In Figure 4 we show the output spot size as a function of the waveguide length for a 135μm wide waveguide launched with a λ = 0.633 μm laser light. The central channel width was d=31μm. Clearly seen is the periodicity of the spot size as a function of waveguide length. This behavior is an indication of a self-imaging distance of 8±0.75 mm. When launched with λ = 0.543 μm, the self-imaging distance was 9.4±0.75 mm, demonstrating an inverse dependence on wavelength as expected from Eq. 1.
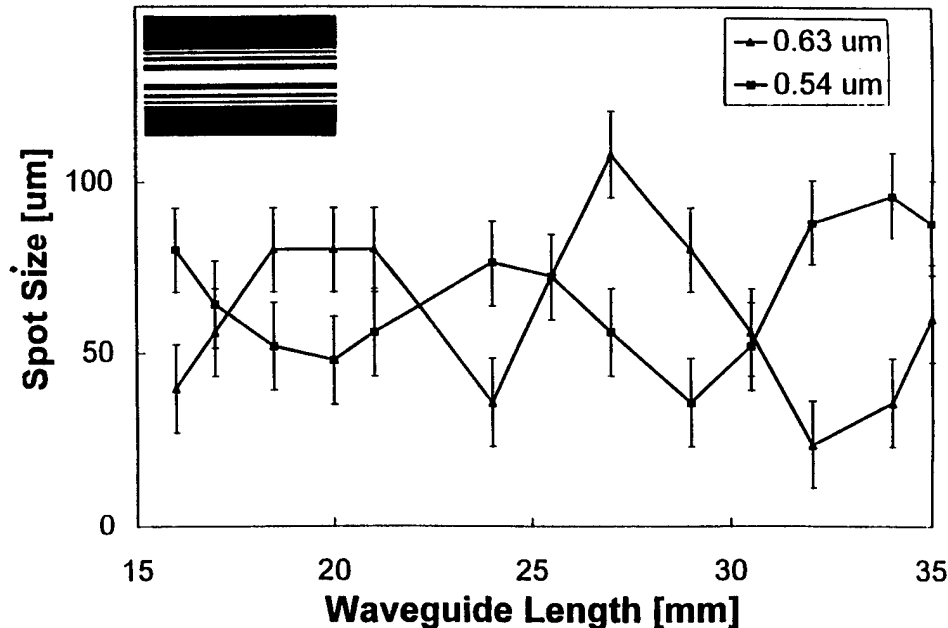
In conclusion, we explored the self-imaging effect in optical waveguides governed by index chirp modulations across its axis and along the entire waveguide. In addition to the ease of fabrication process, this demonstration may help to realize a wide variety of one or two dimensional, passive or active, optical interconnects, filters, dispersion lines and fiber-to-fiber couplers.

1. H. F. Talbot, Philos. Mag., 9, 401-407 (1836); Lord Rayleigh, Philos. Mag., 11, 196 (1881)

2. H. Grebel and W. Zhong, Opt. Letts., 18, 1123 (1993)

3. S-C. Tsay and H. Grebel, J. App. Opt., 33, 6747-6752 (1994).

4. J. Yardley in "Science and Technology of Thin Films for Waveguiding Non-Linear Optics", ed. by F. Kajar and J. D. Swalen, 1995.

Application of UV Cured Epoxy Resin to Polymeric Optical Waveguide Components

Satoru Tomaru, Koji Enbutsu, Makoto Hikita, Ryoko Yoshimura and Saburo Imamura
NTT Opto-electronics Laboratories Tokai, Naka-gun, Ibaraki, 319-11 Japan
TEL 81-292-87-7749 FAX 81-292-87-7870
*Tohru Maruno, Junya Kobayashi
NTT Opto-electronics Laboratories 9-11, Midori-cho, 3-chome, Musashino- shi,
*Tokyo 180 Japan TEL 81-422-59-2474   FAX 81-422-59-4490

1.*Introduction*   Many polymeric optical waveguides have been studied for use in the field of optical interconnection [1-3] because they offer such advantages as routing flexibility, process compatibility with electronic devices, and mass productivity. In particular, their application to multimode optical waveguide devices in the 0.85 μm wavelength region is attractive because polymeric materials generally have low loss. We have already realized polymeric multimode optical devices for optical interconnection[4,5].

In this paper, we report a multimode optical waveguide with low loss and an optical waveguide component with a V groove for a passive fiber alignment which we realized UV cured epoxy resins.

2.*UV cured epoxy resin*   The UV cured epoxy resin we used has certain advantages as an optical waveguide material. They are as follows.

(1)High thermal stability: The resin shows a high glass transition temperature
(Tg~ 200 °C). Therefore, it is expected to have good thermal stability.

(2)Precise controllability of refractive index: Their refractive indices can be easily controlled by mixing several UV curable epoxy resins[6]. The indices can be controlled precisely in the 1.48- 1.60 region with a 0.001 order accuracy.

(3)Simple processability as a negative-tone photoresist: Figure 1 shows a SEM photograph of a high aspect ratio microstructure formed by UV photolithography. The resin can be easily patterned with a conventional mask process using a UV light source.

We used the photocurable property of the epoxy resin to fabricate the multimode optical waveguide component.

3.*Fabrication of optical waveguide using UV cured epoxy resin*

We employed a photolithographic technique to fabricate the waveguide on the basis of the photocurable property of the resin. The details of the method are shown in Fig. 2. After forming an undercladding layer, core ridges are patterned directly by using a conventional mask process. Finally, these ridges are covered with an overcladding layer. Table 1 shows the parameters of the fabricated multimode waveguide. We measured the propagation loss of the fabricated waveguides using a singlemode fiber and a multimode 50 μm GI fiber as input and output fibers, respectively.   Figure 3 shows the near field pattern of the waveguide. Table 2 shows the losses at several wavelengths. Optical waveguides with a loss less than 0.1dB/cm

were obtained in the 0.85 μm wavelength region which is often used in the field of optical interconnection. The minimum loss was estimated to be 0.06 dB/cm at 0.83 μm. Because the UV cured epoxy resin used in the experiment has a high Tg (>200℃), the waveguide has good thermal stability. This thermal stability is now being investigated in detail.

4. Fabrication of optical waveguide component with V grooves by replication

Next, we fabricated an optical waveguide component with V grooves to provide passive fiber alignment with the polymer waveguide. Figure 4 shows the fabrication process of the component. We utilized the photocurable properties of the epoxy resin to fabricate a precise replica of the V grooves. We fabricated the master V grooves by the anisotropic etching of a Si wafer in a KOH solution. First, a replica of the V grooves was fabricated on a silica-glass substrate by curing UV curable epoxy oligomers inserted between the master V grooves and the substrate. Next, V grooves were replicated on a Si substrate by curing epoxy oligomers also inserted between the V groove replica and the Si substrate. The final replica which has V grooves and also act as a cladding layer in the optical waveguide structure can be obtained by selecting a UV resin with a suitable refractive index. We called the replica a polymeric optical bench (POB). Finally, a polymer optical waveguide was fabricated on the POB by photolithography. In that process, a mask aligner was used to ensure that the center position of the waveguide coincided precisely with that of the V grooves on the POB.

The width differences (Δw) between the replica on the POB and the master V grooves were almost all less than 1.0μm as shown in Fig. 5. The small Δw is considered to be due to the a small volume shrinking of the epoxy resin and is within the size tolerance needed for multimode fiber passive alignment. Figure 6 shows a SEM photograph of the 35mm-long straight waveguides we fabricated which were connected to multimode fibers inserted in the V grooves on the POB. The connection loss was estimated to be about 0.9 dB/point at 0.83 μm by measuring the insertion loss of the component.

5.Conclusions   We have realized a multimode optical waveguide with low loss (0.06 dB/cm) at a wavelength of around 0.85μm by using UV cured epoxy resin. Furthermore, an optical waveguide component which enabled passive fiber alignment to be achieved easily was obtained by a replication technique. Therefore, this UV cured epoxy resin is a promising material for use in fabricating polymeric optical waveguide components.

References 1. B. L. Booth, in Polymers for Electronic and Photonic Applications, C. P. Wong, Ed., New York : Academic, 1993, p 549. 2. J. Bristow et al., in Proc. SPIE, 2400, 1995, p.61 3. Kenneth H. Hahn et al., in Proc SPIE CR62, 1996, p. 393 4. A. Kaneko et al., POF'96, Paris, France, 1996, p.113 5.R.Yoshimura et al., Technical report of IEICE, 1996, p.43 6. N.Murata et al., J.Adhesion, 35, 1991, p.25
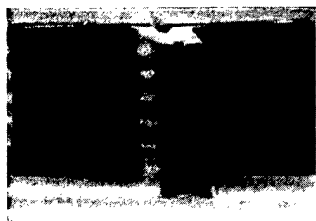
Figure 1.SEM photograph of microstructure
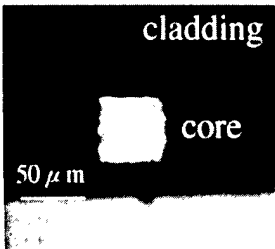
Figure 3. Near field pattern of multimode optical waveguide

Si substrate with V grooves
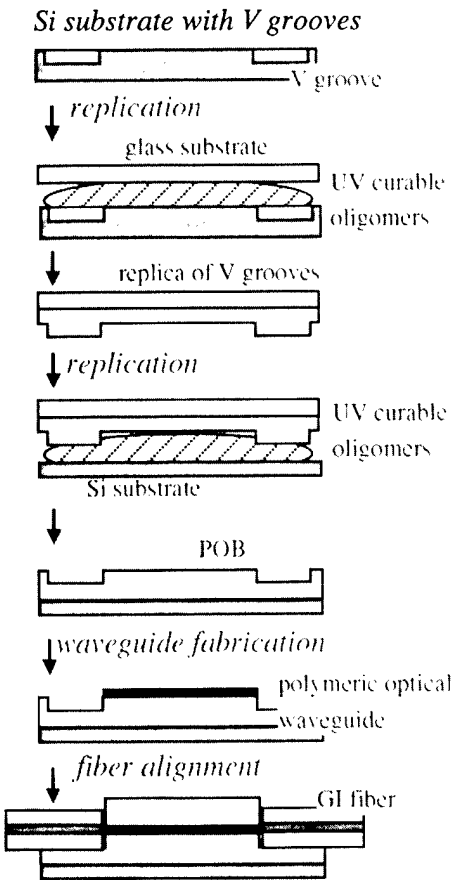
Figure 4 Polymeric optical waveguide component fabrication
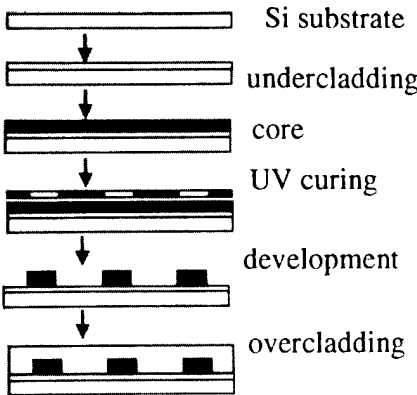
Figure 2.Multimode optical waveguide fabrication

Table 1   Multimode optical waveguide parameters

core	width	height	Δn
	45μm	42μm	0.85%

Table 2   Losses of multimode optical waveguides made of UV cured epoxy resin

Wavelength	680nm	830nm	1310nm	1550nm
Loss (dB/cm)	0.12	0.06	0.54	3.95
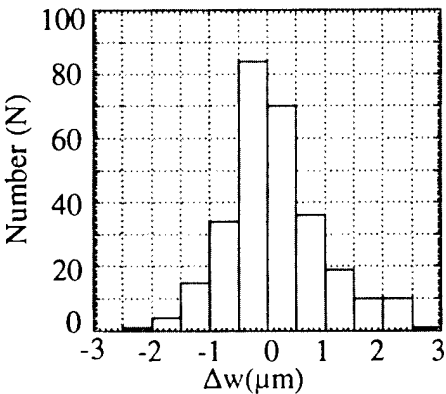
Figure 5 Width differences (Δw) of V grooves between replica and master multimode optical waveguide
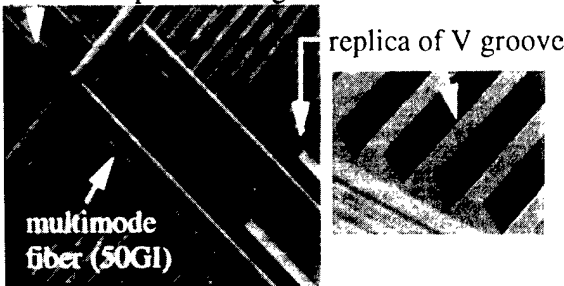
Figure 6 SEM photograph of optical waveguide component

Organic Thin Films for Photonics Applications

EO Devices II

Friday, October 17, 1997

Paul R. Ashley, U.S. Army Missile Command
Presider

FC
1:30pm–3:00pm
Seaview A&B

Next Generation Ultra-High Frequency Integrated EO Modulators

Datong Chen, Harold R. Fetterman, Boris Tsap, *Department of electrical Engineering, University of California at Los Angeles,*
Antao Chen, William H. Steier, *Department of Electrical Engineering, University of Southern California,*
Larry R. Dalton, Department of Chemistry, *University of Southern California,*
Wenshen Wang, Yongqiang Shi, *TACAN Corporation.*

Measurements of traveling wave modulators made from electrooptic polymer materials have now been extended to over 110 GHz using high frequency commercial probes. An optical heterodyne detection system (figure 1) has been developed to characterize those devices at high frequencies. The use of both YAG and tunable semiconductor lasers (tunable range of 8 THz) has helped to improve the detection range and sensitivity of the system. The frequency response of the system was limited only by the operation of our coplanar connecting probes.

The response as a function of frequency for these devices is shown in figure 2 and was virtually flat from 75 to 113 GHz. Combined with our previous measurements up to 60 GHz these results indicate that these devices have a remarkable broadband capability. In order to develop a integrated microwave packaging approach we have designed a configuration which incorporates microwave transitions from waveguide to microstrip. These transitions use anti-podal fin line on Mylar substrates, shown in figure 3 that have been characterized at W-band frequencies. As a result of the spin processing of these materials dozens of these phase modulators can be fabricated at once. The individual units in this design are separated and mounted with the straight portion comprising the travelling wave optical region.

Using these basic sections, with their lithographically defined transitions, it is possible now to look into new circuits and systems at frequencies in the range from 30 GHz to 140 GHz.. Instead of phase modulators our new balanced Y-branch technology will facilitate the use of Mach-Zehnders in both series and parallel configurations. The major losses in these modulators are not in the material absorption or scattering, but rather in the coupling in and out from fibers. Therefore low cost arrays, capable of performing critical signal processing roles, are now being designed for the next generation.
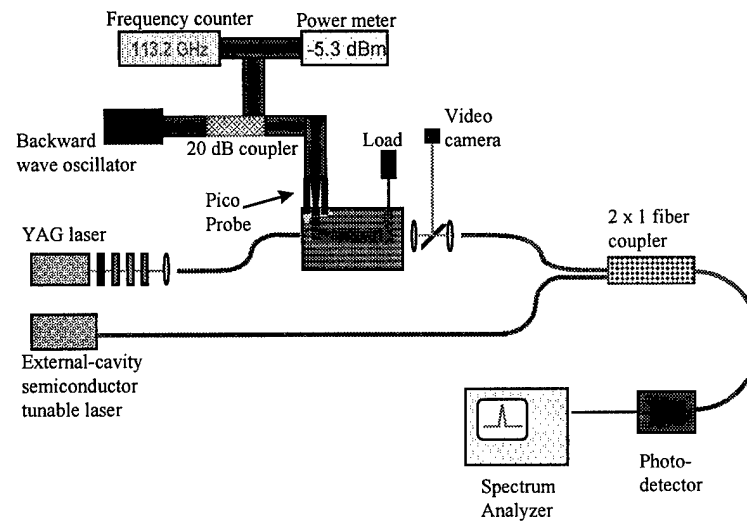
Figure 1. Heterodyne setup with semiconductor external cavity tunable lasers.
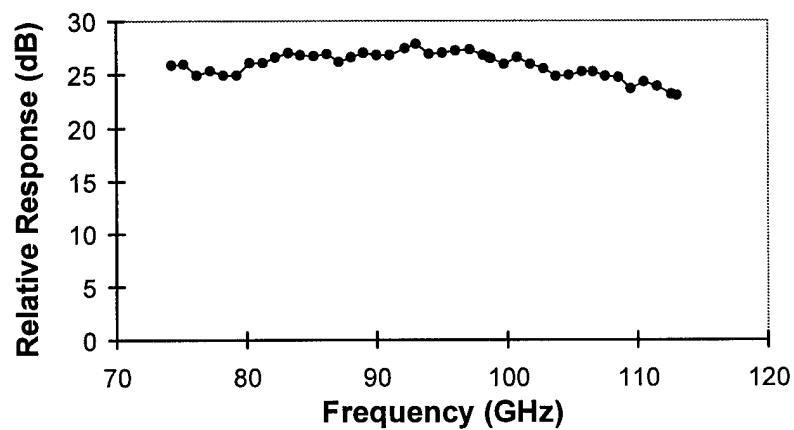
Figure 2. Modulator frequency response from 74 GHz to 113 GHz.
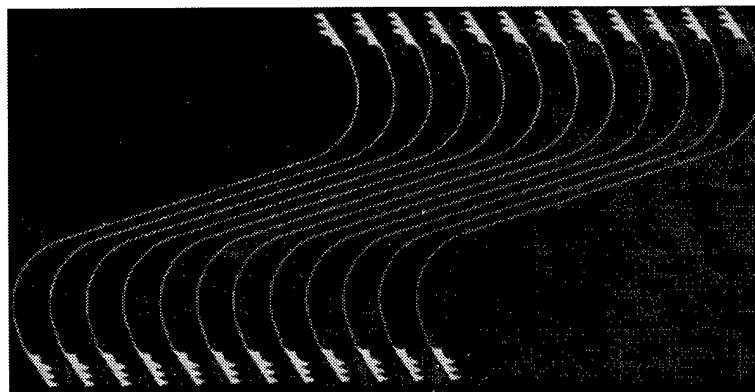
Figure 3. Top view of twelve W-band polymer modulators with integrated fin line transitions.

Characterization of Electro-Optic Polymer Films using Decal Deposited Reflection Fabry-Perot Modulators

L.-M. Wu, Ph. Prêtre, R. A. Hill and A. Knoesen
Department of Electrical and Computer Engineering
University of California, Davis, CA 95616
Phone: (916) 752 6251

Introduction. Electro-optic (EO) properties of nonlinear optical polymers (NLPs), of key interest in any device application, are most widely measured with ellipsometric(1, 2) or interferometric methods.(3) The major drawbacks of these techniques are: a) with ellipsometry, the Pockels coefficients cannot be extracted independently, b) refractive indices must be obtained from other measurements, and c) these methods ignore multiple reflection effects in stratified samples. Waveguiding methods such as attenuated total reflection (ATR) measurements are capable of a complete linear optical and EO characterization of NLPs.(4) But the ATR prism complicates the angular scans, and waveguiding conditions over a large spectral range are difficult to fulfill with a single sample.

For these reasons, Fabry-Perot étalon devices have attracted increasing interest for the characterization of poled NLP films.(5-9) NLPs are well suited for this type of device since they can be readily processed into thin films by spin coating. Metallic electrodes, a natural element in a Fabry-Perot étalon, can be used to apply an electric field across the NLP for the investigation of the EO effect. The interferometric nature of the cavity converts phase changes to amplitude changes, a distinct experimental advantage over external interferometric configurations.

This paper reports the use of reflection mode Fabry-Perot modulators (RFPM) as characterization tool. In contrast to the configurations mentioned above, with this structure, all of the desired linear optical and EO information of a NLP film can be extracted from angular scans of measured reflectance and change in reflectance due to a applied modulation field. The method is capable of performing dispersive measurements even at wavelengths with significant absorption therefore allowing the determination of complex linear and EO properties. The accuracy of the method has been studied in details.

In order to exhibit electro-optic activity, NLPs have to be poled either by applying an electric field across electrodes which are in contact with the NLP or by applying an electric field via a corona discharge.(10) To fabricate the RFPM, we utilized a processing technique, first developed for fabricating quasi-phasematched polymeric structures, which involves decal deposition of high quality, corona poled films selectively onto substrates without spin coating.(11) This lift-off technique allows a sequential device preparation with an accurate control over the processing conditions in every step, e.g. NLP thicknesses can be determined before the final assembly of the device.

Decal Deposition of Poled NLP Films. The decal deposition technique involves the deposition of the NLP onto a temporary substrate which is treated with a "release layer" (e.g. water soluble poly(acrylic acid)). Following deposition and corona poling, the NLP film is cut to the desired final size and released from the temporary substrate. The prepared and poled NLP film is then deposited onto the final substrate which is covered with a thick (~ 150 nm) metal ground electrode. As final step, a thin (~ 30 nm) top metal electrode is evaporated.

Experiments and Analysis. The reflection and modulation characteristics were measured using a $\theta - 2\theta$ rotation stage. From these TE and TM polarization scans the ordinary and extraordinary refractive indices are obtained from the analysis of reflection of light by an anisotropic stratified multilayer system.*(12, 13)* Knowing the linear parameters the Pockels coefficients r_{13} and r_{33} are then independently extracted from the modulation data. As an illustration of this characterization technique, the refractive indices of a 10 mole % Disperse Red 1/ PMMA side chain NLP have been determined to within ± 0.005, the NLP layer thicknesses to within 1% and electro-optic coefficients to within 5%. Corresponding reflectance and modulation scans for this NLP are shown in Fig. 1 and 2, respectively.
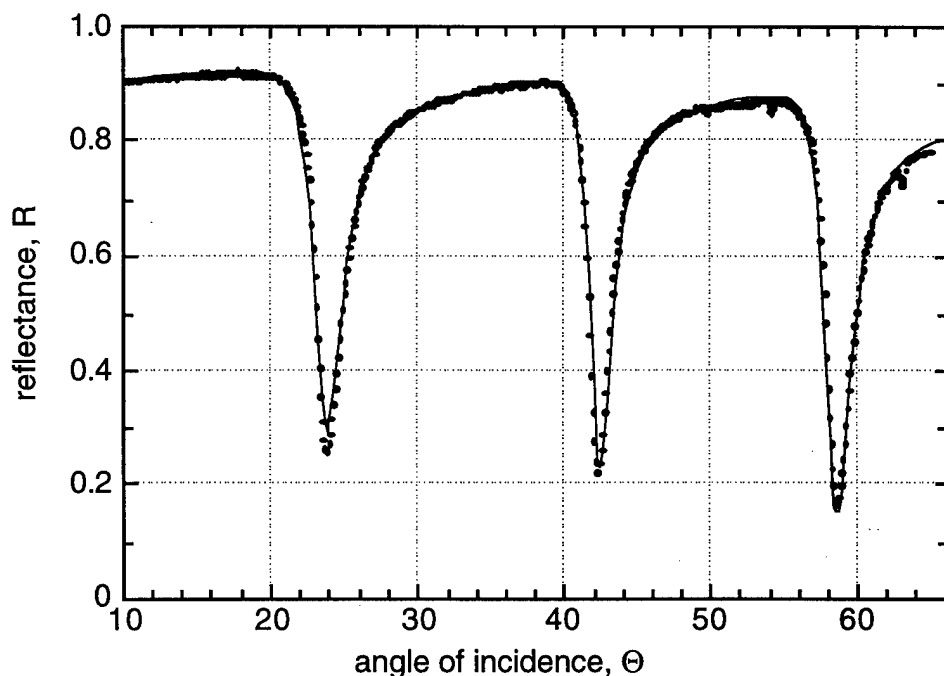
Fig. 1: Reflectance of a DR1-PMMA RFPM with gold electrodes for TM polarization as function of angle of incidence at $\lambda = 633$ nm. Solid line: least-squares fit from the stratified multilayer analysis.
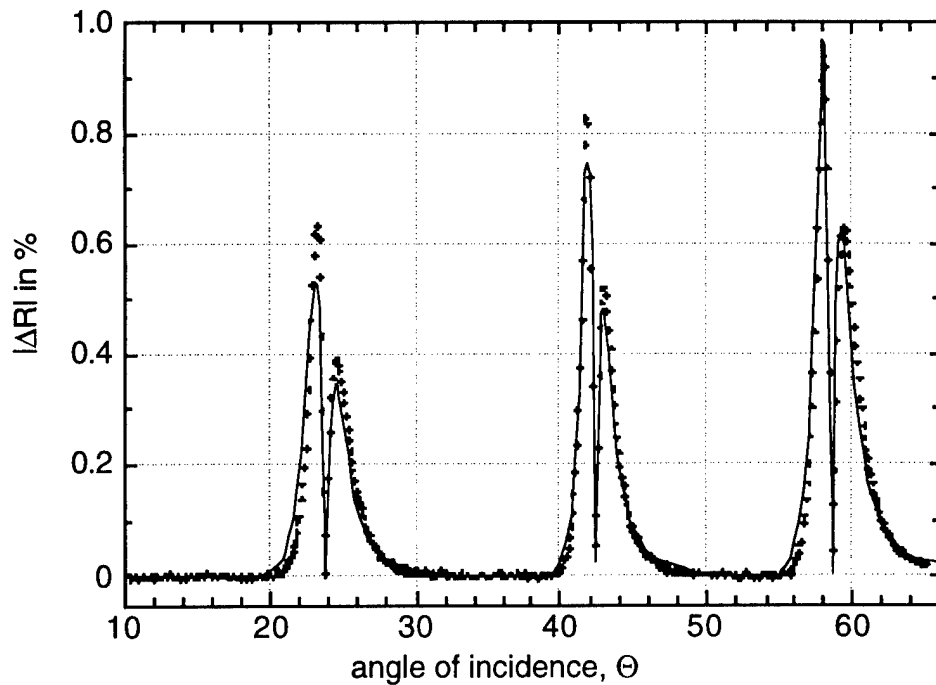
Fig. 2: Change in reflectance of the DR1-PMMA RFPM with gold electrodes for
TM polarization at $\lambda = 633$ nm.

References.

(1)   Teng, C. C.; Man, T. H., *Appl. Phys. Lett.* **1990**, *56*, 1734-1736.

(2)   Schildkraut, J. S., *Appl. Opt.* **1990**, *29*, 2839 - 2841.

(3)   Singer, K. D.; Kuzyk, M. G.; Holland, W. R.; Sohn, J. E.; Lalama, S. J.;
       Comizzoli, R. B.; Katz, H. E.; Schilling, M. L., *Appl. Phys. Lett.* **1988**, *53*, 1800.

(4)   Herminghaus, S.; Smith, B. A.; Swalen, J. D., *J. Opt. Soc. Am. B* **1991**, *8*, 2311.

(5)   Eldering, C. A.; Kowel, S. T.; Knoesen, A., *Appl. Opt.* **1989**, *28*, 4442-4445.

(6)   Uchiki, H.; Kobayashi, T., *J. Appl. Phys.* **1988**, *64*, 2625-2629.

(7)   Meyrueix, R.; Lecomte, J. P.; Tapolsky, G., *Nonlinear Optics* **1991**, *1*, 201 - 211.

(8)   Yankelevich, D. R.; Hill, R. A.; Knoesen, A.; Mortazavi, M. A.; Yoon, H. N.;
       Kowel, S. T., *IEEE Phot. Technol. Lett.* **1994**, *6*, 386-389.

(9)   O'Brien, N. F.; Dominic, V.; Caracci, S., *J. Appl. Phys.* **1996**, *79*, 7493.

(10)   Mortazavi, M. A.; Knoesen, A.; Kowel, S. T.; Higgins, B. G.; Dienes, A., *J. Opt.
       Soc. Am. B* **1989**, *6*, 733 -741.

(11)   Khanarian, G.; Mortazavi, M. A.; East, A. J., *Appl. Phys. Lett.* **1993**, *63*, 1462.

(12)   Azzam, R. M. A.; Bashara, N. M., *Ellipsometry and Polarized Light*, ed., North-
       Holland: Amsterdam, 1987.

(13)   Knoesen, A., *Appl. Opt.* **1991**, *30*, 4017.

Integrated electrooptic polymer devices for optical communications

Yongqiang Shi, Wenshen Wang, and James H. Bechtel
TACAN Corporation, 2330 Faraday Avenue, Carlsbad, CA 92008
Tel: (760)438-1010, Fax: (760)438-2412

William H. Steier and Larry Dalton
Department of Electrical Engineering, University of Southern California, Los Angeles, CA 90089

Harold R. Fetterman
Department of Electrical Engineering, University of California, Los Angeles, CA 90095

The rapid development in high speed optical communications has prompted a large demand in electrooptic (EO) modulators and switches which are currently made of $LiNbO_3$ and semiconductor materials. In order to reduce manufacturing cost and driving voltage, and extend the bandwidth of the EO devices, an intense research in EO polymer materials and devices is underway.

Device fabrication and applications tests are important parts of EO polymer research. The device fabrication process tells us whether the polymer materials can be coated into high quality thin films and are chemically compatible with other layers. The device tests will not only give a precise measurement of the EO coefficients of the materials, but also provide the information on the waveguide loss, thermal/temporal stability, photochemical stability, and the electrical compatibility of guiding layer with cladding layers. In this summary, we present our integrated EO polymer device design, fabrication, test, and performance optimization efforts aiming at the optical communication applications. Other devices such as electric field sensors and wavelength division multiplexers also can be fabricated with minor modifications.

EO polymer modulator fabrication

The EO polymer modulators we fabricated were based on two thermally crosslinked EO polymers, a polyurethane with Disperse Red 19 side chains (PUR-DR19) and an amino-sulfone chromophore based double-end crosslinked EO polymer LD-3. Both PUR-DR19 and LD-3 have moderate EO coefficients (7-14 pm/V) and can be crosslinked thermally at temperatures 130-200°C during electric field poling. The polymer thin films were spin-coated on a polyurethane lower cladding layer with compatible chemical and electrical properties. The waveguide patterns were defined by reactive ion etching, and sandwiched between the cladding layers to form a buried ridge waveguide structure. The device chips consist of a modulator array with matching microstrip line electrodes for high speed operation. The end-faces of the modulator chips were polished for fiber coupling. The top view of a typical modulator chip is shown in Fig. 1.
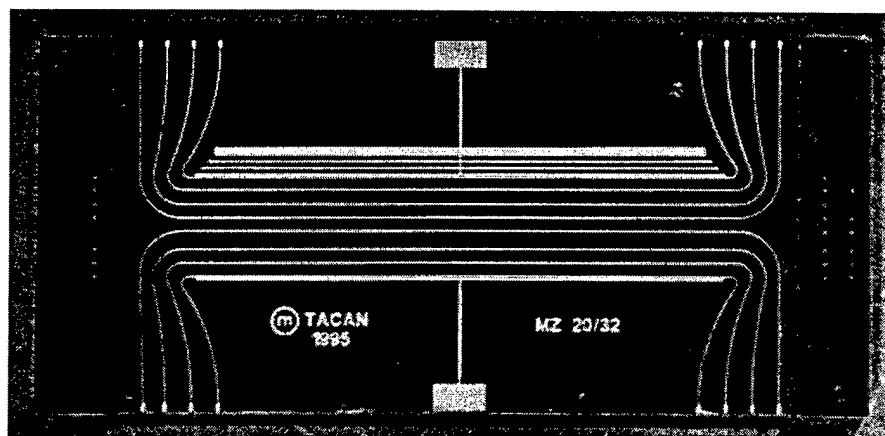
Fig.1   A PUR-DR19 Mach-Zehnder modulator array chip with microstrip line electrodes.

EO modulator test

Our modulator tests are focused on optical communication performance. These tests include halfwave voltage V_π, frequency response, insertion loss, and device operation stability. The measured V_π values ranged from 7.5-30 V depending on the modulator structure and material type. The frequency response of our EO polymer modulators was tested with an HP Lightwave Signal Analyzer. To the frequency limit of our tracking generator (2.7-18 GHz), the test E-O polymer modulator chip showed a very flat response, as shown in Fig.2(a). Good impedance match was obtained for the modulation electrode as measured by a network analyzer, shown in Fig. 2(b). Higher frequency modulation has been characterized on similar polymer modulator chips using optical heterodyne detection method.[1,2] The waveguide loss of the EO polymer waveguide was typically on the order of 0.8-1.5 dB/cm at 1.3 μm.

(a)   (b)
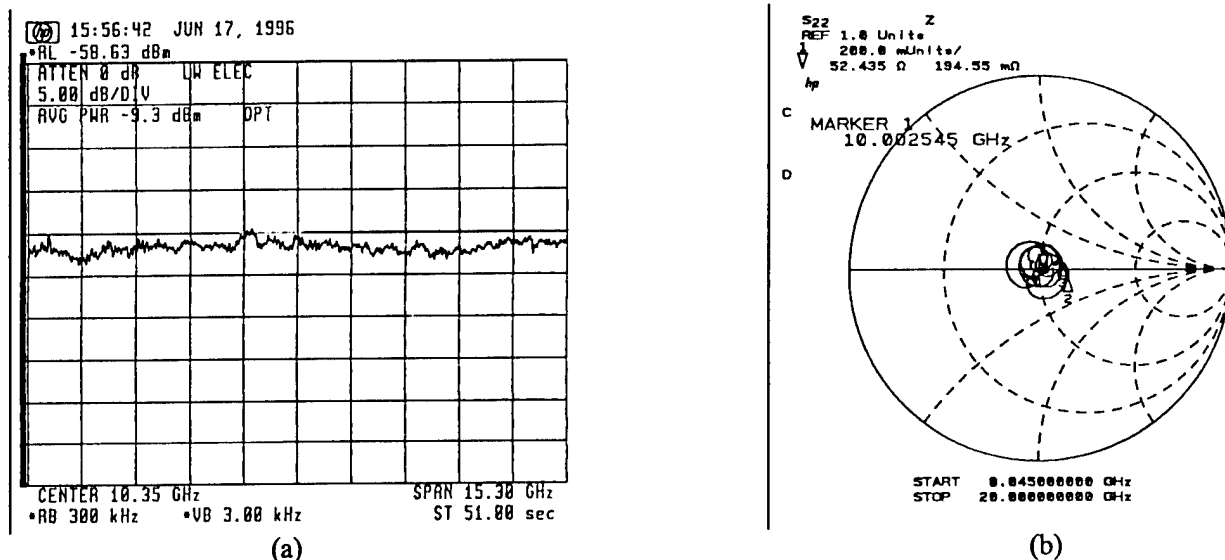
Fig. 2   Measured RF performance of EO polymer modulators. (a) Lightwave Analyzer scan from 2.7 to 18 GHz and (b) Smith chart of the microstrip line electrode.

Our EO polymer modulators have shown a stable second order nonlinearity at normal operation temperatures. For examples, the halfwave voltage of a packaged PUR-DR19 modulator has remained stable for nearly two years at room temperature and occasionally cycled to 60 °C. A grating modulator made of LD-3 showed a stable response when baked at 100 °C in air for over 1000 hours. The EO polymer modulators we fabricated also showed a traceable DC bias voltage for linear operations.

In our photochemical stability tests, modulators made of LD-3 and PUR-DR19 have exhibited photochemical stability better than those made of dimethylaminonitrostilbene containing polymer. Particularly, at an input optical intensity near 1 MW/cm^2, the test LD-3 modulator remained stable over the testing period of more than a week.[3]

Analog and digital optical communication applications

We have used a PUR-DR19 modulator for both analog and digital signal transmission system tests. The experimental signal transmission system consists of a Nd:YAG laser, polymer modulator, a Matrix Multiple Signal Generator, IPITEK CATV and digital receivers, HP Lightwave Analyzer and error detector, a Microwave Logic gigaBERT digital signal generator, and a Tektronix digital sampling oscilloscope. The analog signal transmission test used up to 80 CATV carrier frequencies as the modulation RF sources. With an optical modulation index of 3.4%, a carrier-to-noise ratio of 53 dB was obtained. A predistortion circuit was used to correct the third order intermodulation distortions. A spectrum analyzer scan of the output signal of a CATV channel (NTSC channel 2) is shown in Fig. 3(a).

In our digital signal transmission test, a clear eye pattern was obtained at 1.2 Gb/sec (receiver limit) with only $2V_{p-p}$ modulation level. At a received optical power of -16 dBm, no error was detected during the 200 second testing period, indicating a bit-error rate less than $4x10^{-12}$.

(a)   (b)
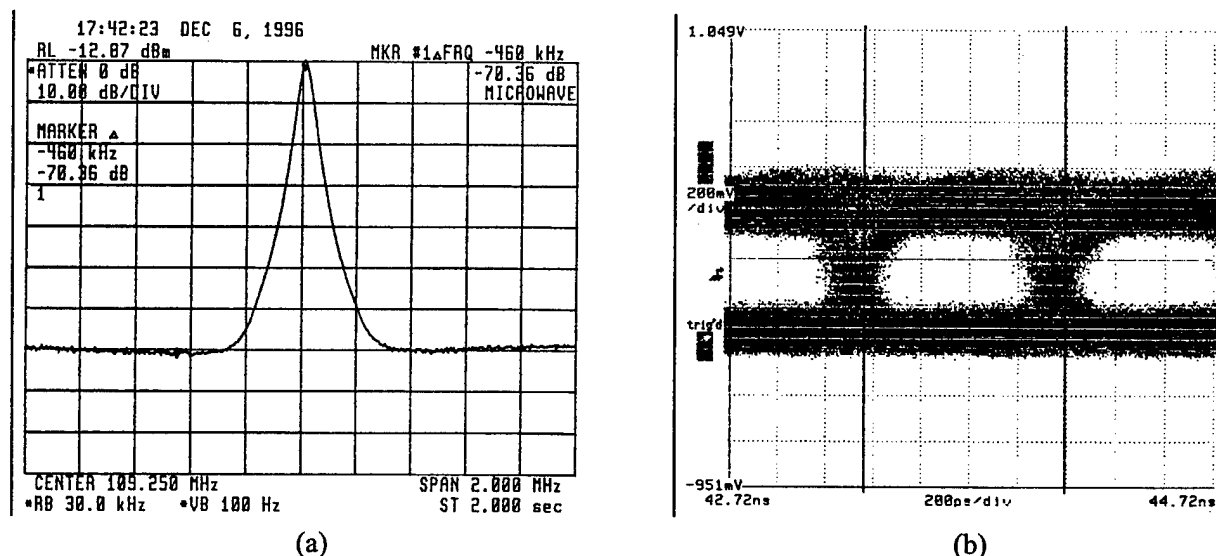
Fig. 3   (a) Spectrum analyzer scan of the transmitted CATV signal of the analog system, and (b) the eye pattern of 1.2 Gb/sec digital signal of the digital transmission system.

Device performance optimization

Our device performance optimization is focused on the reduction of halfwave voltage and the device optical insertion loss. Several approaches have been investigated to reduce the driving voltage of EO polymer modulators. One approach we implemented is the "optical push-pull" in which the modulation field generates opposite refractive index change between the two arms of a Mach-Zehnder modulator, yielding a doubled index change. In our devices, the two arms of the modulator are poled in opposite directions so that only one modulation electrode is required. We have successfully observed a reduction of V_π by a factor of 2 using this optical push-pull method.[4] Another approach is to use an active cladding layer to improve the modulation efficiency. In this case, the tail of the guided wave in the claddings will also experience the modulated index change and therefore the effective index modulation is higher than the structures with only an active guiding layer. The optical insertion loss in our devices is mainly due to the mode mismatch between the fiber/waveguide interface. The use of tapered waveguide coupling section can reduce the optical insertion loss significantly.

Summary

We have fabricated and tested high speed, stable, and low driving voltage EO polymer modulators and demonstrated their applications in analog and digital optical communication systems. Recent developments in optimizing EO polymer device performances are presented.

References

1.   D. Chen, et al., Proc. SPIE, **3006**, 314 (1997).
2.   W. Wang, et al., *Appl. Phys. Lett.*, **67**, 1806 (1995).
3.   Y. Shi, et al., *Appl. Phys. Lett.*, **70**, 1342 (1997).
4.   W. Wang, et al., unpublished result.

Recent Advances in the Translation of Large Microscopic Nonlinearities to Large Macroscopic Nonlinearities in Electro-Optic Polymer Films

Aaron W. Harper, Mingqian He, Fang Wang, Jinghong Chen, Jingsong Zhu,
Sam S. Sun, Larry R. Dalton*
Department of Chemistry, Loker Hydrocarbon Research Institute, University of
Southern California, Los Angeles, CA 90089-1661, (213)740-7103

Antao Chen, Sean M. Garner, Araz Yacoubian, William H. Steier
Department of Electrical Engineering-Electrophysics, University of Southern California,
Los Angeles, CA 90089-0483, (213)740-8781

Datong Chen, H.R. Fetterman
Department of Electrical Engineering, University of California at Los Angeles,
Los Angeles, CA 90095, (310)206-9457

Typical electro-optic polymers are characterized by second-order nonlinear optical (NLO) chromophores arranged polar-asymmetrically in an amorphous polymer matrix. It is believed that the electro-optic activity of workhorse NLO chromophores (e.g., DANS and Disperse Red) are of insufficient magnitude to be viable candidates for commercial device-quality materials.[1] Consequently, much effort has been directed in the past few years toward the development of chromophores with device-quality magnitudes of molecular optical nonlinearities. Unfortunately, the translation of these so-called high-β chromophores to the expected bulk electro-optic activities in polymers generally has not been achieved. Recently, we have shown that this lack of electro-optic activity is due primarily to strong intermolecular electrostatic interactions between chromophores, which tend to align the chromophores in an antiparallel fashion, resulting in no net polar asymmetry in the bulk material.[2,3] Modification of the equation used to describe the polar order, to account for electrostatic intermolecular interactions (orientation, induction, and dispersion effects) gives

$$\left\langle \cos^3 \theta \right\rangle = \frac{\mu f E}{5kT}\left[1 - L^2\left(\frac{W}{kT}\right)\right] \tag{1}$$

where L is the Langevin function, $L(x) = \coth(x) - 1/x$, the argument being the reduced crystallization potential energy and W is the crystallization potential energy,

$$W = -\frac{1}{r^6}\left[\frac{2\mu^4}{3kT(4\pi\varepsilon_0)^2} + \frac{2\mu^2\alpha}{(4\pi\varepsilon_0)} + \frac{3}{4}\alpha^2 I\right] \tag{2}$$

Substitution of equation (1) into equation (3),

$$r_{eff} = \frac{2NF\beta}{n^4}\langle\cos^3\theta\rangle \qquad (3)$$

allows for the calculation of the effective electro-optic coefficient. Figure 1 demonstrates that this model accurately describes the behavior of both conventional and high-β chromophores. Magnitudes of W calculated for a variety of chromophores indicates that intermolecular electrostatic interactions are of sufficient magnitude in high-β chromophores to overcome the dipole alignment energy (arising from the interaction of the molecular dipoles with the poling electric field) at modest chromophore loading densities.[4] This is reflected in the positions of the inflections in the curves of figure 1.
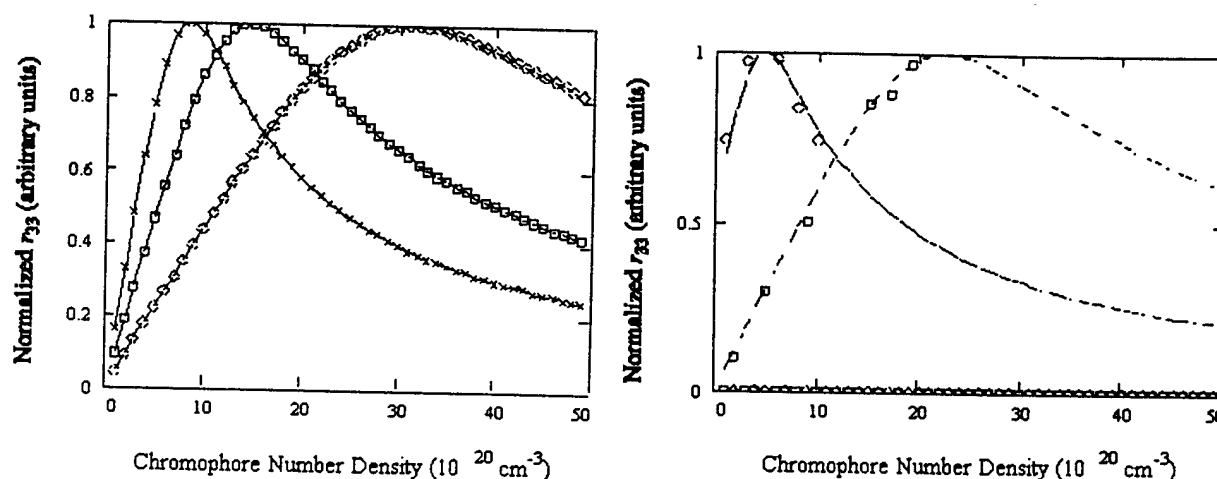
Figure 1. (left) Theoretical plot of normalized electro-optic coefficient as a function of chromophore loading density for azobenzene and stilbene-type chromophores. (right) Comparison of experiment to theory for Disperse Red/PMMA and ISX/Polycarbonate films.

Other support for this model comes from the electrochromic behavior of polymer films containing high-β chromophores. Thermal depoling of such films results in a total disappearance of second-harmonic generation, but no recovery of the absorption attenuation incurred upon the initial poling treatment. We believe that thermal treatment of these films results in the formation of ordered domains of anti-parallel arranged chromophore aggregates. Further evidence comes from pulsed poling field treatments of these films. Electro-optic coefficients obtained from periodically spiked poling fields are typically more than four times larger than those poled under static fields. These observations suggest that intermolecular electrostatic interactions cannot be neglected in the design and preparation of high-β chromophore-containing electro-optic films.

We have explored the chemical derivatization of high-β chromophores to defeat these deleterious electrostatic intermolecular interactions.[5-7] Examples of some of these chromophores, as well as their behavior in polymer films, are shown in Figure 2. In each case, the chromophores possess architectures that sterically interfere with close approach of neighboring chromophores, to an extent that diminishes the magnitude of the electostatic interactions. This results in more

effective dipole alignment of the chromophores in the film, and so a greater electro-optic coefficient is obtained (compared to the underivatized analog, at the same number loading density).
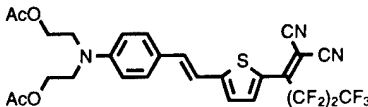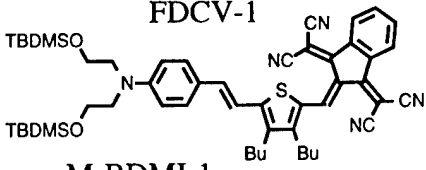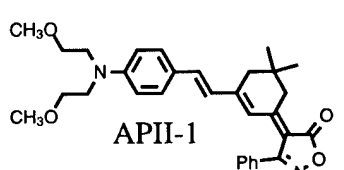
Chromophore	weight % in PMMA	r_{33} (pm/V) at 1.064 μm	optical loss at 1.3 μm (dB/cm)
FDCV-1	25	28	1
M-BDMI-1	40	42	-
APII-1	45	30	0.98

Figure 2. Performance of chromophores designed to defeat intermolecular electrostatic interactions.

References

1. L.R. Dalton, A.W. Harper, R. Ghosn, W.H. Steier, M. Ziari, H. Fetterman, Y. Shi, R.V. Mustacich, A.K.-Y. Jen, K.J. Shea, Chem. Mater. **7**, 1060(1995)
2. L.R. Dalton, A.W. Harper, B.H. Robinson, *Proc. Natl. Acad. Sci. USA, in press.*
3. A.W. Harper, S. Sun, M. He, J. Zhu, L.R. Dalton, S.M. Garner, A. Chen, A. Yacoubian, S. Kalluri, W.H. Steier, B.H. Robinson, *J. Opt. Soc. Am. B, Opt. Phys., in press.*
4. A.W. Harper, L.R. Dalton, *J. Am. Chem. Soc., submitted.*
5. Fang Wang, Aaron W. Harper, Mingqian He, Larry R. Dalton, Sean M. Garner, Araz Yacoubian, William H. Steier, *Polymer Preprints* **38(1)**, 971-972(1997).
6. Jingsong Zhu, Mingqian He, Aaron W. Harper, Sam-Shajing Sun, Larry R. Dalton, Sean M. Garner, William H. Steier, *Polymer Preprints* **38(1)**, 973-974(1997).
7. Jinghong Chen, Jingsong Zhu, Aaron W. Harper, Fang Wang, Mingqian He, Shane S.H. Mao, Larry R. Dalton, Antao Chen, William H. Steier, *Polymer Preprints* **38(2)**, *in press.*

Photorefraction

Friday, October 17, 1997

Kenneth D. Singer, Case Western Reserve University
Presider

FD
3:30pm-5:15pm
Seaview A&B

High performance photorefractive polymers and their applications

B. Kippelen, B. L. Volodin, E. Hendrickx, D. D. Steele, Sandalphon, Y. Enami,
J. F. Wang, H. Röckel, F. Meyers S. R. Marder,[1], [2] and N. Peyghambarian
Optical Sciences Center, The University of Arizona, Tucson, AZ 85721
[1] *Beckman Institute, California Institute of Technology, Pasadena, CA 91125*
[2] *Jet Propulsion Laboratory, California Institute of Technology, Pasadena, CA 91109*

Within the past years, photorefractive polymers have gained in maturity and are emerging as a promising new class of materials for photonic applications.[1,2] Several applications ranging from holographic storage to real-time optical processing[3] have been demonstrated with highly efficient photorefractive polymers. In polymers with a low glass transition temperature, orientational effects were identified[4] and were found to have the strongest contribution to the overall refractive index modulation amplitude.[5] Due to these orientational effects, the design criteria or figure of merit of chromophores for photorefractive applications differ from those of purely electro-optic applications. When both the orientational birefringence and the electro-optic effects contribute to the total refractive index modulation amplitude, the new molecular figure of merit F becomes:

$$F = \left[A(T) \Delta\alpha \, \mu^2 + \beta \, \mu \right] \tag{1}$$

where $\Delta\alpha$ is the molecular polarizability anisotropy, μ the dipole moment of the molecule, β the first hyperpolarizability, and $A(T) = 2/9kT$ is a numerical scaling factor. Calculations in the frame of the BOA (bond order alternation) performed on the chromophore $(CH_3)_2N(CH=CH)_4CHO$ show that the orientational contribution $A(T)\Delta\alpha\mu^2$ is optimized when the molecule is polarized beyond the cyanine limit in a region of BOA where the electro-optic contribution $\beta\mu$ peaks, but is opposite in sign.[6] This result can be explained as follows: calculations show that the polarizability α exhibits a peak at BOA = 0 at the cyanine limit for this molecule.[7] However, the dipole moment μ increases nearly linearly with BOA over the region considered, and thus μ^2 increases quadratically with BOA. Consequently, $\Delta\alpha\mu^2$ has its peak shifted to higher BOA values beyond the cyanine limit.

Based on these results, we synthesized the polyene molecule 2-N,N-dihexylamino-7-dicyanomethylidenyl-3,4,5,6,10-pentahydronaphthalene (DHADCMPN) shown in Fig. 1. Its structure is different from linear polymethines and has been modified to comply with the practical requirements of a well-performing photorefractive polymer: (i) *n*-hexyl groups on the amine donor group to impart high solubility and low aggregation; (ii) a fused ring bridge to prevent photoisomerization, to reduce aggregation, and to improve thermal and photochemical stability; (iii) CN which are thermally stable and contribute to a large dipole moment; (iv) sufficient ground-state charge transfer to lead to low BOA and therefore a sharp absorption edge. The molecule was used as a

dopant molecule in mixtures of poly(N-vinylcarbazole) (PVK) and ethylcarbazole (ECZ) that act as the photoconducting matrix. The photorefractive properties were tested by four-wave mixing and two-beam coupling experiments in the tilted geometry described in Ref. 5.
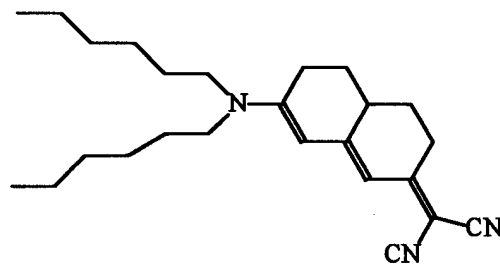
Fig. 1: Chemical structure of the DHADCMPN photorefractive chromophore

To compare the performance of DHADCMPN with that of previous organic photorefractive materials, we fabricated samples with 2,4,7-trinitrofluorenone (TNF) as a sensitizer. The diffraction efficiency corrected for the linear zero-field absorption in the sample (normalized diffraction efficiency) measured at 633 nm is shown in Fig. 2. for 105 μm-thick samples with composition DHADCMPN:PVK:ECZ:TNF (40:38:20:2 % wt.). As shown in Fig. 2, maximum diffraction is observed 105-μm-thick samples at an applied field of 30 V/μm at 633 nm, corresponding to an improvement of Δn by a factor of four compared to previous DMNPAA-based polymers with 50% wt. chromophore loading.[5] To investigate the long term stability of DHADCMPN-based samples we performed optical scattering experiments as a function of time and temperature. In order to observe crystallization on a reasonable time scale, we accelerated the process by heating the samples to 85 °C (below the melting point of the chromophores) in air. The degree of crystallization was quantified by measuring the amount of light scattered by the samples within a fixed solid angle. A reference time which is related to the lifetime of the sample was defined as the onset of crystallization after the nucleation period. DMNPAA-based samples with 40% wt. doping exhibited a reference time of 1 min. In contrast, DHADCMPN-based samples with the same chromophore loading had a reference time of 220 min, corresponding to two orders of magnitude improvement over DMNPAA-based samples.

To enable new applications we developed photorefractive polymers that have high efficiency in the near infra-red (IR) part of the spectrum (> 800 nm). This work is driven by: (i) the compatibility with the emission of high quality GaAs semiconductor laser diodes and commercial solid-state femtosecond lasers, such as Ti:Sapphire lasers; (ii) overlap with the transparency window of biological tissues to enable medical imaging applications. For that purpose, we developed new polymers based on the sensitizer (2,4,7-trinitro-9-fluorenylidene)malonitrile (TNFDM). The charge transfer complex formed by TNFDM and carbazole moieties provides spectral sensitivity up to 900 nm. At 830 nm, total diffraction is observed in samples of DHADCMPN:PVK:ECZ:TNFDM samples with composition (40:38:20:2 % wt.) at an applied field of 50 V/μm in 105-μm-thick samples, exceeding the performance of previous polymers in the visible.
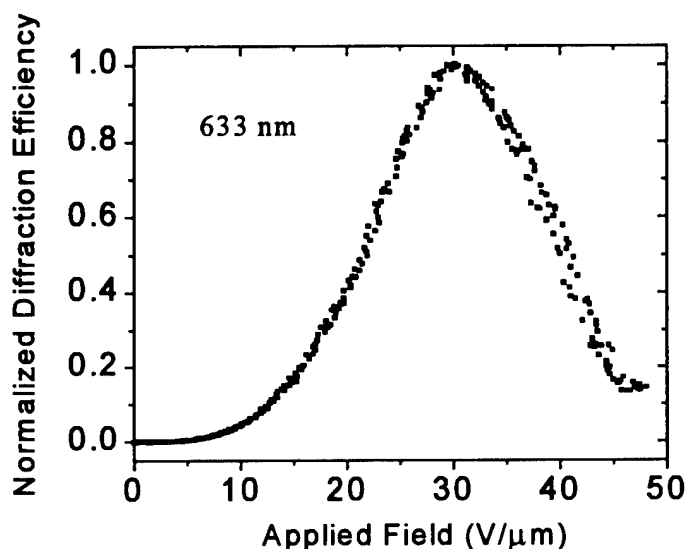
Fig. 2: Normalized diffraction efficiency measured by four-wave mixing experiments at 633 nm in a 105 μm-thick samples of DHADCMPN:PVK:ECZ:TNF (40:38:20:2 % wt.)

With these new IR-sensitive photorefractive polymers we developed an application that enables the imaging through scattering media using ballistic photons in an all-optical, femtosecond holographic time-gate. Imaging through scattering media with an effective optical density of four was demonstrated at 800 nm using a mode-locked/continuous-wave Ti:sapphire laser.[8]

[1] Moerner, W. E., Silence, S. M., *Chem. Rev.* **94**, 127 (1994)

[2] Kippelen, B., Meerholz, K. & Peyghambarian, N. in *Nonlinear Optics of Organic Molecules and Polymers,* Nalwa, H. S. & Miyata, S., Eds. (CRC Press, Boca Raton 1997);

[3] Volodin, B. L., Kippelen, B., Meerholz, K., Javidi, B. & Peyghambarian, N., *Nature* **383**, 58-60 (1996).

[4] Moerner, W. E., Silence, S. M., Hache, F. & Bjorklund, G. C. *J. Opt. Soc. Am. B*, **11**, 320 (1994).

[5] Meerholz, K., Volodin, B. L., Sandalphon, Kippelen, B. & Peyghambarian, N. *Nature* **371**, 497-500 (1994).

[6] Kippelen, B., Meyers, F., Peyghambarian, N. & Marder, S. R., *J. Am. Chem. Soc.* in press (1997).

[7] Meyers, F., Marder, S. R., Pierce, B. M., and Brédas, J. L. *J. Am. Chem. Soc.* **116**, 10703 (1994).

[8] Steele, D.D., Volodin, B. L., Savina, O., Röckel, H., Marder, S. R., Kippelen, B., Peyghambarian, N., submitted (1997).

Organic photorefractive composite dynamics

JD Shakos, AM Cox, DP West*, KS West and TA King
Laser Photonics Group, University of Manchester, Manchester M13 9PL, UK

RD Blackburn
Liverpool John Moores University, Byrom Street, Liverpool L3 3AF, UK

*Email: Dave.West@man.ac.uk
Tel +44 161 275 4103

Several devices such as holographic memory elements and adaptive optical components benefit from a rapid rate of recording of diffraction gratings. In reorientationally-enhanced photorefractive materials[1], the total electro-optic response is due to a combination of the electronic electro-optic effect (or Pockels effect) and the reorientation of polar birefringent molecules in the presence of the local electric field. This reorientational effect can be significantly larger than the Pockels effect in these materials, but may be slow due to the characteristic reorientation times of these polar molecules. This effect depends largely on the reorientational mobility of the molecules, which correlates with the material viscosity.

The polymer composites tested here consisted of poly(N-vinylcarbazole) (PVK) as the charge transporting polymer; 2,4,7-trinitro-9-fluorenone (TNF) as a charge generation sensitiser and an azo-dye derivative 1-(2'-ethylhexyloxy)-2,5-dimethyl-4-(4''nitrophenylazo)benzene (EHDNPB) added to provide the electro-optic response (both electronic and reorientational). No separate plasticiser is used as the composite is plasticised by a high content of electro-optic dye. The resulting polymer composite (EHDNPB:PVK:TNF) is stable with good optical quality and longevity of the resulting device[2].

Composites with 47.5% and 55% by weight of the EHDNPB dye were synthesised. The percentage of the charge generation sensitiser, TNF, was in both cases 1% by weight. PVK making up the remainder of the composite. Concentrations of up to a maximum of 55% wt. of dye in the polymer matrix were found to be free from crystallisation over many months. Composites with less than 47.5% wt. dye tended to be brittle with an increased material viscosity. Within the composition range 47.5% wt. to 55% wt. electro-optic dye, observations of strong photorefractive behaviour were possible.

In the regime of low intensity writing beams, charge generation is the limiting factor in grating formation, but at higher intensities, charge transport or reorientation of dye molecules can be the rate limiting step in grating formation. By Degenerate Four Wave Mixing (DFWM) techniques grating risetimes of 700 ms and 400 ms were measured in composites of 47.5% wt. and 55% wt. of electro-optic dye (fig. 1) respectively. In the high dye concentration case it is proposed that the charge carrier mobility of the doped poly(N-vinylcarbazole):2,4,7-trinitro-9-fluorenone (PVK:TNF) matrix is the limiting factor in grating response rates.

A Mach-Zehnder interferometer was constructed in which the phase of a beam of light passed through an optical medium is compared with that of a reference arm to detect small changes in phase and consequently in the refractive index. This technique enabled measurement of electro-optic response as a function of frequency of modulation of the poling field (fig 2). At high frequencies, the reorientational effect is insignificant and only the electronic Pockels electro-optic effect is observed. At low frequencies, both electronic and reorientational effects contribute to the r_{13} coefficient. Results for modulation frequencies lower than 15 Hz are distorted by low-frequency instability of the lock-in amplifier, hence the statistical errors involved in such measurements are much larger than for the higher frequency measurements. As the temperature increases, the reorientational mobility of the dye molecules increases. At high enough temperatures, the increased reorientational mobility permits the maximum orientational response to occur at an elevated frequency measurable with this experimental setup.

The alignment parameter is inversely proportional to the absolute temperature[3] and proportional to the poling field when far from alignment saturation[4]. The reduction in electro-optic response, due to thermal noise, at higher temperatures can therefore be normalised. The normalised steady state electro-optic response at room temperature (20 °C) is 0.85 pm/(V/μm) for the 47.5 % dye content sample and 0.89 pm/(V/μm) for the 55 % wt. dye content sample. We calculate a carrier mobility in the composite of $5 \times 10^{-10} cm^2 V^{-1} s^{-1}$. This figure is well in excess of two orders of magnitude lower than the well documented carrier mobility for a pure PVK:TNF matrix of $10^{-7} cm^2 V^{-1} s^{-1}$[5]. The composite system used in the work described here is doped over 50% wt. with highly polar chromophores. A similar reduction in the magnitude of the mobility in PVK:TNF systems when doped with polar molecular species has been reported previously[6,7,8]. The value of mobility obtained in this work is consistent with mobility values reported for these analogous systems.

Mach-Zehnder Interferometry and DFWM techniques indicate that the rate of response of the photorefractive polymer composite (EHDNPB:PVK:TNF) is not limited critically by charge generation, once above a specific optical intensity threshold. The reorientation of birefringent molecules is also significantly faster than the build-up time of the space charge field for the fastest, high dye-content sample. The reduced charge carrier mobility distribution in the PVK:TNF:dye composite is the limiting factor to the photorefractive response rate.

[1] M.C.J.M. Donckers, S.M. Silence, C.A. Walsh, F. Hache, D.M. Burland, W.E. Moerner and R.J. Twieg, Opt. Lett., 18, 1044 (1993).
[2] A.M. Cox, R.D. Blackburn, D.P. West, T.A. King, F.A. Wade and D.A. Leigh, Appl. Phys. Lett. 68, 2801 (1996).
[3] D.J. Williams, Nonlinear optical properties of organic molecules and crystals, D.S. Chemla and J. Zyss, ed. (Academic Press, 1987), Vol. 1, Chap. II.7.
[4] C.J.F. Bottcher, Theory of Electric Polarisation, (Elsevier, 1973), Vol. 1, pp. 161.
[5] M.D. Tabak, D.M. Pai and M.E. Scharfe, J. Non-Cryst. Solids, 6, 357 (1971).
[6] G.G. Malliaras, V.V. Krasnikov, H.J. Bolink and G. Hadziioannou, Phys. Rev. B, 52, 14324 (1995).

[7] G. G. Malliaras, V.V. Krasnikov, H.J. Bolink and G.Hadziioannou, Appl. Phys. Lett., **67**, 455 (1995).

[8] A. Dieckmann, H. Bässler and P.M. Borsenberger, J. Chem. Phys., **99**, 8136 (1993).
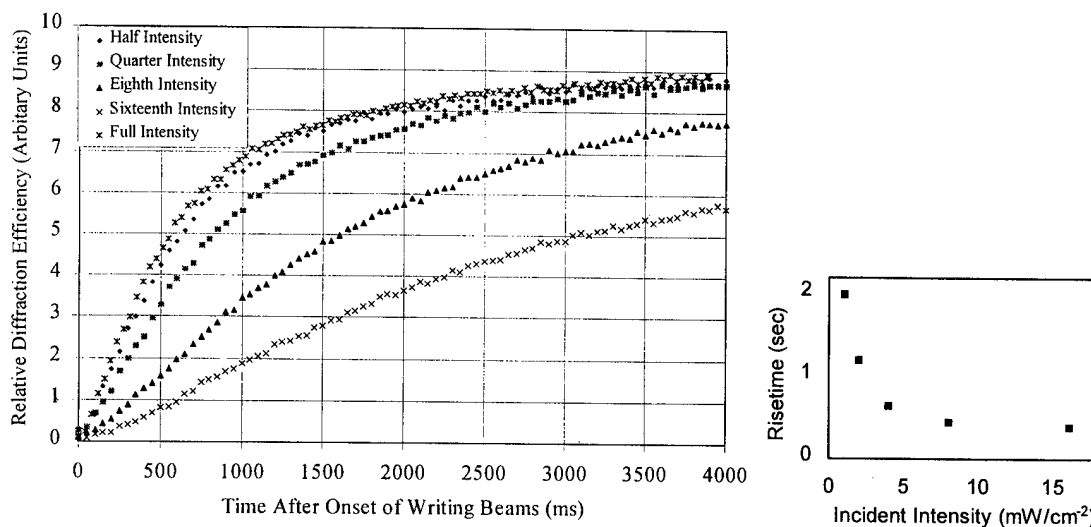
Fig. 1: Holographic diffraction efficiency risetime of the photorefractive device over a range of pump beam intensities for 55% wt. composite (both writing beams are of same intensity; full pump beam intensity is approximately 16 mWcm^{-2}). Right: Charge generation ceases to be the limiting factor for intensities greater than 8 mWcm^{-2}.
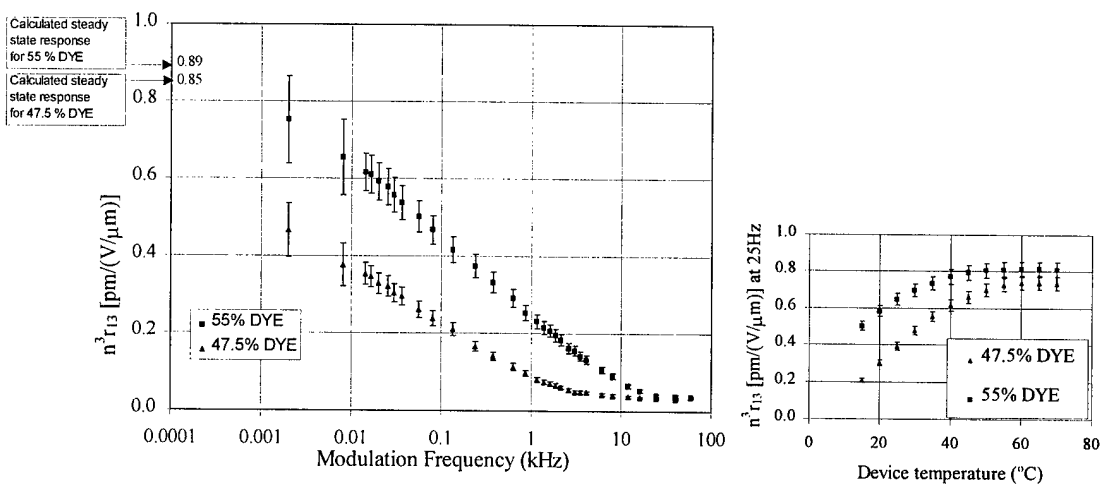
Fig. 2: Electro-optic response as a function of field modulation frequency for the two compositions at 20 °C, normalised to sample thickness. The right hand chart shows how the temperature affects the electro-optic response at 25 Hz modulation from which the steady state electro-optic response can be estimated.

Recent Advances in High Gain Photorefractive Polymers

A. Grunnet-Jepsen and W. E. Moerner

Department of Chemistry and Biochemistry, University of California San Diego
9500 Gilman Dr. M/C 0340, La Jolla, CA 92093-0340
phone: 619 822 0243, fax: 619 534 7244, email: agrunnet@ucsd.edu

With the discovery of photorefractivity in inorganic crystals in the late sixties [1,2], it was soon realized that the photorefractive (PR) effect had a large potential within the field of nonlinear optics. The versatility of the effect has since been clearly demonstrated by numerous applications ranging from holographic data storage and image processing to Bragg interference filters, optical interconnects, optical tracking systems, and self-pumped phase conjugate mirrors [3]. The class of photoconductive, electrooptic crystals that exhibited the PR effect quickly expanded to include ferroelectric oxides ($BaTiO_3$, $LiNbO_3$), sillenites ($Bi_{12}SiO_{20}$, $Bi_{12}TiO_{20}$, $Bi_{12}GeO_{20}$) and compound semiconductors (GaAs, InP, CdTe), to mention just a few. Recently completely new classes of materials have been proposed based on polymeric materials, organic glasses, and liquid crystals [4-6]. With the advantage of ease of processing, low cost, and high performance, these materials promise to be good candidates for present and future applications.

We report here on the development and characterization of high gain photorefractive polymers. Emphasis will be placed on a novel stable composite of the photoconductor poly(n-vinyl carbazole), PVK, the charge generator C_{60}, the nonlinear optical chromophore 4-piperidino-benzylidene-malononitrile (PDCST provided by R. J. Twieg), and the liquid plasticizer
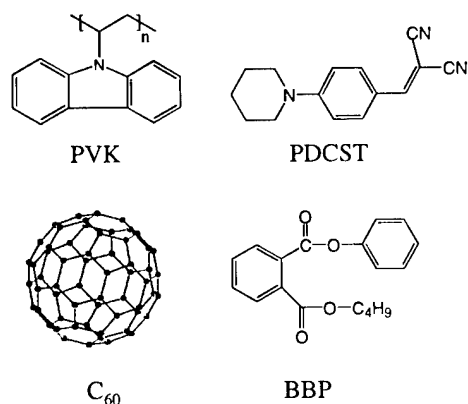
Figure 1 Sample components: charge-transporting network poly(n-vinyl carbazole) (PVK), nonlinear optical chromophore 4-piperidinobenzylidene-malononitrile (PDCST), the fullerene C_{60}, and the liquid plasticizer butyl benzyl phthalate (BBP).

butyl benzyl phthalate, BBP (see Fig. 1). The optical properties of this material, denoted PVK:PDCST:BBP:C_{60}, have been reported recently [7], and the material has been shown to exhibit a high two-beam coupling gain coefficient (Γ=200/cm at 120V/μm), fast response time (τ_g=50 ms at 1W/cm^2), over-modulation of diffraction efficiency, high sensitivity, and high stability.

Using such high gain coefficients, we have recently observed amplified scattering (beam fanning) in a photorefractive polymer for the first time. The manifestations of beam fanning and the implications for two-beam coupling measurements are investigated experimentally, and optimal geometries for observing or avoiding fanning are presented.

Optical processing with photorefractive polymers depends upon achieving high optical gain, which depends exponentially upon the product of the interaction length and the gain coefficient, gain=exp(ΓL) assuming no pump depletion. Unfortunately, the thickness of PR polymers have typically been limited to ~100μm due to technical reasons. We present one approach to overcoming the low ΓL: the use of several polymer layers to increase the overall interaction length. This configuration produces optical one-pass gains as large as a factor of 5 in a three-layer sample (See Fig. 2). For a two-layer sample placed in an optical cavity made with two concave mirrors, the PR gain can exceed the total optical losses and *spontaneous* oscillation can be observed. Because only one
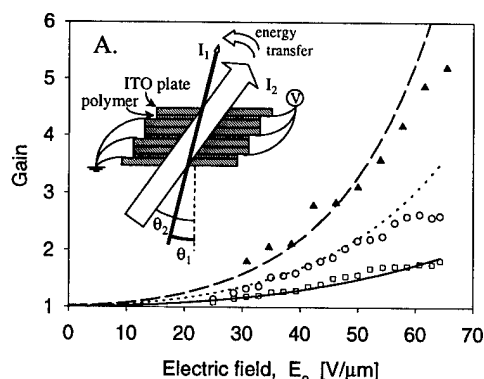
Figure 2. Two-beam coupling gain in a single sample (□), a two-layer stack (O), and a three-layer stack (▲) of the polymer composite PVK:PDCST:BBP:C_{60} with symbols the measured data and the curves a model fit .
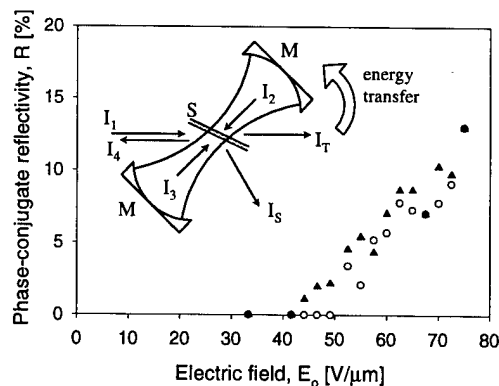
Figure 3. Self-pumped phase-conjugate (SPPC) reflectivity as a function of applied electric field for a 2-layer sample of PVK:PDCST:BBP:C_{60} for an incident intensity of I_1=180 mW/cm^2 (▲) I_1=90 mW/cm^2 (O) The inset shows the experimental arrangement for the linear cavity SPPC.

pumping beam is required, this configuration also acts as a self-pumped phase conjugating mirror. With phase-conjugate reflectivities as high as 13% for an applied electric field of 75 V/μm (Fig. 3), this marks a crucial milestone for this growing class of optoelectronic materials.

Another approach to enhancing the overall two-beam coupling gain is to use a moving interference pattern instead of a stationary one [8-10]; see Fig. 4. Dramatic enhancement of the gain has been demonstrated in our polymer composite, with values as large as 500 being achieved using a three-layer sample. This is the highest gain reported to date in a photorefractive polymer.
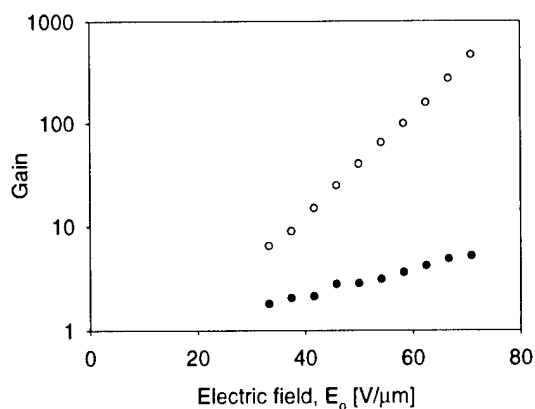
Figure 4 The steady-state gain as a function of applied electric field for a three-layer PR polymer sample. Gain is shown for stationary fringes (●) and for moving fringes (O).

From an investigation of the time dependence and velocity of fringe motion, we also determine that hole conduction is dominant and that the mobility life-time product reaches $\mu\tau=3\times10^{-10}$ cm^2/V at an applied electric field E_o=71 V/μm.

References

1. A. Ashkin, G. D. Boyd, J. M. Dzierdzic, R. G. Smith, A. A. Ballman, H. J. Levenstein, and K. Nassau, *Appl. Phys. Lett.* **9**, 72 (1966).
2. F. S. Chen, J. T. LaMacchia, and D. B. Fraser, *J. Appl. Phys.* **38**, 3389 (1968).
3. See e.g. L. Solymar, D. J. Webb, and A. Grunnet-Jepsen, *The physics and applications of photorefractive materials*, Oxford University Press, New York, 1996.
4. S. Ducharme, J. C. Scott, R. J. Twieg, and W. E. Moerner, *Phys. Rev. Lett.* **66**, 1846 (1991).
5. K. Meerholz, B. L. Volodin, Sandalphon, B. Kippelen, and N. Peyghambarian, *Nature* **371**, 497 (1994); M. Liphardt et al., *Science* **263**, 367 (1994); P. M. Lundquist et al., *ibid.* **274**, 1182 (1996). G. P. Wiederrecht, B. A. Yoon, and M. R. Wasielewski, *ibid.* **270**, 1794 (1995).
6. W. E. Moerner, A. Grunnet-Jepsen, and C. L. Thompson, *Ann. Rev. Mat. Sci.* **27** (in press 1997).
7. A. Grunnet-Jepsen, C. L. Thompson, R. J. Twieg, and W. E. Moerner, *Appl. Phys. Lett.*, **70**, 1515 (1997).
8. S. I. Stepanov, V. V. Kulikov, and M. P. Petrov, *Opt. Commun.* **44**, 19 (1982).
9. J. P. Huignard, H. Rajbenbach, Ph. Refregier, L. Solymar, *Opt. Eng.* **24**, 586 (1985).
10. Ph. Refregier, L. Solymar, H. Rajbenbach, and J. P. Huignard, *J. Appl. Phys.* **58**, 45 (1985).

Phase stability of guest/host photorefractive polymers studied by light scattering experiments

E. Hendrickx, B. L. Volodin, D. D. Steele, J. L. Maldonado Rivera, J. F. Wang,
B. Kippelen and N. Peyghambarian
Optical Sciences Center, The University of Arizona, Tucson, AZ 85721
Tel : (520) 621-4341; Fax (520) 626-4221; kippelen@ccit.arizona.edu

In recent years, we developed plasticized guest-host photorefractive polymers with a glass transition temperature below room temperature.[1] However, in these guest/host polymers a gradual crystallization of the chromophores (50% wt.) limits the shelf lifetime of the samples. The lifetime of DMNPAA(2,5-dimethyl-4-(p-nitrophenylazo)anisole) : PVK(poly-vinylcarbazole) : ECZ(N-ethylcarbazole) : TNF(tri-nitrofluorenone) samples with 50% wt. of DMNPAA was found to vary between a few hours and a few months depending on the starting materials and the processing conditions. Here we present a new guest/host photorefractive composite based on isomeric mixtures of the chromophore NPADVBB (4-(4'-nitrophenylazo)1,3-di[(3"or 4"-vinyl)benzyloxy] benzene). These composites exhibit a performance level that is identical to that of DMNPAA-based samples but have an estimated shelf lifetime of several years at room temperature.

The photorefractive properties of the sample were tested by four-wave mixing and two-beam coupling experiments in the tilted geometry described previously. The laser source was a HeNe laser (633 nm). The steady-state diffraction efficiencies as a function of applied field in samples with composition DMNPAA:PVK:ECZ:TNF (40:39:19:2 %wt.) and NPADVBB:PVK:ECZ:TNF (40:39:19:2 %wt.) were found to be identical within experimental error. For both samples maximum diffraction efficiency is observed at an applied field of approximately 65 V/μm in 105 μm thick samples. The photorefractive origin of both signals was confirmed by two-beam coupling experiments. The dynamics of the build-up of the photorefractive grating was similar in both samples and was sub-second.

To quantify the shelf lifetime of these different samples, we studied the crystallization behavior of the chromophores in the polymer matrix as a function of temperature. The crystallization was followed by monitoring the intensity of the light scattered from the sample within a fixed solid angle.[2] The scattered light intensity measured as a function of time in a sample of DMNPAA:PVK:ECZ (39:41:20 %wt.) held at 55 °C is shown in Figure 1. Crystallization does not start immediately upon heating: an induction period for the formation of nucleation sites that scatter light is observed and followed by a period of accelerated crystallization during which the nuclei grow in radius. This behavior is characteristic of phase separations occurring through the mechanism of nucleation and growth. The crystals appear as isolated spots in the composite matrix. Finally, the intensity of the scattered light decreases exponentially with time due to multiple scattering, which broadens the distribution of the scattered light and increases the absorption of light. This behavior is typical and very reproducible within 25% in the samples investigated in this study. To quantify the shelf lifetime of

guest/host photorefractive polymers we define a reference time t_{ref} that corresponds to the intercept of the linear extrapolations of the induction and growth phases. That reference time corresponds to the first visible appearance of crystallites in the polymer matrix.
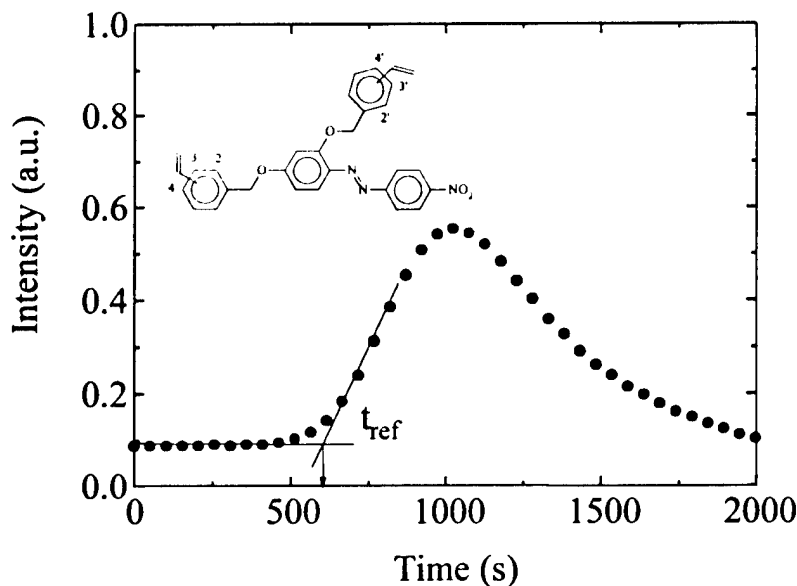
Figure 1 : Intensity of the scattered light as a function of time for a polymer composite DMNPAA:PVK:ECZ (39:41:20 % wt.) and at 55 °C. The inset shows the structure of NPADVBB.

We investigated the crystallization onset as a function of several parameters including the sample composition, sample temperature, plasticizer to polymer ratio (ECZ/PVK), and the nature of the dopant chromophore. The results are summarized in Table I. A first factor that strongly influences the sample lifetime is the temperature at which the sample is stored. The reference time t_{ref} drops drastically upon heating the samples. Theories developed for crystallization processes usually describe their temperature dependence by the Arrhenius velocity equation, commonly used for the rate of a thermally activated process :

$$\frac{1}{t_c} \propto k = A\exp\left(-\frac{E}{RT}\right) \qquad (1)$$

where t_c is a time constant characteristic for the process, k is the rate constant (s^{-1}), R the gas constant (8.314 J K^{-1} mol^{-1}), A a prefactor, E the activation energy (J mol^{-1}) and T the temperature (K). Our results show that the nucleation period can be described by an Arrhenius plot in the temperature range 45-85 °C. An activation energy of $E = 71 \pm 4$ kJ mol^{-1} (0.74 eV) can be deduced. This value is close to the activation energy for diffusion of gases and liquids in polymers, 20-80 kJ mol^{-1}, and suggests that the speed of diffusion of the polar molecules in the polymer matrix is the rate-limiting step in the crystallization process.

Table I : Reference time measured in guest/host photorefractive composites as a function of dopant chromophore, chromophore concentration, PVK/ECZ ratio (% wt.), and temperature. T_M is the melting point of the chromophore.

Dye (% wt.)	T_M (°C)	PVK / ECZ	T (°C)	t_{ref} (s)
DMNPAA 21%	161	3/2	75	1650
DMNPAA 19%	161	1/1	75	250
DMNPAA 39%	161	2/1	35	94000
DMNPAA 39%	161	2/1	45	1200
DMNPAA 39%	161	2/1	55	500
DMNPAA 39%	161	2/1	65	200
DMNPAA 39%	161	2/1	75	110
DMNPAA 39%	161	2/1	85	60
NPDAB 39%	149	2/1	85	140
NPADVBB 39%	127	2/1	85	6600

Table I also shows that the reference time t_{ref} depends not only on the nature of the chromophore and the temperature, but also on the composition of the matrix and in particular the polymer/plasticizer ratio. This behavior can be seen from the decrease in lifetime, from 27.5 min. to 4.2 min. at 75 °C, in samples doped with DMNPAA chromophores when the PVK/ECZ ratio is varied from 3/2 to 1/1. The addition of a plasticizer to a polymer increases the free volume and the segmental mobility. This results in an increased rate of diffusion and consequently a lower sample lifetime.

All these measurements were carried out at temperatures that are well above room temperature, i.e. well above the glass transition temperature which, for composites with PVK/ECZ 2:1 weight ratio, falls in the temperature range of 0 °C to 40 °C. If we compare the lifetime of DMNPAA-samples at 85 °C to that of PVK-based composites doped with other dyes at the same temperature, we can see an increase in lifetime upon going from DMNPAA, to NPDAB (4-(4'-nitrophenylazo)1,3-di(benzyloxy)benzene) and NPADVBB. This increase in lifetime also corresponds to a decrease of the melting point of the polar dye. Upon going from DMNPAA to NPADB, it can be seen that the extra phenyl substituents already induce a lowering of the melting point and an increase in the sample lifetime. For NPADVBB, however, the vinyl bonds on both phenyl rings can be either in the 3 or 4-position. Hence NPADVBB is a mixture of four isomers, with the vinyl groups in positions (3,3'), (3,4'), (4,3') and (4,4'). As a result the melting point is lowered further and the sample remains optically clear for 110 minutes at 85 °C. From this behavior, we can estimate a room temperature shelf lifetime of several years for samples containing 40% wt. of NPADVBB and with a PVK:ECZ ratio of 2:1.

1 K. Meerholz, B.L. Volodin, Sandalphon, B. Kippelen and N. Peyghambarian *Nature* 371, 497 (1994).
2 E. Hendrickx, B.L. Volodin, D.D. Steele, J.L. Maldonado Rivera, J.F. Wang, B. Kippelen and N. Peyghambarian Submitted for publication (1997).

REDUCED HOLE MOBILITY IN PHOTOREFRACTIVE POLYMERS DUE TO THE CHROMOPHORE DIPOLE MOMENT

Arosha Goonesekera and Stephen Ducharme, Department of Physics and Astronomy

Center for Material Research and Analysis
University of Nebraska-Lincoln, Lincoln, NE 68588-0111
Tel: (402) 472-8590, Fax: (402) 472-2879, EMail: awg@unlinfo.unl.edu

The recent demonstrations of low-cost high performance photorefractive polymers has encouraged more detailed studies of charge carrier transport mechanisms in photorefractive polymers as charge transport is a limiting factor in the sensitivity of these materials. The photorefractive effect is a mechanism for non local refractive index grating formation in an electro-optic material due to nonuniform illumination, through photoconduction and linear electro-optic response. The speed of photorefractive effect which remains low at present, is proportional to photoconductivity, hence improved understanding of transport mechanisms is vital. This report describes the negative effect the dipole moment of the non-linear chromophore has on the hole mobility in photorefractive polymers.

Recent studies[1] and theoretical models[2, 3] of reduced carrier mobilities due to dipolar disorder in xerographic polymers underline the importance of the detailed study of the effect of polar molecules on charge transport in photorefractive polymers because xerographic and photorefractive polymers share many of the same components and operate by similar physical mechanisms.[4] Due to these similarities, one expects there will be a good correlation between the transport mechanisms in these two systems.

Photorefractive polymer composites generally consist of a polymer backbone, a non-linear chromophore, a photosensitizer, and the charge transport agent. The model system for the present study, as shown in Fig. 1, is the bisA-NAS:DEH photorefractive polymer consisting of a bisphenol-A polycarbonate host (bisA-PC) polymer with the electro-optic chromophore 4-4'-nitroaminostilbene (NAS) incorporated either as a guest or covalently (bisA-NAS), plus a guest hole transport agent diethylamino-benzaldehyde-diphenyl hydrazone (DEH). Fours compositions were studied: 1) the bisA-NAS:DEH composite with effectively 28 wt. % NAS, and the bisA-PC host polymer with 2) 0 %, 3) 3.5 % and 4) 7 % NAS by weight. The DEH concentration was 30 wt. % in all samples.

a) bisphenol-A-polycarbonate (**BPPC**)

b) Diethylamino-benzaldehyde diphenyl hydrazone (**DEH**)

c) 4- nitro-4' aminostilbene (**NAS**)

d) Bisphenol-A-4, 4' Nitro-AminoStilbene (**bisA-NAS**)
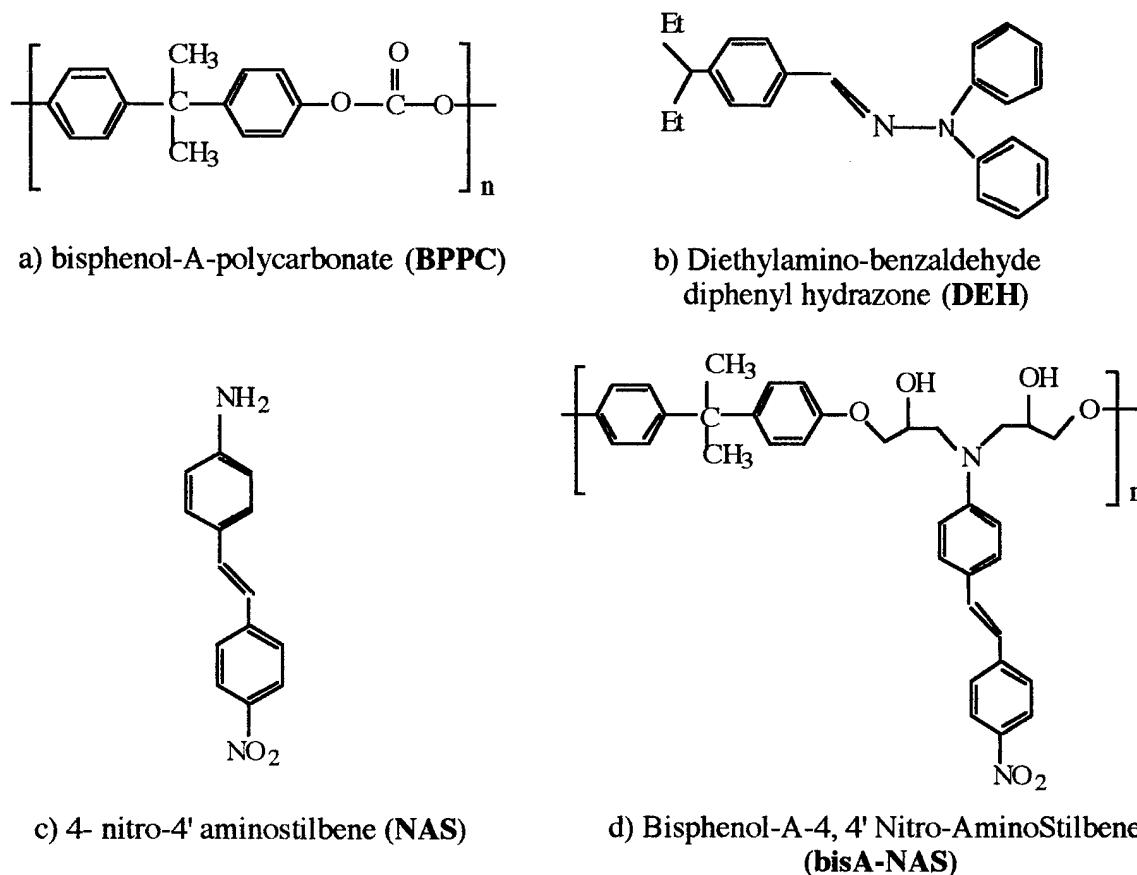
Figure 1: Components of the molecularly doped polymers.

The mobility was measured by the conventional time-of-flight technique with carriers generated at high electrical bias in a thin selenium layer on one side of a thin film of the subject polymer and an aluminum counter electrode. A plateau in the current transient was used to determine the time of flight and calculate the mobility as a function of the average electric field in the sample. Care was taken to ensure that charge depletion was negligible. A detailed description of sample fabrication and the time-of-flight techniques have been published elsewhere.[5]

Figure 2 shows a significant reduction in hole mobility with increasing chromophore concentration in guest NAS systems while in the NAS-attached system shows a further reduced hole mobility, especially at the large electric fields used in photorefractive recording. This trend is indicative of the effect produce by the dipole moment of the chromophore.

According to the models,[2, 3] the large dipole moment of the NAS chromophore at 6.7 DeBye results in reduced mobility at high fields because the randomly placed and oriented dipoles introduce considerable additional energetic disorder in the hopping manifold. The consequence of this additional energetic disorder is the generation of more high-potential-mismatch hopping transitions and reduced mobility on average. It also appears that the

covalent NAS photorefractive polymer (28 wt. % NAS) has its mobility reduced much more than can be attributed to the effects of the NAS chromophore dipole on the energetic disorder.
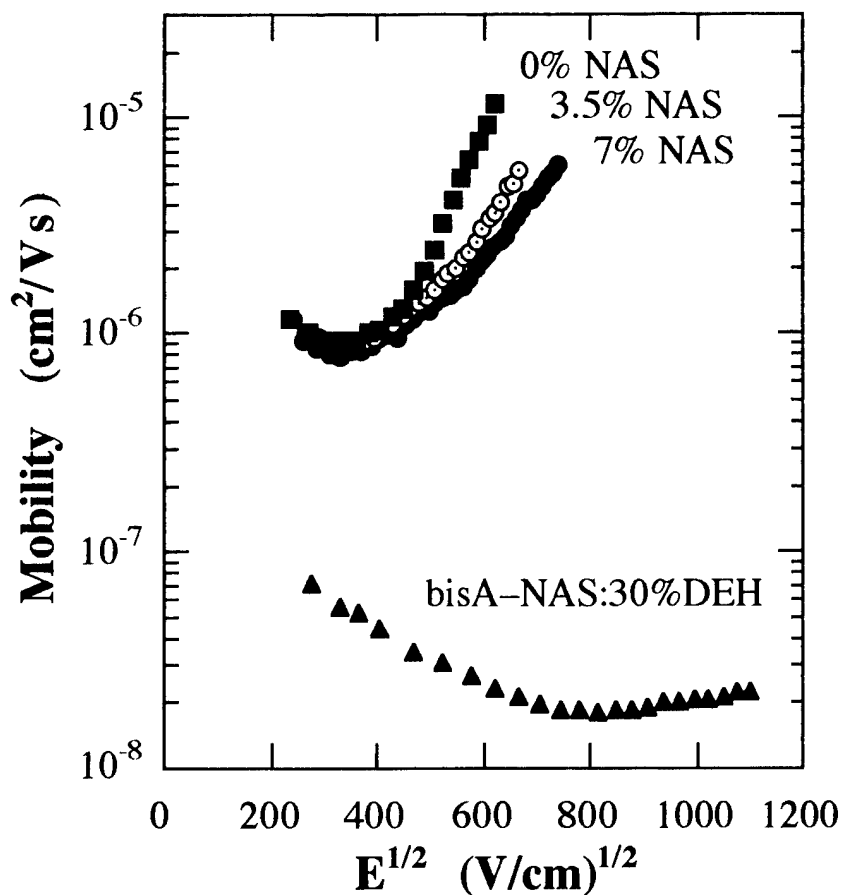
Figure 2: Mobility of the polymer composites with varying concentrations of NAS.

In conclusion, this investigation indicates that the presence of molecules of with large dipole moments can result in reduction of carrier mobility in photorefractive polymers. Since chromophores with large electro-optic response, and consequently large dipole moments, are necessary for improved photorefractive gain or diffraction efficiency, these results bode ill for the prospect of significant increases in the photorefractive speed through conventional considerations. Therefore, it is essential to continue probing the effects of polar molecules (many of the hole transport agents, including DEH, are also highly polar) on charge transport in molecularly doped polymers and to consider means of either reducing dipole moments while maintaining electro-optic response, or reducing the sensitivity of the carrier mobility to dipolar disorder.

ACKNOWLEDGMENTS

REFERENCES

[1] P. M. Borsenberger, H. Bässler, *J. Chem. Phys.* **95**, 5327 (1991).

[2] R. H. Young, *Philos. Mag. B* **72**, 435-457 (1995).

[3] D. H. Dunlap, P. E. Parris, V. M. Kenkre, *Phys. Rev. Lett.* **77**, 542-544 (1996).

[4] S. Ducharme, R. W. Twieg, J. C. Scott, W. E. Moerner, *Phys. Rev. Lett.* **66**, 1846-1849 (1991).

[5] A. Goonesekera, S. Ducharme, J. M. Takacs, L. Zhang, Hole Mobilities in a Photorefractive Polymer, S. Ducharme, J. M. Stasiak, Eds., Organic Photorefractive Materials and Xerographic Photoreceptors, Denver (SPIE, 1996).

Maslyanitsin, I. A. ▪ ThE8
Matsuda, Hiro ▪ ThE1
Matsumoto, Osamu ▪ ThE5
Matsumoto, Shiro ▪ ThC5
Matsuura, Tohru ▪ FA4
McBranch, D. W. ▪ ThE17
McGehee, M. ▪ WD1
Medvedev, G. A. ▪ WB2
Meier, Urs ▪ ThD2
Meyers, F. ▪ FD1
Miyata, S. ▪ ThE22
Mizukami, F. ▪ ThE10
Moerner, William E. ▪ FD3
Morrell, M. M. ▪ WD4
Muller, Jacques ▪ WC4
Mungan, Carl E. ▪ ThE25

Nadler, M. P. ▪ ThE7
Nakashima, M. ▪ ThE2
Nihei, Eisuke ▪ WA1, WD2
Norwood, Robert A. ▪ WA2, ThB, ThE19, FB4
Nunzi, Jean-Michel ▪ WC1

Oh, M. C. ▪ ThE26, ThE27, ThE28
Ohta, T. ▪ ThE10
Okada, Akane ▪ ThE4
Olbrechts, Geert ▪ ThD3
Olson, David J. ▪ FA2

Palffy-Muhoray, P. ▪ WB5
Park, H. ▪ ThE27, ThE28
Perry, J. W. ▪ ThA3
Persoons, André ▪ ThD1, ThD3
Petschek, R. G. ▪ ThC3
Peyghambarian, N. ▪ WD4, FD1, FD4
Pong, Richard G. S. ▪ ThA2
Prayaga, Chandra S. ▪ ThE25
Prêtre, Ph. ▪ FC2
Przhonska, Olga ▪ ThA1

Quintero-Torres, R. ▪ WC3

Ra, Younsoo ▪ WA3, ThE23, FB2
Ramírez-del-Solar, M. ▪ ThE2
Rao, D. Narayana ▪ ThE2
Rao, D. V. G. L. N. ▪ ThE2
Ratna, B. R. ▪ ThE13
Roberts, M. J. ▪ ThC6, ThE7
Robinson, J. M. ▪ ThE17
Röckel, H. ▪ ThA3, FD1
Rubner, Michael ▪ WD5

Saavedra, S. Scott ▪ ThE9
Sakai, Wataru ▪ ThE5
Sakata, Seizou ▪ ThC5
Sandalphon ▪ FD1
Sarkisov, Sergey ▪ ThE12
Sasabe, Hiroyuki ▪ ThB3, ThC2
Sasaki, Keisuke ▪ WD2
Sasaki, Shigekuni ▪ FA4
Savranskii, V. V. ▪ ThE8
Schülzgen, A. ▪ WD4
Schwartz, B. J. ▪ WD1
Shacklette, Lawrence W. ▪ WA2, FB4
Shakos, J. D. ▪ FD2
Shashidhar, R. ▪ ThE13
Shelton, David P. ▪ ThE11
Shi, R. F. ▪ ThB1
Shi, Yongqiang ▪ FA2, FB2, FC1, FC3
Shin, Sang-Yung ▪ ThE29
Shirk, James S. ▪ ThA2
Shu, Ching-Fong ▪ ThE6
Singer, K. D. ▪ WB1, ThC3, FD
Smilowitz, L. ▪ ThE17
Snow, Arthur W. ▪ ThA2
Sokoloff, J. P. ▪ ThB3
Sourisseau, C. ▪ WB4
Spiegelberg, Ch. ▪ WD4
Steele, D. D. ▪ FD1, FD4
Stegeman, George I. ▪ WC2, WC5
Steier, William H. ▪ WA3, WA4, ThE16, ThE18, ThE21, ThE23, FA, FB2, FC1, FC3, FC4
Stengel, K. M. T. ▪ FB4
Stenger-Smith, J. D. ▪ ThC6, ThE7
Stevenson, S. ▪ ThE15
Strutz, Shane J. ▪ WB3
Sugiyama, Yasuyuki ▪ ThC5
Sun, Diechi ▪ WC6
Sun, Meng ▪ WC6
Sun, Sam S. ▪ FC4
Sun, Shajing ▪ WA3, ThE23

Tanaka, K. ▪ ThE22
Thakur, M. K. ▪ WC3, ThE14, ThE24
Tkachenko, N. A. ▪ ThE8
Tomaru, Satoru ▪ FB5
Tripathy, Sukant K. ▪ ThC4, ThE2, FB3
Tsap, Boris ▪ FC1
Tsuchimori, Masaaki ▪ ThE4
Tsutsumi, Naoto ▪ ThE5
Turner, M. L. ▪ WD3

Ushijima, Hirobumi ▪ ThE1
Usui, H. ▪ ThE22

Van Elshocht, Sven ▪ ThD1
Van Steenwinckel, David ▪ ThD3
Van Stryland, Eric ▪ ThA1
Verbiest, Thierry ▪ ThD1
Vijayalakshmi, S. ▪ FB4
Volodin, B. L. ▪ FD1, FD4
Vydra, Jan ▪ ThE20

Wada, Tatsuo ▪ ThC2
Wang, C. H. ▪ ThE6
Wang, Fang ▪ ThE23, FC4
Wang, J. F. ▪ FD1, FD4
Wang, S. ▪ ThE15
Wang, Wenshen ▪ FA2, FC1, FC3
Wang, X. ▪ ThC4
Wang, Yuh-Kai ▪ ThE6
Watanabe, T. ▪ ThE22
Watanbe, Osamu ▪ ThE4
West, D. P. ▪ FD2
West, K. S. ▪ FD2
Wilkosz, Aaron ▪ ThE12
Won, Y. H. ▪ ThE26, ThE27, ThE28
Wong, Man Shing ▪ ThD2
Woo, E. P. ▪ WD3
Wood, Laurie L. ▪ ThE9
Wu, X. L. ▪ ThA3
Wu, L. M. ▪ FC2
Wynne, K. J. ▪ ThE7

Xu, Jianjun ▪ ThE14, ThE24

Yacoubian, Araz ▪ ThE23, FC4
Yamamoto, Kaoru ▪ ThE10
Yang, W. S. ▪ ThE17
Yardley, James T. ▪ WA2, FB4
Yase, Kiyoshi ▪ ThE10
Yoshida, Yuji ▪ ThE10
Yoshimura, Ryoko ▪ FB5

Zang, Yi-Liang ▪ ThE6
Zarras, P. ▪ ThE7
Zhang, Cheng ▪ ThE23
Zhang, Qiang ▪ WC5
Zhang, Yadong ▪ ThC2
Zhou, Jun ▪ WC6
Zhou, Ligui ▪ ThE24
Zhu, Jingsong ▪ ThE23, FC4
Ziari, Mehrdad ▪ ThE21
Zyss, Joseph ▪ ThD, FB1

Organic Thin Films for Photonics Applications
Technical Program Committee